Contribution à l'étude du trafic routier sur réseaux à l'aide des équations d'Hamilton-Jacobi

Guillaume Costeseque

UNIVERSITÉ PARIS-EST

École Doctorale **Mathématiques et STIC**

THÈSE

présentée pour l'obtention du titre de

Docteur de l'Université Paris-Est

Spécialité : **Mathématiques Appliquées**

par

Guillaume COSTESEQUE

Soutenue publiquement le 12 Septembre 2014

Contribution à l'étude du trafic routier sur réseaux à l'aide des équations d'Hamilton-Jacobi

---

Directeur de thèse: **Régis MONNEAU**
Co-encadrant de thèse: **Jean-Patrick LEBACQUE**

Jury

M.	Ludovic LECLERCQ,	Univ. Lyon, IFSTTAR/ENTPE	Président
Mme	Paola GOATIN,	Inria Sophia-Antipolis	Rapporteur
M.	Saïd MAMMAR,	Univ. Evry Val d'Essonne	Rapporteur
M.	Chris M.J. TAMPÈRE,	KU Leuven – Belgique	Rapporteur
M.	Fabio CAMILLI,	Univ. di Roma – Italie	Examinateur
M.	Jean-Patrick LEBACQUE,	Univ. Paris-Est, IFSTTAR	Examinateur
M.	Markos PAPAGEORGIOU,	TU Crete – Grèce	Examinateur
M.	Régis MONNEAU,	Univ. Paris-Est, ENPC	Directeur de thèse

À ma famille, qui a toujours tout fait pour me permettre de réussir,

À mon grand-père François, disparu quelques jours avant ma soutenance.

"Le mieux est le mortel ennemi du bien."
— Charles De Montesquieu, *Cahiers*

Résumé

Ce travail porte sur la modélisation et la simulation du trafic routier sur un réseau. Modéliser le trafic sur une section homogène (c'est-à-dire sans entrée, ni sortie) trouve ses racines au milieu du XX$^{\text{ème}}$ siècle et a généré une importante littérature depuis. Cependant, la prise en compte des discontinuités des réseaux comme les jonctions, n'a attiré l'attention du cercle scientifique que bien plus récemment. Pourtant, ces discontinuités sont les sources majeures des congestions, récurrentes ou non, qui dégradent la qualité de service des infrastructures. Ce travail se propose donc d'apporter un éclairage particulier sur cette question, tout en s'intéressant aux problèmes d'échelle et plus particulièrement au passage microscopique-macroscopique dans les modèles existants.

La première partie de cette thèse est consacrée au lien existant entre les modèles de poursuite microscopiques et les modèles d'écoulement macroscopiques. Le passage asymptotique est assuré par une technique d'homogénéisation pour les équations d'Hamilton-Jacobi. Dans une deuxième partie, nous nous intéressons à la modélisation et à la simulation des flux de véhicules au travers d'une jonction. Le modèle macroscopique considéré est bâti autour des équations d'Hamilton-Jacobi. La troisième partie enfin, se concentre sur la recherche de solutions analytiques ou semi-analytiques, grâce à l'utilisation de formules de représentation permettant de résoudre les équations d'Hamilton-Jacobi sous de bonnes hypothèses. Nous nous intéressons également dans cette thèse, à l'application des techniques Hamilton-Jacobi à la classe générique des modèles macroscopiques de trafic de second ordre, dits *modèles GSOM*.

Mots-clés: Trafic routier, micro, macro, réseau, jonction, Hamilton-Jacobi, schéma numérique, Lax-Hopf

Abstract

This work focuses on modeling and simulation of traffic flows on a network. Modeling road traffic on a homogeneous section takes its roots in the middle of XX^{th} century and it has generated a substantial literature since then. However, taking into account discontinuities of the network such as junctions, has attracted the attention of the scientific circle more recently. However, these discontinuities are the major sources of traffic congestion, recurring or not, that basically degrades the level of service of road infrastructure. This work therefore aims to provide a unique perspective on this issue, while focusing on scale problems and more precisely on microscopic-macroscopic passage in existing models.

The first part of this thesis is devoted to the relationship between microscopic car-following models and macroscopic continuous flow models. The asymptotic passage is based on a homogenization technique for Hamilton-Jacobi equations. In a second part, we focus on the modeling and simulation of vehicular traffic flow through a junction. The considered macroscopic model is built on Hamilton-Jacobi equations as well. Finally, the third part focuses on finding analytical or semi-analytical solutions, through representation formulas aiming to solve Hamilton-Jacobi equations under adequate assumptions. In this thesis, we are also interested in the application of Hamilton-Jacobi technique to a generic class of second order macroscopic traffic flow models, the so-called *GSOM models*.

Keywords: Traffic flow, micro, macro, network, junction, Hamilton-Jacobi, numerical scheme, Lax-Hopf

Remerciements

C'est avec un grand soin que je rédige ces quelques lignes afin de remercier les différentes personnes dont les contributions, à des degrés divers, m'ont été précieuses durant ces trois années de thèse. D'avance pardon à ceux que j'aurais malgré tout oublier.

Pour commencer, j'adresse toute ma reconnaissance à mes deux encadrants, Régis Monneau et Jean-Patrick Lebacque, respectivement Ingénieur en Chef et Ingénieur Général du corps des Ponts, Eaux et Forêts. Cela a été un réel plaisir de travailler sous leurs directions. Avec des styles différents mais poussés par une même passion pour la science et la recherche, ils ont su faire émerger chez moi un intérêt sans cesse renouvelé pour des sujets auxquels ma formation m'avait peu ou prou destinée. Je pense avoir su, plus ou moins habilement, tirer partie des qualités, des (immenses) connaissances mais aussi des disponibilités de chacun. En passant outre les petites (et grandes) turbulences qui accompagnent nécessairement une "cohabitation" à trois pendant la durée d'une thèse, j'espère que ce travail aura permis de créer des ponts entre la rigeur des *mathématiques appliquées* et les enjeux réels en *transport*.

Je tiens bien évidemment à remercier les membres de mon jury de thèse. Ce travail étant à la frontière entre deux thématiques, des spécialistes de chaque ont accepté d'évaluer mon travail. Je remercie ainsi Mme Paola Goatin, M. Saïd Mammar et M. Chris Tampère qui ont accepté la lourde tâche de rapporter ce mémoire – et ce dans un délai très court, mais aussi M. Fabio Camilli, M. Ludovic Leclercq et M. Markos Papageorgiou qui me font l'immense honneur de faire partie de mon jury d'évaluation. Je les remercie pour le temps et l'énergie consacrés à l'évalutation de ma contribution et pour leurs remarques judicieuses et constructives.

Mes remerciements vont également à l'endroit de mon employeur, le Ministère de l'Ecologie, du Développement Durable et de l'Energie (MEDDE), à Jean-François Delmas et Alexandre Ern, respectivement directeur et directeur adjoint du CERMICS, à l'ensemble des membres de la commission de suivi des thèses ITPE présidée par Jacques Roudier, Ingénieur Général du Corps des Ponts, Eaux et Forêts, mais aussi Christine Buisson et Ludovic Leclercq (LICIT / ENTPE et IFSTTAR), qui ont suivi périodiquement mon avancée. Pour le rôle qu'il a eu dans mon orientation vers une thèse, j'adresse mes plus sincères remerciements à Aurélien Duret.

Je ne peux pas oublier mes collègues de travail qui ont partagé mon quotidien, tout au long de ces trois années, que ce soit à l'Ecole des Ponts ou à l'IFSTTAR (je vous prie de m'excuser de ne pas tous vous citer). Du côté du CERMICS, je tiens à saluer l'ensemble des doctorants et plus particulièrement mes collègues de bureau : Oliver Hénard, Patrick Hoscheit, Maria Adela Puscas, Yannick Masson, mais aussi Julien Reygner, William Minvielle, Thomas Pradeau, Pauline Sarrabezolles et Laurent Monasse avec qui j'ai eu l'occasion de

discuter d'autres choses que de mathématiques. Je remercie également tous les membres (anciens ou actuels) de l'équipe "EDP et matériaux" : Danny El-Khass (qui m'a le premier accueilli au laboratoire), Mohammad Al Haj, Ghada Chmaycen, Amin Ghorbel, Elefthe-rios Ntvoris et Jérémy Firozali ; ainsi que ceux qui ne seront rester que sur une courte (mais intense) période : Łukasz Paszkowski et Matija Hustić (qui m'ont énormément aidé dans la rédaction de mon premier article), Avetik Arakelyan, Liutang Xue et Erik Lind-gren. J'aurais un mot spécialement pour mon collègue et ami Arnaud Le Guilcher, avec lequel j'ai eu énormément de plaisir à discuter.

Du côté de l'IFSTTAR, la liste est également longue (et n'est certainement pas ex-haustive) mais voici une tentative : Dihya Atmani, Johanna Baro, Hani El-Assaad, Jos-quin Fouillaron, Matthieu Mastio, Andry Randriamanamihaga, Rony Rozas, Wissam Sam-mouri, Moncef Toumi et ceux de passage David Abellanas, Arthur de La Rochefoucauld, Asma Khelifi ou encore Luis Blanche. Pour le rôle particulier qu'ils ont eu dans mon début de thèse, je remercie mes collègues "irréductibles" à savoir Thomas Monamy et Tibye Saumtally. Et je tiens à remercier Tibye pour tous les bons conseils qu'il a su me distiller tout au long de cette aventure (professionnelle et humaine). Pour nos discussions diverses, j'adresse un remerciement spécial à Virginie Boutueil ainsi qu'à Rémi Sainct, que je n'ai pas su classer entre Ecole des Ponts et IFSTTAR.

Pour leurs aides diverses (mais ô combien appréciées), je tiens à remercier Cathe-rine Baccaert, Nathalie Quelleu et Isabelle Simunic du secrétariat du CERMICS, Joëlle Guillot et Annie Thuilot du secrétariat du GRETTIA, Méranh Karounna et Nathalie Galéa du secrétariat général de l'IFSTTAR, Sylvie Cach du secrétariat de l'Ecole Doctorale MSTIC et également Mustapha Tendjaoui (sans qui rien ne fonctionnerait au GRETTIA). Pour les discussions scientifiques et éclectiques, je remercie Xavier Louis. Pour m'avoir permis d'intervenir dans leur groupe de travail à l'Université Paris-Est Marne-la-Vallée, merci à Michel Roussignol, Sylvain Lassarre et Antoine Tordeux. Je suis reconnaissant à Si-mon Cohen et l'ensemble du jury *abertis* qui m'on attribué le prix de recherche pour mon mémoire de master, formidable catalyseur pour ce travail de thèse.

Durant cette thèse, j'ai pris l'initiative de contacter énormément de personnes afin d'obtenir des réponses directes à certaines de mes questions. J'ai toujours eu des retours de leur part, ce qui a bien souvent donné lieu à des échanges passionants. J'en remercie très vivement : Ke Han (Penn. SU puis Imperial College London) dont le travail et la réussite ont été de véritables inspirations pour moi, Jia Li (UC Davis), Maurizio Falcone (Univ. Roma), Smita Sahu (Univ. Roma), Lawrence Evans (UC Berkeley), Alexandre Bayen (UC Berkeley), Christian Claudel (KAUST), Aude Hofleitner (UC Berkeley puis Face-book), Sébastien Blandin (IBM), Meng Wang (TU Delft), Paola Goatin (Inria), Nico-las Seguin (UPMC), Martin Treiber (TU Dresden), Alberto Bressan (Penn State Univ.), Italo Capuzzo-Dolcetta (Univ. Roma) et Fabio Ancona (Univ. Padova). Merci également à mes collègues ITPE du LICIT, Julien Monteil, Florian Marczak et Pierre-Antoine La-harotte, pour les éclairages sur leurs sujets de thèse, ainsi qu'à Céline Parzani (LICIT) et Boris Ly (*ex*-SETRA) pour l'intérêt porté à mes travaux.

Je porte une attention toute particulière à remercier Jean-Pierre Aubin, qui m'a grand ouvert les portes de son univers pour m'instruire à la théorie de la *viabilité*. Il a été d'une grande bonté à mon égard ainsi qu'à l'adresse de mes enfants. Je lui suis redevable du "second souffle" de mon travail de thèse et des opportunités de post-doctorat qui m'ont été offertes. Jean-Pierre a su m'introduire auprès de personnes chaleureuses et de grande qualité comme Alexandre Bayen, Christian Claudel, Luxi Chen, Marie-Hélène Durand, Sophie Martin ou encore Anna Désilles avec qui j'espère avoir le plaisir de travailler.

J'espère pouvoir "rembourser les générations futures" comme lui cherchait à rembourser l'encadrement que lui avait prodigué Jacques-Louis Lions. Je remercie également son épouse Hélène Frankowska qui m'a fort gentimment proposé un financement afin de pouvoir concilier mes aspirations professionnelles et ma situation familiale.

Je remercie également l'ensemble des membres de l'ANR "HJnet" qui ont été d'une grande bienveillance envers moi : Olivier Ley, Guy Barles, Ariela Briani, Yves Achdou, Pierre Cardialaguet, Hasnaa Zidani mais aussi les deux proches collaborateurs de Régis, à savoir Cyril Imbert et Nicolas Forcadel.

Enfin, mes derniers mots et mes plus tendres pensées vont à ma famille et à mes proches, à mon frère Benoît pour sa relecture attentive et tout particulièrement à mon épouse Virginie et à nos deux enfants, Jules et Maxime. Merci pour votre soutien constant, vos encouragements et l'affection indéfectible que vous me prodiguez. Merci infiniment de tout abandonner pour me suivre dans la suite de cette aventure de recherche.

Sommaire

Glossaire

ARZ	Aw-Rascle-Zhang (modèle de)
BAU	Bande d'Arrêt d'Urgence
CFL	Courant-Friedrichs-Lewy (condition)
DF	Diagramme Fondamental
DNL	Dynamic Network Loading
DTA	Dynamic Traffic Assignment
EDO	Equation aux Dérivées Ordinaires
EDP	Equation aux Dérivées Partielles
ENO	Essentially Non Oscillatory (scheme)
FD	Fundamental Diagram
GDV	Gestion Dynamique des Voies
GSOM	Generic Second Order Models
HJ	Hamilton-Jacobi (équation de)
ITS	Intelligent Transportation Systems
l.h.s.	left hand side
lsc	lower semi-continuous
LWR	Lighthill-Whitham-Richards (modèle de)
ODE	Ordinary Differential Equation
PDE	Partial Differential Equation
RDV	Régulation Dynamique des Vitesses
r.h.s.	right hand side
sci	semi-continue inférieurement
scs	semi-continue supérieurement
TIV	Temps Inter-Véhiculaire
usc	upper semi-continuous
V2I	Vehicle to Infrastructure (communication)
V2V	Vehicle to Vehicle (communication)
WENO	Weighted Essentially Non Oscillatory (scheme)

Introduction générale

Cette thèse porte sur la modélisation et la simulation du *trafic routier sur un réseau* avec une attention particulière portée aux phénomènes dynamiques aux jonctions. Sans perte de généralité, étant donné que les ondes caractéristiques en trafic ne se déplacent qu'à vitesse finie, nous nous limiterons à l'étude d'une seule jonction par la suite. Cette thèse a la particularité de traiter les deux aspects, modélisation et simulation, en mathématiques appliquées ainsi qu'en transport. Il est intéressant de noter qu'un des buts principaux de l'analyse mathématique est de déterminer l'existence et l'unicité de la solution du modèle tel qu'il est défini, ou de montrer les propriétés de convergence de la solution numérique vers la solution exacte du problème, dans le cas de schémas numériques. En transport, les finalités sont essentiellement la compréhension et l'explication de la physique du phénomène mais aussi l'applicabilité des méthodes.

1 Motivations issues de l'ingénierie du trafic

1.1 Constat

Devant la concentration des lieux de vie et des activités en milieu urbain ou périurbain où la voiture reste le moyen de déplacement privilégié et face au besoin renouvelé de mobilité, la congestion routière est devenue un enjeu majeur pour les sociétés modernes en termes de perte de productivité, de perte de temps, d'émissions de gaz à effet de serre et d'autres externalités négatives. Pour illustration, rappelons que le coût de la congestion dans les villes européennes représenterait une charge d'environ 1% du produit intérieur brut (PIB) total de l'Europe chaque année[1]. Ce chiffre est bien sûr à nuancer car il est sujet de débats (voir par exemple [219]).

L'efficience des infrastructures et des systèmes de transports d'un pays est un paramètre majeur dans son économie. Sur cet échiquier, le mode routier conserve une part prépondérante. Au cours des dernières décennies, avec l'intensification des échanges, *motif* de déplacement, et la multiplication du nombre de véhicules, *vecteur* de déplacement, les infrastructures ont toujours dû être adaptées au volume de circulation. Cette politique d'expansion des réseaux n'est aujourd'hui plus tenable économiquement et n'est plus acceptable socialement. En effet, dans un environnement global contraint, la prise de conscience collective des impacts négatifs d'un tel fonctionnement conduit à changer de paradigme. L'usage des infrastructures aujourd'hui congestionnées doit donc être optimisée afin d'apporter aux usagers un niveau de service accru. L'apparition de la congestion est un phénomène qui est étudié depuis plus d'une cinquantaine d'années et les mécanismes en jeu sur les sections homogènes sont relativement bien compris. Cela est un peu moins vrai concernant l'approche globale d'un *réseau* composé de sections homogènes mais aussi

1. http://tinyurl.com/cqzf52p, voir en particulier l'appendice 5 du Papier Blanc, SEC(2011) 358, pour la méthode d'estimation de l'impact de la congestion.

de discontinuités. Ce qui est également moins compris, est de savoir comment intervenir efficacement sur ce système afin d'en tirer un fonctionnement optimal.

Considérons un réseau routier donné et identifions-le à un *graphe orienté*, c'est-à-dire un ensemble composé de sommets reliés entre eux par des arcs induisant un sens privilégié de déplacement. Les véhicules se répartissent sur ce réseau en fonction de leur origine et de leur destination. Les gestionnaires de trafic ne peuvent pas influencer le choix de l'utilisateur de son couple origine-destination. Toutefois, ils peuvent soit influencer les heures de départ, par des incitations comme le péage modulable ou par de l'information sur l'état de trafic par exemple, ou ils peuvent améliorer le guidage dynamique des conducteurs déjà présents sur le réseau en leur conseillant l'itinéraire le plus adapté en temps réel. Le premier exemple sort de l'objectif de ce travail et nous ne nous intéresserons pas davantage à celui-ci dans ce manuscrit. Le second exemple nous amène à considérer les modèles d'affectation dynamique des véhicules sur le réseau ou *Dynamic Traffic Assignment* (DTA).

Les modèles dynamiques d'affectation du trafic sont souvent remaniés pour constituer des problèmes mathématiques, englobant des problèmes de programmation, des problèmes de contrôle optimal ou des problèmes d'inégalités variationnelles, qui sont généralement résolus par des méthodes classiques d'optimisation sous de bonnes hypothèses (voir par exemple [121] ou encore [239]). Au coeur des modèles de type DTA, se trouvent les modèles de chargement dynamique du réseau, communément appelés *Dynamic Network Loading* (DNL). Ces modèles doivent décrire de façon réaliste la variation des flux de trafic dans le temps, sur des réseaux à grande échelle, tout en respectant la théorie du trafic routier. Ce point a tout particulièrement motivé mon travail de recherche.

1.2 Origines de la congestion et pratiques de gestion du trafic

Nous nous proposons de réaliser un tour rapide des raisons majeures de l'apparition de la congestion ainsi que des méthodes existantes d'optimisation de l'usage des infrastructures de transport. Avant cela, nous nous attardons sur deux notions clés pour la compréhension du phénomène de congestion, que sont l'*offre* et la *demande* de trafic. Ce sont des notions locales qui déterminent respectivement, le débit maximal réel pouvant s'écouler vers l'aval et le débit maximal réel souhaitant être écoulé depuis l'amont. Les notions d'offre et demande sont connexes à la notion de *capacité* de l'infrastructure qui définit le flux maximal théorique pouvant s'écouler localement sur la section considérée. Notons que la capacité est une borne supérieure à l'offre et à la demande. La congestion que tout usager a pu expérimenter est principalement due à une situation où l'offre est inférieure à la demande. Le volume de véhicules souhaitant s'écouler ne peut donc pas être satisfait. Une partie, égale à l'offre, va pouvoir effectivement circuler mais la partie résiduelle va être stockée sur le réseau, générerant de la congestion. Ces cas proviennent (voir Figure 1) :

- soit d'une baisse temporaire ou durable de la capacité de l'infrastructure. Cela peut notamment être consécutif à une réduction du nombre de voies de circulation, à un abaissement de la vitesse maximale autorisée par de la signalisation dynamique ou encore à une limitation de la vitesse maximale à cause du gradient physique (même si la capacité d'une infrastructure n'est pas nécessairement atteinte pour la vitesse maximale).

- soit d'une hausse de la demande. En effet, la demande est un phénomène hautement temporel qui présente de fortes variations, comme aux heures de pointe du matin ou du soir. La demande sur un réseau se trouve être également la résultante de flux qui

peuvent s'additionner comme aux points d'entrée sur le réseau ou aux convergents entre réseaux. Ce phénomène est au coeur de nos préoccupations pour cette thèse.

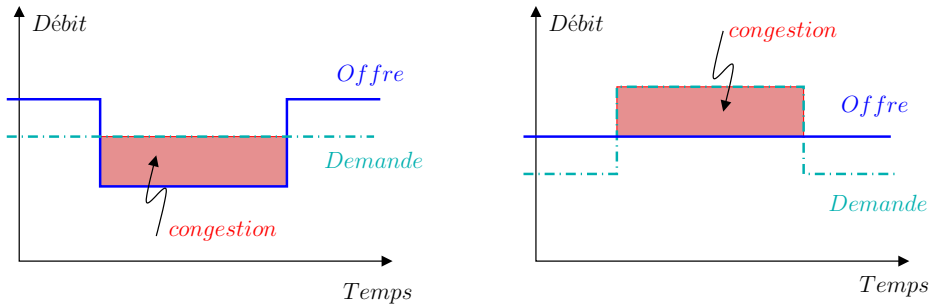

FIGURE 1 – Représentation schématique des deux cas d'occurence de congestion

Cependant, il est observé que la congestion apparaît bien souvent avant que le système n'atteigne sa capacité. Cela s'explique en partie par la diversité des comportements individuels des usagers et de l'instabilité du trafic. En effet, un simple freinage brusque peut entraîner la propagation de perturbations qui sont plus ou moins accentuées selon le temps de réaction des conducteurs et les interdistances entre véhicules.

Représentation imagée des ondes en trafic. *Par analogie, considérons un ensemble de dominos disposés séparément les uns à la suite des autres sur une table (repère eulérien fixe, équivalent en trafic au repère lagrangien si on considère que tous les véhicules circulent à la même vitesse). Plus les dominos seront rapprochés les uns des autres (plus la densité est élevée), plus vite ira une perturbation (par exemple la chute du premier) pour passer de l'un à l'autre. Si les dominos sont tous accolés (densité maximale), alors la chute du premier entraînera la chute immédiate du dernier (vitesse de l'onde infinie). En revanche, si deux dominos consécutifs sont suffisamment espacés pour que la chute de l'un n'impacte pas le suivant, alors l'onde mettra en temps infini pour atteindre le dernier domino (elle ne l'atteindra jamais : la vitesse de l'onde est nulle). Dans le cas du trafic, l'idée est semblable. Malgré tout, les véhicules sont conduits par des "agents" humains qui ont des temps de réaction et des comportements variables. Ce qui fait que l'onde de perturbation peut être accentuée (conducteur "agressif" avec un temps de réaction court ou une interdistance faible) ou atténuée (conducteur "passif" avec un temps de réaction long ou une interdistance plus grande).*

A l'origine de ces perturbations, nous trouvons principalement les changements de voie de circulation qui forcent les véhicules qui arrivent à une vitesse supérieure sur le véhicule venant de s'insérer à adapter leur vitesse pour rétablir une interdistance de confort. Le temps de réaction des conducteurs tend à produire des espaces de vide entre véhicules, périodes transitoires séparant les phases d'accélération et de décélération de chaque véhicule. La propagation d'une telle perturbation génère des ondes dites de *stop-and-go*. Les vides créés entre véhicules participent à une dégradation de la capacité théorique de l'infrastructure. On parle alors de chute de capacité [191]. Cette thématique de recherche sort néanmoins du cadre de ce travail.

Les mesures de gestion possibles afin de pallier à ces perturbations dépendent du type de réseau car les réponses seront différentes selon l'environnement :

- en milieu urbain, en excluant les cas pathogènes d'accidents, la congestion récurrente apparait principalement à partir des intersections. La plupart des intersections se compose soit de rond-points, soit de feux tricolores. Une solution est alors de gérer les plans de feux de façon synchronisée sur l'ensemble des intersections du réseau et non pas localement. En effet l'amélioration d'une seule intersection, par un processus d'optimisation locale, peut entraîner une dégradation du fonctionnement d'une intersection suivante, en augmentant son débit d'arrivée.

- en milieu inter-urbain, diverses méthodes de gestion existent comme :

  - le contrôle d'accès (ou *ramp metering* en anglais) pour gérer les flux d'entrée vers la voie principale et éviter de perturber le flux majeur. Concrètement, il s'agit d'implanter un feu de signalisation sur la voie d'entrée pour permettre l'insertion des véhicules au compte-goutte. Cette méthode peut cependant avoir l'inconvénient de repousser le problème de la congestion sur les réseaux secondaires ;
  - la gestion dynamique des voies (GDV) avec l'utilisation localement de la bande d'arrêt d'urgence (BAU) permettant d'augmenter l'offre, avec également le risque de reporter la demande sur un point en aval du réseau et d'en dégrader les conditions de circulation ;
  - la régulation dynamique des vitesses (RDV) qui, paradoxalement, permet d'uniformiser les vitesses entre les différentes voies de circulation et entre les usagers (véhicules légers et poids lourds classiquement) en abaissant la vitesse maximale autorisée. L'usager n'ayant plus d'intérêt de changer de voie en termes de gain de vitesse, cela permet de diminuer le nombre de changements de voie et ainsi de réduire la probabilité de générer des perturbations (voir par exemple [87]). Cela permet en outre de retarder l'arrivée des véhicules sur les bouchons en aval.

Un point à traiter est de déterminer quand il faut déclencher l'une ou l'autre des méthodes de régulation. Ce point fait l'objet de nombreuses recherches mais ne sera pas traité dans le présent travail de thèse. Le gestionnaire doit pouvoir connaître précisément et en temps réel, l'état du trafic sur son réseau et disposer de modèles lui permettant d'évaluer *a priori* l'impact d'une mesure de gestion.

1.3 Une note sur les Systèmes de Transports Intelligents

Les Systèmes de Transports Intelligents (ou ITS de l'anglais *Intelligent Transportation Systems*) forment un ensemble de solutions techniques et technologiques dont les promesses en gestion du trafic routier ne sont pas négligeables.

Toutefois, il est nécessaire de bien définir de quels systèmes l'on parle à l'évocation des Systèmes de Transports Intelligents. En effet, une définition assez générique peut être la suivante : tout système provenant de l'application des nouvelles technologies de l'information et de la communication. Il y a de fait une popularisation des équipements technologiques dans les véhicules, avec des finalités très diverses. Il est ainsi possible de penser aux différents systèmes portant sur la sécurité et le confort, comme l'intégration de nouveaux types de capteurs dont le but est de compléter la perception partielle qu'a un usager de son environnement de conduite. Citons par exemple :

- les caméras et les radars de recul pour le stationnement,

- la surveillance des angles morts pour les manoeuvres de dépassement,

- les systèmes de géo-positionnement et de guidage afin de choisir l'itinéraire le plus adapté.

Peuvent s'ajouter à cette liste, la variété de systèmes d'informations trafic avec la transmission par radio ou par le biais des Panneaux à Messages Variables (PMV). Une des technologies qui a le plus marqué les transports ces dernières années est sans aucun doute l'arrivée de l'internet mobile et de l'information proposée par les téléphones portables équipés. Les modes de communication sans fil comme le Blutetooth ainsi que le Wifi sont également de nouvelles sources d'innovation en trafic. Globalement, l'intérêt de ces technologies est d'étendre le domaine spatio-temporel considéré, alors que classiquement, il se réduit aux seules capacités de perception des usagers. Comme nous pouvons le voir, la définition des ITS est très vague et englobe toute une panoplie de technologies. Aussi, pour ce travail, nous préfèrons recadrer notre intérêt sur les systèmes coopératifs, qui forment une sous-classe de l'ensemble des ITS. Les véhicules coopératifs sont des véhicules équipés qui permettent de transmettre sur des canaux dédiés, des informations diverses et variées comme l'état du trafic, la présence d'une congestion, la présence d'un obstacle ou la présence d'un feu de trafic. La transmission peut se faire vers les autres véhicules engendrant des communications du type *vehicule to vehicule* (V2V) ou échanger avec l'infrastucture constituée d'unités en bord de route. On parle dans ce cas de communications *vehicule to infrastructure* (V2I). L'enjeu est donc de pouvoir évaluer l'impact macroscopique induit par ces communications microscopiques au niveau des véhicules.

1.4 Problématiques

Grâce à de nouveaux outils, allant des résultats théoriques à de nouvelles technologies de mesures, renforcées par l'utilisation en plein essor des technologies de géo-positonnement et la démocratisation des appareils proposant de l'Internet mobile, il est désormais imaginable d'optimiser l'ensemble du système routier. Jusqu'à maintenant, les variables macroscopiques du trafic routier étaient mesurées uniquement en certains points fixes du réseau, là où les chaussées étaient équipées de systèmes de mesure comme les boucles électromagnétiques. Désormais, la multiplication des systèmes de géolocalisation embarquée permet d'obtenir une quantité considérable de nouvelles données microscopiques, d'une grande richesse. Ces nouvelles données sont essentiellement les trajectoires des véhicules sondes (*probe data* ou *floating car data* en anglais) à partir desquelles il est possible de déterminer les temps de parcours ou les vitesses instantanées mais aussi d'estimer les variables macroscopiques comme la densité ou le flux de véhicules. L'enjeu est donc de mettre à profit ces nouvelles données au sein des modèles d'écoulement macroscopique du trafic. A notre connaissance, il n'existe que peu de travaux réalisés sur la prise en compte de ces informations. Citons néanmoins [58,59], ainsi que [216]. Les approches actuelles requièrent toutefois des hypothèses simplificatrices fortes que nous aimerions relâcher. L'une d'elle suppose que la fonction qui donne le flux selon la densité est linéaire par morceaux. Ces questions nous amènent à étudier les liens entre microscopique et macroscopique au sein des modèles de trafic routier. Nous parlons bien ici de modèles d'écoulement dynamique, en considérant la dichotomie classique réalisée entre les modèles microscopiques pour lesquels les véhicules sont individualisés et les modèles macroscopiques où l'on considère un comportement global des véhicules par une approche hydrodynamique. Nous souhaitons englober dans notre démarche micro-macro un passage du discret au continu pour les modèles dynamiques d'écoulement des véhicules mais aussi un passage d'une structure de réseau discrète à un *continuum* de voies. Le lien entre microscopique et macroscopique dans les modèles d'écoulement sera appréhendé soit par une technique d'homogénéisation (du microscopique vers le macroscopique), soit à l'inverse par des schémas numériques

(du macroscopique vers le microscopique). Le dénominateur commun à ce travail réside dans la manipulation des équations d'Hamilton-Jacobi qui sont des équations aux dérivées partielles (EDP) non linéaires. Ces équations interviennent naturellement dans de nombreux champs de la mécanique. Nous essaierons également d'exploiter le lien entre lois de conservation scalaires qui sont classiquement utilisées en théorie du trafic et les équations d'Hamilton-Jacobi du premier ordre.

2 Aperçu des équations d'Hamilton-Jacobi

Dans cette section, nous nous proposons de donner un aperçu simplifié des équations d'Hamilton-Jacobi et de leur utilisation en théorie du trafic. Cette section n'est pas absolument nécessaire pour la compréhension du reste du manuscrit mais permet au lecteur de se familiariser avec les équations d'Hamilton-Jacobi qui n'ont été appliquées à la théorie du trafic routier que très récemment. Le lecteur souhaitant approfondir certaines des notions évoquées dans ce qui suit, pourra se référer aux livres d'Evans sur les équations aux dérivées partielles [89] mais aussi à Bardi et Capuzzo-Dolcetta [16] et à celui de Barles [19] présentant la classe des solutions faibles pour Hamilton-Jacobi, communément appelées *solutions de viscosité*. Une théorie dite de *viabilité* a été développée en parallèle et englobe les équations d'Hamilton-Jacobi et leurs implications en théorie du contrôle optimal. Le lecteur est renvoyé à [9].

Le lecteur s'intéressant plus particulièrement aux contributions de la thèse pourra se diriger directement à la Section 3.

2.1 Motivation physique des équations d'Hamilton-Jacobi

Les équations d'Hamilton-Jacobi forment une classe d'équations aux dérivées partielles (EDP) fortement non linéaires. Cela signifie que l'évolution de la solution d'une telle équation n'est pas proportionelle à la perturbation qui lui est appliquée. Dans le cas le plus simple, les équations d'Hamilton-Jacobi peuvent s'écrire de la façon suivante

$$u_t + H(D_x u) = 0, \quad \text{dans} \quad (0,+\infty)\times\mathbb{R}^n, \tag{1}$$

où $u : [0,+\infty)\times\mathbb{R}^n \to \mathbb{R}$ est l'inconnue, $D_x u = (u_{x_1},...,u_{x_n}) \in \mathbb{R}^n$ son gradient et $H : \mathbb{R}^n \to \mathbb{R}$ désigne l'Hamiltonien. Il n'existe pas en règle générale de solutions régulières continues pour tout temps. Prenons l'exemple de l'équation Eikonale avec conditions de Dirichlet

$$\begin{cases} |Du| = 1, & \text{sur} \quad \Omega = (-1,1), \\ u = 0, & \text{sur} \quad \partial\Omega. \end{cases} \tag{2}$$

Si l'on cherche des solutions régulières $u \in C^1(\Omega)$, alors le théorème de Rolle nous enseigne qu'il existe un point x_0 tel que

$$Du(x_0) = \frac{u(1)-u(-1)}{2} = 0.$$

Ainsi l'équation Eikonale (2) n'est plus satisfaite au voisinage de x_0.

Une notion de solutions faibles ou solutions *généralisées* a donc été proposée conjointement au début des années 1980 par Crandall, Ishii et Lions [71–73]. Elles sont appelées *solution de viscosité*. Notons qu'une autre classe de solutions faibles a été définie par Barron, Jensen et Frankowska [24, 102] et qu'elles diffèrent des solutions de viscosité dans le sens où les fonctions candidates doivent être semi-continues inférieurement mais doivent satisfaire une certaine égalité lorsqu'on les teste par des fonctions auxiliaires.

Les équations d'Hamilton-Jacobi sont issues d'un formalisme mathématique qui trouve sa motivation dans la résolution des équations de la mécanique hamiltonienne, dites équations de Hamilton. Ces équations peuvent être décrites par le système d'équations différentielles du premier ordre suivant

$$\begin{cases} \dot{\mathbf{x}} = D_p H(\mathbf{p}, \mathbf{x}) \\ \dot{\mathbf{p}} = -D_x H(\mathbf{p}, \mathbf{x}), \end{cases} \tag{3}$$

où H dénote l'Hamiltonien, $\mathbf{x}$ le vecteur position des particules et $\mathbf{p}$ est une quantité d'intérêt pour le système, définissant la quantité de mouvement et remplaçant la vitesse des particules. La formulation hamiltonienne, tout comme la formulation lagrangienne qui lui est connexe, sont des reformulations de la mécanique classique régie par les lois de Newton (voir par exemple [6]). La mécanique hamiltonienne s'appuie sur le principle de moindre action, un principe vérifié par un grand nombre de systèmes physiques. Ce principe a été établi très tôt dans l'Histoire, par différents éminents scientifiques parmi lesquels nous pouvons citer Fermat, Maupertuis, Euler ou encore Lagrange (par ordre chronologique). Le principe de moindre action peut se résumer de la façon suivante : un système physique dynamique en mouvement entre deux points va chercher à minimiser son coût de déplacement entre ces deux points. Il est notable que le principe de moindre action donne naissance au calcul des variations, discipline qui s'intéresse à trouver des méthodes de minimisation de fonctionnelle, ainsi qu'aux méthodes variationnelles. Relevons également que les équations de Hamilton forment un système d'équations différentielles que l'on cherche à résoudre par une équation aux dérivées partielles, l'équation d'Hamilton-Jacobi. Les EDP étant généralement plus difficiles à résoudre que les EDO, cette opération entraîne un surcoût de complexité mais elle permet de déterminer l'ensemble des trajectoires des mobiles du système dynamique considéré.

Le lien existant entre les formulations hamiltonienne et lagrangienne, qui sont deux visions différents du même problème, est assuré par la transformation de Legendre. Cette transformation permet de changer le Lagrangien en Hamiltonien sous de bonnes hypothèses et inversement. En outre, la transformation de Legendre permet de convertir un système lagrangien de n équations différentielles du second ordre en un système hamiltonien remarquablement symétrique de $2n$ équations du premier ordre.

Definition 1 (Transformée de Legendre-Fenchel)**.** *Si le Lagrangien L ne dépend pas de la variable x, si l'application $q \to L(q)$ est convexe (et donc continue) et si de plus nous avons que le Lagrangien est coercif, c'est-à-dire qu'il vérifie*

$$\lim_{|q| \to +\infty} \frac{L(q)}{|q|} = +\infty$$

alors la transformée de Legendre-Fenchel du Lagrangien L dénoté L^* est définie par

$$L^*(p) = \sup_{q \in \mathbb{R}^n} \{p.q - L(q)\}, \quad pour \quad p \in \mathbb{R}^n, \tag{4}$$

où "." dénote le produit scalaire dans $\mathbb{R}^n$. La formule (4) est exactement la définition de l'Hamiltonien H. De façon identique, la transformée de Legendre de l'Hamiltonien H est le Lagrangien L. Ce sont des variables duales convexes.

$$L^* = H \quad et \quad H^* = L.$$

Nous pouvons en déduire que l'Hamiltonien est lui aussi convexe et coercif.

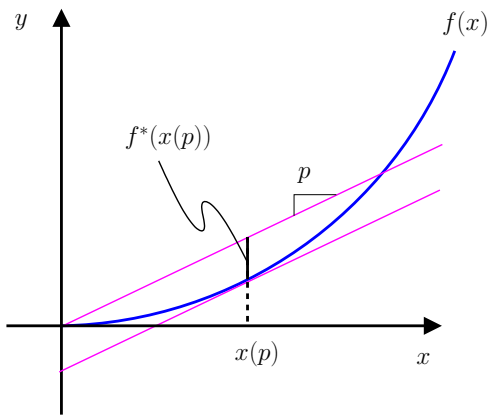

FIGURE 2 – Transformée de Legendre pour une fonction convexe f

La transformée de Legendre-Fenchel pour une fonction convexe est illustrée sur la Figure 2.

Historiquement, la transformation de Legendre, antérieure à la transformation de Fenchel, suppose la différentiabilité de la fonction. Fenchel a étendu cette transformation par la conjuguaison convexe. Lorsque la fonction est à la fois différentiable et convexe, les deux transformations sont donc équivalentes et on parle de transformation de Legendre-Fenchel. D'après le théorème de Fenchel-Moreau, la propriété de dualité $f^{**} = f$ est valable lorsque la fonction f est convexe et semi-continue inférieurement.

2.2 Solutions de viscosité, contrôle optimal et formule de représentation

L'idée pour obtenir des formules explicites, dites *formules de représentation*, des solutions d'équations d'Hamilton-Jacobi est d'écrire l'hamiltonien de l'équation comme l'hamiltonien d'un problème de contrôle optimal. Dans ce cas alors et si l'hamiltonien $H(p)$ est convexe en p (où en généralisant $H(x,u,p)$ convexe en (u,p)), la fonction valeur du problème de contrôle donne une (voire l'unique) solution de l'équation d'Hamilton-Jacobi.

Nous avons défini la conjuguée de Legendre-Fenchel pour une fonction H convexe, continue et coercive par

$$H^*(p) = \sup_{q\in\mathbb{R}^n} \left[p.q - H(q)\right].$$

Sous les hypothèses de convexité, continuité et coercivité on récupère alors que $(H^*)^* = H$. On peut donc réécrire l'équation d'Hamilton-Jacobi (1) comme suit :

$$u_t + \sup_{v\in\mathbb{R}^n} \left[u_x.v - H^*(v)\right] = 0.$$

Il s'agit de la version de Bellman du problème de contrôle en horizon fini. La dynamique étant donnée par $-v$ et le coût instantané par le Lagrangien L, c'est-à-dire la conjuguée de Fenchel de l'Hamiltonien $L = H^*$ (et de même $H = L^*$). La solution du problème de Cauchy

$$\begin{cases} u_t + H(D_x u) = 0, & \text{sur} \quad (0,+\infty)\times\mathbb{R}^n, \\ u(0,x) = u_0(x), & \text{sur} \quad \mathbb{R}^n, \end{cases}$$

est donc donnée par

$$u(t,x) = \inf_{X(.)} \left[\int_0^t H^*(\dot{X}(s))ds + u_0(X(0))\right],$$

où $X(.)$ dénote la trajectoire telle que $X(t) = x$. Il est possible de montrer (voir [19]) que le contrôle constant $v = \dfrac{x - X(0)}{t}$ est optimal. La trajectoire optimale est donc le segment de droite qui relie le point de départ $(0, X(0))$ au point final (t, x). On en déduit la première formule de Lax-Hopf(-Oleinik)

$$u(t,x) = \inf_{y \in \mathbb{R}^n} \left[tH^* \left(\frac{x-y}{t} \right) + u_0(y) \right].$$

Plus généralement, l'équation d'Hamilton-Jacobi avec un hamiltonien dépendant de la variable spatiale mais satisfaisant toujours les hypothèses de continuité (c'est précisément cette hypothèse que l'on ne vérifie pas dans le cas d'une jonction en trafic), de convexité et de coercivité en p uniformément par rapport à x, est toujours associée à un problème de contrôle où la dynamique est $-v$ et le coût instantané est $H^*(x, v)$.

2.3 Une note sur la formule de Lax-Hopf

La formule de Lax-Hopf que nous venons d'ébaucher dans la précédente section trouve de nombreuses applications, notamment en trafic. Nous souhaitons revenir sur la construction de cette formule et sur les hypothèses nécessaires pour que cette formule donne la solution de viscosité au problème d'Hamilton-Jacobi asscoié. Nous nous basons sur l'article de Bardi et Evans [17]. Les papiers de référence sont également [137, 159] ainsi que [207].

Considérons l'équation d'Hamilton-Jacobi du premier ordre suivante

$$u_t + H(D_x u) = 0 \tag{5}$$

avec $u : \mathbb{R}^n \times (0, +\infty) \to \mathbb{R}$ et $H : \mathbb{R}^n \to \mathbb{R}$. On peut vérifier alors que la famille des solutions linéaires suivantes

$$\hat{u}(t,x) = \alpha.x - tH(\alpha) + \beta, \quad \text{pour tout} \quad \alpha \in \mathbb{R}^n,\ \beta \in \mathbb{R}$$

est solution de l'équation (5). L'idée énoncée par Hopf en 1965 est alors de construire une famille plus générale de solutions en prenant une enveloppe de ces solutions élémentaires [137].

Considérons désormais le problème de Cauchy suivant

$$\begin{cases} u_t + H(Du) = 0, & \text{sur} \quad (0, +\infty) \times \mathbb{R}^n, \\ u(.,0) = u_0(.), & \text{sur} \quad \mathbb{R}^n. \end{cases} \tag{6}$$

Il est alors possible de distinguer deux types de formules selon les hypthèses prises sur la régularité de l'Hamiltonien H ainsi que de la donnée initiale u_0.

Theorem 2.1 (Première formule de Hopf ou formule de Lax-Hopf-Oleinik)**.** *Supposons que l'Hamiltonien $H : \mathbb{R}^n \to \mathbb{R}$ est convexe et que la donnée initiale $u_0 : \mathbb{R}^n \to \mathbb{R}$ est uniformément Lipschitz continue. Alors,*

$$u(t,x) := \inf_{z \in \mathbb{R}^n} \sup_{y \in \mathbb{R}^n} \left[u_0(z) + y.(x - z) - tH(y) \right] \tag{7}$$

est l'unique solution de viscosité uniformément continue du problème (6).

On peut remarquer que la première formule de Hopf (7) peut être réécrite comme ceci

$$u(t,x) := \inf_{z \in \mathbb{R}^n} \left[u_0(z) - tH^* \left(\frac{x-z}{t} \right) \right],$$

grâce à la transformée de Legendre-Fenchel de l'Hamiltonien et au fait que la donnée initiale est indépendante de y.

Le second résultat est le suivant :

Theorem 2.2 (Seconde formule de Hopf)**.** *Supposons que l'Hamiltonien $H : \mathbb{R}^n \to \mathbb{R}$ est continu et que la donnée initiale $u_0 : \mathbb{R}^n \to \mathbb{R}$ est uniformément Lipschitz continue et convexe. Alors,*

$$u(t,x) := \sup_{y\in\mathbb{R}^n} \inf_{z\in\mathbb{R}^n} [u_0(z) + y.(x-z) - tH(y)] \tag{8}$$

est l'unique solution de viscosité uniformément continue du problème (6).

L'équation (8) peut être réécrite comme

$$\begin{aligned} u(t,x) &= \sup_{y\in\mathbb{R}^n} \{y.x - tH(y) - u_0^*(y)\} \\ &= [u_0^* + tH]^* (x). \end{aligned}$$

Il est intéressant de noter que dans ce cas-là, la transformation de Legendre-Fenchel s'applique à la donnée initiale u_0 et non plus à l'Hamiltonien.

L'existence et l'unicité de la solution de viscosité pour le problème de Cauchy sont des résultats classiques en théorie de la viscosité. Les preuves démontrant que les formules de Lax-Hopf (7) et (8) sont solutions de viscosité sont détaillées dans [17]. Il existe deux manières de prouver ces résultats. L'une d'elle privilégie une approche EDP en utilisant les inégalités de sous et sur-solutions de viscosité. La seconde consiste à utiliser l'approche de contrôle optimal et l'équation de la programmation dynamique.

2.4 Applications en théorie du trafic routier

La formulation variationnelle sous-jacente aux équations d'Hamilton-Jacobi a été étudiée en théorie du trafic par plusieurs auteurs. Les plus marquants sont G.F. Newell qui a intuité une formule explicite et ses propriétés pratiques [199–201], propriétés qui ont ensuite été proprement démontrées par C.F. Daganzo [78–80]. Le lecteur intéressé pourra également se référer à [57, 158, 186].

Nous nous intéressons à la fonction $N : [0, +\infty) \times \mathbb{R} \to \mathbb{R}$ qui donne le nombre total de véhicules $N(t,x)$ s'étant écoulés au point x entre un temps initial (ici, pris égal à 0) et le temps courant $t \geq 0$. Nous supposons que cette fonction est continue selon ses deux variables, quitte à interpoler la fonction initialement constante par morceaux pour un x fixé. La surface $N(t,x)$ est parfois appelée dans la littérature *surface de Moskowitz*, du nom d'un ingénieur californien qui aurait été un des premiers à utiliser ce graphe [196]. En projetant séparément la surface de Moskowitz sur les trois plans de l'espace $t-x-n$, il est possible de retrouver :

(i) Les trajectoires $\mathcal{X}(t, n_j)$ des véhicules n_j, pour tout $j \in \mathbb{Z}$, en projetant les courbes de niveau sur le plan $t-x$ à indice n_j fixé.

(ii) Les courbes de véhicules cumulés locales $N(t, x_j)$, en projetant les courbes de niveau x_i, pour tout $i \in \mathbb{Z}$, sur le plan $t-n$. Cela permet en outre de calculer les grandeurs intéressantes et caractéristiques du trafic comme :

- le débit au point x_i donné par la pente $Q = \partial_t N$, définissant le nombre de véhicules par unité de temps,

- le nombre de véhicules présents entre deux positions x_i et x_{i+1},
- ou encore le temps de parcours entre deux positions x_i et x_{i+1}.

(iii) La répartition des véhicules $N(t_k, x)$ repérés par leurs numéros, sur le réseau à l'instant t_k, $k \in \mathbb{N}$, en projetant sur le plan $x-n$. On retrouve là également des grandeurs caractéristiques du trafic à savoir :

- la densité des véhicules au temps t_k donnée par l'opposée de la pente, soit $\rho = -\partial_x N$,
- le nombre de véhicules étant passés au-dessus de la position x entre deux temps t_k et t_{k+1},
- ou encore la distance parcourue par un véhicule entre deux temps t_k et t_{k+1}.

Il est alors possible de vérifier simplement que si la densité ρ satisfait à la loi de conservation

$$\rho_t + (Q(\rho))_x = 0,$$

alors la fonction de Moskowitz N qui satisfait

$$N_x(t,x) = -\rho(t,x) \quad \text{et} \quad N_t(t,x) = f(\rho(t,x)),$$

est une solution de l'équation d'Hamilton-Jacobi du premier ordre,

$$N_t + H(N_x) = 0, \quad \text{sur} \quad (0,+\infty) \times \mathbb{R}, \tag{9}$$

où l'Hamiltonien H est défini pour tout $p \in \mathbb{R}$ par

$$H(p) = -Q(-p).$$

Si de plus, nous supposons que l'Hamiltonien H est continu, convexe et coercif, et que nous définissons le Lagrangien L comme la transformée de Legendre de l'Hamiltonien H (voir Figure 3),

$$L(p) = H^*(p) = \sup_{q \in \mathbb{R}} \{pq - H(q)\},$$

alors la première formule de Hopf (et le principe de programmation dynamique de Bellman) nous donne que

$$N(t,x) = \inf_{y \in \mathbb{R}} \left\{ N(s,y) + (t-s) L\left(\frac{x-y}{t-s}\right) \right\}, \quad \text{pour tout} \quad 0 \le s < t, \tag{10}$$

est une solution de viscosité de l'équation (9).

Parmi les candidats, il est connu que les trajectoires qui minimisent la borne inférieure dans (10) sont données par les courbes caractéristiques. Dans notre cas, puisque l'Hamilton ne dépend pas de la position spatiale x, les caractéristiques sont des droites dans le plan $t-x$ (voir Figure 4 (a)).

En outre, si nous supposons que l'Hamiltonien est triangulaire (ou de manière équivalente, supposons que la fonction de débit-densité est triangulaire, voir Figure 4 (b)), alors la solution au point (t,x) est simplement affectée par deux ondes. Il s'agit de l'onde de congestion se déplaçant depuis l'aval vers l'amont, à la vitesse $-w < 0$ et de l'onde cinématique avançant à la vitesse $u > 0$ (voir Figure 4 (b)). En remarquant que

$$u = \frac{x}{t-s} \quad \text{et} \quad -w = \frac{x-y}{t},$$

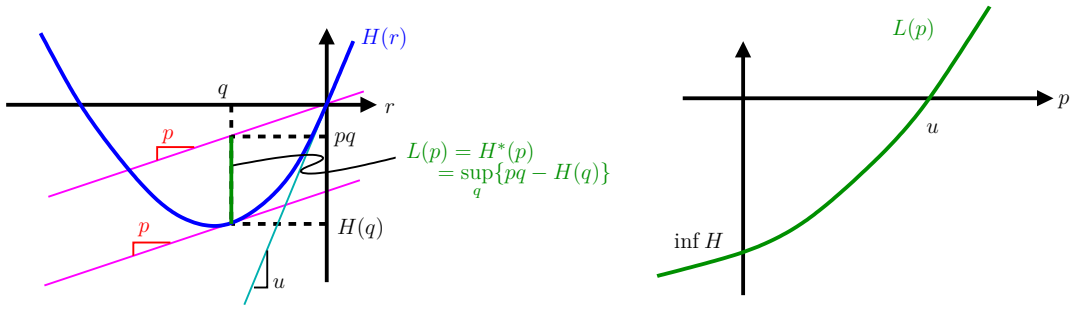

FIGURE 3 – Transformée de Legendre de l'Hamiltonien H

et que nous avons $L(u) = 0$ et $L(-w) = w\rho_{max}$, la formule de Lax-Hopf (7) peut être réécrite comme

$$N(t,x) = \min\left\{N\left(t - \frac{x}{u}, 0\right), N(0,y) + (y-x)\rho_{max}\right\}. \tag{11}$$

Il est intéressant de noter que sous l'hypothèse du diagramme triangulaire, la formule de Lax-Hopf se réduit à prendre le minimum entre deux éléments. Le premier terme apparaissant dans la minimisation (11) correspond à la valeur de N obtenue dans des conditions fluides tandis que la seconde correspond à la valeur pour des conditions congestionnées. Cette simplification illustre l'efficience de la formule de Lax-Hopf appliquée au trafic.

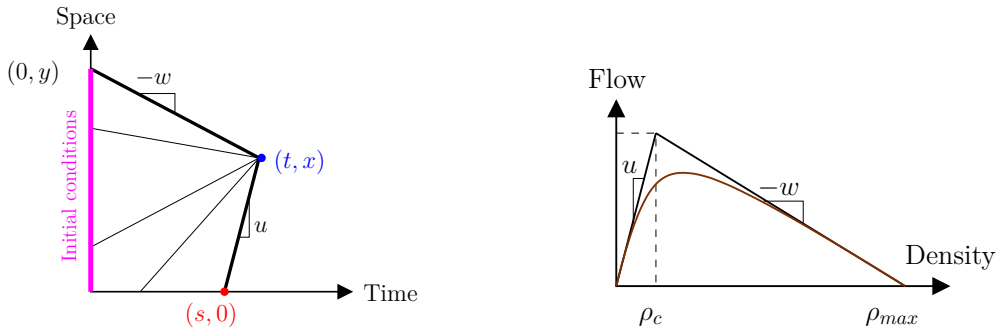

(a) caractéristiques atteignant (t,x) (b) Loi de débit-densité de forme triangulaire

FIGURE 4 – Illustration de l'utilisation de la formule de Lax-Hopf en trafic

3 Positionnement et contributions de la thèse

Cette section s'applique à présenter de façon synthétique les approches qui ont été étudiées dans cette thèse et les résultats qui en ont été obtenus. Nous avertissons le lecteur que les résultats mathématiques ont été volontairement retranscris de façon littérale pour homogénéiser la présentation avec les résultats non mathématiques. Nous essayons de faire ainsi apparaitre les contributions du travail de thèse, en comparaison à ce qui a été entrepris dans la littérature.

3.1 Passage du microscopique au macroscopique par homogénéisation

Comme dans de nombreux domaines de la mécanique classique, il existe plusieurs échelles d'observation du trafic routier. Les échelles sont illustrées sur la Figure 5.

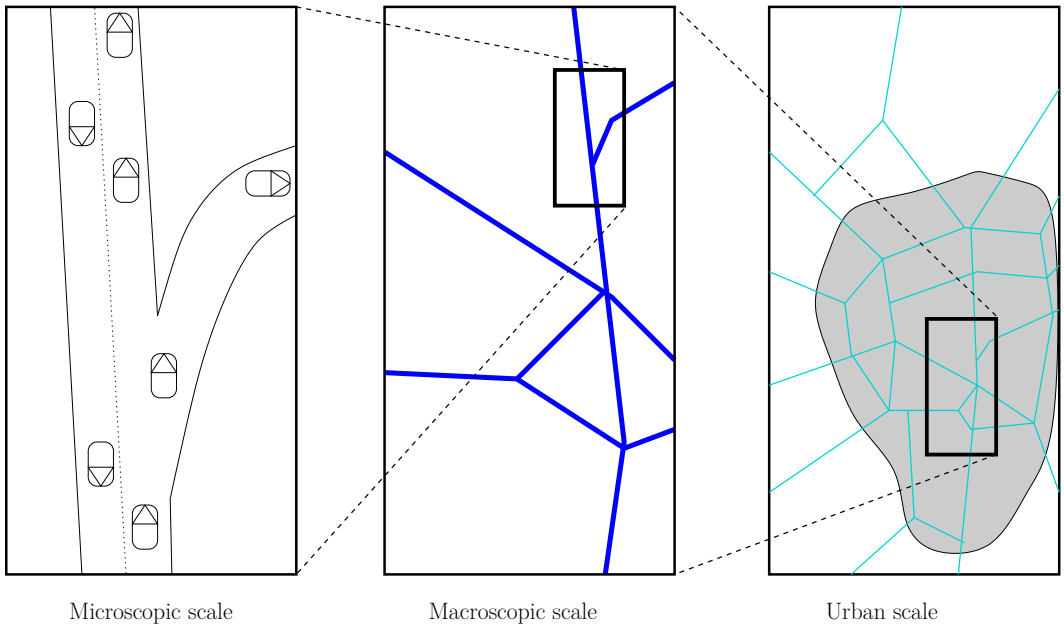

FIGURE 5 – Illustration des échelles caractéristiques en trafic

Littérature. Comme il est décrit dans l'Annexe A ci-après, nous considèrons les modèles d'écoulement du trafic selon la dichotomie réalisée classiquement entre modèles microscopiques et modèles macroscopiques. Tandis que les modèles microscopiques cherchent à reproduire le comportement individuel des usagers, les modèles macroscopiques tendent à caractériser l'écoulement moyen du flux de trafic en agrégeant les données des particules. Il existe une multitude de modèles, tant microscopiques que macroscopiques.

- Au niveau microscopique, la plupart des modèles se composent d'un système infini d'équations aux dérivées ordinaires (EDO) qui régit la trajectoire de chaque véhicule.
- Au niveau macroscopique, la brique élémentaire repose sur une approche hydrodynamique, assimilant le trafic à un fluide. Pour les sections homogènes, les modèles s'appuient donc pour la plupart sur un système d'équations aux dérivées partielles (EDP), et plus précisément de lois de conservation.

La première contribution consiste donc au passage du microscopique au macroscopique pour les modèles de trafic dynamiques, réalisé pour les lois de poursuite sans temps de retard. Les lois de poursuite forment classiquement un système couplé d'ODE qui donnent la trajectoire d'un véhicule en fonction de la trajectoire du véhicule précédent. Considérons $(x_i)_{i\in Z}$ l'ensemble des trajectoires des véhicules $i \in \mathbb{Z}$ dont les évolutions sont données par le modèle suivant

$$\dot{x}_i(s) = F\left(x_{i+1}(s) - x_i(s)\right), \quad \text{pour tout} \quad i \in \mathbb{Z}, \quad s \in [0, +\infty) \tag{12}$$

où $F : \mathbb{R} \to \mathbb{R}$ décrit la relation entre l'interdistance et la vitesse du véhicule. Nous supposons que les véhicules se déplacent sur une route uni-dimensionnelle et ne peuvent pas se dépasser. Nous introduisons un facteur d'échelle $\varepsilon > 0$ ainsi que la position échelonnée X^ε définie telle que

$$x_i(s) =: \frac{1}{\varepsilon} X^\varepsilon(\varepsilon s, i\varepsilon), \quad \text{pour} \quad i \in \mathbb{Z}, \quad s \in [0, +\infty), \tag{13}$$

Contribution (R. Monneau). *Nous montrons alors que la position re-échelonnée X^ε s'homogénéise vers la solution de viscosité X^0 de l'équation d'Hamilton-Jacobi*

$$X_t^0(t,y) = F(X_y^0(t,y)), \quad \textit{pour} \quad y \in \mathbb{R}, \quad t \in [0,+\infty), \tag{14}$$

lorsque le facteur d'échelle ε tend vers zéro.
Cela correspond à effectuer un dé-zoom c'est-à-dire de considérer l'écoulement des véhicules de plus en plus haut, jusqu'à ne plus distinguer qu'un milieu continu. Il est alors classique de montrer que la solution de viscosité X^0 à l'équation d'Hamilton-Jacobi (14) est une primitive de la solution faible entropique ρ de la loi de conservation scalaire

$$\rho_t + (F(\rho))_x = 0, \quad \text{pour} \quad y \in \mathbb{R}, \quad t \in [0,+\infty). \tag{15}$$

Cette équation détermine le modèle d'écoulement macroscopique dit *modèle LWR* (pour Lighthill, Whitham et Richards [184,221]). Ce modèle est détaillé par la suite, voir également l'Annexe A.

Contribution (R. Monneau). *Outre la convergence de la solution re-échelonnée vers la solution de viscosité du problème continu, nous avons également obtenu une estimation de l'erreur entre ces deux solutions.*
Plus précisément, nous démontrons qu'il existe une constante $C_T > 0$, dépendant uniquement du temps final T considéré, telle que

$$|X^\varepsilon(t,y) - X^0(t,y)| \leq C_T\sqrt{\varepsilon}, \quad \text{pour} \quad y \in \mathbb{R}, \quad t \in [0,T).$$

Cette estimation d'erreur permet de quantifier la perte d'informations lorsque l'on considère le modèle macroscopique en lieu et place du modèle microscopique. En effet, au niveau du flux, les variables sont déduites par une "moyennisation" des informations individuelles des véhicules, intrinsèquement plus riches.

Littérature. Cette technique d'homogénéisation est relativement classique pour l'étude des problèmes de compatibilité entre les différentes formes de représentation d'un phénomène physique à différentes échelles. Par exemple, elle a été utilisée précédemment pour les modèles de dislocation dans les cristaux [99]. La plupart des phénomènes observés dans la nature sont caractérisés par plusieurs échelles spatiales ou temporelles. En physique, la plupart des quantités intéressantes, accessibles à l'expérience et nécessaires pour les applications sont macroscopiques : volume, pression, densité. Afin de les calculer à partir des quantités microscopiques, il est nécessaire de les lier à des moyennes statistiques faisant intervenir des concepts et méthodes probabilistes. Il apparaît que sous certaines conditions au niveau microscopique, le niveau macroscopique peut être décrit, avec une bonne approximation, par des équations bien plus simples où les particularités microscopiques agissent au travers de leurs caractéristiques moyennées. De nombreuses théories mathématiques et physiques ont été développées sur la base de cette observation dont la théorie de l'homogénéisation. La théorie de l'homogénéisation ne donne qu'une image asymptotique en ce sens qu'elle donne un résultat exact seulement lorsque le ratio entre les différentes échelles tend vers zéro. Dans ce travail, nous nous sommes limités au cas de l'homogénéisation déterministe, c'est-à-dire que toutes les variables considérés suivent un comportement connu, non sujet à l'aléa.

Un travail préliminaire a également été mené pour les modèles du premier ordre incorporant un temps de retard non nul, comme par exemple l'équation suivante

$$\dot{x}_i(s) = F\left(x_{i+1}(s-\tau) - x_i(s-\tau)\right), \quad \text{pour tout} \quad i \in \mathbb{Z}, \quad s \in [0,+\infty). \tag{16}$$

Dans ce cas, le conducteur réagit aux *stimulii*, c'est-à-dire aux variations dans le comportement de conduite de son véhicule leader, avec un temps de retard $\tau \neq 0$ qui englobe le temps de réaction du conducteur ainsi que le temps d'action mécanique. Ce premier travail avec temps de retard a eu pour résultat d'établir une valeur limite pour le temps de retard $\tau \leq \frac{1}{e}$ avec l'hypothèse que $0 \leq F \leq 1$ et $0 \leq F' \leq 1$. Au-delà de cette valeur, nous ne pouvons pas garantir l'homogénéisation des modèles microscopiques. Cette borne supérieure justifie l'approximation du temps de retard négligeable.

Contribution (R. Monneau). *La seconde contribution est donc la preuve de l'existence d'un principe de comparaison pour des temps de retard suffisamment petits et des données initiales bien "conditionnées". Ce principe de comparaison assure la convergence de la solution rééchelonnée vers la solution continue du problème macroscopique.*
Le conditionnement des données initiales traduit le fait qu'en trafic, les véhicules ne doivent pas être générés avec des interdistances trop faibles, en comparaison au produit du temps de réaction et de la vitesse initiale des véhicules. En effet, ce produit donne la distance parcourue par le véhicule avant que le conducteur n'ait pu prendre en considération les informations utiles pour modifier sa vitesse. Ce principe de comparaison permet d'obtenir l'homogénéisation du système couplé d'ODEs vers l'équation d'Hamilton-Jacobi, de façon identique à la démarche précédente.

Littérature. Notons que la borne établie sur la valeur du temps de retard se retrouve dans plusieurs travaux d'étude de la stabilité linéaire d'un peloton de véhicules (voir par exemple [227] et [208,210]). Dans la litérature, apparaissent deux valeurs de seuil, que nous noterons τ_1 et τ_2 avec $0 < \tau_1 < \tau_2$. En deçà du premier seuil τ_1 (qui ne dépend que du choix de normalisation de la fonction de vitesse F), il apparait que l'homogénéisation est possible alors qu'au-delà du second seuil τ_2, il est acquis qu'il n'y a pas d'homogénéisation possible et même que le modèle microscopique produit des collisions entre les véhicules. L'impact macroscopique du temps de réaction a été étudié notamment dans [205].

3.2 Premiers pas vers l'évaluation des systèmes coopératifs

Littérature. Nos premiers résultats d'homogénéisation des modèles de poursuite laissent à penser que les modèles multi-anticipatifs du type

$$\dot{x}_i(t+\tau) = F\left((x_{i+j}(t) - x_i(t))_{j=1,\dots,n}, \dot{x}_i(t), (\dot{x}_{i+j}(t))_{j=1,\dots,n}\right), \quad \text{pour tout} \quad i \in \mathbb{Z}, \quad n \in \mathbb{Z}, \quad t > 0,$$

peuvent également être étudiés de façon similaire. Les modèles multi-anticipatifs sont majoritairement des extensions de modèles de poursuite existants mais ils permettent de considérer plus d'un véhicule leader dans le comportement de conduite. Cette caractéristique est très intéressante lorsque l'on souhaite comprendre l'impact macroscopique des Systèmes de Transports Intelligents et plus particulièrement les systèmes coopératifs comme présentés dans la Section 1.3.

Quelques travaux ont déjà proposé une approche sur les systèmes coopératifs (voir par exemple [144, 194, 224, 226] sans exhaustivité) mais peu mettent en avant l'impact de ces technologies en faisant l'analogie avec des modèles multi-anticipatifs.

Contribution. *Initialement guidés par la volonté de comparer les comportements multi-anticipatifs sur les jeux de données réelles, nous avons proposé un modèle macroscopique de trafic de second ordre, appartenant à la famille GSOM, qui rend compte macroscopiquement des comportements multi-voies et multi-anticipatifs.*

Les modèles de la famille des GSOM (pour *Generic Second Order Traffic Models family*) sont des modèles étendant les notions présentées par le modèle LWR qui permet de rendre compte de plusieurs éléments significatifs en dynamique du trafic comme la capacité, le stockage, le diagramme fondamental ou les phases de trafic. La famille GSOM englobe de nombreux modèles de la littérature comme les modèles de Aw et Rascle [11] et celui de Zhang [240,241], les modèles multi-classes de Bagnerini et Rascle [12] ou Jin et Zhang [143], le modèle à transition de phase déduit du modèle à deux phases de Colombo [61] ou encore le modèle multivoies de Greenberg, Klar et Rascle [150]. Les modèles GSOM présentés pour la première fois dans Lebacque, Mammar, Haj-Salem [174] s'écrivent de la manière suivante :

$$\begin{cases} \partial_t \rho + \partial_x(\rho v) = 0, \\ \partial_t(\rho I) + \partial_x(\rho v I) = \rho\varphi(I), \\ v = \mathfrak{I}(\rho, I) \end{cases} \tag{17}$$

avec ρ qui définit la densité, v la vitesse, x la position et t le temps. La première équation permet de traduire la conservation des véhicules tandis que la seconde équation permet de décrire la dynamique de l'attribut comportemental I, dépendant du conducteur. Cet attribut peut correspondre au type du véhicule, à la propension à un comportement plus ou moins agressif, à la destination, aux flux d'informations depuis et vers le véhicule, etc. La dernière équation du système (17) reproduit la loi phénoménologique dite Diagramme Fondamental en vitesse-interdistance, qui dépend de l'attribut du conducteur.

Le modèle que nous avons proposé, permet de prendre en compte un comportement multi-anticipatif ainsi que multi-voies. L'attribut advecté avec le trafic est alors la composition du trafic, c'est-à-dire la proportion de véhicules considérant chacun p véhicules leaders. Une des particularités du modèle est sa simplification lorsqu'il est projeté dans les variables lagrangiennes. Cela simplifie notablement l'étude des ondes dues aux discontinuités de contact, pour différents attributs I.

Le caractère multi-anticipatif des véhicules permet de relever le seuil du temps de retard critique en-deça duquel il est possible d'homogénéiser le modèle. Ce modèle peut avoir une utilité directe dans l'identification et l'estimation des impacts macroscopiques des communications au niveau microscopique.

3.3 Modélisation et simulation du trafic sur jonction

Littérature. Il existe dans la littérature "transport" un grand nombre de modèles de jonctions qui sont essentiellement utilisés pour l'ingénierie du trafic. Le lecteur est renvoyé aux travaux de R. Corthout [64] et aux articles connexes de Tampère, Flöterröd et Rhode [65, 225]. Les travaux de Khoshyaran et Lebacque [147–149] ou encore [167, 173] ont également permis des avancées significatives dans la modélisation des jonctions en trafic. Les modèles de jonction forment une brique essentielle des modèles de chargement dynamique d'un réseau, au sein même des modèles d'affectation dynamique du trafic [7]. En effet, nous rappelons que c'est principalement en aux points de jonction du réseau que se forment les congestions.

D'un point de vue mathématique, l'étude de systèmes dynamiques sur des réseaux (et de leur contrôle) a attiré l'attention des mathématiciens tout particulièrement lors de la dernière décennie, en lien avec des applications très diverses dont le trafic routier, mais aussi pour l'étude de fluides sur d'autres types de réseaux comme les réseaux de gaz, les réseaux de télécommunications, les vaisseaux sanguins ou encore les réseaux en économie. Le lecteur pourra s'appuyer sur l'ouvrage-référence de Garavello et Piccoli [106] mais aussi sur le papier de Bressan *et alii* [37] faisant un tour des différentes applications de la théorie des systèmes hyperboliques sur réseaux.

Afin d'outrepasser un certain nombre de limitations théoriques rencontrées par les mathématiciens pour la modélisation du trafic routier sur des réseaux par le biais de l'approche hyperbolique, dont notamment la difficulté de trouver une caractérisation différentielle de la solution au problème dans le cas de jonctions avec plus de deux voies entrantes, il a été proposé dans la littérature d'intégrer le problème et de le considérer dans le cadre des équations d'Hamilton-Jacobi.

Il y a de nombreux papiers dans la littérature traitant des équations d'Hamilton-Jacobi avec des Hamiltoniens discontinus en espace et/ou sur des réseaux. Le lecteur intéressé pourra se référer à [114] et à [140] pour une revue très large de la littérature. Globalement, la difficulté réside en la définition d'une notion de solution de viscosité au point de discontinuité des Hamiltoniens. Le problème au noeud réside dans la définition des fonctions test à droite et à gauche du point de jonction, sachant l'irrégularité différentielle en ce point. En dehors de ce point, les auteurs utilisent la notion classique des solutions de viscosité, à la Crandall, Evans et Lions. Différentes approches pour traiter la discontinuité ont été effectuées jusqu'à présent. Les notions de solutions proposées sont généralement associées à une motivation particulière, ce qui rend les notions a priori étrangères les unes aux autres.

Notons par exemple que l'article d'Achdou, Camilli, Cutrì et Tchou [2], s'intéresse à un problème de contrôle d'un réseau et à l'équation de Bellman qui en découle. Pour définir la solution à la discontinuité, les auteurs utilisent la distance géodésique qui leur donne une fonction-test admissible. Il a été démontré par Camilli et Marchi [49] que cette notion de solution de viscosité est équivalente à la définition indépendante introduite par Imbert, Monneau et Zidani [141].

Il est également possible de démontrer que dans le cas d'un réseau en une seule dimension d'espace, les solutions construites dans [114] pour ces équations d'Hamilton-Jacobi avec des Hamiltoniens discontinus tombent dans la famille des solutions construites dans le papier d'Imbert et Monneau [140].

Les premiers résultats d'Achdou et al. [2] et d'Imbert et al. [141] ont été complétés par des travaux plus récents et plus généraux [3]. Le récent papier d'Imbert et Monneau [140] contient notamment les résultats d'unicité et de comparaison les plus généraux (hypothèses relaxées sur les Hamiltoniens par exemple, avec condition de bi-monotonie), avec des démonstrations essentiellement basées sur une approche EDP, au contraire des preuves de type "contrôle optimal" développées dans [2, 3, 20].

Nous nous sommes intéressés au modèle s'appuyant sur les équations d'Hamilton-Jacobi proposé dans [141] et qui s'écrit comme suit

$$\begin{cases} u_t^\alpha + H_\alpha(u_x^\alpha) = 0 & \text{sur} \quad (0,T)\times(0,+\infty), \quad \text{pour} \quad \alpha = 1,\dots,N, \\ u^\beta =: u, \quad \text{pour tout} \quad \beta = 1,\dots,N & \\ u_t + \max\limits_{\beta=1,\dots,N} H_\beta^-(u_x^\beta) = 0 & \text{sur} \quad (0,T)\times\{0\}, \end{cases} \tag{18}$$

avec H_α l'Hamiltonien défini sur la branche α, $\alpha \in \{1,...,N\}$, et H_α^- la partie décroissante de l'Hamiltonien soit

$$H_\alpha^-(p) = \inf_{q\le p} H_\alpha(q), \quad \text{pour tout} \quad \alpha = 1,...,N.$$

Dans [141], il est démontré que si l'Hamiltonien H est strictement convexe (et sous d'autres conditions, voir notamment le Théorème 1.1), alors la solution de viscosité du

problème (18) existe et est unique. En revanche, du fait des méthodes de preuve bâties sur le contrôle optimal, si l'on suppose que H est uniquement Lipschitz continu, ce qui a du sens dans notre application trafic, alors l'unicité n'est plus garantie *a priori*.

Bien que le modèle Hamilton-Jacobi de la jonction sur lequel nous nous sommes appuyés [141], fasse appel à la formulation contrôle optimal des équations et qu'il exhibe une formule de représentation à la Hopf-Lax, la solution ne peut pas être calculée simplement. Il est nécessaire d'utiliser un schéma numérique. Il existe de nombreux exemples de schémas numériques pour les équations d'Hamilton-Jacobi avec des Hamiltoniens continus, comme par exemple

- les schémas semi-Lagrangiens (voir [82, 83, 90, 91] ou également [21, 22, 156]) qui utilisent l'expression de type contrôle optimal des équations ainsi que le principe de programmation dynamique de Bellman. La technique est de coupler une méthode d'intégration pour des ODEs et une méthode d'interpolation. Ces schémas ne nécessitent pas l'introduction d'une condition de type Courant-Friedrichs-Lewy (CFL) [70].

- les méthodes aux différences finies. Ces schémas ont été les premiers exemples historiquement utilisés, notamment par Crandall and Lions [74]. Il est également possible d'enrichir les modèles basiques pour corriger certains imperfections des schémas monotones. Cela a donné naissance aux méthodes Essentially Non Oscillatory (ENO) et Weighted Essentially Non Oscillatory (WENO) (voir par exemple [91, 212]). Des méthodes éléments finis ont aussi été étudiées dans [138, 243].

Il existe d'autres méthodes comme les méthodes anti-diffusives, les méthodes Fast-Marching ou Level-Sets [211, 223, 231] ou encore les méthodes Galerkin discontinues [30, 54]. Le lecteur intéressé pourra également se référer à [21–23, 154, 155].

En revanche il n'existe que peu de travaux sur la résolution numérique des équations d'Hamilton-Jacobi présentant une discontinuité en espace, comme c'est le cas auquel nous sommes confrontés au niveau de la jonction. Parmi les quelques papiers existants, citons le travail de Camilli, Festa et Schieborn [48] qui s'intéresse à l'équation eikonale sur un espace métrique et propose un schéma semi-Lagrangien. Cela est permis en outre car l'équation eikonale choisie a la particularité d'avoir le même minimum quelle que soit la branche, ce qui n'est pas nécessairement le cas dans notre travail.

Contribution. *La cinquième contribution de cette thèse est le développement d'un schéma numérique aux différences finies dont la solution converge vers une (voire la) solution à l'équation d'Hamilton-Jacobi (18) que l'on considère posée sur une jonction (dans un réseau).*
Nous avons fait le choix d'un schéma aux différences finies. Notre schéma a été testé grâce à des simulations numériques pour différentes configurations de jonctions (convergent, divergent, plusieurs voies entrantes et sortantes), en prenant en compte différents cas d'études (exprimés en pratique sous forme de problèmes de Riemann pour les densités de véhicules).

Nous introduisons des pas discrets en temps et en espace $(\Delta t, \Delta x)$ qui doivent satisfaire une condition de stabilité, à savoir la condition CFL. Nous considérons $(U_i^{\alpha,n})_{\alpha,i,n}$ la solution du schéma numérique suivant qui discrétise le modèle continu (18) pour des temps

discrets $n\Delta t$ avec $n \geq 0$:

$$\begin{cases} \dfrac{U_i^{\alpha,n+1} - U_i^{\alpha,n}}{\Delta t} + \max\left\{H_\alpha^+(p_{i,-}^{\alpha,n}), H_\alpha^-(p_{i,+}^{\alpha,n})\right\} = 0, & \text{pour} \quad i \geq 1, \quad \alpha = 1, \ldots, N, \\ U_0^{\beta,n} =: U_0^n, \quad \text{pour tout} \quad \beta = 1, \ldots, N \\ \dfrac{U_0^{n+1} - U_0^n}{\Delta t} + \max\limits_{\beta=1,\ldots,N} H_\beta^-(p_{0,+}^{\beta,n}) = 0 \end{cases} \Bigg| \quad \text{pour} \quad i = 0, \tag{19}$$

où nous avons défini les gradients discrets en espace prograde et rétrograde (respectivement *forward* et *backward* en anglais)

$$p_{i,+}^{\alpha,n} := \frac{U_{i+1}^{\alpha,n} - U_i^{\alpha,n}}{\Delta x} \quad \text{et} \quad p_{i,-}^{\alpha,n} := \frac{U_i^{\alpha,n} - U_{i-1}^{\alpha,n}}{\Delta x},$$

et de la même façon, les gradients discrets en temps

$$W_i^{\alpha,n} := \frac{U_i^{\alpha,n+1} - U_i^{\alpha,n}}{\Delta t}.$$

Nous prouvons alors la convergence de la solution numérique vers la solution de viscosité du problème continu (18) à sous-suite convergente près, lorsque $\varepsilon := (\Delta t, \Delta x)$ tend vers zéro. Nous retrouvons la convergence complète vers l'unique solution lorsque l'Hamiltonien est strictement convexe. Suivant [140], il est possible d'espérer que le schéma numérique converge vers l'unique solution de viscosité de (18) sous des hypothèses plus faibles sur les Hamiltoniens mais cela n'a pas été proprement établi dans le présent travail.

Contribution. *Une interprétation "trafic" du schéma numérique pour les équations d'Hamilton-Jacobi sur une jonction a été développée, avec notamment un schéma dérivé pour les densités satisfaisant au modèle LWR [184, 221] posé sur une jonction.*
Le point délicat est le traitement de la condition de raccord à la jonction. Nous proposons ainsi un tour d'horizon des différentes formes de conditions à la jonction, basées presque toujours sur des problèmes d'optimisation sous contraintes. Ce tour d'horizon s'attache à décrire l'interprétation du schéma dérivé pour les densités et donne de nouveaux exemples numériques. Il s'attache également à lister les possibles points d'amélioration du schéma numérique dans une visée pratique en trafic. Parmi les perspectives, nous soulevons notamment la nécessité de prendre en compte un limiteur de flux pouvant traduire la sous-optimalité du flux passant à la jonction. Cela permettrait de rendre compte également du phénomène de chute de capacité observé en trafic. Notons à ce propos que la théorie a été étendue au cas de fonctions à la jonction avec limiteur de flux dans [139, 140].

Contribution. *Nous avons étudié numériquement les cas d'homogénéisation sur plusieurs types de réseaux, sous l'hypothèse de périodicité du motif du réseau. Cela a permis d'intuiter un certain nombre de résultats théoriques comme l'expression du flux homogénéisé sur le réseau considéré.*
La condition de périodicité du réseau est essentielle pour l'homogénéisation comme indiqué dans [140]. Nous avons également abordé un problème d'optimisation des coefficients de partage des flux à la jonction afin de maximiser l'écoulement du trafic, sous une donnée initiale et des données aux bords. L'Hamiltonien homogénéisé se rapproche du concept de Diagramme Fondamental macroscopique (ou *Macroscopic Fundamental Diagram* en anglais) très en vogue en trafic depuis les travaux de N. Geroliminis et C.F. Daganzo [81, 110].

Nous nous sommes également intéressé au cas de l'homogénéisation numérique d'un réseau constitué d'une route unidimensionnelle avec deux feux de trafic. Nous caractérisons le limiteur de flux selon la distance séparant les deux feux et le déphasage entre les phases de feux.

3.4 Modèles GSOM de trafic et formule de représentation à la Lax-Hopf

Littérature. Comme nous l'avons présenté en Section 2, il existe des formules dites de représentation permettant le calcul des solutions aux équations d'Hamilton-Jacobi. Ce type de formule découle notamment de la formulation variationnelle du problème. Cette approche a été utilisée en modélisation du trafic par C. Daganzo [78,79] puis a été reprise par A. Bayen et son équipe à UC Berkeley afin de permettre l'assimilation de données lagrangiennes dans le modèle macroscopique d'écoulement [58,59]. Cependant l'utilisation de la première formule de Hopf (7), permettant un calcul explicite de la solution, n'est plus pertinente lorsque l'Hamiltonien (ou de façon équivalentale, le Diagramme Fondamental) dépend de la variable spatiale x. Cela brise en effet certaines propriétés de la solution comme l'invariance par translation en espace par exemple, les caractéristiques n'étant plus nécessairement des droites.

Il seraitt intéressant de développer une formule analytique ou semi-analytique, relativement peu coûteuse en temps de calcul, pour les équations d'Hamilton-Jacobi sur une jonction. Ce travail n'a pas été éffectué dans la littérature, bien que certains auteurs se soient intéressés à des équations d'Hamilton-Jacobi avec termes sources [182]. Les termes sources permettent de prendre en compte les discontinuités spatiales comme les entrées et les sorties (vues comme des sources et des "puits" de trafic) sur un réseau. Pour notre part, nous nous sommes intéressés à un problème connexe qui est de se donner une méthodologie de calcul des solutions à une équation d'Hamilton-Jacobi lorsque l'Hamiltonien dépend d'une variable exogène.

Contribution. *Nous avons développé une méthode numérique basée sur la formule de représentation "à la Lax-Hopf" pour déterminer la solution du problème variationnel associé aux modèles d'écoulement de second ordre dit GSOM (Generic Second Order Modeling).* Nous travaillons pour une section homogène, c'est-à-dire sans sources de trafic. L'Hamiltonien est donc indépendant de la variable spatiale. Nous reprenons les pistes évoquées dans le papier de Lebacque et Khoshyaran [172], à savoir la formulation variationnelle des modèles GSOM dans le cadre Lagrangien. Notons que la formulation variationnelle n'est autre que la formulation de type contrôle optimal des équations d'Hamilton-Jacobi. Cela permet de découpler l'équation d'évolution de la densité et celle de l'attribut des véhicules I (voir équation (17)). Le problème se simplifie donc et permet d'utiliser les grands principes de l'approche Lax-Hopf formulée par Claudel et Bayen [58,59] pour le modèle LWR, modèle macroscopique de type premier ordre. Les deux éléments clés de la méthode de résolution sont donc :

- la simplification du problème global comprenant des conditions initiales, des conditions internes et des conditions limites, en un ensemble fini de sous-problèmes plus simples. La solution globale est alors donnée par le minimum de toutes les solutions partielles qui résolvent chacun des sous-problèmes (propriété d'inf-morphisme) ;
- les solutions partielles sont calculées grâce à la formule de représentation "à la Lax-Hopf", le long des trajectoires optimales qui sont données par les caractéristiques.

Contribution. *En complément du travail mentionné ci-dessus, un schéma numérique aux différences finies est également proposé pour résoudre les modèles GSOM, réécrits*

dans leurs coordonnées lagrangiennes, sur une jonction.
Ce travail fait l'objet de recherches en cours. Les résultats numériques de cette approche "différences finies" pourraient notamment être comparés aux résultats numériques obtenus avec la formule de Lax-Hopf (qui n'est pour l'instant pas adaptée pour le problème à la jonction), en termes de temps de calcul et d'erreur numérique.

4 Organisation de la thèse

Cette thèse se compose de sept chapitres organisés en trois parties. Certains chapitres de ce manuscrit sont issus d'articles en cours de rédaction, soumis ou publiés. Ils correspondent donc à l'origine à des travaux indépendants les uns des autres, écrits en langue anglaise. L'auteur s'excuse des quelques répétitions et changements de notation qui en résultent.

4.1 Première partie

La première partie se consacre aux modèles d'écoulement sur section homogène.

Le **premier chapitre** porte sur le passage du microscopique au macroscopique dans les modèles d'écoulement sur section homogène, c'est-à-dire sans jonction. Le lien micro-macro est effecté par passage à la limite et est appelé dans la littérature *homogénéisation* des équations d'Hamilton-Jacobi. Nous étudions également ce même type de passage à la limite avec un modèle microscopique prenant en compte un temps de retard non nul.

Le **deuxième chapitre** s'articule autour d'un modèle macroscopique prenant en considération le caractère multi-anticipatif des conducteurs au niveau microscopique. Il utilise les résultats d'homogénéisation du deuxième chapitre. Nous en proposons également une déclinaison capable de modéliser une section multi-voies.

4.2 Deuxième partie

La deuxième partie du travail est axée autour de la modélisation des jonctions, lieux de difficulté pour l'écoulement du trafic sur un réseau.

Le **troisième chapitre** s'intéresse à un état de l'art approfondi des modèles de jonction en trafic. Il propose également une déclinaison "trafic" du schéma numérique qui est étudié dans le chapitre suivant. Enfin, quelques simulations numériques sont proposées et des pistes d'amélioration sont discutées.

Le **quatrième chapitre** introduit le schéma numérique utilisé pour la résolution d'un modèle de jonction, bâti sur les équations d'Hamilton-Jacobi. Les propriétés mathématiques du schéma et de la solution numérique sont ainsi détaillées. Un exemple numérique permet d'illustrer le comportement du schéma dans un cas simple.

Le **cinquième chapitre** porte sur l'homogénéisation numérique de l'écoulement du trafic sur un réseau périodique. Nous utilisons le schéma numérique précédemment défini dans le cinquième chapitre, pour étudier le problème d'homogénéisation des flux sur un réseau périodique. La périodicité nous permet en outre de nous intéresser particulièrement au problème dans une cellule. Nous étudions numériquement des cas qui ne sont pas (encore) couverts par la théorie.

4.3 Troisième partie

La troisième partie s'articule autour des formules de représentation, dites *formules de Lax-Hopf* pour les équations d'Hamilton-Jacobi.

Le **sixième chapitre** s'intéresse à une résolution numérique des modèles macroscopiques de la famille GSOM, par une méthode qui utilise la formulation variationnelle des modèles et les formules de Lax-Hopf.

Le **septième chapitre** se veut complémentaire du chapitre précédent tout en considérant le cas des jonctions. Il est effectivement axé sur une méthodologie de résolution numérique des modèles de la famille GSOM, réécrits dans les coordonnées Lagrangiennes, et posés sur une jonction avec état interne. Il est donc nécessaire de considérer la jonction (fixe dans le repère eulérien) comme une condition limite particulière dans le repère lagrangien.

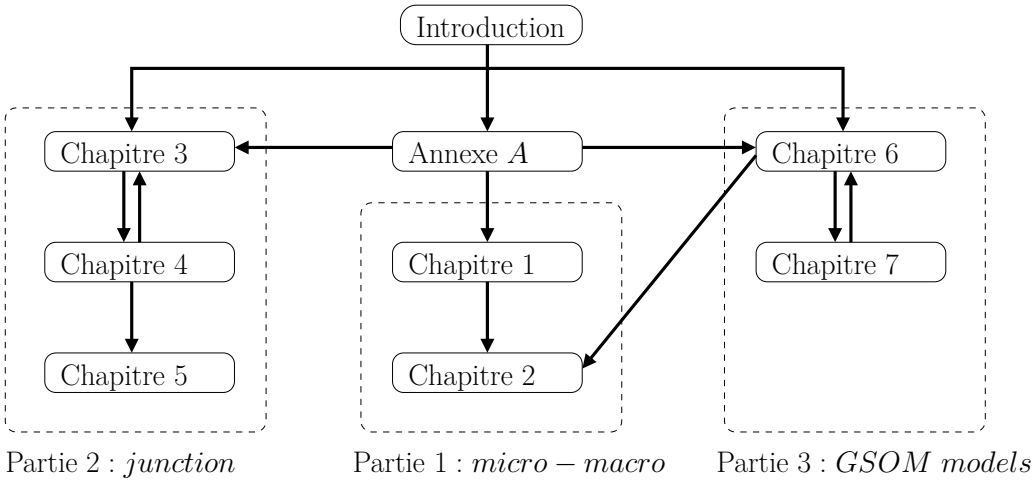

FIGURE 6 – Organisation structurelle du manuscrit de thèse et liens entre chapitres : l'**Annexe A** fait le tour des modèles utilisés en trafic pour les sections homogènes ; le **Chapitre 1** traite du passage micro-macro ; le **Chapitre 2** propose un modèle macroscopique prenant en compte le comportement multi-anticipatif microscopique ; le **Chapitre 3** donne une interprétation trafic des modèles Hamilton-Jacobi (discret et continu) posé sur une jonction ; le **Chapitre 4** décrit le schéma numérique utilisé pour résoudre les équations HJ sur jonction et présente ses propriétés ; le **Chapitre 5** est une étude numérique de l'homogénéisation sur des réseaux ; le **Chapitre 6** détaille une méthodologie de résolution des modèles GSOM se basant sur la formule de Lax-Hopf ; le **Chapitre 7** traite numériquement les modèles GSOM sur jonction.

L'**annexe** A est une introduction à la modélisation et à la simulation du trafic, au niveau microscopique et macroscopique, sur section. Le but est de préciser le cadre de l'étude et de décrire les outils mathématiques existants. L'accent est mis sur les limites de chaque modèle et de chaque approche afin de montrer qu'il est nécessaire de bien connaitre les domaines d'utilisation de chacun d'eux.

Avertissements au lecteur

Hormis l'annexe A, écrite en langue française, tous les autres chapitres composant cette thèse sont rédigés en langue anglaise.

Les chapitres 1, 5 et 7 sont des versions préliminaires de travaux qui sont actuellement considérés par l'auteur et ses co-auteurs. Les résultats énoncés et les preuves afférentes sont présentés de façon formelle dans la présente version du manuscrit. Les travaux actuels cherchent à les rendre rigoureux.

5 Publications

Revue à comité de lecture

Costeseque, G., Lebacque, J.P., Monneau, R., (2013). A convergent scheme for Hamilton-Jacobi equations on a junction : application to traffic, *Num. Math.* (accepted).

Costeseque, G., Lebacque, J.P., (2014). A variational formulation for higher order macroscopic traffic flow models : numerical investigation, *Transp. Res. B* (accepted).

Ouvrage collectif

Costeseque, G., (2013). Modélisation et simulation dans le contexte du trafic routier, In F. Varenne et M. Silberstein Eds, *Modéliser & simuler. Epistémologies et pratiques de la modélisation et de la simulation*, Editions Matériologiques.

Actes de congrès à comité de sélection ou lecture

Costeseque, G., Lebacque, J.P., (2012). Intersection modeling using a convergent scheme based on Hamilton-Jacobi equation, Proceedings of 15th EWGT, *Social & Behavioral Sciences*, Volume 54, 736-748.

Costeseque, G., Lebacque, J.P., (2014). Discussion about traffic junction modelling : conservation laws VS Hamilton-Jacobi equations, *Discrete Cont. Dyn. Syst. S*, 7 (3), 411-433.

Costeseque, G., Lebacque, J.P., (2014). Multi-anticipative car-following behaviour : macroscopic modeling, Proceedings of the Traffic and Granular Flow'13 conference (TGF'13), Julich, Germany.

En cours de rédaction

Costeseque, G., GSOM macroscopic traffic flow models on junctions : Lagrangian perspective.

Costeseque, G., Numerical homogenization of Hamilton-Jacobi equations on networks : application to traffic.

Première partie

Du microscopique au macroscopique sur une section homogène

Chapitre 1

Homogenization of microscopic traffic flow models

Most of this Chapter 2 are the transcription notes of private lectures by R. Monneau. More precisely, these private lectures cover Subsections 1.1, 1.2 and Sections 3, 4 and 5. Proofs were written and detailed by the author. Some proofs of Section 5 have been written in collaboration with Mohammad Al Haj, from Université of Paris-Est.

Sommaire

Abstract

In this chapter, we highlight a rigorous link between microscopic and macroscopic traffic models. In this way, we consider some models using systems of ODEs that describe the dynamics of vehicles. At the microscopic level, each vehicle satisfies a given function depending on the gap, the speed and/or the relative speed from the leader vehicle. After a proper asymptotic rescaling, we show that solutions of these systems of ODEs converge to solutions of some macroscopic traffic flow models, based on Hamilton-Jacobi (HJ) equations on one dimensional domain.

1 Introduction

The aim of this chapter is to present some homogenization results for traffic models. Roughly speaking, it is possible to divide traffic models into two main categories depending on time and space scales : on one hand we consider the microscopic car-following models and on the other hand, the macroscopic flow models (see Annex A). The homogenization results presented in this chapter allow to build a rigorous bridge between both types of models, showing that passing to the limit in microscopic models under specific assumptions leads to macroscopic models.

1.1 Settings

We consider a one-dimensional infinite road without any entry or exit. Assume that the vehicles are labeled such that any vehicle $i \in \mathbb{Z}$ has its leader numbered as $(i+1)$. Assume also that vehicles cannot overtake. At time $s \in \mathbb{R}$, we denote :

- the i^{th} vehicle position by $x_i(s)$,
- its instantaneous speed by $\dot{x}_i(s)$ and
- its acceleration by $\ddot{x}_i(s)$.

We are interested in two specific microscopic car-following models described below.

First order model without delay : Assume that the vehicles position satisfies the first microscopic model equation previously referenced as (1) in Table A.2, given by the following Ordinary Differential Equation (ODE)

$$\dot{x}_i(s) = F\left(x_{i+1}(s) - x_i(s)\right), \quad \text{for any} \quad i \in \mathbb{Z}, \quad s \in [0, +\infty), \tag{1.1.1}$$

where $F : \mathbb{R} \to \mathbb{R}$ denotes the speed function of vehicles.

First order model with time delay : We also consider an other model in which a time delay $\tau > 0$ is introduced such that (1.1.1) is modified as follows

$$\dot{x}_i(s) = F\left(x_{i+1}(s-\tau) - x_i(s-\tau)\right), \quad \text{for any} \quad i \in \mathbb{Z}, \quad s \in [0, +\infty). \tag{1.1.2}$$

The time delay $\tau > 0$ is supposed to be the same for every vehicle and does not depend on $i \in \mathbb{Z}$. As above, the function $F : r \mapsto F(r)$ denotes the speed function.

We assume that there exits a function X^ε such that

$$x_i(s) =: \frac{1}{\varepsilon} X^\varepsilon(i\varepsilon, \varepsilon s), \quad \text{for} \quad i \in \mathbb{Z}, \quad s \in [0, +\infty), \tag{1.1.3}$$

with $\varepsilon > 0$ representing a scale factor and i the position index. The index $i \in \mathbb{Z}$ is a discrete variable. In order to work with a pseudo continuum of vehicles, we define continuous

variables $n \in \mathbb{R}$ and $t \in [0,T]$ such as $n := i\varepsilon$ and $t := \varepsilon s$. In this way, X^ε describes the re-scaled position of the vehicles. Then we have that

$$X^\varepsilon(n,t) = \varepsilon x_{\lfloor \frac{n}{\varepsilon} \rfloor}\left(\frac{t}{\varepsilon}\right), \quad \text{for} \quad n \in \mathbb{R}, \quad t \in [0,+\infty)$$

where $\lfloor . \rfloor$ denotes the floor integer.

We are also interested in a first order traffic flow model which is given under the form of a Hamilton-Jacobi (HJ) equation. We show later that this HJ equation is strictly equivalent to the celebrated first order traffic flow model called LWR model [184, 221].

Hamilton-Jacobi equation : We consider the Cauchy problem for the Hamilton-Jacobi (HJ) equation as follows

$$\begin{cases} X^0_t(n,t) = F\left(X^0_n(n,t)\right), & \text{for} \quad n \in \mathbb{R}, \quad t \in [0,+\infty), \\ \\ X^0(n,0) = X_0(n), & \text{for} \quad n \in \mathbb{R}, \end{cases} \tag{1.1.4}$$

where the (macroscopic) initial condition X_0 satisfies assumption (A3) below.

Let us consider the following assumptions :

(A1) **(Regularity of the speed-spacing function F)**

$$\begin{cases} F & \text{is continuous,} \\ F & \text{is Lipschitz continuous in} \quad (x_{i+1} - x_i)(s). \end{cases}$$

(A2) **(Monotonicity of the speed-spacing function F)**

$$F \quad \text{is non-decreasing in} \quad (x_{i+1} - x_i)(s).$$

(A3) **(Initial conditions)** The initial vehicles density is bounded

$$0 < \frac{1}{\rho_0} \leq (X_0)_n \leq \rho_0 \quad \text{with} \quad \rho_0 \geq 1$$

and $X_0 : \mathbb{R} \to \mathbb{R}$ is Lipschitz.

Let us set

$$x_i^0 := x_i(0) = \frac{1}{\varepsilon} X_0(i\varepsilon).$$

such that x_i^0 is bounded for any $i \in \mathbb{Z}$.

(A4) **(Regularity of the ODE solutions)**

$$\begin{cases} x_i \in \mathcal{C}^1\left([0,+\infty)\right), & \text{for any} \quad i \in \mathbb{Z}, \\ \\ x_i & \text{is Lipschitz continuous in} \quad t \in [0,+\infty), \quad \text{for any} \quad i \in \mathbb{Z}. \end{cases}$$

Remark 1.1 (Zero initial conditions)**.** *It is noteworthy that assumption (A3) leads to consider non-zero initial conditions. In terms of traffic, it means that there are some vehicles on the road at time $t = 0$. If the road is empty at initial time, it will stay like that for any times $t \geq 0$. Indeed, at the macroscopic level, we satisfy (1.1.4) with (phenomenological) condition $F(0) = 0$.*

1.2 Main results

In this section, we briefly present the main results of the Chapter for each of both microscopic models described in (1.1.1 and (1.1.2.

For the first model without time delay (1.1.1), we have the following homogenization results :

Theorem 1.2 ((R. Monneau) Micro to macro for ODE (1.1.1))**.** *Assume that (A1), (A2), (A3) and (A4) are satisfied.*

Let $(x_i)_{i\in\mathbb{Z}}$ be a solution of the system of ODEs (1.1.1) submitted to the initial conditions

$$x_i(0) = \frac{1}{\varepsilon}X_0(i\varepsilon), \quad \text{for} \quad i \in \mathbb{Z}.$$

Let X^0 be the unique solution of (1.1.4).

Consider $\varepsilon > 0$ and X^ε defined in (1.1.3). Then we have

(i) **Convergence :** *for all compact set $\mathcal{K} \subset \mathbb{R}\times[0,+\infty)$, X^ε converges uniformly to X^0 on $\mathcal{K}$ when $\varepsilon \to 0$ and*

(ii) **Error estimate :** *there exists $C_T > 0$ such that*

$$|X^\varepsilon(n,t) - X^0(n,t)| \le C_T\sqrt{\varepsilon}, \quad \text{for} \quad n \in \mathbb{R}, \quad t \in [0,T).$$

For the second model with time delay described in (1.1.2), as first main result we have the existence of a comparison principle :

Proposition 1.3 ((R. Monneau) Strict comparison principle for model (1.1.2))**.** *Assume that*

$$0 \le F' \le 1 \quad \text{and} \quad F \in C^1(\mathbb{R}) \cap L^\infty(\mathbb{R}).$$

Let us consider $(x_i)_i$ and $(y_i)_i$ two solutions of (1.1.2) over $[-\tau,+\infty)$.

Let us define for any $i \in \mathbb{Z}$ and any $t \ge 0$:

$$d_i(t) := x_i(t) - y_i(t).$$

If there exists a constant $\delta > 0$ and a positive and non-decreasing function $\rho : \mathbb{R} \to \mathbb{R}$ satisfying

$$\rho(\tau)\tau' < 1 - \frac{1}{\rho(\tau')} \tag{1.1.5}$$

such that

$$(1)_0^\rho \qquad 0 < \delta \le d_i(s-\tau') \le \rho(\tau')d_i(s), \quad \text{for all} \quad i \in \mathbb{Z}, \quad \tau' \in [0,\tau], \quad s \in [-\tau,0]$$

and

$$(2)_0^\rho \qquad \dot{d}_i(s) \ge -\rho(\tau)d_i(s), \quad \text{for all} \quad i \in \mathbb{Z}, \quad s \in [-\tau,0]$$

Then we have

$$0 < \delta \le d_i(t), \quad \text{for all} \quad i \in \mathbb{Z}, \quad t \ge 0$$

The second main result we have is the following homogenization result :

Proposition 1.4 ((R. Monneau) Convergence to the viscosity solution and error estimate)**.** *Assume that assumptions of Proposition 1.3 hold true.*

Assume also that (A1), (A2), (A3) and (A4) are satisfied.

Consider X^0 the unique solution of (1.1.4).

Let $\varepsilon > 0$ and X^ε defined in (1.1.3) for $(x_i)_{i\in\mathbb{Z}}$ a solution of (1.1.2) submitted to the initial conditions

$$x_i(0) = \frac{1}{\varepsilon} X_0(i\varepsilon), \quad \text{for} \quad i \in \mathbb{Z}.$$

Then we have

(i) **Convergence :** *for all compact set $\mathcal{K} \subset \mathbb{R} \times [0, +\infty)$, X^ε converges uniformly to X^0 on $\mathcal{K}$ when $\varepsilon \to 0$ and*

(ii) **Error estimate :** *there exists $C_T > 0$ such that*

$$|X^\varepsilon(n,t) - X^0(n,t)| \leq C_T\sqrt{\varepsilon}, \quad \text{for} \quad n \in \mathbb{R}, \quad t \in [0,T).$$

1.3 Organization of the document

We first review the results for micro-macro approaches in the traffic literature. in Section 2. We define the viscosity solution for Hamilton-Jacobi equation in Section 3. Then the proofs of the main results for first order models are presented in the section 4. The section 5 deals with delayed first order models for which the delay time could not be neglected.

2 Micro-to-Macro approaches : a review

This section is devoted to a quick review of the literature applied to traffic flow modeling and multi-scales methods. The interested reader could refer to Annex A for a more detailed review of the literature about traffic flow models.

Microscopic models : microscopic traffic models purpose is to represent individual driving behaviors. Here, we deal with the so-called car-following models which state that a vehicle trajectory depends on the driving behavior of its nearest leader vehicle. These models have been investigated for almost half a century [52, 109, 217] and give birth to huge literature. For a more complete presentation of car-following models, the interested reader could refer to [34, 135].

Notice that our first ODE (1.1.1) recovers the models of Pipes [217] and Forbes [98] while the second ODE (1.1.2) recovers the ones of Chandler *et al.* [52], Gazis *et al.* [109] and Newell [198]. It is easy to check that the models of Kometani *et al.* [151], Gipps [115] and Krauss [153] are also recovered by the extensions of (1.1.2) (see Subsection 5.4). However, it should be interesting to deal with the more specific form of the models of Bando [14], Helly [127] and Treiber *et al.* [228].

Macroscopic models : In this chapter, we only focused on macroscopic models that were deduced from an hydrodynamics analogy. Adopting a aerial viewpoint, the traffic flow is assumed to behave like any other fluid on a network. The simplest macroscopic model is the so-called LWR model which stands for Lighthill, Whitham [184] and Richards [221]. In the LWR model, the vehicles density ρ is given by the following scalar conservation law :

$$\partial_t \rho(x,t) + \partial_x Q(\rho(x,t)) = 0 \tag{1.2.6}$$

where Q denotes the flow of vehicles. It is the simplest traffic flow model because it assumes that the flow is always at a steady state of equilibrium. Many other macroscopic models tried to improve this assumption of equilibrium by taking into account transitional traffic states.

Microscopic to macroscopic approaches : One of the first micro-macro approach in traffic models was performed in the 1950's and early 1960's by researchers from the General Motors Corporation, namely Robert Herman, Denos C. Gazis, Elliott W. Montroll and Robert E. Chandler among others. Indeed, they not only create car-following theory, they also make a link between such models and traffic flow ones. For instance, in [109], assuming that the leading vehicle in traffic stream has a constant speed u and integrating the expression for the acceleration of $(n+1)$st vehicle, it gives the expression for the velocity of that vehicle, which in turn is intended to be the steady-state velocity of the traffic stream. This velocity solves an appropriate equation mixing the flow and the density.

For example, consider the application of this procedure to the simplest linear car-following model

$$\ddot{x}_{n+1}(t) = \alpha\left[\dot{x}_n(t-T) - \dot{x}_{n+1}(t-T)\right]$$

giving the acceleration of $(n+1)$st vehicle with respect to the relative speed modulo a time delay $T > 0$. By integration and up to a shift in time, we get the velocity

$$u := \dot{x}_{n+1}(t) = \alpha\underbrace{[x_n(t-T) - x_{n+1}(t-T)]}_{=:s=\frac{1}{\rho}} + C_0.$$

The constant C_0 can be computed thanks to the condition for null speed $u = 0$ obtained at maximal density ρ_{jam}. Then from the definition of flow $q = u\rho$, it proceeds that

$$q = \alpha\left[1 - \frac{\rho}{\rho_{\text{jam}}}\right].$$

The constant α is given for the condition $q(\rho = 0) = q_m$ with $q_m \neq 0$. It is noteworthy to underline that this choice is not realistic for low densities or equivalently for high spacing, say that the car-following model is not consistent near to vacuum.

The same (formal) procedure could be used for other type of microscopic models. For instance, if doing so for the following model

$$\ddot{x}_{n+1}(t+T) = \alpha_0 \frac{[\dot{x}_n(t) - \dot{x}_{n+1}(t)]}{[x_n(t) - x_{n+1}(t)]^l}\,[\dot{x}_{n+1}(t+T)]^m$$

first proposed by Gazis, Herman and Rothery [109] and then examined by May and Keller [189], it follows the steady-state equations given in Table 1.1.

Macro-to-Micro approach is often based on a discretization of macroscopic models thanks to finite difference numerical schemes. The main one is Godunov scheme [117] which is equivalent in traffic to the Daganzo's Cell Transmission model [76, 77]. Moreover Godunov numerical scheme has been translated into traffic through the notions of Supply and Demand highlighted in [164].

In traffic literature, for micro-to-macro passage, the reader can refer to [10] which shows that a particular time-discrete microscopic model converges to a second order macroscopic model, and to [157] where the macroscopic limit of a micro kinetic model is shown to be equal to the Kruzhkov entropy solution of the LWR model. There is also the recent paper [62]. The papers [208, 209] and [13] are more precisely dedicated to study stability properties of microscopic models (and so their macroscopic behavior).

	m=0	**m=1**
l=0	$q = q_m \left[1 - \frac{\rho}{\rho_{\text{jam}}}\right]$ Chandler et al. [52] ; Pipes [217]	
l=1	$q = u_{\text{free}} \rho \ln\left(\frac{\rho}{\rho_{\text{jam}}}\right)$ Greenberg [119] ; Gazis et al. [109]	
l=3/2	$q = u_{\text{free}} \rho \left[1 - \sqrt{\frac{\rho}{\rho_{\text{jam}}}}\right]$ Drew [85]	
l=2	$q = u_{\text{free}} \rho \left[1 - \frac{\rho}{\rho_{\text{jam}}}\right]$ Greenshields [120]	$q = u_{\text{free}} \exp\left(\frac{\rho}{\rho_{crit}}\right)$ Edie [88]
l=3		$q = u_{\text{free}} \exp -\frac{1}{2}\left(\frac{\rho}{\rho_{crit}}\right)^2$ Drake et al. [84]

TABLE 1.1 – From GHR model to steady-state models : a classification

There are also a certain number of works about meso to macro passage, where "mesoscopic" stands for kinetic models of traffic flow. We can quote the (numerous) works of Ngoduy on that subject [202–206] or the work using Vlasov-like equation [28].

Let us also mention many homogenization results for Hamilton-Jacobi equations for which the literature is now huge. Homogenization is a general technique which have been used for several different models. For instance, we could mention the homogenization results for the Frenkel-Kontorova (FK) model involving interactions with an infinite number of particles has been studied in Forcadel, Imbert, Monneau [99, 100] and references therein. The FK model allows describing dislocation dynamics. For application to traffic, see [101, 112, 193].

The passage to the limit from microscopic to macroscopic works pretty well in the existing results because it is often assumed that the particles (vehicles in our case) are of the same type except the work of Forcadel, Imbert, Monneau [100] which deals with homogenization for n type of particles. We would like to investigate what homogenization results give if one assume for instance

$$\dot{x}_i(s) = F_i\left(x_{i+1}(s-\tau) - x_i(s-\tau)\right), \quad \text{for any} \quad i \in \mathbb{Z}, \quad s \in [0, +\infty), \tag{1.2.7}$$

with a flow function F_i which depends itself on the driver.

3 Viscosity solution

For a more general introduction to viscosity solutions, the reader could refer to Barles [19] and above all to the user's guide of Crandall, Ishii, Lions [72].

3.1 Definitions

Now, we introduce the main definitions used along this chapter.

Definition 2 (Upper and lower semi-continuous envelopes)**.** *For any function $X : \mathbb{R} \times [0, +\infty) \to \mathbb{R}$, upper and lower semi-continuous envelopes are respectfully defined as*

$$X^*(y,t) = \limsup_{(y',t')\to(y,t)} X(y',t')$$

and

$$X_*(y,t) = \liminf_{(y',t')\to(y,t)} X(y',t').$$

Moreover, we say that

$$\begin{cases} X \quad \text{is upper semi continuous if and only if} \quad X = X^*, \\ X \quad \text{is lower semi continuous if and only if} \quad X = X_*, \\ X \quad \text{is continuous if and only if} \quad X_* = X^*. \end{cases}$$

Definition 3 (Viscosity solutions)**.** *We say that a function $X : \mathbb{R} \times [0, +\infty) \to \mathbb{R}$ is a subsolution (resp. a supersolution) of (1.1.4) on an open set $\Omega \subset \mathbb{R} \times [0, T)$ if its upper semi-continuous (resp. lower semi-continuous) function is locally bounded, and if for any $(y,t) \in \Omega$ and any test function $\varphi \in \mathcal{C}^1(\Omega)$ such that $X - \varphi$ attains a strict local maximum (resp. a local minimum) at the point (y,t), we have*

$$\begin{cases} \varphi_t(y,t) \le F(\varphi_y) \\ \\ (resp. \quad \varphi_t(y,t) \ge F(\varphi_y)) \,. \end{cases} \tag{1.3.8}$$

The function X^* (resp. X_*) is said to be a subsolution (resp. supersolution) on $\mathbb{R} \times [0, T)$, if X^* is a subsolution (resp. X_* is a supersolution) on $\Omega = \mathbb{R} \times [0, T)$ and if moreover it satisfies :

$$\begin{cases} X^*(y,0) \le X_0(y) \quad for \quad y \in \mathbb{R} \\ \\ (resp. \quad X_*(y,0) \ge X_0(y) \quad for \quad y \in \mathbb{R}) \end{cases}$$

where the initial data X_0 is assumed continuous.

A function X is said a viscosity solution of (1.1.4) if X^* is a subsolution and X_* is a supersolution.

3.2 Main results for HJ equation

The first main property of this notion of solution is its stability when passing to the limit. Indeed, we have

Proposition 3.1 (Stability of viscosity solutions)**.** *Assume (A1)-(A2) and $0 < T < +\infty$. Assume that $(X^\varepsilon)_\varepsilon$ is a sequence of subsolutions (resp. supersolutions) of equation (1.1.4) on $\mathbb{R} \times [0, T)$ satisfying (1.1.4) with the same constant $C > 0$, and let us set*

$$\overline{X}(y,t) = \limsup_\varepsilon{}^* \, X^\varepsilon(y,t) = \limsup_{\substack{\varepsilon\to 0 \\ (y',t')\to(y,t)}} X^\varepsilon(y',t')$$

$$\left(resp. \quad \underline{X}(y,t) = \liminf_\varepsilon{}_* \, X^\varepsilon(y,t) = \liminf_{\substack{\varepsilon\to 0 \\ (y',t')\to(y,t)}} X^\varepsilon(y',t') \right)$$

Then $\overline{X}$ is a subsolution (resp. $\underline{X}$ is a supersolution) of (1.1.4) on $\mathbb{R} \times [0, T)$.

We skip the proof which is straightforward adaptation of the classical proof proposed in [19]).

The second main property is the following

Proposition 3.2 (Comparison principle)**.** *Assume (A1)-(A2)-(A3). Assume that* $\overline{X}$ *and* $\underline{X}$ *are respectively a subsolution and a supersolution of (1.1.4) on* $\mathbb{R} \times [0,T)$*. Then we have* $\overline{X} \leq \underline{X}$ *on* $\mathbb{R} \times [0,T)$*.*

We will also need to localize the comparison principle :

Proposition 3.3 (Comparison principle on bounded sets)**.** *Assume (A1)-(A2). Let us fix a point* $(y_0, t_0) \in \mathbb{R} \times [0,T)$ *and for any* $r, R > 0$*, let us set*

$$Q_{r,R} = (y_0 - r, y_0 + r) \times (t_0 - R, t_0 + R).$$

Assume that $\overline{X}$ *is a subsolution (resp.* $\underline{X}$ *a supersolution) of (1.1.4) on the open set* $Q_{r,R} \subset \mathbb{R} \times [0,T)$*. Then*

$$\begin{cases} \overline{X} \leq \underline{X} & \text{on} \quad Q_{r,R} \\ \\ \overline{X} \leq \underline{X} & \text{on} \quad \partial_p\, Q_{r,R} \end{cases}$$

Where

$$\begin{aligned} \partial_p\, Q_{r,R} = &([y_0 - r; y_0 + r] \times \{t_0 - R\}) \\ &\cup\ (\{y_0 - r\} \times [t_0 - R; t_0 + R]\ \cup\ \{y_0 + r\} \times [t_0 - R; t_0 + R]) \end{aligned}$$

The third main property of viscosity solutions is the following :

Proposition 3.4 (Existence by Perron's method)**.** *Assume (A1)-(A2). Assume that* $\overline{X}$ *is a subsolution (resp.* $\underline{X}$ *is a supersolution) of (1.1.4) on* $\mathbb{R} \times [0,T)$ *such that*

$$\overline{X} \leq \underline{X} \quad \text{on} \quad \mathbb{R} \times [0,T)$$

Let $\mathcal{S}$ *the set of all supersolution* $\underline{\tilde{X}}$ *of (1.1.4) on* $\mathbb{R} \times [0,T)$ *satisfying* $\underline{\tilde{X}} \geq \overline{X}$*. Let*

$$Y(y,t) = \inf \left\{ \underline{\tilde{X}}(y,t) \quad \text{such that} \quad \underline{\tilde{X}} \in \mathcal{S} \right\}$$

Then Y_* *is a solution of (1.1.4) on* $\mathbb{R} \times [0,T)$ *satisfying* $\overline{X} \leq Y_* \leq \underline{X}$*.*

The proofs of Propositions 3.2, 3.3 and 3.4 (which follow the classical method ; see for instance Crandall Ishii, Lions [72]) are recalled here after.

3.3 Proof of the main results for the HJ equation

Theorem 3.5 ((R. Monneau) Comparison principle for HJ equation)**.** *Assume (A1), (A2) and (A3). Let* $\overline{X}$ *and* $\underline{X}$ *be respectively a subsolution and a supersolution of (1.1.4), such that*

$$\overline{X}(x,0) \leq \underline{X}(x,0), \quad \text{for} \quad x \in \mathbb{R}.$$

Moreover, assume that there exists a real B *such that*

$$\overline{X}(x,t) - \underline{X}(x,t) \leq B, \quad \text{for} \quad x \in \mathbb{R}.$$

Then for any $T > 0$ *we get*

$$\overline{X}(x,t) \leq \underline{X}(x,t), \quad \text{for} \quad x \in \mathbb{R}, \quad t \in [0,T).$$

Proof Let $T > 0$. Assume that $\overline{X}$ is a subsolution and $\underline{X}$ a supersolution of (1.1.4).

We argue by contradiction by assuming

$$M := \sup_{\substack{x\in\mathbb{R}\\ 0\le t\le T}} \left\{\overline{X}(x,t) - \underline{X}(x,t)\right\} > 0.$$

We set up to a duplication of variables and penalization

$$M_{\alpha,\eta,\varepsilon,\delta} = \sup_{\substack{x,y\in\mathbb{R}\\ 0\le t,s\le T}} \left\{\overline{X}(x,t) - \underline{X}(y,s) - \frac{|x-y|^2}{2\varepsilon} - \frac{|t-s|^2}{2\delta} - \alpha\frac{x^2}{2} - \frac{\eta}{T-t}\right\}$$

where $\alpha, \eta, \varepsilon, \delta > 0$.

Step 1 : Barriers for subsolution and supersolution

From (A1) F is Lipschitz and its Lipschitz constant is denoted C. Using the definitions of sub and supersolution, we can check that $\begin{cases}\overline{X}(x,t) < X_0(y) + Ct\\ \underline{X}(x,t) > X_0(y) - Ct\end{cases}$.

Step 2 : Settings

Let us denote

$$\phi(x,y) := \overline{X}(x,t) - \underline{X}(y,s) - \frac{|x-y|^2}{2\varepsilon} - \frac{|t-s|^2}{2\delta} - \alpha\frac{x^2}{2} - \frac{\eta}{T-t},$$

where $s, t \in [0,T)$ are fixed.

Since ϕ is upper semi-continuous ($\overline{X}$ and $\underline{X}$ are by definition upper semi-continuous) with

$$\phi(x,y) \underset{|x|,|y|\to 0}{\longrightarrow} -\infty,$$

then the minimum $M_{\alpha,\eta,\varepsilon,\delta}$ is attained for a certain set of data $(x_\varepsilon, y_\varepsilon, t_\varepsilon, s_\varepsilon)$, that is

$$M_{\alpha,\eta,\varepsilon,\delta} = \overline{X}(x_\varepsilon,t_\varepsilon) - \underline{X}(y_\varepsilon,s_\varepsilon) - \frac{|x_\varepsilon-y_\varepsilon|^2}{2\varepsilon} - \frac{|t_\varepsilon-s_\varepsilon|^2}{2\delta} - \alpha\frac{x_\varepsilon^2}{2} - \frac{\eta}{T-t_\varepsilon}.$$

Notice that for any $\gamma > 0$, there exist (x_γ, t_γ) such that

$$M \ge \overline{X}(x_\gamma,t_\gamma) - \underline{X}(x_\gamma,y_\gamma) \ge M - \gamma$$

Then we have

$$\begin{aligned} M_{\alpha,\eta,\varepsilon,\delta} &\ge \overline{X}(x_\gamma,t_\gamma) - \underline{X}(x_\gamma,y_\gamma) - \alpha\frac{x_\gamma^2}{2} - \frac{\eta}{T-t_\gamma}\\ &\ge M - \gamma - \alpha\frac{x_\gamma^2}{2} - \frac{\eta}{T-t_\gamma}\\ &\ge \frac{M}{2} > 0 \end{aligned}$$

where we use in the last line that $\gamma = \dfrac{M}{4}$ and that α and η are small enough :

$$\alpha\frac{x_\gamma^2}{2} + \frac{\eta}{T-t_\gamma} < \frac{M}{4}.$$

Let us prove that $\alpha|x_\varepsilon| \underset{\alpha\to 0}{\longrightarrow} 0$. We have that

$$0 < \frac{M}{2} \le M_{\alpha,\eta,\varepsilon,\delta} \le \overline{X}(x_\varepsilon,t_\varepsilon) - \underline{X}(y_\varepsilon,s_\varepsilon) - \alpha\frac{x_\varepsilon^2}{2},$$

and

$$\overline{X}(x_\varepsilon,t_\varepsilon)-\underline{X}(y_\varepsilon,s_\varepsilon)\leq \sup_{\substack{x\in\mathbb{R}\\0\leq t\leq T}}\left\{\overline{X}(x,t)-\underline{X}(x,t)\right\}\leq B.$$

Then it follows

$$0\leq B-\alpha\frac{x_\varepsilon^2}{2}\leq B.$$

From where we deduce

$$\alpha|x_\varepsilon|\leq\sqrt{\alpha B}.$$

Step 3 : Distinction of cases

Case A : $t_\varepsilon=s_\varepsilon=0$. Then it follows that

$$M_{\alpha,\eta,\varepsilon,\delta}=\overline{X}(x_\varepsilon,0)-\underline{X}(y_\varepsilon,0)-\frac{|x_\varepsilon-y_\varepsilon|^2}{2\varepsilon}-\alpha\frac{x_\varepsilon^2}{2}-\frac{\eta}{T},$$

where $\overline{X}(x_\varepsilon,0)-\underline{X}(y_\varepsilon,0)\leq 0$ by assumption.

Hence there is a contradiction because

$$0<\frac{M}{2}\leq M_{\alpha,\eta,\varepsilon,\delta}<0.$$

Case B : $t_\varepsilon=0$ and $s_\varepsilon>0$. Two subcases are thus possible : either $t_\varepsilon=0$ or $s_\varepsilon=0$. Both cases are similar and we only focus on one which is $t_\varepsilon=0$. Indeed to take $s_\varepsilon=0$ and $t_\varepsilon>0$ only makes appear an extra term $\dfrac{\eta}{T-t_\varepsilon}$ which is less than $\dfrac{\eta}{T}$.

We have in this case

$$M_{\alpha,\eta,\varepsilon,\delta}=\overline{X}(x_\varepsilon,0)-\underline{X}(y_\varepsilon,s_\varepsilon)-\frac{|x_\varepsilon-y_\varepsilon|^2}{2\varepsilon}-\frac{|s_\varepsilon|^2}{2\delta}-\alpha\frac{x_\varepsilon^2}{2}-\frac{\eta}{T}.$$

Notice that we have

$$\begin{aligned}\overline{X}(x_\varepsilon,0)-\underline{X}(y_\varepsilon,s_\varepsilon)=&\overline{X}(x_\varepsilon,0)-\underline{X}(x_\varepsilon,0)\\&+\overline{X}(x_\varepsilon,0)-\underline{X}(y_\varepsilon,0)\\&+\underline{X}(y_\varepsilon,0)-\underline{X}(y_\varepsilon,s_\varepsilon),\end{aligned}$$

where the first term is negative by assumption, the second one satisfies

$$\overline{X}(x_\varepsilon,0)-\underline{X}(y_\varepsilon,0)\leq Lip(X_0)|x_\varepsilon-y_\varepsilon|$$

if $\underline{X}$ is a solution and the last one is such that

$$\underline{X}(y_\varepsilon,0)-\underline{X}(y_\varepsilon,s_\varepsilon)\leq Cs_\varepsilon,$$

from the barriers on sub and supersolution in Step 1. Thus we obtain

$$\overline{X}(x_\varepsilon,0)-\underline{X}(y_\varepsilon,s_\varepsilon)\leq Lip(X_0)|x_\varepsilon-y_\varepsilon|+Cs_\varepsilon.$$

Hence up to choose ε small enough such that

$$Lip(X_0)|x_\varepsilon-y_\varepsilon|\leq\frac{|x_\varepsilon-y_\varepsilon|^2}{2\varepsilon}$$

and δ small enough such that

$$Cs_\varepsilon\leq\frac{|s_\varepsilon|^2}{2\delta},$$

we get a contradiction

$$0 < \frac{M}{2} \leq M_{\alpha,\eta,\varepsilon,\delta} \leq Lip(X_0)|x_\varepsilon - y_\varepsilon| + Cs_\varepsilon - \frac{|x_\varepsilon - y_\varepsilon|^2}{2\varepsilon} - \frac{|s_\varepsilon|^2}{2\delta} - \alpha\frac{x_\varepsilon^2}{2} - \frac{\eta}{T} < 0.$$

Case C : $t_\varepsilon, s_\varepsilon > 0$. We use the viscosity inequalities in this case.

Let the test function φ smooth enough such that

$$\varphi(x,t) := M_{\alpha,\eta,\varepsilon,\delta} + \underline{X}(y_\varepsilon, s_\varepsilon) + \frac{|x - y_\varepsilon|^2}{2\varepsilon} + \frac{|t - s_\varepsilon|^2}{2\delta} + \frac{\alpha x^2}{2} + \frac{\eta}{T - t}, \quad \text{for} \quad x \in \mathbb{R}, \quad t \in [0, T).$$

We then get

$$\begin{cases} \overline{X}(x,t) \leq \varphi(x,t), & \text{for} \quad x \in \mathbb{R}, \quad t \in [0,T), \\ \\ \overline{X}(x,t) = \varphi(x,t), & \text{at} \quad \overline{P} = (x_\varepsilon, t_\varepsilon). \end{cases}$$

The subsolution inequality reads $\varphi_t \leq F(\varphi_x)$ at $\overline{P} = (x_\varepsilon, t_\varepsilon)$, that gives

$$\frac{\eta}{(T - t_\varepsilon)^2} + \frac{t_\varepsilon - s_\varepsilon}{\delta} \leq F\left(\frac{x_\varepsilon - y_\varepsilon}{\varepsilon} + \alpha x_\varepsilon\right). \tag{1.3.9}$$

Similarly, let the test function ψ smooth enough such that

$$\psi(y,s) := -M_{\alpha,\eta,\varepsilon,\delta} + \overline{X}(x_\varepsilon, t_\varepsilon) - \frac{|x_\varepsilon - y|^2}{2\varepsilon} - \frac{|t_\varepsilon - s|^2}{2\delta} - \frac{\alpha x_\varepsilon^2}{2} - \frac{\eta}{T - t_\varepsilon}, \quad \text{for} \quad x \in \mathbb{R}, \quad t \in [0, T).$$

We then get

$$\begin{cases} \underline{X}(y,s) \geq \psi(y,s), & \text{for} \quad y \in \mathbb{R}, \quad s \in [0,T), \\ \\ \underline{X}(y,s) = \psi(y,s), & \text{at} \quad \underline{P} = (x_\varepsilon, t_\varepsilon). \end{cases}$$

The supersolution inequality reads $\psi_s \geq F(\psi_y)$ at $\underline{P} = (y_\varepsilon, s_\varepsilon)$, that gives

$$\frac{t_\varepsilon - s_\varepsilon}{\delta} \geq F\left(\frac{x_\varepsilon - y_\varepsilon}{\varepsilon}\right) \tag{1.3.10}$$

Then (1.3.9)-(1.3.10) imply that

$$\begin{aligned} 0 < \frac{\eta}{(T - t_\varepsilon)^2} &\leq F\left(\frac{x_\varepsilon - y_\varepsilon}{\varepsilon} + \alpha x_\varepsilon\right) - F\left(\frac{x_\varepsilon - y_\varepsilon}{\varepsilon}\right) \\ &\leq C\alpha|x_\varepsilon| \end{aligned}$$

Since $\alpha|x_\varepsilon| \underset{\alpha \to 0}{\longrightarrow} 0$, we obtain a contradiction that ends the proof. □

Theorem 3.6 (Uniqueness of HJ solution)**.** *Assume (A1), (A2) and (A3). There exists a unique solution X^0 to the Hamilton-Jacobi equation (1.1.4).*

Proof The proof is very classical and we do not reproduce it here. It is based on three steps which are (1) getting barriers on the solutions, (2) proof of the existence by Perron's method (see [142]) and (3) conclude. □

4 First order model with no delay

We are interested here in the first order microscopic model depicted in (1.1.1) :

$$\dot{x}_i(s) = F\left(x_{i+1}(s) - x_i(s)\right), \quad \text{for} \quad i \in \mathbb{Z}$$

For sake of simplicity (and without any loss of generality), we assume that the function F satisfies

$$\sup_{z\in\mathbb{R}} F(z) = 1 \quad \text{and} \quad \sup_{z\in\mathbb{R}} F'(z) = 1$$

4.1 Settings for the ODE

Theorem 4.1 ((R. Monneau) Uniqueness of the ODE solution)**.** *We consider the equation defined by (1.1.4) completed by the initial data $(x_i^0)_{i\in\mathbb{Z}}$ such as (A3) is respected i.e. the space gradient is bounded and thus, the time gradient $(x_i^0)_t$ too.*

If F satisfies (A1), then there exists an unique solution $x_i^0(t)$ of (1.1.1) and

$$|x_i(t) - x_i^0| \leq Ct$$

Proof **Step 1 : Reformulation of the problem in a Banach space**
We have

$$\dot{x_i} = F(x_{i+1} - x_i)$$

where F is a Lipschitz function

$$\exists L > 0 \ : \ \forall (a,b) \in \mathbb{R}^2, \ |F(a) - F(b)| \leq L|a-b|$$

Let $U = \left((x_i)_{i\in\mathbb{Z}}\right) \in \mathbb{R}^{\mathbb{Z}}$ and we assume that we can find a function $\mathcal{F}$ such $\dot{U} = \mathcal{F}(U)$.
Consider $\mathcal{B} \subset \mathbb{R}^{\mathbb{Z}}$ given by

$$\mathcal{B} = \{U \in \mathbb{R}^{\mathbb{Z}}, (u_i - x_i^0) \leq r\}$$

where $(x_i^0)_i$ is the initial data and $r > 0$ is the ball radius.

Notice that $U : [0,T] \to \mathcal{B}$ where $\mathcal{B}$ is a Banach space equipped with its norm defined as

$$\|U\| = \sup_{i\in\mathbb{Z}} |x_i|$$

Step 2 : $\mathcal{F}$ is Lipschitz
We obtain

$$\begin{aligned}
\|\mathcal{F}(U) - \mathcal{F}(V)\| &= \sup_i |\mathcal{F}_i(U) - \mathcal{F}_i(V)| \\
&= \sup_i |F_i(u_{i+1} - u_i) - F_i(v_{i+1} - v_i)| \\
&\leq L \sup_i |(U_{i+1} - V_{i+1}) - (U_i - V_i)| \\
&\leq 2L \sup_i |U_i - V_i| = 2L\|U - V\|
\end{aligned}$$

Step 3 : Contraction

We consider :

$$U(t) = U(0) + \int_0^t \mathcal{F}(U(s))ds = \Big(A(U(t))\Big)$$

where A is a function satisfying

$$\begin{aligned} A(U(t)) - A(V(t)) &= \int_0^t ds\Big(\mathcal{F}(U(s)) - \mathcal{F}(V(s))\Big) \\ &\leq \int_0^t Lip(\mathcal{F})\|U(s) - V(s)\|ds \\ &\leq TLip(\mathcal{F}) \sup_{0\leq t\leq T} \|U(t) - V(t)\| \\ &\leq \alpha \sup_{0\leq t\leq T} \|U(t) - V(t)\| \end{aligned}$$

We have just proved that :

$$\sup_{0\leq t\leq T} \Big\|\Big(A(U(t))\Big) - \Big(A(V(t))\Big)\Big\| \leq \alpha \sup_{0\leq t\leq T} \|U(t) - V(t)\|$$

If the time period T is small enough for example $T < \dfrac{1}{Lip(\mathcal{F})}$ with $Lip(\mathcal{F}) > 0$, then $TLip(\mathcal{F}) =: \alpha < 1$. This condition on T implies that we have to work with a succession of small time periods such as $[0, T]$, $[T, 2T]$ etc.

Step 4 : Conclusion
As A is a contracting function, according to the fixed point theorem in a Banach space, we know that there exists a unique $U \in \mathcal{B}$ such that $U(t) = A\,(U(t))$. □

Lemma 4.2 ((R. Monneau) Formal conservation of order)**.** *On a single lane road, the vehicles keep ordered according to their initial order, that is to say there is no overtaking manœuvre. More precisely, if*

$$x_{i+1}(0) \geq x_i(0) \quad , \quad \forall i \in \mathbb{Z}$$

Then

$$x_{i+1}(t) \geq x_i(t) \quad , \quad \forall i \in \mathbb{Z}, \forall t > 0$$

Proof Let's consider for any $i \in \mathbb{Z}$ and $t > 0$, $S_i(t) = x_{i+1}(t) - x_i(t)$ and $\min\limits_{i\in\mathbb{Z}} S_i(t) = m(t)$. Let's suppose that $m(t)$ is reached for $i = i_0$. Then

$$m'(t) = \dot{S}_{i_0}(t) = \dot{x}_{i_0+1}(t) - \dot{x}_{i_0}(t) = F(S_{i_0+1}) - F(S_{i_0})$$

Under the assumption that F is a non-decreasing function (A2), we obtained that $m'(t) \geq 0$. So

$$m(t) \geq m(0) \geq 0$$

□

Remark 4.3. *The function F represents the speed of the considered vehicle. It is not surprising to choose the speed as a non-decreasing function of the headway distance. However, many recent studies have showed that there exists a cycle of hysteresis. In the case of first order model, the main causes of hysteresis lap, for example time delay and leader vehicle speed, are not considered.*

Theorem 4.4 ((R. Monneau) Comparison principle for ODE (1.1.1))**.** *Let us consider* $(x_i)_{i\in\mathbb{Z}}$ *and* $(y_i)_{i\in\mathbb{Z}}$ *two solutions of (1.1.1). Moreover we assume that we have* $x_i(0) \leq y_i(0), \quad \forall i \in \mathbb{Z}$ *and we assume that* $(x_i)_{i\in\mathbb{Z}}$ *and* $(y_i)_{i\in\mathbb{Z}}$ *satisfy both assumption (A4) and Theorem 4.1. As* $(x_i)_{i\in\mathbb{Z}}$ *and* $(y_i)_{i\in\mathbb{Z}}$ *are both Lipschitz, we can also consider that we have*

$$\begin{cases} x_i(t) \leq x_i(0) + Ct \\ y_i(t) \geq y_i(0) - Ct \end{cases}, \quad \text{for} \quad i \in \mathbb{Z}, \quad t \geq 0$$

with C *a constant which is independent from* i*.*

Then, under the assumptions (A1) and (A2), we have :

$$x_i(t) \leq y_i(t), \quad \text{for} \quad i \in \mathbb{Z}, \quad t \geq 0$$

Proof **Step 1 : Setting**
Let $T > 0$. We will suppose that the inequality is false, trying to highlight a contradiction. Therefore, we consider that :

$$M = \sup_{\substack{i\in\mathbb{Z} \\ 0\leq t\leq T}} x_i(t) - y_i(t) > 0.$$

We introduce another supremum, using a duplication of variables by penalization. This one allows to consider that the index i and the time t are not huge and their expansions are in some way bounded :

$$M_{\alpha,\eta} = \sup_{\substack{i\in\mathbb{Z} \\ 0\leq t\leq T}} x_i(t) - y_i(t) - \alpha i^2 - \eta t$$

Where $\alpha > 0$ and $\eta > 0$.

We assume that for α and η small enough, we have :

$$M_{\alpha,\eta} > \frac{M}{2} > 0$$

Step 1.1 : proof of inequality $M_{\alpha,\eta} > M/2$
Actually, we have $M_{\alpha,\eta} \geq M_{\alpha,0} - \eta T$ where we can assume that $\eta < M/4T$.

We could raise $M_{\alpha,0}$ for a certain α, recalling that

$$\forall \delta > 0, \quad \exists (i_\delta, t_\delta) \in \mathbb{Z} \times [0,T), \quad M \geq |x_{i_\delta}(t_\delta) - y_{i_\delta}(t_\delta)| \geq M - \delta$$

Thus, we have for any $\delta > 0$ the existence of $(i_\delta, t_\delta) \in \mathbb{Z} \times [0,T)$ such that

$$\begin{aligned} M_{\alpha,0} \geq x_{i_\delta}(t_\delta) - y_{i_\delta}(t_\delta) - \alpha(i_\delta)^2 &\geq M - \delta - \alpha(i_\delta)^2 \\ &\geq \frac{3M}{4} \qquad \text{for} \quad \alpha < \alpha_0 = \frac{1}{(i_\delta)^2}\left(\frac{M}{4} - \delta\right) \end{aligned}$$

From which we find back the inequality, according to the one complied by η :

$$M_{\alpha,\eta} \geq \frac{M}{2}$$

Step 1.2
Consider that $M_{\alpha,\eta}$ is reached for $i = i_\alpha$ and $t = t_\alpha$.
Then

$$M_{\alpha,\eta} = x_{i_\alpha}(t_\alpha) - y_{i_\alpha}(t_\alpha) - \alpha {i_\alpha}^2 - \eta t_\alpha > \frac{M}{2} > 0$$

One can remark that $t_\alpha > 0$ because of the assumptions $M = \sup_{i\in\mathbb{Z}}\ x_i(t) - y_i(t) > 0$ for $t = 0$ and $x_i(0) \leq y_i(0), \quad \forall i \in \mathbb{Z}$.

Step 2 : Obtaining inequalities
We now consider the following function :

$$\begin{aligned}\varphi : [0,T] &\to \mathbb{R}\\ t &\mapsto x_{i_\alpha}(t) - y_{i_\alpha}(t) - \alpha {i_\alpha}^2 - \eta t\end{aligned}$$

As $M_{\alpha,\eta}$ is a supremum, we assume that $\dot{\varphi}(t_\alpha) \geq 0$, thus

$$\dot{x_{i_\alpha}}(t_\alpha) - \dot{y_{i_\alpha}}(t_\alpha) - \eta \geq 0$$

$$F\big(x_{i_\alpha+1}(t_\alpha) - x_{i_\alpha}(t_\alpha)\big) - F\big(y_{i_\alpha+1}(t_\alpha) - y_{i_\alpha}(t_\alpha)\big) \geq \eta$$

We also have that :

$$M_{\alpha,\eta} = x_{i_\alpha}(t_\alpha) - y_{i_\alpha}(t_\alpha) - \alpha\big(i_\alpha\big)^2 \geq x_{i_\alpha+1}(t_\alpha) - y_{i_\alpha+1}(t_\alpha) - \alpha\big(i_\alpha+1\big)^2$$

$$y_{i_\alpha+1}(t_\alpha) - y_{i_\alpha}(t_\alpha) + 2\alpha(i_\alpha) + \alpha \geq x_{i_\alpha+1}(t_\alpha) - x_{i_\alpha}(t_\alpha)$$

Then

$$Lip(F)|2\alpha i_\alpha + \alpha| \geq F\big(y_{i_\alpha+1}(t_\alpha) - y_{i_\alpha}(t_\alpha) + 2\alpha i_\alpha + \alpha\big) - F\big(y_{i_\alpha+1}(t_\alpha) - y_{i_\alpha}(t_\alpha)\big) \geq \eta > 0$$

Step 3 : Proof of $\alpha i_\alpha \underset{\alpha\to 0}{\longrightarrow} 0$
As we have

$$x_i(t) \leq x_i(0) + Ct \quad \text{and} \quad y_i(t) \geq y_i(0) - Ct$$

Thus

$$2CT \geq M_{\alpha,\eta} \geq \frac{M}{2} > 0$$

$$2CT - \alpha\big(i_\alpha\big)^2 \geq x_{i_\alpha}(t_\alpha) - y_{i_\alpha}(t_\alpha) - \alpha.{i_\alpha}^2 - \eta t_\alpha \geq x_0(0) - y_0(0)$$

And

$$\alpha\big(i_\alpha\big)^2 \leq 2CT - \Big(x_0(0) - y_0(0)\Big) = C'$$

So

$$\alpha|i_\alpha| \leq \sqrt{C'}\alpha$$

Step 4 : Contradiction
Under the assumption of $\alpha i_\alpha \underset{\alpha\to 0}{\longrightarrow} 0$, we obtain a contradiction while

$$0 \geq \eta > 0$$

So $M < 0$ and $x_i(t) \leq y_i(t),\ \forall t \geq 0$. □

Corollary 4.5 ((R. Monneau) Conservation of initial order)**.** *Considering $(x_i)_{i\in\mathbb{Z}}$ solution of (1.1.1) such that $x_{i+1}(0) \leq x_i(0)$, with x_i satisfying both assumption (A4) and Theorem 2.12.*

Then, under the assumptions (A1) and (A2), we have :

$$x_{i+1}(t) \leq x_i(t), \quad \forall t \geq 0$$

Proof We consider x_i and x_{i+1} such as both are solutions of (1.1.1) such as :

$$x_i(0) \leq x_{i+1}(0), \forall i \in \mathbb{Z}$$

With $\forall i \in \mathbb{Z},\ x_i \in \mathcal{C}^1(\mathbb{R})$ and $(x_i)_i$ Lipschitz.

And

$$|x_i(t) - x_i(0)| \leq Ct, \forall i \in \mathbb{Z}$$

Applying the previous theorem for $y_i = x_{i+1}$, the proof is direct. □

Proposition 4.6 ((R. Monneau) PDE solved at ε-level)**.** *If x_i is a solution of (1.1.1), then X^ε given by (1.1.3) solves formally the following equation :*

$$\frac{\partial X^\varepsilon}{\partial t}(y,t) = F\left(\frac{X^\varepsilon(y+\varepsilon,t) - X^\varepsilon(y,t)}{\varepsilon}\right) \tag{1.4.11}$$

Proof We have

$$X_t^\varepsilon = \frac{\partial X^\varepsilon}{\partial t}(i\varepsilon,\varepsilon s) = \frac{1}{\varepsilon}\frac{\partial X^\varepsilon}{\partial s}(i\varepsilon,\varepsilon s) = \frac{\partial x_i}{\partial s}(s) = \dot{x}_i(s)$$

And

$$x_{i+1}(s) - x_i(s) = \frac{X^\varepsilon((i+1)\varepsilon,\varepsilon s) - X^\varepsilon(i\varepsilon,\varepsilon s)}{\varepsilon} = X_y^\varepsilon$$

Thus

$$\frac{\partial X^\varepsilon}{\partial t}(i\varepsilon,\varepsilon s) = F\left(x_{i+1} - x_i\right) = F\left(\frac{X^\varepsilon((i+1)\varepsilon,\varepsilon s) - X^\varepsilon(i\varepsilon,\varepsilon s)}{\varepsilon}\right)$$

So

$$X_t^\varepsilon = F\left(X_y^\varepsilon\right)$$

□

4.2 Proof of the main results for the non-delayed model

Theorem 4.7 ((R. Monneau) Convergence to the viscosity solution)**.** *Consider X^0 the unique solution of (1.1.4) satisfying the assumptions (A1), (A2) and (A3).*

We set X^ε defined as follows

$$x_i(t) := \frac{1}{\varepsilon}X^\varepsilon(i\varepsilon,\varepsilon t) \quad \textit{for any} \quad i \in \mathbb{Z}, \quad t \in [0,+\infty)$$

with $(x_i)_{i\in\mathbb{Z}}$ solution of (1.1.1), such that X^ε satisfies (1.1.4).

Then for all compact set $\mathcal{K} \subset \mathbb{R} \times [0,+\infty)$, X^ε converges uniformly to X^0 on $\mathcal{K}$ when $\varepsilon \to 0$, i.e.

$$|X^\varepsilon - X^0|_{L^\infty(\mathcal{K})} \underset{\varepsilon\to 0}{\longrightarrow} 0$$

Proof **Step 1 : Barriers** Notice that u_0 is Lipschitz according to assumption (A0). Hence we can easily deduce that

$$\begin{cases} X^- \leq X^0 \leq X^+ \\ X^- \leq X^\varepsilon \leq X^+ \end{cases}$$

with $X^{\pm}(y,t) := X_0(y) \pm Ct$ for any $(y,t) \in \mathbb{R} \times [0,+\infty)$ and for $C = \|F\|_\infty$.

Indeed we have that

$$|x_i(t) - x_i(0)| \leq Ct$$

We can also consider

$$\left|\varepsilon x_i\left(\frac{t}{\varepsilon}\right) - \varepsilon x_i(0)\right| \leq C\frac{t}{\varepsilon}\varepsilon$$

So

$$|X^\varepsilon(y = i\varepsilon, t) - X^0(y = i\varepsilon)| \leq Ct$$

As $i\varepsilon \leq y < (i+1)\varepsilon$ and $|X^0(i\varepsilon) - X^0(y)| \leq Lip(X^0)\varepsilon$, we finally obtain that :

$$|X^\varepsilon(y,t) - X^0(y)| \leq Ct + Lip(X^0)\varepsilon$$

It also implies that we can properly define the upper semi-continuous enveloppe (resp. lower) of X^ε such that

$$\overline{X}(y,t) := \limsup_{\substack{\varepsilon\to 0 \\ (y',t')\to(y,t)}} X^\varepsilon(y',t') =: \limsup_{\varepsilon}{}^{*}\ X^\varepsilon$$

$$\text{and} \quad \underline{X}(y,t) := \liminf_{\substack{\varepsilon\to 0 \\ (y',t')\to(y,t)}} X^\varepsilon(y',t') =: \liminf_{\varepsilon}{}_{*}\ X^\varepsilon$$

Step 2 : $\overline{X}$ is a subsolution of (1.1.4) As usual we prove that $\overline{X}$ is a subsolution of (1.1.4). We argue by contradiction. If $\overline{X}$ is not a subsolution of (1.1.4), then there exists $P_0 := (y_0, t_0)$ and a test function φ smooth enough defined such that

$$\begin{cases} \overline{X} \leq \varphi & \text{over} \quad B_{2r,r}(P_0) \\ \overline{X} = \varphi & \text{at} \quad P_0 \end{cases}$$

and satisfying that

$$\varphi_t > F(\varphi_y) \quad \text{at} \quad P_0 \tag{1.4.12}$$

Up to replace φ by $P \mapsto \varphi(P) + |P - P_0|$, we can assume that

$$\begin{cases} \overline{X} < \varphi & \text{over} \quad B_{2r,r}(P_0) \setminus \{P_0\} \\ \overline{X} = \varphi & \text{at} \quad P_0 \end{cases}$$

Moreover, we assume that there exists $\eta_r > 0$ such that

$$\overline{X} - \varphi \leq -\eta_r < 0 \quad \text{over} \quad B_{2r,r}(P_0) \setminus B_{r,r}(P_0) \tag{1.4.13}$$

By definition of $\overline{X}$ and for ε small enough, we have that

$$X^\varepsilon \leq \overline{X} + \frac{\eta_r}{2}$$

Thus for ε small enough, from (1.4.13) it is obvious that

$$X^\varepsilon - \varphi \leq -\frac{\eta_r}{2} \quad \text{over} \quad B_{2r,r}(P_0) \setminus B_{r,r}(P_0) \tag{1.4.14}$$

We have also that $\overline{X}(P_0) = \lim_{\varepsilon\to 0} X^\varepsilon(P_\varepsilon)$ with $X^\varepsilon \underset{\varepsilon\to 0}{\longrightarrow} u^0$. As φ is smooth enough, we get that

$$(X^\varepsilon - \varphi)(P_\varepsilon) \underset{\varepsilon\to 0}{\longrightarrow} (u^0_\varphi)(P_0) = 0 \tag{1.4.15}$$

We set

$$M_\varepsilon := \sup_{P\in\overline{B_{r,r}(P_0)}} (X^\varepsilon - \varphi)(P)$$

and we assume that M_ε is reached for $\bar{P}_\varepsilon \in \overline{B_{r,r}(P_0)}$ that is

$$M_\varepsilon = (X^\varepsilon - \varphi)(\bar{P}_\varepsilon)$$

Let us prove that $\bar{P}_\varepsilon \to P_0$ for $\varepsilon \to 0$. We argue by contradiction. As $\bar{P}_\varepsilon \in \overline{B_{r,r}(P_0)}$ which is a compact set, we can extract a subsequence ε' from ε such that $\bar{P}_\varepsilon$ converges to $\bar{P}_0 \neq P_0$. By abuse of notation, we will consider ε instead of the subsequence ε'. Moreover we have that $(\overline{X} - \varphi)(\bar{P}_\varepsilon) \underset{\varepsilon\to 0}{\longrightarrow} (\overline{X} - \varphi)(\bar{P}_0)$ with $(\overline{X} - \varphi)(\bar{P}_0) < 0$ by definition of φ over $B_{2r,r}(P_0) \setminus \{P_0\}$. Then for ε small enough and for

$$\delta := -\frac{(\overline{X} - \varphi)(\bar{P}_0)}{2} > 0$$

we have that

$$(X^\varepsilon - \varphi)(\bar{P}_\varepsilon) \leq (\overline{X} - \varphi)(\bar{P}_0) + \delta < -\frac{\delta}{2} < (X^\varepsilon - \varphi)(P_\varepsilon)$$

where we use that $(X^\varepsilon - \varphi)(P_\varepsilon)$ converges to 0 according to (1.4.15).

Hence we get a contradiction since $(\overline{X} - \varphi)(\bar{P}_0) \geq (\overline{X} - \varphi)(\bar{P}_0)$.

Since $\bar{P}_\varepsilon \to P_0$ for $\varepsilon \to 0$, it is obvious that for ε and r small enough, we have that $\bar{P}_\varepsilon$ is in the open ball $B_{r,r}(P_0)$.

As X^ε is a solution of (1.1.4) (of course it is also a subsolution), we can consider a test function $\bar{\varphi}$ such that

$$\begin{cases} X^\varepsilon \leq M^\varepsilon - \varphi =: \bar{\varphi} & \text{over} \quad B_{2r,r}(P_0) \\ X^\varepsilon = \bar{\varphi} & \text{at} \quad \bar{P}_\varepsilon \end{cases}$$

and we have that

$$\begin{aligned} \bar{\varphi}_t(y,t) &\leq F\left(\frac{1}{\varepsilon}(\bar{\varphi}(y+\varepsilon,t) - \bar{\varphi}(y,t))\right) \quad \text{for any} \quad (y,t) \in \mathbb{R}\times[0,+\infty)\bar{\varphi} \\ &\leq F\left(\frac{1}{\varepsilon}(\varphi(y+\varepsilon,t) - \varphi(y,t))\right) \end{aligned}$$

We notice that $\bar{\varphi}_t = \varphi_t$. Then passing to the limit for $\varepsilon \to 0$, we get

$$\varphi_t(P_0) \leq F(\varphi_y(P_0))$$

which is in contradiction with (1.4.12).

Step 3 : Conclusion We have proved that $\overline{X}$ is a subsolution of (1.1.4) and we can also prove that $\underline{X}$ is a supersolution of (1.1.4). By definition, we have that

$$\overline{X} \geq \underline{X}$$

Both $\overline{X}$ and $\underline{X}$ satisfy the comparison principle that gives us :

$$\overline{X} \leq \underline{X}$$

Hence, we get that $\overline{X} = \underline{X}$ is the viscoity solution of (1.1.4). That ends the proof. □

Theorem 4.8 ((R. Monneau) General error estimate)**.** *If $\tilde{X}^\varepsilon$ is a general solution of equation (1.1.4),*
Then we have

$$|\tilde{X}^\varepsilon(y,t) - X^0(y,t)| \leq C_T\sqrt{\varepsilon}$$

for $y \in \mathbb{R},\ t \in [0,T]$.

Corollary 4.9 ((R. Monneau) Particular error estimate)**.** *If $X^\varepsilon(y,t) = \varepsilon x_{\lfloor \frac{y}{\varepsilon} \rfloor}(\frac{t}{\varepsilon})$ is a particular solution of equation (1.1.4),*
Then we have

$$|X^\varepsilon(y,t) - X^0(y,t)| \leq C_T\sqrt{\varepsilon}$$

for $y \in \mathbb{R},\ t \in [0,T]$.

Proof **Step 0 : Preliminary**
Considering (1.1.1), we introduce $x(y,t) = x_i(t)$ where we considerate a continuum of vehicles which indices pass from $i \in \mathbb{Z}$ to $y \in \mathbb{R}$. Thus,

$$\frac{\partial X}{\partial t}(y,t) = F\Big(x(y+1,t) - x(y,t)\Big)$$

If X^ε defined as follows

$$X^\varepsilon(y,t) = \varepsilon x_{\lfloor \frac{y}{\varepsilon} \rfloor}(\frac{t}{\varepsilon})$$

$$X^\varepsilon(y,t=0) = X_0(\varepsilon \lfloor \frac{y}{\varepsilon} \rfloor) = X_0^\varepsilon(y)$$

solves

$$\begin{cases} \dfrac{\partial}{\partial t}\tilde{X}^\varepsilon(y,t) = F\Big(\dfrac{\tilde{X}^\varepsilon(y+\varepsilon,t) - \tilde{X}^\varepsilon(y,t)}{\varepsilon}\Big) \\ \\ \tilde{X}^\varepsilon(y,0) = X_0(y) \end{cases} \tag{1.4.16}$$

Then

$$X_0^\varepsilon(y) \leq X_0(y) \leq X_0^\varepsilon(y) + \varepsilon Lip(X_0)$$

$$X^\varepsilon(y,t) \leq \tilde{X}_0^\varepsilon(y) \leq X^\varepsilon(y,t) + \varepsilon Lip(X_0)$$

The aim of this proof is to show that $|\tilde{X}^\varepsilon - X^0| \leq C_T\sqrt{\varepsilon}$
Let $T > 0$. Consider

$$M_\eta = \sup_{\substack{x\in\mathbb{R} \\ 0\leq t\leq T}} X^\varepsilon(x,t) - X^0(x,t) - \eta t$$

And

$$M_{\alpha,\eta,\gamma,\delta} = \sup_{\substack{x,y\in\mathbb{R} \\ 0\leq t,s\leq T}} X^\varepsilon(x,t) - X^0(y,s) - \frac{|x-y|^2}{2\gamma} - \frac{|t-s|^2}{2\delta} - \alpha\frac{y^2}{2} - \frac{\eta}{T-t} > \frac{M}{2} > 0$$

Where $\alpha > 0$, $\eta > 0$, $\gamma > 0$ and $\delta > 0$.

Step 1 : Obtaining barriers

$$M_{\alpha,\eta,\gamma,\delta} > \frac{M_\eta}{2} > 0$$

for α and η small enough.

$$M_{\alpha,\eta,\gamma,\delta} \geq X^{\varepsilon}(0,0) - X^{0}(0,0) - \frac{\eta}{T} = -C^{(0)}$$

and

$$X_0(x) - X_0(y) + Ct + Cs - P \geq M_{\alpha,\eta,\gamma,\delta}$$

Let $d = |x-y|$ and $C^{(1)} = 2CT + C^{(0)} \geq P - Ld$.

$$\begin{aligned}
&\frac{\eta}{T-t} + \alpha\frac{x^2}{2} + \frac{|x-y|^2}{2\varepsilon} + \frac{|t-s|^2}{2\delta} - L|x-y| \leq C^{(1)} \\
&\frac{|x-y|^2}{2\varepsilon} - L|x-y| \leq C^{(1)} \\
&\frac{d^2}{2\varepsilon} - Ld \leq C^{(1)}
\end{aligned}$$

We then deduce that $d = |x-y| \leq C^{(2)}$ from where we obtain that

$$\frac{\eta}{T-t} + \alpha\frac{x^2}{2} + \frac{|t-s|^2}{2\delta} \leq C^{(3)}$$

Step 2 : viscosity inequalities

Step 2.1 : Subsolution inequality

$$X^{\varepsilon}(x,t) \leq M_{\alpha,\eta,\gamma,\delta} + X^{0}(y,s) + \frac{|x-y|^2}{2\gamma} + \frac{|t-s|^2}{2\delta} + \frac{\alpha y^2}{2} + \frac{\eta}{T-t} = \varphi(x,t)$$

The equality is available when $M_{\alpha,\eta,\gamma,\delta}$ is reached.

$$\Rightarrow \varphi_t \leq F(\varphi_x)$$

at the sup point.

$$\eta + \frac{t-s}{\delta} \leq F(\frac{x-y}{\gamma} + \frac{\varepsilon}{2\gamma}x) \tag{1.4.17}$$

Step 2.2 : Supersolution inequality

$$X^{0}(y,s) \geq -\psi(y,s) = -M_{\alpha,\eta,\gamma,\delta} + X^{\varepsilon}(x,t) - \frac{|x-y|^2}{2\gamma} - \frac{|t-s|^2}{2\delta} - \frac{\alpha y^2}{2} - \frac{\eta}{T-t} = \psi(y,t)$$

$$\Rightarrow \psi_s \leq F(\psi_y)$$

$$\frac{t-s}{\delta} \geq F(-\alpha y + \frac{x-y}{\gamma}) \tag{1.4.18}$$

Step 2.3 : Difference (1.4.17)-(1.4.18)

$$\begin{aligned}
\Rightarrow \frac{\eta}{T^2} \leq \frac{\eta}{(T-t)^2} &\leq F(\frac{x-y}{\gamma} + \frac{\varepsilon}{2\gamma}) - F(\frac{x-y}{\gamma} - \alpha y) \\
&\leq Lip(F)(\frac{\varepsilon}{2\gamma} + \alpha|y|)
\end{aligned}$$

$$\frac{\eta}{2T^2} \leq Lip(F)\frac{\varepsilon}{2\gamma}$$

We choose $\frac{\eta}{T^2} > Lip(F)\frac{\varepsilon}{\gamma} \Rightarrow t = 0 \ or \ s = 0.$

Step 3 : $t = 0$ **or** $s = 0$

Two cases are possible : either $t = 0$ or $s = 0$. Both are similar and we only focus on one which is $t = 0$.

As

$$\frac{|x-y|^2}{2\gamma} + \frac{|t-s|^2}{2\delta} \leq C$$

$$\begin{aligned} 0 < \frac{M_\eta}{2} < M_{\alpha,\eta,\gamma,\delta} &\leq X_0(x) - X_0(y) + Cs - \frac{|x-y|^2}{2\gamma} \\ &\leq Lip(X_0)|x-y| + C|t-s| - \frac{|x-y|^2}{2\gamma} \\ &\leq C'(\sqrt{\gamma} + \sqrt{\delta} + \delta) \end{aligned}$$

Step 4 : Conclusion

$$\begin{aligned} \hat{M}_{\alpha,\eta,\gamma,\delta} &= \sup_{\substack{x=y \\ t=s}} X^\varepsilon(x,t) - X^0(y,s) - \frac{|x-y|^2}{2\gamma} - \frac{|t-s|^2}{2\delta} - \alpha\frac{y^2}{2} - \frac{\eta}{T-t} \\ &= \sup_{\substack{x\in\mathbb{R} \\ 0\leq t\leq T}} X^\varepsilon(x,t) - X^0(x,t) - \alpha\frac{x^2}{2} - \frac{\eta}{T-t} \\ &\leq \sup_{\substack{x,y\in\mathbb{R} \\ 0\leq t,s\leq T}} X^\varepsilon(x,t) - X^0(y,s) - \frac{|x-y|^2}{2\gamma} - \frac{|t-s|^2}{2\delta} - \alpha\frac{y^2}{2} - \frac{\eta}{T-t} \\ &\leq C'(\sqrt{\gamma} + \sqrt{\delta}) \end{aligned}$$

From where

$$\begin{aligned} X^\varepsilon(x,t) - X^0(x,t) &\leq \alpha\frac{x^2}{2} - \frac{\eta}{T-t} + C'(\sqrt{\gamma} + \sqrt{\delta}) \\ &\leq \frac{T^2}{T-t} Lip(F)\frac{\varepsilon}{\gamma} + C'(\sqrt{\gamma} + \sqrt{\delta}) \\ &\leq TLip(F)\frac{\varepsilon}{\gamma} + C'\gamma \\ &\leq [C' + TLip(F)]\sqrt{\varepsilon} \end{aligned}$$

Note that we select $\gamma = \sqrt{\varepsilon}$ □

4.3 Equivalence with the LWR model

Proposition 4.10 ((R. Monneau) (Formal) PDE for the macroscopic first order model)**.** *Assume (A1), (A2) and (A3). Assume that X^0 satisfies the HJ equation (1.1.4). If the vehicles density ρ is defined such that*

$$\rho(x,t) = \frac{1}{X_n^0}, \quad \textit{with} \quad x := X^0(n,t), \tag{1.4.19}$$

then ρ solves the conservation law (1.2.6).

Proof (Formal) We assume that $X(.,t)$ is invertible and $X^{-1}(.,t)$ its reciprocal function, which leads to

$$\rho(x,t) = \frac{1}{X_n(n,t)} = \frac{1}{X_n(X^{-1}(.,t)(x),t)} = \partial_x X^{-1}(.,t)(x)$$

and

$$\rho_t(t,x) = \partial_x(\partial_t X^{-1}(.,t)(x))$$

Let's calculate $\partial_t X^{-1}(.,t)(x)$.
We differentiate $x = X(n,t) = X(X^{-1}(.,t)(x),t)$ with respect to t, we get

$$\partial_t X^{-1}(.,t)(x) = -\frac{X_t}{X_y}. \tag{1.4.20}$$

We set

$$F\left(\frac{1}{\rho}\right) =: V(\rho)$$

Combining previous equations, we get

$$\partial_t X^{-1}(.,t)(x) = -\rho V(\rho)(x,t)$$

which leads to

$$\partial_t \rho(t,x) = \partial_x(-\rho V(\rho)(x,t))$$

Thus we get the result

$$\rho_t + (\rho V(\rho))_x = 0$$

□

5 Delayed first order model

In this part, we will focus on the delayed model (1.1.2). As before, the function F represents the speed function and it satisfies the previous assumptions (A1) and (A2) i.e. we assume that F is non-decreasing on its first variable and it is Lipschitz continuous.

5.1 Comparison principle

We consider $(x_i)_{i\in\mathbb{Z}}$ solution of the previous system of ODEs (1.1.2) over $[-\tau,+\infty)$. We assume that the $(x_i)_i$ are also defined for $t \in [-2\tau,-\tau]$ with time delay $\tau > 0$ such that :

$$x_i(s) = x_i(-\tau), \quad \text{for all} \quad i \in \mathbb{Z}, \quad s \in [-2\tau,-\tau].$$

This condition gives necessary information about initial data due to the delay time τ.

We also assume that F satisfies (which can always be done, up to rescale x_i and t :

$$0 \le F' \le 1 \quad \text{and} \quad F \in C^1(\mathbb{R}) \cap L^\infty(\mathbb{R}) \tag{1.5.21}$$

Proposition 5.1 ((R. Monneau) Strict comparison principle)**.** *Assume (1.5.21). Let us consider $(x_i)_i$ and $(y_i)_i$ two solutions of (1.1.2) over $[-\tau,+\infty)$. Let us define for any $i \in \mathbb{Z}$ and any $t \ge 0$:*

$$d_i(t) := x_i(t) - y_i(t)$$

Assume there exists a constant $\delta > 0$ and a positive and non-decreasing function $\rho : \mathbb{R} \to \mathbb{R}$ satisfying

$$\rho(\tau)\tau' < 1 - \frac{1}{\rho(\tau')}. \tag{1.5.22}$$

If we have

$$(1)_0^\rho \qquad 0 < \delta \le d_i(s-\tau') \le \rho(\tau')d_i(s), \quad \textit{for all} \quad i \in \mathbb{Z}, \quad \tau' \in [0,\tau], \quad s \in [-\tau,0]$$

and

$$(2)_0^\rho \qquad \dot{d}_i(s) \geq -\rho(\tau) d_i(s), \quad \textit{for all} \quad i \in \mathbb{Z}, \quad s \in [-\tau, 0]$$

Then we have

$$0 < \delta \leq d_i(t), \quad \textit{for all} \quad i \in \mathbb{Z}, \quad t \geq 0$$

Remark 5.2. *Taking the limit for $\delta \to 0$, we can recover a (non strict) comparison principle.*

Proof We argue by contradiction. Assume that there exists $t_0 > 0$ such that $(1)_{t_0}^\rho$ is not true. Let $t^* \geq 0$ the last point such that $(1)_{t^*}^\rho$ holds true, that is :

$$(1)_{t^*}^\rho \qquad 0 < \delta \leq d_i(s - \tau') \leq \rho(\tau') d_i(s), \quad \text{for all} \quad i \in \mathbb{Z}, \quad \tau' \in [0, \tau], \quad s \in [-\tau, t^*]$$

Let $\varepsilon > 0$ and choose $t_\varepsilon \in (t_*, t_* + \varepsilon)$. We have that

$$d_i(t_\varepsilon - \tau') > \rho(\tau') d_i(t_\varepsilon), \quad \text{for all} \quad i \in \mathbb{Z}, \quad \tau' \in [0, \tau].$$

Step 1 : $(1)_{t^*}^\rho \Longrightarrow (2)_{t^*}^\rho$
We set for any $i \in \mathbb{Z}$ and any $s \geq -\tau$:

$$a_i(s) = (y_{i+1} - y_i)(s - \tau)$$

From $(1)_{t^*}^\rho$ we have for any $-\tau \leq s \leq t^*$:

$$\begin{aligned} \dot{d}_i(s) &= F\left(a_i(s) + (d_{i+1} - d_i)(s - \tau)\right) - F(a_i(s)) \\ &= F'(\xi_i(s)) \left\{(d_{i+1} - d_i)(s - \tau)\right\} \\ &\geq -d_i(s - \tau) \end{aligned}$$

where we have used that (1.5.21) in the last line.

We deduce from $(1)_{t^*}^\rho$ that

$$(2)_{t^*}^\rho \qquad \dot{d}_i(s) \geq -\rho(\tau) d_i(s), \quad \text{for all} \quad i \in \mathbb{Z}, \quad s \in [-\tau, t^*]$$

Step 2 : $(1)_{t^*}^\rho \cup (2)_{t^*}^\rho \Longrightarrow (1)_{t^*}^{\tilde{\rho}}$
Let $s \in [0, t^*]$. For any $\tau' \in [0, \tau)$, we have that :

$$\begin{aligned} d_i(s - \tau') - d_i(s) &= -\int_{s-\tau'}^{s} \dot{d}_i(t) dt \\ &\leq \rho(\tau) \int_{s-\tau'}^{s} d_i(t) dt \\ &\leq \rho(\tau) \int_{s-\tau'}^{s} \rho(s - t) d_i(s) dt \\ &\leq \rho(\tau) d_i(s) \int_0^{\tau'} d\bar{\tau} \rho(\bar{\tau}) \end{aligned}$$

where we have used $(2)_{t^*}^\rho$ in the second line, and $(1)_{t^*}^\rho$ in the third line after an appropriate shift of variable.

We get that

$$(1)_{t^*}^{\tilde{\rho}} \qquad d_i(s - \tau') \leq \tilde{\rho}(\tau') d_i(s), \quad \text{for all} \quad i \in \mathbb{Z}, \quad \tau' \in [0, \tau], \quad s \in [0, t^*]$$

where we defined

$$\tilde{\rho}(\tau') := 1 + \rho(\tau) \int_0^{\tau'} d\bar{\tau}\rho(\bar{\tau}) \tag{1.5.23}$$

Step 3 : $\rho(\tau') > \tilde{\rho}(\tau')$
Since ρ is monotone, it is obvious that

$$\tilde{\rho}(\tau') \leq 1 + \rho(\tau)\rho(\tau')\tau'$$

According to the condition (1.5.22), we get the result

$$\rho(\tau') > \tilde{\rho}(\tau'), \quad \text{for} \quad \tau' \in [0, \tau]. \tag{1.5.24}$$

Step 4 : conclusion
It is obvious to check that d_i is Lipschitz and that $Lip(d_i) \leq 2$.

From $(1)^{\tilde{\rho}}_{t^*}$, we obtain that :

$$\begin{aligned} d_i(t_\varepsilon - \tau') &\leq d_i(t^* - \tau') + 2\varepsilon \\ &\leq \tilde{\rho}(\tau')d_i(t^*) + 2\varepsilon \\ &\leq \tilde{\rho}(\tau')d_i(t_\varepsilon) + 2\varepsilon(1 + \tilde{\rho}(\tau')) \end{aligned}$$

Notice that $d_i(t_\varepsilon) > 0$. Indeed we have that

$$\begin{aligned} d_i(t_\varepsilon) &\geq d_i(t^*) - 2\varepsilon \\ &\geq \bar{\delta}e^{-\rho(\tau)t^*} - 2\varepsilon > 0 \end{aligned}$$

where we use $(2)^{\rho}_{t^*}$ and we choose ε such that :

$$\varepsilon < \frac{\bar{\delta}}{2}e^{-\rho(\tau)t^*} =: \varepsilon_1$$

According to (1.5.24) and up to choose ε such that

$$\varepsilon \leq \frac{\bar{\delta}}{2}e^{-\rho(\tau)t^*}\frac{\rho(\tau') - \tilde{\rho}(\tau')}{1 + \rho(\tau')} =: \varepsilon_2$$

we can easily show that

$$\tilde{\rho}(\tau')d_i(t_\varepsilon) + 2\varepsilon(1 + \tilde{\rho}(\tau')) \leq \rho(\tau')d_i(t_\varepsilon)$$

Then for $\varepsilon \leq \min\{\varepsilon_1, \varepsilon_2\}$ (it is obvious to check that $\varepsilon_1 > \varepsilon_2$), we get that

$$d_i(t_\varepsilon - \tau') \leq \rho(\tau')d_i(t_\varepsilon)$$

This ends the proof because $(1)^{\rho}_{t^*}$ is still true at $t_\varepsilon > t^*$ for ε small enough. □

Corollary 5.3 ((R. Monneau) Conservation of initial order)**.** *Let us consider $(y_i)_{i\in\mathbb{Z}}$ solution of (1.1.2) over $[-\tau, +\infty)$. Let us define for any $i \in \mathbb{Z}$ and any $t \geq 0$:*

$$d_i(t) := y_{i+1}(t) - y_i(t)$$

If there exists a constant $\delta > 0$ and a positive and non-decreasing function $\rho : \mathbb{R} \to \mathbb{R}$ satisfying (1.5.22) such that $(1)^{\rho}_0$ and $(2)^{\rho}_0$ hold true,

Then we have that :

$$y_{i+1}(t) \geq y_i(t), \quad \text{for all} \quad t \geq 0$$

Proof We apply the previous theorem for $x_i = y_{i+1}$ and then the proof is direct. □

Remark 5.4 (Traffic interpretation of comparison principle)**.** *The conditions* $(1)_0^\rho$ *and* $(2)_0^\rho$ *have easy interpretations in terms of traffic. We recall that the comparison principle leads to the conservation of initial order of vehicles. Due to the time delay* $\tau > 0$*, we need to control the vehicle trajectories on a wider initial time set. Precisely, we need the speeds and the accelerations not to be too high with respect to initial spacings and the distance traveled by vehicles during a time period* τ*. By the way, the condition on function* ρ *implies that (under the normalization of function* F*)*

$$\tau < \frac{1}{e}.$$

This condition is related to stability results that can be found in traffic literature.

5.2 Convergence

Let us consider that

$$X^\varepsilon(y,t) := \varepsilon x_{\lfloor \frac{y}{\varepsilon} \rfloor}(\frac{t}{\varepsilon})$$

The idea is to show that

$$X^\varepsilon(y,t) \to X(y,t) \quad \text{for} \quad \varepsilon \to 0$$

with X solution of

$$X_t = F(X_y).$$

Moreover we have that X^ε is solution of

$$X_t^\varepsilon(y, t+\varepsilon\tau) = F\left(\frac{X^\varepsilon(y+\varepsilon,t) - X^\varepsilon(y,t)}{\varepsilon}\right) \tag{1.5.25}$$

Proposition 5.5 ((R. Monneau) Convergence to the viscosity solution)**.** *Consider* X^0 *the unique solution of (1.5.25), checking the assumptions (A1), (A2) and (A3). If the function* X^ε *is defined as*

$$X^\varepsilon : \mathbb{R} \times [0,+\infty) \to \mathbb{R}$$
$$(y,t) \mapsto \varepsilon x_{\lfloor \frac{y}{\varepsilon} \rfloor}\left(\frac{t}{\varepsilon}\right)$$

With $(x_i)_{i\in\mathbb{Z}}$ *solution of (1.1.2).*

Then for all compact set $\mathcal{K} \subset \mathbb{R} \times [0,+\infty)$*,* X^ε *converges uniformly to* X^0 *on* $\mathcal{K}$ *when* $\varepsilon \to 0$*, i.e.*

$$|X^\varepsilon - X^0|_{L^\infty(\mathcal{K})} \underset{\varepsilon\to 0}{\longrightarrow} 0$$

Proof **Step 1 : estimates**
Let us consider the initial conditions $X^\varepsilon(y,s)$ with $-\varepsilon\tau \le s \le 0$ or on the semi-infinite set $s \le 0$. We want to get $X^\varepsilon(y,s)$ bounded for $s \le 0$ in order to avoid infinite propagation speeds or collision. For the time gradient X_t^ε the problem is quite simple because the function F is assumed to be bounded itself ($0 \le F \le 1$). For the space gradient, we have that

$$x_{i+1}(s) - x_i(s) = \frac{X^\varepsilon(y+\varepsilon, s+\varepsilon\tau) - X^\varepsilon(y, s+\varepsilon\tau)}{\varepsilon}$$

We assume that X^ε is 1-periodic according to its first variable such that :

$$X^\varepsilon(y+1,t) = X^\varepsilon(y,t) + L \tag{1.5.26}$$

Then from $0 \leq X_t^\varepsilon \leq 1$ we get that $0 \leq X^\varepsilon(0,t) \leq t$. By generalizing for any y, we obtain what follows :

$$L\lfloor y \rfloor \leq t + L(1 + \lfloor y \rfloor)$$

As $y - 1 \leq \lfloor y \rfloor \leq y$, we finally get that X^ε admits ε-independent bounds.

$$L(y-1) \leq X^\varepsilon(y,t) \leq t + L(y+1) \tag{1.5.27}$$

Let us consider the upper semi-relaxed enveloppe $\bar{X}$ of X^ε defined such that :

$$\begin{aligned} \bar{X}(y,t) &:= \limsup_{\varepsilon \to 0}{}^* X^\varepsilon(y,t) \\ &= \limsup_{(y',t',\varepsilon) \to (y,t,0)} X^\varepsilon(y',t') \end{aligned}$$

In the next step, we prove using a contradiction that $\bar{X}$ is a viscosity subsolution of (1.5.25).

Step 2 : $\bar{X}$ subsolution

Let us assume that $\bar{X}$ is not a viscosity subsolution of (1.5.25). That means that there exists a test function φ smooth enough and defined such that :

$$\varphi_t > F(\varphi_y) \quad \text{at} \quad P_0 = (y_0, t_0) \tag{1.5.28}$$

Up to modify φ, we can assume that on $\left(B_{\frac{r}{2}}(P_0)\right)^C$ we have that

$$\varphi - \bar{X} \geq 2\eta > 0$$

Where for any $r > 0$, we define $B_r(P_0)$ such as :

$$B_r(P_0) := [y_0 - r, y_0 + r] \times [t_0 - r, t_0 + r]$$

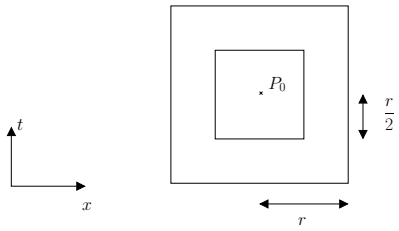

FIGURE 1.1 – Illustration of the set $B_r(P_0)$

From where we get that

$$\begin{cases} \varphi - X^\varepsilon \geq \eta > 0 \quad \text{on} \quad \left(B_{\frac{r}{2}}(P_0)\right)^C \\ (\varphi - X^\varepsilon)(P_0) < \dfrac{\eta}{2} \end{cases}$$

Let us set

$$M_\varepsilon = \inf_{B_r(P_0)} (\varphi - X^\varepsilon) \leq (\varphi - X^\varepsilon)(P_0) < \frac{\eta}{2}$$

We assume that M_ε is reached at $P_\varepsilon = (y_\varepsilon, t_\varepsilon) \in B_{\frac{r}{2}}(P_0)$ i.e.

$$M_\varepsilon = (\varphi - X^\varepsilon)(P_\varepsilon)$$

We can easily prove that

$$\begin{cases} M_\varepsilon \to 0 \\ P_\varepsilon \to P_0 \end{cases}, \quad \text{for} \quad \varepsilon \to 0 \tag{1.5.29}$$

because of $\varphi - \bar{X} > 0$ except at P_0.

Let us consider $\varphi^\varepsilon := \varphi - M_\varepsilon$ such that :

$$\begin{cases} \varphi^\varepsilon = \varphi - M_\varepsilon \geq X^\varepsilon & \text{on} \quad B_r(P_0) \\ \varphi^\varepsilon = X^\varepsilon & \text{at} \quad P_\varepsilon \in B_{\frac{r}{2}}(P_0) \end{cases} \tag{1.5.30}$$

Up to decrease the value of r, we can assume that $\forall \theta > 0$ we have what follows :

$$\varphi_t^\varepsilon \geq \theta + F(\varphi_y^\varepsilon) \quad \text{on} \quad B_r(P_0) \tag{1.5.31}$$

Notice that by abuse of notation, we replace φ^ε by φ. We have that :

$$\begin{aligned} \varphi_t^\varepsilon(y, t+\varepsilon\tau) - F\left(\frac{\varphi^\varepsilon(y+\varepsilon,t) - \varphi^\varepsilon(y,t)}{\varepsilon}\right) &= \varphi_t(y,t) - F(\varphi_y(y,t)) \\ &+ \varphi_t(y, t+\varepsilon\tau) - \varphi_t(y,t) \\ &- \left(F\left(\frac{\varphi(y+\varepsilon,t) - \varphi(y,t)}{\varepsilon}\right) - F(\varphi_y(y,t))\right) \end{aligned}$$

As we obviously have that $\varphi_t(y, t+\varepsilon\tau) - \varphi_t(y,t) = o_\varepsilon(1)$ and $\varphi(y+\varepsilon,t) - \varphi(y,t) = o_\varepsilon(1)$, using the regularity of F, we get that :

$$\varphi_t^\varepsilon(y, t+\varepsilon\tau) - F\left(\frac{\varphi^\varepsilon(y+\varepsilon,t) - \varphi^\varepsilon(y,t)}{\varepsilon}\right) = \varphi_t(y,t) - F(\varphi_y(y,t)) + o_\varepsilon(1)$$

We assume that $\varphi_t(y,t) - F(\varphi_y(y,t)) \geq \theta > 0$. Up to choose ε small enough, we also get that $o_\varepsilon(1) \leq \theta/2$. From where we obtain that

$$\varphi_t^\varepsilon(y, t+\varepsilon\tau) - F\left(\frac{\varphi^\varepsilon(y+\varepsilon,t) - \varphi^\varepsilon(y,t)}{\varepsilon}\right) \geq \frac{\theta}{2} > 0 \quad \text{on} \quad b_{\frac{r}{2}}(P_0)$$

We could notice that φ^ε is then a strict supersolution and X^ε a solution of the same equation (1.5.25).

Then we have that

$$X^\varepsilon(y+\varepsilon,t) \leq \varphi^\varepsilon(y+\varepsilon,t) \quad \text{on} \quad B_{r/2}(P_0)$$

And

$$X^\varepsilon(y,t) = \varphi^\varepsilon(y,t) \quad \text{at} \quad P_\varepsilon \in B_{r/2}(P_0)$$

From where using the fact that F is non-decreasing on its first argument, we deduce that

$$F\left(\frac{X^\varepsilon(y+\varepsilon,t) - X^\varepsilon(y,t)}{\varepsilon}\right) \leq F\left(\frac{\varphi^\varepsilon(y+\varepsilon,t) - \varphi^\varepsilon(y,t)}{\varepsilon}\right)$$

If we assume that $X^\varepsilon(y, t+\varepsilon\tau) \geq \varphi_t^\varepsilon(y, t+\varepsilon\tau)$ then we get the contradiction :

$$\begin{aligned} 0 = X_t^\varepsilon(y, t+\varepsilon\tau) - F\left(\frac{X^\varepsilon(y+\varepsilon,t) - X^\varepsilon(y,t)}{\varepsilon}\right) &\geq \varphi_t^\varepsilon(y, t+\varepsilon\tau) - F\left(\frac{\varphi^\varepsilon(y+\varepsilon,t) - \varphi^\varepsilon(y,t)}{\varepsilon}\right) \\ &\geq \frac{\theta}{2} > 0. \end{aligned}$$

Let us consider

$$d_i(t) = \frac{\varphi^\varepsilon(i\varepsilon, \varepsilon t) - X^\varepsilon(i\varepsilon, \varepsilon t)}{\varepsilon}$$

As we have that

$$d_i(t+\tau) = d_i(t) + \int_0^\tau ds\ \dot{d}_i(s)$$

Then using the fact that X^ε is solution of (1.5.25) with F such that $0 \leq F \leq 1$ and the fact that φ^ε is as smooth as we want, we get that

$$|d_i(t+\tau) - d_i(t)| \leq C\tau$$

Moreover as we have that $\inf_{B_r(P_0)\setminus B_{r/2}(P_0)} (\varphi^\varepsilon - X^\varepsilon) \geq \frac{\eta}{2}$, we finally get that

$$d_i(t) \geq \frac{\eta}{2\varepsilon}$$

From where we deduce that

$$d_i(t-\tau) \leq \rho d_i(t) \quad \text{with} \quad \rho = 1 + \varepsilon\tau$$

We notice that ρ is as close of 1 as we want it. We then could apply the comparison principle and we get :

$$d_i(t) = \frac{\varphi^\varepsilon - X^\varepsilon}{\varepsilon} \geq \frac{\eta}{2\varepsilon} > 0, \quad \text{for all} \quad t > 0$$

this is in contradiction with the fact that $\varphi^\varepsilon = X^\varepsilon$ at P_ε.

Step 3 : Conclusion

We can similarly prove that $\underline{X}$ is a supersolution of (1.5.25). Then the comparison principle leads to $\underline{X} \geq \overline{X}$. But by construction, we have that $\underline{X} \leq \overline{X}$. Then we finally get that :

$$\underline{X} = \overline{X} = X$$

□

5.3 Error estimate

Let us consider the following equation :

$$\begin{cases} X_t^\varepsilon(y,t) = F\left(\dfrac{X^\varepsilon(y+\varepsilon,t) - X^\varepsilon(y,t)}{\varepsilon}\right) \\ X^\varepsilon(y,0) = X_0(y) \end{cases} \tag{1.5.32}$$

Theorem 5.6 ((R. Monneau) General error estimate)**.** *If $\tilde{X}^\varepsilon$ is a general solution of equation (1.5.32) and if X^0 is the unique viscosity solution of (1.1.4), then we have*

$$|\tilde{X}^\varepsilon(y,t) - X^0(y,t)| \leq C_T\sqrt{\varepsilon}$$

for $y \in \mathbb{R},\ t \in [0,T]$.

Corollary 5.7 ((R. Monneau) Particular error estimate)**.** *If $X^\varepsilon(y,t) = \varepsilon x_{\lfloor \frac{y}{\varepsilon} \rfloor}(\frac{t}{\varepsilon})$ is a particular solution of equation (1.5.32)and if X^0 is the unique viscosity solution of (1.1.4), then we have*

$$|X^\varepsilon(y,t) - X^0(y,t)| \leq C_T\sqrt{\varepsilon}$$

for $y \in \mathbb{R},\ t \in [0,T]$.

Proof **Step 0 : Preliminary**
Let us consider that X^0 solves the HJ equation (1.1.4) and X^ε defined such as $X^\varepsilon(y,t) = \varepsilon x_{\lfloor \frac{y}{\varepsilon} \rfloor}\left(\frac{t}{\varepsilon}\right)$ solves the ε-level PDE (1.5.32).

Consider $T > 0$ and let us set the following supremum, considering variables duplication and penalization as follows :

$$M_{\eta,\gamma,\delta} = \sup_{\substack{x,y\in\mathbb{R} \\ 0\leq t,s\leq T}} X^\varepsilon(x,t) - X^0(y,s) - \frac{|x-y|^2}{2\gamma} - \frac{|t-s|^2}{2\delta} - \frac{\eta}{T-t}$$

Where $\eta, \gamma, \delta > 0$. Let us assume that the supremum $M_{\eta,\gamma,\delta}$ is reached for a certain set of the variables denoted by (x^*, y^*, t^*, s^*). For sake of clarity, we will drop out the stars in the notations. Thus let us consider that (with the abuse of notation)

$$M_{\eta,\gamma,\delta} = X^\varepsilon(x,t) - X^0(y,s) - \frac{|x-y|^2}{2\gamma} - \frac{|t-s|^2}{2\delta} - \frac{\eta}{T-t}$$

Step 1 : viscosity inequalities
We have that

$$X^\varepsilon_t(x,t) = \frac{t-s}{\delta} + \frac{\eta}{(T-t)^2} = F\left(\frac{X^\varepsilon(y+\varepsilon,t) - X^\varepsilon(y,t)}{\varepsilon}\right)$$

Let us set

$$\psi(x,t) = \frac{|x-y|^2}{2\gamma} + \frac{|t-s|^2}{2\delta} + \frac{\eta}{T-t}$$

We can easily prove that ψ is a strict supersolution of the equation (1.1.4) (which is also satisfied by X^0) i.e. we can find a real $\theta > 0$ such that we get what follows :

$$\psi_t \geq F(\psi_y) + \theta \quad \text{at} \quad P(x,t) \tag{1.5.33}$$

Indeed we have that at the point $P = (x,t)$

$$\begin{aligned} F\left(\frac{\psi(x+\varepsilon,t-\tau\varepsilon) - \psi(x,t-\tau\varepsilon)}{\varepsilon}\right) &= F\left(\frac{|x+\varepsilon-y|^2 - |x-y|^2}{2\gamma\varepsilon}\right) \\ &= F\left(\frac{x-y}{\delta} + \frac{\varepsilon}{2\gamma}\right) \\ &\geq F\left(\frac{x-y}{\delta}\right) + Lip(F)\frac{\varepsilon}{2\gamma} \end{aligned}$$

Thus we get the strict inequality at $P = (x,t)$

$$\psi_t = \frac{t-s}{\delta} + \frac{\eta}{(T-t)^2} \geq F\left(\frac{x-y}{\gamma}\right) + \theta$$

with $\theta = \frac{\eta}{T^2} - \frac{Lip(F)\varepsilon}{2\gamma} > 0$ if $\frac{\varepsilon}{\gamma} < \frac{2\eta}{Lip(F)T^2}$. Moreover this late inequality shows that η should be high enough in such a way the supremum could not be reached for t or $s = 0$ (see the discussion in the Proof of Error Estimate for the no-delay first order model).

Then if we consider the slightly different supremum $M = \sup_{x,t} X^\varepsilon(x,t) - \psi(x,t) - X^0(y,s)$ where $X^0(y,s)$ is seen as a constant, up to modify M by $\tilde{M} = \sup_{x,t} X^\varepsilon(x,t) - \psi(x,t)$, we

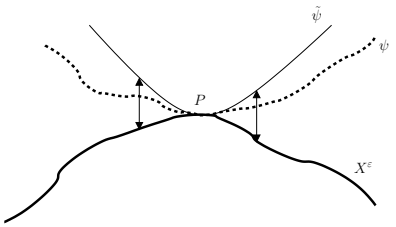

FIGURE 1.2 – Comparison of the solution with the test function

have that $\tilde{M} = 0$ for a certain couple $P = (x^*, t^*)$. We then can do the same reasoning than for Comparison Principle, up to modify ψ by $\tilde{\psi}$ such that $|X^\varepsilon - \tilde{\psi}| \geq C$ outside a square domain (as illustrated on Figure 5.3 below).

Step 2 : Conclusion

As usual, we set the following supremum

$$M_\gamma := \sup \left\{ u^\varepsilon(x,t) - u^0(y,s) - \frac{|x-y|^2}{2\gamma} - \frac{|t-s|^2}{2\delta} - \eta s \right\}$$

By the classical arguments, we can obtain the two viscosity inequalities, first one for u^ε and second one for u^0 :

$$\begin{cases} \dfrac{t-s}{\delta} \leq F_\varepsilon(u^\varepsilon) \\ \\ \dfrac{t-s}{\delta} - \eta \geq F\left(\dfrac{x-y}{\gamma}\right) \end{cases}$$

Then we get that

$$u^\varepsilon(x,t) \leq M_\gamma + u^0(y,s) + \frac{|x-y|^2}{2\gamma} + \frac{|t-s|^2}{2\delta} + \eta s =: \varphi(x,t)$$

and we assume that the equality is reached above at $P_0 = (x_0, t_0)$. We can thus write that

$$\varphi(x,t) = \varphi(P_0) + D_{x,t}\varphi(P_0)(P - P_0) + o(P - P_0)$$

It is also possible to get

$$u^0(y,s) \geq -M_\gamma + u^\varepsilon(x,t) - \frac{|x-y|^2}{2\gamma} - \frac{|t-s|^2}{2\delta} - \eta s =: \psi(y,s)$$

where we assume that the equality is obtained at $\bar{P}_0 = (y_0, s_0)$. That means in particular :

$$\psi(y,s) = \psi(\bar{P}_0) + D_{y,s}\psi(\bar{P}_0)(P - \bar{P}_0) + o(P - \bar{P}_0)$$

Notice that the space gradients are equal :

$$\begin{cases} D_{x,t}\varphi(P_0) = (p, \sigma) \\ \\ D_{y,s}\psi(\bar{P}_0) = (p, \bar{\sigma}) \end{cases}, \quad \text{with} \quad p = \frac{x_0 - y_0}{\gamma}, \quad \sigma = \frac{t_0 - s_0}{\delta}, \quad \bar{\sigma} = \sigma - \eta$$

Let

$$\begin{aligned} \bar{u}^0(y,s) &= u^0(y,s) + \eta(s - s_0) - \psi(\bar{P}_0) \\ &\geq p(y - y_0) + \sigma(s - s_0) + o\left(|y - y_0| + |s - s_0|\right) \end{aligned}$$

and

$$\begin{aligned}\bar{u}^\varepsilon(x,t) &= u^\varepsilon(x,t) - \varphi(P_0)\\ &\leq p(x-x_0) + \sigma(t-t_0) + o\left(|x-x_0| + |t-t_0|\right)\end{aligned}$$

Up to replace $\bar{P}_0$ by P_0, we can get that $\bar{u}^0$ and $\bar{u}^\varepsilon$ are locally comparable :

$$\begin{aligned}\bar{u}^0(x,t) &\geq p(x-x_0) + \sigma(t-t_0) + o(|x-x_0| + |t-t_0|)\\ &\geq \bar{u}^\varepsilon(x,t) + o(|x-x_0| + |t-t_0|).\end{aligned}$$

□

5.4 Extensions : speed-dependent and multi-anticipative models

Proposition 5.8 ((R. Monneau) Formal extensions of homogenization results)**.** *All the previous results could be easily extended to other classes of models say :*

- *The models taking into account (with a delay time) the speed of two consecutive vehicles which would be expressed under the following form*

$$\dot{x}_i(t+\tau) = F\left(x_{i+1}(t) - x_i(t), \dot{x}_i(t), \dot{x}_{i+1}(t)\right), \quad \text{for all} \quad i \in \mathbb{Z}, \quad t > 0 \qquad (1.5.34)$$

- *The models taking in account many leader vehicles (and even encompassing the previous case of a speed-dependence law)*

$$\dot{x}_i(t+\tau) = F\left((x_{i+j}(t) - x_i(t))_{j=1,\dots,n}, \dot{x}_i(t), (\dot{x}_{i+j}(t))_{j=1,\dots,n}\right), \quad \text{for all} \quad i \in \mathbb{Z}, \quad t > 0 \qquad (1.5.35)$$

Proof (R. Monneau) How to modify the propositions and adapt the corresponding proofs.
Case 1 : speed-dependent models (1.5.34)

- Comparison principle : if we have the following conditions

$$\begin{cases} 1 \geq F_a' \geq \rho(\tau) F_b' \geq 0 \\ \\ d_i(t-\tau) \leq \rho(\tau) d_i(t) \end{cases}$$

then we get

$$\begin{aligned}\dot{d}_i(t) &= F\left(d_{i+1}(t), \dot{x}_{i+1}(t)\right) - F\left(d_i(t), \dot{x}_i(t)\right)\\ &= F_a'(d_{i+1} - d_i) + F_b'(d_{i+1})\\ &\geq (F_a' - \rho(\tau)F_b')d_{i+1} - F_a' d_i\\ &\geq -d_i(t-\tau)\\ &\geq -\rho(\tau) d_i(t)\end{aligned}$$

- Convergence : we set $\bar{v} = \bar{F}(\bar{d}) = F(\bar{d}, \bar{v})$ which could be solved be finding a fixed point as $\bar{v} = v(\bar{d}) = \bar{F}(\bar{d})$ in the case of F invertible (possible if $0 < F_b' < 1$).

Case 2 : multi-anticipative models (1.5.35)

- Comparison principle : if we have the following conditions

$$\begin{cases} 1 \geq \sum_j (F_a')_j \geq \rho(\tau) F_b' \geq 0 \\ \\ d_i(t-\tau) \leq \rho(\tau) d_i(t) \end{cases}$$

then we get

$$\begin{aligned} \dot{d_i}(t) &= \sum_j (F_a')_j (d_{i+j} - d_i) + (F_b')_j (d_{i+j}) \\ &\geq \sum_j ((F_a')_j - \rho(\tau) F_b') d_{i+j} - (F_a')_j d_i \\ &\geq -d_i(t-\tau) \\ &\geq -\rho(\tau) d_i(t) \end{aligned}$$

- Convergence : we set $\bar{v} = \bar{F}(\bar{d}) = F(\bar{d}, 2\bar{d}, ..., n\bar{d}, \bar{v}, ..., \bar{v})$ which could be solved be finding a fixed point as $\bar{v} = v(\bar{d})$ in the case of F invertible (possible if $0 < \sum_j (F_b')_j < 1$).

□

6 Conclusion

This Chapter is dedicated to the rigorous passage from microscopic car-following models to hydrodynamics macroscopic models, thanks to a homogenization technique for Hamilton-Jacobi equations. The HJ equations are thus useful for the change of scale in the models. It is worth noticing that the re-scaled macroscopic model is the *Lagrangian formulation* of the Hamilton-Jacobi counterpart of the seminal LWR traffic flow model.

The material for non-delayed car-following models is somehow very classical for Hamilton-Jacobi equations. However, at our best knowledge, it is totally original for delayed microscopic models but it has to be deepened for sake of mathematical rigor. We first cast elementary results.

Let us give some comments on the results presented in this Chapter. It is noteworthy that the comparison principle which is absolutely necessary for the homogenization of Hamilton-Jacobi equations means that the vehicles have to stay ordered during the observed duration. It prevents us from considering overtaking maneuvers or multi-lanes behavior. However, one can think to a re-labeling of vehicles such that the vehicles stay artificially ordered. It imposes to keep track of previous and new labels. It has not been considered in this work.

Chapitre 2

Multi-anticipative car-following behaviour : macroscopic modeling

This chapter is extracted from a paper in collaboration with Jean-Patrick Lebacque and submitted in the Proceedings of TGF'13 Conference.

Sommaire

Abstract

In this work we will deal with a macroscopic model of multi-anticipative car-following behaviour i.e. driving demeanour taking into account many vehicles ahead. Some empirical studies have suggested that drivers not only react to the closest leader vehicle but also anticipate on traffic conditions further ahead. Using a recent mathematical result of homogenization for a general class of car-following models (and also available for multi-anticipative models), we will deeply investigate the effects of multi-anticipation at the microscopic level on the macroscopic traffic flow. To investigate multi-anticipation behaviour may be fundamental to understand better cooperative traffic flow dynamics.

1 Introduction

1.1 Motivation

Our motivation comes from the sky-rocketing development of new technologies in transportation leading to the multiplication of Intelligent Transportation Systems (ITS). More precisely we would like to assess the impact of cooperative systems on general traffic flow. Cooperative systems include vehicle-to-vehicle (V2V) or vehicle-to-infrastructure (V2I) communications, generally designated as V2X technologies. There is a fast growing literature about cooperative systems. The interested reader can refer for instance to [195] and references therein.

The fact that the observed headway between two consecutive vehicles is often strictly less than the reaction time of the drivers, suggests that drivers anticipate on more than one leader. Indeed, if not, the proportion of accidents should be dramatically increased. The multi-anticipation has been shown as a key element for the stabilization of traffic flow, above all in dense traffic situations.

However multi-anticipation behaviour has only been taken into consideration at a microscopic scale. Indeed such macroscopic models as the Payne-Whitham one only account for anticipation in time. The macroscopic issues encompass multi-lane traffic with lane changing and assignment but also multi-anticipation on each lane or the combination of those both processes. In classical approaches, the whole traffic is projected on a single line to simplify the problem in a one-dimensional framework.

1.2 Notations

Let x denotes the position and $t > 0$ the time. $x_i(t)$ refers to the trajectory of the vehicle $i \in \mathbb{Z}$. The speed and the acceleration of vehicle i are described by the first and second derivative of x_i w.r.t. time. Notice that we also introduce a time delay $T \geq 0$.

We assume that the vehicles are labelled according to a snapshot of a section of road from upstream to downstream (see Figure 2.1). Vehicle labels increase with x. Thus $(x_{i+1} - x_i)(t)$ is the spacing and $(\dot{x}_{i+1} - \dot{x}_i)(t)$ the relative speed at time t between vehicle i and its leader $(i+1)$. We also denote by $m \geq 1$ the total number of leaders that are considered by vehicle $i \in \mathbb{N}$.

At the macroscopic level, we denote respectively the density and the flow of vehicles at location x and time t as $\rho(x,t)$ and $Q(x,t)$.

1.3 Main results and organization of the paper

As a main result we describe a new macroscopic model that encompass multi-anticipative car-following behaviour that are classically taken into account only at the microscopic scale. Moreover our model is able to consider multi-lane dynamics.

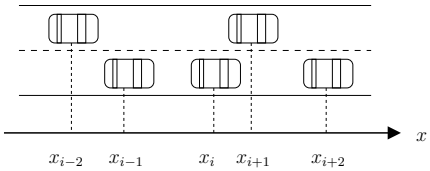

FIGURE 2.1 – Notations for the microscopic car-following models

The rest of the paper is organized as follows : we first recall some existing multi-anticipative car-following models in Section 2. We particularly highlight what we think to be the seminal form of such a model. In Section 3, we describe the formal mathematical result that allows us to pass from microscopic models to equivalent macroscopic ones. Our macro model is also described in Section 4. Finally we provide some numerical considerations in Section 5 before to discuss the results and to conclude.

2 Multi-anticipative traffic modelling : an introduction

Multi-anticipative models. The main existing multi-anticipative car-following models come from adaptations of classical car-following ones with a single leader vehicle. We recall below some examples. The interested reader could refer to [96] for references. We can quote for instance

- the model of Bexelius [26]

$$\ddot{x}_i(t+T) = \sum_{j=1}^{m} \alpha_j \left(\dot{x}_{i+j} - \dot{x}_i\right)(t)$$

extends the car-following model of Chandler *et al.* [52]

$$\ddot{x}_i(t+T) = \alpha \left(\dot{x}_{i+1}(t) - \dot{x}_i(t)\right).$$

We recall that the model of Chandler *et al.* is a specific case of the model of Gazis, Herman and Rothery

$$\ddot{x}_i(t+T) = \alpha \left(\dot{x}_i(t+T)\right)^p \frac{\dot{x}_{i+1}(t) - \dot{x}_i(t)}{\left(x_{i+1}(t) - x_i(t)\right)^l},$$

where we assume that $p = 0 = l$.

- Lenz *et al.* [179]

$$\ddot{x}_i(t+T) = \sum_{j=1}^{m} \alpha_j \left[V_e\left(\frac{x_{i+j}(t) - x_i(t)}{j}\right) - \dot{x}_i(t+T)\right]$$

extend the model of Bando *et al.* [14], yielding a second order multi-anticipative model

$$\ddot{x}_i(t+T) = \alpha \left[V_e(x_{i+1}(t) - x_i(t)) - \dot{x}_i(t+T)\right],$$

where V_e is the optimal velocity function given by

$$V_e(x) = \tanh(x-h) + \tanh(h), \quad \text{with} \quad h \text{ constant}.$$

- Hoogendoorn *et al.* [136] propose an extension of the model of Helly [127]

$$\ddot{x}_i(t+T) = \sum_{j=1}^{m_1} \alpha_j \left(\dot{x}_{i+j} - \dot{x}_i\right)(t) + \sum_{j=1}^{m_2} \beta_j \left[\left(x_{i+j} - x_i\right)(t) - S_0 - jT\dot{x}_i(t)\right], \quad (2.2.1)$$

  with two different number of considered leaders $m_1 \geq 1$ and $m_2 \geq 1$ according to either speed variations or headway variations.

- Treiber *et al.* [230] introduces the Human Driver Model (HDM) as an extension of his well-known Intelligent Driver Model (IDM) [228]. The HDM model reads as follows

$$\ddot{x}_i(t+T) = \ddot{x}_i^f(t) + \sum_{j=1}^{m} \ddot{x}_{i,j}^c(t)$$

  with $\ddot{x}_i^f$ (resp. $\ddot{x}_{i,j}^c$) the free acceleration (resp. the constrained acceleration) defined as

$$\begin{cases} \ddot{x}_i^f(t) = \alpha\left[1 - \left(\frac{\dot{x}_i(t)}{v_0}\right)^4\right], \\ \\ \ddot{x}_{i,j}^c(t) = -\alpha\left(S_0 + \dot{x}_i(t)\tau + \frac{\dot{x}_i(t)(\dot{x}_{i+j} - \dot{x}_i)(t)}{2\sqrt{\alpha\beta}}\right)^2 \left(\frac{1}{x_{i+j}(t) - x_i(t)}\right)^2 \end{cases}$$

  where

v_0	desirated velocity
α	maximal acceleration
β	comfort acceleration
S_0	minimal interdistance
τ	time headway

- Farhi *et al.* [96] describes a first order model that extends the Min-Plus car-following model. This model is described in Section 3. As it is based on algebra Min-Plus, it is easy to check its global properties.

Remark 2.1. *The additive form in the multi-anticipative models yields models which are easier to study analytically. But the minimum form expresses the fact that a driver will adapt its velocity (or equivalently its acceleration) according to the worst behaviour of all the considered leaders and thus offers more physical interpretation.*

Experimental results. In [136, 213], the model (2.2.1) is calibrated on real data and it fits best for $m_1 = 3$ and $m_2 = 1$, meaning that the drivers are more sensitive to speed variations than headway variations. It is also shown that the multi-anticipative models improves the representation of driving behaviour. However there is a high variance in driving behaviour which is not totally accounted for.

In many studies (for instance [195, 230] and references therein), platoon stability (on a single lane) is shown to decrease when the reaction time increases, and to increase when the spatial and/or temporal anticipation are increased.

3 Macroscopic model for multi-anticipative traffic.

3.1 First result in the Min-Plus algebra

First order multi-anticipative models can be viewed as high-viscosity approximation of second order models (such as the Frenkel-Kontorova model studied in [100]). For instance,

in [96] the model is a first order and based on a piecewise linear fundamental diagram (FD). The velocity is computed by taking the minimum of all constraints imposed by preceding vehicles. The model is expressed in the Min-Plus algebra as follows

$$x_i(t+1) = x_i(t) + \min_{1\leq j\leq m} (1+\lambda)^{m-1} \min_{v\in\mathcal{U}} \max_{w\in\mathcal{W}} \left[\alpha_{vw}\left(\frac{x_{i+j}(t)-x_i(t)}{j}\right)+\beta_{vw}\right] \tag{2.3.2}$$

where $\mathcal{U}$ and $\mathcal{W}$ are two finite sets of indices. The $\lambda \geq 0$ is a discount parameter favouring closer leaders over the farther ones.

The authors obtain semi-analytical results concerning the stability of the model and the existence of fixed points. These fixed points match invariant states for the macroscopic traffic flow.

Notice moreover that the simulation results in [96] show the smoothing effects of multi-anticipative driving on the macroscopic traffic flow.

3.2 Multi-anticipative first order models and Hamilton-Jacobi equation

One approach to micro-macro passage relies on the mathematical homogenization of car-following models into Hamilton-Jacobi equation.

Let us first consider the following first order multi-anticipative model

$$\dot{x}_i(t+T) = \max\left[0, V_{max} - \sum_{j=1}^{m} f\left(x_{i+j}(t)-x_i(t)\right)\right] \tag{2.3.3}$$

with $T \geq 0$, $m \geq 1$ fixed and $f : \mathbb{R}_+^* \mapsto \mathbb{R}_+$ which needs to be a non-negative and non-increasing function describing the speed-spacing relationship. Let us choose

$$f(r) = \beta \exp(-\gamma r), \quad \text{for any} \quad r > 0, \tag{2.3.4}$$

with β, $\gamma > 0$. This choice is mathematically convenient because if we set

$$F\left(\{x_k - x_i\}_{i+1\leq k\leq i+m}\right) := V_{max} - \sum_{j=1}^{m} f\left(x_{i+j}(t)-x_i(t)\right),$$

then we can check that $\dfrac{\partial F}{\partial x_k - x_i} \geq 0$, for any $k = \{i+1, ..., i+m\}$. Thus, it is possible to recover (at least formally) homogenization results.

Remark 3.1. *Notice that qualitatively this choice of an exponential speed-spacing fundamental diagram (FD) implies that the more the vehicles anticipate on their leaders, the lower their speeds and the higher their spacings. However one would expect that multi-anticipation allows shorter spacing and with high speeds.*

Remark 3.2 (Equivalence result)**.** *One can check that if we consider a piecewise linear speed-spacing relationship, then the model (2.3.3) can be approximated by the Min-Plus model (2.3.2).*

Let us consider the model (2.3.3). If we apply an unzooming procedure by introducing the rescaled position of vehicles as follows

$$X^\varepsilon(y,t) = \varepsilon x_{\lfloor \frac{y}{\varepsilon} \rfloor}\left(\frac{t}{\varepsilon}\right), \quad \text{for} \quad y \in \mathbb{R}, \quad t \in [0, +\infty) \tag{2.3.5}$$

where $\lfloor . \rfloor$ denotes the floor integer, then we can recover a Hamilton-Jacobi equation by homogenization when the scale factor ε goes down to zero :

$$\frac{\partial X^0}{\partial t} = \bar{V}\left(\frac{\partial X^0}{\partial n}, m\right) \tag{2.3.6}$$

with m the number of considered leaders and the (macroscopic) flow speed as follows

$$\bar{V}(r,m) = \max\left[0, V_{max} - \sum_{j=1}^{m} f(jr)\right].$$

The unknown $X^0(n,t)$ denotes the position of the vehicle labeled n at time t :

$$\frac{\partial X^0}{\partial t} = v \quad \text{and} \quad \frac{\partial X^0}{\partial n} = r,$$

where v and r describe respectively the speed and the spacing.

We recover the classical LWR model (standing for Lighthill, Whitham [184] and Richards [221]) in Lagrangian coordinates (n,t) that is

$$\begin{cases} \partial_t r + \partial_n v = 0, \\ v = \bar{V}(r,m). \end{cases} \tag{2.3.7}$$

We recall that the LWR model in Eulerian coordinates (t,x) expresses the conservation of vehicles on a section

$$\begin{cases} \partial_t \rho + \partial_x(\rho v) = 0, \\ v = V(\rho,m) := \bar{V}(1/\rho, m). \end{cases}$$

with ρ the density of vehicles and the *modified* speed-density fundamental diagram (FD) $V : (\rho,m) \mapsto V(\rho,m)$ which is non-negative and non-increasing w.r.t. ρ.

This homogenization result is fully described in [192]. Homogenization is a general technique which has been used for several different models involving interactions with a finite number of particles. The interested reader is referred to [100] and references therein.

3.3 General multi-lane traffic flow model with multi-anticipation

We consider a multi-lane road section and we consider the projection of vehicles on the spatial axis as in Figure 2.1. Assume that the traffic flow on such a section is composed of a mixture of multi-anticipative vehicles. The model (2.3.7) implies that low anticipation vehicles will be stuck behind high anticipation vehicles. In the case of multi-lane traffic such behaviour is precluded by the fact that vehicles can overtake each other.

Therefore let us denote by χ_j the fraction of j-anticipative vehicles, whatever the number of lanes. Then the traffic flow is the superposition of traffic of j-anticipative vehicles, i.e.

$$\chi = (\chi_j)_{j=1,\dots,m},$$

with $0 \leq \chi_j \leq 1$ for any $j = \{1,\dots,m\}$ and $\sum_{j=1}^{m} \chi_j = 1$. It is then obvious that the composition is advected with the traffic flow. We can express this concept using a model of the Generic Second Order Modelling (GSOM) familly as it has been introduced by

Lebacque *et al.* in [174]. The driver attribute is the composition χ. We get the following expression

$$\begin{cases} \partial_t \rho + \partial_x (\rho v) = 0, \\ v := \sum_{j=1}^{m} \chi_j V(\rho, j) = \sum_{j=1}^{m} \chi_j \bar{V}(1/\rho, j), \\ \partial_t(\rho\chi) + \partial_x(\rho\chi v) = 0. \end{cases} \tag{2.3.8}$$

Let us set

$$\bar{W}(\rho, \chi) := \sum_{j=1}^{m} \chi_j \bar{V}(1/\rho, j), \quad \text{and} \quad W(r, \chi) = \bar{W}(1/r, \chi) = \sum_{j=1}^{m} \chi_j \bar{V}(r, j)).$$

We can check that the third line in equation (2.3.8) could be rewritten as a simple advection equation

$$\partial_t \chi + v \partial_x \chi = 0.$$

As it has been already shown (see for instance [174]), the system (2.3.8) admits only two kinds of waves :

- kinematic waves (rarefaction or shock) for the vehicles density, similar to kinematic waves for the LWR model. Through such a wave, the composition of traffic χ is preserved but not the speed ;
- contact discontinuities for the composition of traffic. In this case, the wave velocity is equal to the speed of traffic v which is conserved through the wave.

In Lagrangian coordinates (t, n), with n the label of cars, the flux variable is v and the stock variable is the spacing $r = 1/\rho$. The model can be recast as :

$$\begin{cases} \partial_t r + \partial_n v = 0 \\ v = W(r, \chi) \\ \partial_t \chi = 0 \end{cases} \tag{2.3.9}$$

The model (2.3.8), (2.3.9) is new in the sense that there already exist some multilanes models such as the model of Greenberg, Klar and Rascle (see [174] and references therein) which belongs to the GSOM family. However to the best authors knowledge, there does not exists any macroscopic PDE model taking into consideration multi-anticipative behaviour in a multi-lane context.

4 Numerical approaches

To numerically solve the system (2.3.8), we can use classical GSOM methodologies [172, 174] that encompass :

- Godunov-like schemes for which we need to introduce finite time and space steps Δt, Δx_k that need to satisfy a CFL condition. Consider the following scheme

$$\begin{cases} \rho_k^{t+1} = \rho_k^t + \dfrac{\Delta t}{\Delta x_k} \left[q_k^t - q_{k+1}^t \right], \\ q_k^t := \min \left\{ \Delta_k \left(\rho_k^t, \chi_k^t \right), \Sigma_{k+1} \left(\rho_{k+1}^t, \chi_{k+1}^t \right) \right\}, \\ \rho_k^{t+1} \chi_k^{t+1} = \rho_k^t \chi_k^t + \dfrac{\Delta t}{\Delta x_k} \left[q_k^t \chi_k^t - q_{k+1}^t \chi_{k+1}^t \right] \end{cases} \tag{2.4.10}$$

where we have defined the supply and demand functions as in [164]

$$\Delta_k(\rho,\chi) = \max_{0\le\xi\le\rho}\left[\xi\bar{W}_k(\xi,\chi)\right], \quad \text{and} \quad \Sigma_k(\rho,\chi) = \max_{\xi\ge\rho}\left[\xi\bar{W}_k(\xi,\chi)\right]$$

and the (numerical) flow q_k^t as the minimum between downstream supply and upstream demand functions.

- variational formulation and dynamic programming techniques [68].
- particle methods in the Lagrangian framework (t,n). A standard way of obtaining these (refer to [172,174]) is to apply a Godunov scheme to (2.3.9). This is easy : the supply is simply v_{max}, the demand is W, because $r \mapsto W(r,\chi)$ is increasing. Since a cell can be associated to a packet of Δn vehicles having a total spacing r_n^t and tail position x_n^t, a simple car-following like model (2.4.11) is derived. Considering Lagrangian finite difference methods, we can either deal with a vectorial attribute χ or with an integer $j = 1,...,m$ with randomization of probability χ_j. We opt here for the first option. The resulting model is described hereafter :

$$\left|\begin{array}{l} x_n^{t+1} = x_n^t + \Delta t W\left(r_n^t, \chi_n^t\right) \\ r_n^t = \left(x_{n+1}^t - x_n^t\right)/\Delta n \\ \chi_n^{t+1} = \chi_n^t \end{array}\right. \tag{2.4.11}$$

The Lagrangian method (2.4.11) is more precise (less smoothing of waves) than (2.4.10) and easier to calculate (the demand being the speed).

4.1 Choice of the fundamental diagram

For this numerical example, we have used the speed-spacing function described in (2.3.4) that is

$$\bar{V}(r,m) = \max\left[0, V_{max} - \sum_{j=1}^{m}\beta\exp(-\gamma j r)\right]$$

with $\beta, \gamma > 0$. As we consider that those coefficients are strictly independent of the number of considered leaders $j \in \{1,...,m\}$, one can easily check that

$$\beta = V_{max}\exp\left(\gamma r_{min}\right)$$

where r_{min} is the minimal spacing between two consecutive vehicles. The maximal speed V_{max} is equal to 25 m/s and γr_{min} is fixed to 0.18 in order to ensure a proper critical density. The maximal number of considered leaders m is equal to 5.

Note that the fundamental diagrams plotted on Figure 2.2 are intended for a single lane. Then the higher the number of considered leaders, the higher the critical spacing (or equivalently the lower the critical density) per single lane.

4.2 Description of the use case

Let us consider a traffic flow on a multi-lane road section. Roughly speaking, assume that entering the section we have two distinct compositions of traffic : high anticipatory, then low anticipatory, then high anticipatory again (see Figure 2.3). The downstream supply is formulated in terms of speed, which is more convenient in the Lagrangian framework. The supply is assumed to drop in the middle of the considered period (from times $t = 250$ to $t = 2200$), generating a high-density wave propagating backwards.

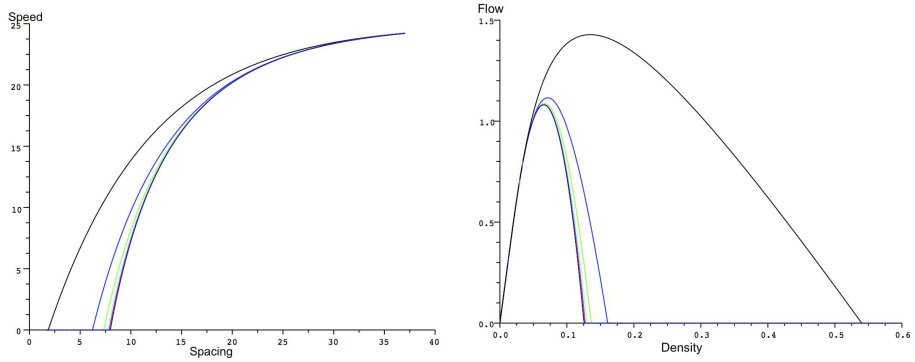

FIGURE 2.2 – Speed-spacing fundamental diagram $r \mapsto \bar{V}(r, m)$ (left) and Flow-density fundamental diagram $\rho \mapsto \rho V(\rho, m)$ (right) for different values of $m \in [1, 5]$. On left hand diagram, the increasing direction for values of m is from left to right. On the right hand diagram, it is the exact inverse, from right to left.

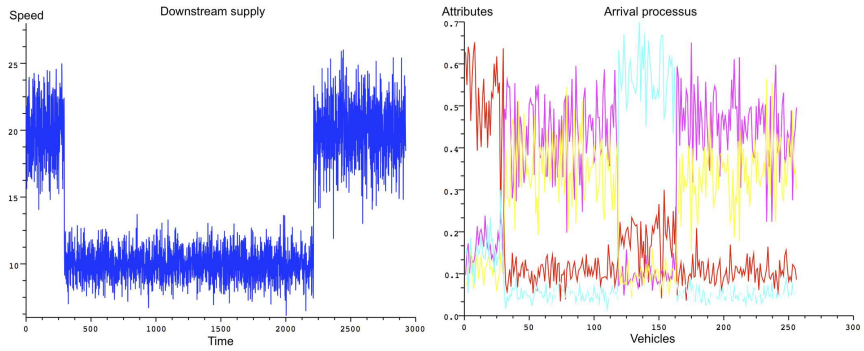

FIGURE 2.3 – Downstream supply value (left) and traffic composition attribute χ (right)

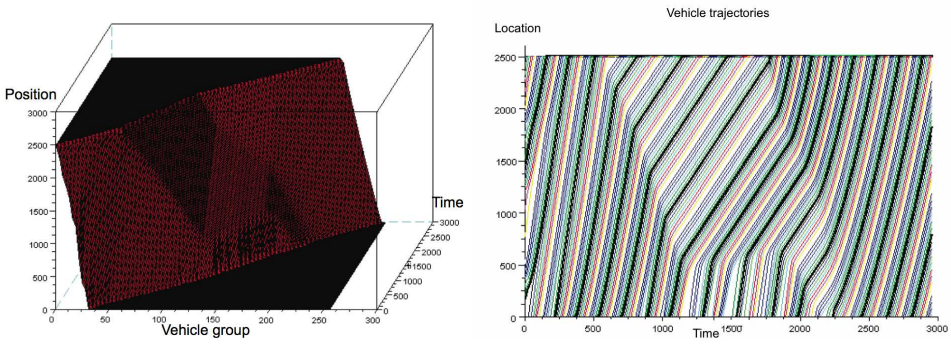

FIGURE 2.4 – Positions in Lagrangian framework (left) and Eulerian trajectories (right)

This shock wave interacts with the contact discontinuities carried by the incoming traffic (at times $t = 1000$ and $t = 1800$). Note that the increase of downstream supply at time $t = 2200$ generates also a rarefaction wave (see Figure 2.4).

This simple numerical example shows that the low anticipatory fraction of the traffic allows to reduce or annihilate the shock wave because drivers accept lower critical spacings. This effect result is strongly dependent on our choice of the speed-spacing relationship $\bar{V}$ which implies that less anticipative drivers drive faster, take more risks. The inclusion of stochastic effects [149] would show another effect : that multi-anticipation smoothens traffic.

5 Conclusion and future directions

Possible extensions include adding source terms for the equation of advection of the composition. This could account for the spatial variability of multi-anticipatory behaviour. See for instance [172]. Moreover our model should be tested on real measurement data. The main problem is the identification of instantaneous traffic composition χ as well the speed-spacing function parameters as it was done in [96].

Another study should be based on the analysis of individual trajectories to recover the results of previous studies which state that the multi-anticipative car-following models improve the representation of individual driving behaviour. While the existing experiments only take into account already congested situations, these work should extend the results by considering congested and also fluid traffic flow situations. Such a study could also confirm or infirm the impact of anticipatory behavior on the traffic (see Remark 3.1).

Deuxième partie

Modélisation du trafic routier sur jonction

Chapitre 3

A convergent scheme for Hamilton-Jacobi equations on a junction : application to traffic

This chapter is an adaptation of [69] written in collaboration with Régis Monneau and Jean-Patrick Lebacque and accepted for publication in *Numerische Mathematik*.

Sommaire

Abstract

In this paper, we consider first order Hamilton-Jacobi (HJ) equations posed on a "junction", that is to say the union of a finite number of half-lines with a unique common point. For this continuous HJ problem, we propose a finite difference scheme and prove two main results. As a first result, we show bounds on the discrete gradient and time derivative of the numerical solution. Our second result is the convergence (for a subsequence) of the numerical solution towards a viscosity solution of the continuous HJ problem, as the mesh size goes to zero. When the solution of the continuous HJ problem is unique, we recover the full convergence of the numerical solution. We apply this scheme to compute the densities of cars for a traffic model. We recover the well-known Godunov scheme outside the junction point and we give a numerical illustration.

1 Introduction

The main goal of this paper is to prove properties of a numerical scheme to solve Hamilton-Jacobi (HJ) equations posed on a junction. We also propose a traffic application that can be directly found in Section 4.

1.1 Setting of the PDE problem

In this subsection, we first define the junction, then the space of functions on the junction and finally the Hamilton-Jacobi equations. We follow [141].

The junction. Let us consider $N \geq 1$ different unit vectors $e_\alpha \in \mathbb{R}^2$ for $\alpha = 1, \dots, N$. We define the branches as the half-lines generated by these unit vectors

$$J_\alpha = [0, +\infty) e_\alpha \quad \text{and} \quad J_\alpha^* = J_\alpha \setminus \{0_{\mathbb{R}^2}\}, \quad \text{for all} \quad \alpha = 1, \dots, N,$$

and the whole *junction* (see Figure 3.1) as

$$J = \bigcup_{\alpha=1,\dots,N} J_\alpha.$$

The origin $y = 0_{\mathbb{R}^2}$ (we just call it "$y = 0$" in the following) is called the *junction point*. For a time $T > 0$, we also consider the time-space domain defined as

$$J_T = (0, T) \times J.$$

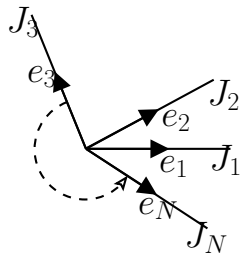

FIGURE 3.1 – Junction model

Space of test functions. For a function $u : J_T \to \mathbb{R}$, we denote by u^α the "restriction" of u to $(0, T) \times J_\alpha$ defined as follows for $x \geq 0$

$$u^\alpha(t, x) := u(t, x e_\alpha).$$

Then we define the natural space of functions on the junction :

$$C^1_*(J_T) = \left\{ u \in C(J_T), \quad u^\alpha \in C^1\left((0,T)\times[0,+\infty)\right) \quad \text{for} \quad \alpha = 1,\dots,N \right\}. \tag{3.1.1}$$

In particular for $u \in C^1_*(J_T)$ and $y = xe_\alpha$ with $x \geq 0$, we define

$$u_t(t,y) = u^\alpha_t(t,x) = \frac{\partial u^\alpha}{\partial t}(t,x) \quad \text{and} \quad u^\alpha_x(t,x) = \frac{\partial u^\alpha}{\partial x}(t,x).$$

HJ equation on the junction. We are interested in continuous functions $u : [0,T)\times J \to \mathbb{R}$ which are *viscosity solutions* (see Definition 5) on J_T of

$$\begin{cases} u^\alpha_t + H_\alpha(u^\alpha_x) = 0 & \text{on} \quad (0,T)\times(0,+\infty), \quad \text{for} \quad \alpha = 1,\dots,N, \\ \\ u^\beta =: u, \quad \text{for all} \quad \beta = 1,\dots,N \\ \\ u_t + \max\limits_{\beta=1,\dots,N} H^-_\beta(u^\beta_x) = 0 \end{cases} \quad \text{on} \quad (0,T)\times\{0\}, \tag{3.1.2}$$

for functions H_α and H^-_α that will be defined below in assumption (A1).

We consider an initial condition

$$u^\alpha(0,x) = u^\alpha_0(x), \quad \text{with} \quad x \in [0,+\infty) \quad \text{for} \quad \alpha = 1,\dots,N. \tag{3.1.3}$$

We make the following assumptions :

(A0) **Initial data**

The initial data $u_0 := (u^\alpha_0)_\alpha$ is globally Lipschitz continuous on J, i.e. each associated u^α_0 is Lipschitz continuous on $[0,+\infty)$ and $u^\alpha_0(0) = u^\beta_0(0)$ for any $\alpha \neq \beta$.

(A1) **Hamiltonians**

For each $\alpha = 1,...,N$,

- we consider functions $H_\alpha \in C^1(\mathbb{R};\mathbb{R})$ which are coercive, i.e. $\lim\limits_{|p|\to+\infty} H_\alpha(p) = +\infty$;
- we assume that there exists a $p^\alpha_0 \in \mathbb{R}$ such that H_α is non-increasing on $(-\infty, p^\alpha_0]$ and non-decreasing on $[p^\alpha_0, +\infty)$, and we set :

$$H^-_\alpha(p) = \begin{cases} H_\alpha(p) & \text{for} \quad p \leq p^\alpha_0 \\ \\ H_\alpha(p^\alpha_0) & \text{for} \quad p \geq p^\alpha_0 \end{cases} \quad \text{and} \quad H^+_\alpha(p) = \begin{cases} H_\alpha(p^\alpha_0) & \text{for} \quad p \leq p^\alpha_0 \\ \\ H_\alpha(p) & \text{for} \quad p \geq p^\alpha_0 \end{cases} \tag{3.1.4}$$

  where H^-_α is non-increasing and H^+_α is non-decreasing.

Remark 1.1. *Assumption (A1) allows the Hamiltonians H_α to have plateaus, in particular at the minimum of H_α. In such a case the value p^α_0 is not unique.*

1.2 Presentation of the scheme

We denote by Δx the space step and by Δt the time step. We denote by $U^{\alpha,n}_i$ an approximation of $u^\alpha(n\Delta t, i\Delta x)$ for $n \in \mathbb{N}$, $i \in \mathbb{N}$, where α stands for the index of the considered branch.

We define the discrete space derivatives

$$p_{i,+}^{\alpha,n} := \frac{U_{i+1}^{\alpha,n} - U_i^{\alpha,n}}{\Delta x} \quad \text{and} \quad p_{i,-}^{\alpha,n} := \frac{U_i^{\alpha,n} - U_{i-1}^{\alpha,n}}{\Delta x}, \tag{3.1.5}$$

and similarly the discrete time derivative

$$W_i^{\alpha,n} := \frac{U_i^{\alpha,n+1} - U_i^{\alpha,n}}{\Delta t}. \tag{3.1.6}$$

Then we consider the following numerical scheme corresponding to the discretization of the HJ equation (3.1.2) for $n \geq 0$:

$$\begin{cases} \dfrac{U_i^{\alpha,n+1} - U_i^{\alpha,n}}{\Delta t} + \max\left\{H_\alpha^+(p_{i,-}^{\alpha,n}), H_\alpha^-(p_{i,+}^{\alpha,n})\right\} = 0, & \text{for} \quad i \geq 1, \quad \alpha = 1, \dots, N, \\ U_0^{\beta,n} =: U_0^n, \quad \text{for all} \quad \beta = 1, \dots, N \\ \dfrac{U_0^{n+1} - U_0^n}{\Delta t} + \max\limits_{\beta=1,\dots,N} H_\beta^-(p_{0,+}^{\beta,n}) = 0 \end{cases} \quad \text{for} \quad i = 0, \tag{3.1.7}$$

with the initial condition

$$U_i^{\alpha,0} = u_0^\alpha(i\Delta x) \quad \text{for} \quad i \geq 0, \quad \alpha = 1, \dots, N. \tag{3.1.8}$$

It is natural to introduce the following Courant-Friedrichs-Lewy (CFL) condition [70] :

$$\frac{\Delta x}{\Delta t} \geq \sup_{\substack{\alpha=1,\dots,N \\ i\geq 0,\ 0\leq n\leq n_T}} |H_\alpha'(p_{i,+}^{\alpha,n})| \tag{3.1.9}$$

where the integer n_T is assumed to be defined as $n_T = \left\lfloor \dfrac{T}{\Delta t} \right\rfloor$ for a given $T > 0$.

We then have

Proposition 1.2. (Monotonicity of the numerical scheme)
Let $U^n := (U_i^{\alpha,n})_{\alpha,i}$ and $V^n := (V_i^{\alpha,n})_{\alpha,i}$ two solutions of (3.1.7). If the CFL condition (3.1.9) is satisfied and if $U^0 \leq V^0$, then the numerical scheme (3.1.7) is monotone, that is

$$U^n \leq V^n \quad \textit{for any} \quad n \in \{0, ..., n_T\}.$$

Our scheme (3.1.7) is related to the Godunov scheme for conservation laws in one space dimension, as it is explained in our application to traffic in Section 4.

1.3 Main results

We first notice that even if we can always check *a posteriori* the CFL condition (3.1.9), it is not obvious to satisfy it *a priori*. Indeed the CFL condition (3.1.9) depends on the discrete gradients $p_{i,\pm}^{\alpha,n}$ which are themselves functions of Δt through the scheme (3.1.7). For this reason, we will consider below a more restrictive CFL condition (see (3.1.12)) that can be checked from the initial data. To this end, we need to introduce a few notations.

For sake of clarity we first consider $\sigma \in \{+1, -1\}$ denoted by abuse of notation $\sigma \in \{+, -\}$ in the remaining, with the convention $-\sigma = -$ if $\sigma = +$ and $-\sigma = +$ if $\sigma = -$.

Under assumption (A1), we need to use a sort of inverse of $(H_\alpha^\pm)$ that we define naturally for $\sigma \in \{+,-\}$ as :

$$(H_\alpha^{-\sigma})^{-1}(a) := \sigma\left(\inf\{\sigma p, \quad H_\alpha^{-\sigma}(p) = a\}\right) \tag{3.1.10}$$

with the additional convention that $(H_\alpha^\pm)^{-1}(+\infty) = \pm\infty$.

We set

$$\begin{cases} \underline{p}_\alpha = (H_\alpha^-)^{-1}(-m^0) \\ \\ \overline{p}_\alpha = (H_\alpha^+)^{-1}(-m^0) \end{cases} \quad \text{with} \quad m^0 = \inf_{\substack{\beta=1,\dots,N,\\ i\in\mathbb{N}}} W_i^{\beta,0} \tag{3.1.11}$$

where $(W_i^{\beta,0})_{\beta,i}$, defined in (3.1.6), is given by the scheme (3.1.7) for $n = 0$ in terms of $(U_i^{\beta,0})_{\beta,i}$ (itself defined in (3.1.8)). It is important to notice that with this construction, $\underline{p}_\alpha$ and $\overline{p}_\alpha$ depend on Δx, but not on Δt.

We now consider another CFL condition which turns out to be more restrictive than CFL condition (3.1.9) (see Theorem 1.3). This condition is given by

$$\frac{\Delta x}{\Delta t} \geq \sup_{\substack{\alpha=1,\dots,N\\ p_\alpha\in[\underline{p}_\alpha,\overline{p}_\alpha]}} |H'_\alpha(p_\alpha)| \tag{3.1.12}$$

which is then satisfied for Δt small enough.

Note that by construction we have $-\infty < \underline{p}_\alpha \leq \overline{p}_\alpha < +\infty$ because $-m^0 \geq \max_{\alpha=1,\dots,N}\left(\min_{\mathbb{R}} H_\alpha\right)$ (see also Remark 2.4 (i)).

Our first main result is the following :

Theorem 1.3. (Gradient and time derivative estimates)
Assume (A1). If $(U_i^{\alpha,n})$ is the numerical solution of (3.1.7)-(3.1.8) and if the CFL condition (3.1.12) is satisfied with m^0 finite, then the following two properties hold for any $n \geq 0$:

(i) For $\underline{p}_\alpha$ and $\overline{p}_\alpha$ defined in (3.1.11), we have the following gradient estimate :

$$\underline{p}_\alpha \leq p_{i,+}^{\alpha,n} \leq \overline{p}_\alpha, \quad \text{for all} \quad i \geq 0, \quad \text{and} \quad \alpha = 1,\dots,N. \tag{3.1.13}$$

(ii) Considering $M^n = \sup_{\alpha,i} W_i^{\alpha,n}$ and $m^n = \inf_{\alpha,i} W_i^{\alpha,n}$, we have the following time derivative estimate :

$$m^0 \leq m^n \leq m^{n+1} \leq M^{n+1} \leq M^n \leq M^0. \tag{3.1.14}$$

Remark 1.4. *Notice that due to (3.1.13), the more restrictive CFL condition (3.1.12) implies the natural CFL condition (3.1.9) for any $n_T \geq 0$.*

Our second main result is the following convergence result which also gives the existence of a solution to equations (3.1.2)-(3.1.3).

Theorem 1.5. (Convergence of the numerical solution up to a subsequence)
Assume (A0)-(A1). Let $T > 0$ and

$$\varepsilon := (\Delta t, \Delta x)$$

such that the CFL condition (3.1.12) is satisfied. Then there exists a subsequence ε' of ε such that the numerical solution $(U_i^{\alpha,n})$ of (3.1.7)-(3.1.8) converges as ε' goes to zero,

locally uniformly on any compact set $\mathcal{K} \subset [0,T) \times J$, *towards a solution* $u := (u^\alpha)_\alpha$ *of (3.1.2)-(3.1.3) in the sense of Definition 5, i.e.*

$$\limsup_{\varepsilon' \to 0} \sup_{(n\Delta t, i\Delta x) \in \mathcal{K}} |u^\alpha(n\Delta t, i\Delta x) - U_i^{\alpha,n}| = 0, \tag{3.1.15}$$

where the index α *in (3.1.15) is chosen such that* $(n\Delta t, i\Delta x) \in \mathcal{K} \cap [0,T) \times J_\alpha$.

In order to give below sharp Lipschitz estimates on the continuous solution u, we first define $L^{\alpha,-}$ and $L^{\alpha,+}$ as the best Lipschitz constants for the initial data u_0^α, i.e. satisfying for any $x \geq 0$ and $a \geq 0$

$$aL^{\alpha,-} \leq u_0^\alpha(x+a) - u_0^\alpha(x) \leq aL^{\alpha,+}. \tag{3.1.16}$$

Let us consider

$$\begin{cases} m_0^0 := \inf\limits_{\substack{\alpha=1,\dots,N \\ L^{\alpha,-} \leq p_\alpha \leq L^{\alpha,+}}} -H_\alpha(p_\alpha), \\ M_0^0 := \max\left[\max\limits_{\alpha=1,\dots,N} \left\{ - \max\limits_{\sigma \in \{+,-\}} H_\alpha^{-\sigma}(L^{\alpha,\sigma}) \right\}, - \max\limits_{\alpha=1,\dots,N} \left\{ H_\alpha^-(L^{\alpha,+}) \right\} \right], \end{cases} \tag{3.1.17}$$

and

$$\begin{cases} \underline{p}_\alpha^0 := (H_\alpha^-)^{-1}(-m_0^0), \\ \overline{p}_\alpha^0 := (H_\alpha^+)^{-1}(-m_0^0). \end{cases} \tag{3.1.18}$$

Corollary 1.6. (Gradient and time derivative estimates for a continuous solution)
Assume (A0)-(A1). Let $T > 0$ *and* $u := (u^\alpha)_\alpha$ *be a solution of (3.1.2)-(3.1.3) constructed in Theorem 1.5. Then for all* $a \geq 0$, *for all* $0 \leq t \leq T$ *and* $x \geq 0$, *the function* u *satisfies the following properties :*

$$\begin{cases} am_0^0 \leq u^\alpha(t+a,x) - u^\alpha(t,x) \leq aM_0^0, \\ a\underline{p}_\alpha^0 \leq u^\alpha(t,x+a) - u^\alpha(t,x) \leq a\overline{p}_\alpha^0, \end{cases} \tag{3.1.19}$$

where m_0^0, M_0^0, $\underline{p}_\alpha^0$ *and* $\overline{p}_\alpha^0$ *are defined in (3.1.17) and (3.1.18).*

Recall that under the general assumptions of Theorem 1.5, i.e. (A0)-(A1), the uniqueness of a solution u of (3.1.2)-(3.1.3) is not known. If we replace condition (A1) by a stronger assumption (A1') below, it is possible to recover the uniqueness of the solution (see [141] and Theorem 1.7 below).
This is the following assumption :

(A1') **Strong convexity**
There exists a constant $\gamma > 0$, such that for each $\alpha = 1, ..., N$, there exists a lagrangian function $L_\alpha \in C^2(\mathbb{R};\mathbb{R})$ satisfying $L_\alpha'' \geq \gamma > 0$ such that H_α is the Legendre-Fenchel transform of L_α, i.e.

$$H_\alpha(p) = L_\alpha^*(p) = \sup_{q \in \mathbb{R}} (pq - L_\alpha(q)) \tag{3.1.20}$$

and

$$H_\alpha^-(p) = \sup_{q \leq 0} (pq - L_\alpha(q)) \quad \text{and} \quad H_\alpha^+(p) = \sup_{q \geq 0} (pq - L_\alpha(q)). \tag{3.1.21}$$

We can easily check that assumption (A1') implies assumption (A1).
We are now ready to recall the following result extracted from [141] :

Theorem 1.7. (Existence and uniqueness for a solution of the HJ problem) *Assume (A0)-(A1') and let $T > 0$. Then there exists a unique viscosity solution u of (3.1.2)-(3.1.3) on J_T in the sense of the Definition 5, satisfying for some constant $C_T > 0$*

$$|u(t,y) - u_0(y)| \leq C_T \quad \text{for all} \quad (t,y) \in J_T.$$

Moreover the function u is Lipschitz continuous with respect to (t,y) on J_T.

Our last main result is the following :

Theorem 1.8. (Convergence of the numerical solution under uniqueness assumption) *Assume (A0)-(A1'). Let $T > 0$ and $\varepsilon = (\Delta t, \Delta x)$ such that the CFL condition (3.1.12) is satisfied. If $u := (u^\alpha)_\alpha$ is the unique solution of (3.1.2)-(3.1.3) in the sense of Definition 5, then the numerical solution $(U_i^{\alpha,n})$ of (3.1.7)-(3.1.8) converges locally uniformly to u when ε goes to zero, on any compact set $\mathcal{K} \subset [0,T) \times J$, i.e.*

$$\limsup_{\varepsilon \to 0} \sup_{(n\Delta t, i\Delta x) \in \mathcal{K}} |u^\alpha(n\Delta t, i\Delta x) - U_i^{\alpha,n}| = 0, \tag{3.1.22}$$

where the index α in (3.1.22) is chosen such that $(n\Delta t, i\Delta x) \in \mathcal{K} \cap [0,T) \times J_\alpha$.

Using our scheme (3.1.7), we will present in Section 5 illustrations by numerical simulations with application to traffic.

1.4 Brief review of the literature

Hamilton-Jacobi formulation. We mainly refer here to the comments provided in [141] and references therein. There is a huge literature dealing with HJ equations and mainly with equations with discontinuous Hamiltonians. However, concerning the study of HJ equation on a network, there exist a few works : the reader is referred to [1, 2] for a general definition of viscosity solutions on a network, and [50] for Eikonal equations. Notice that in those works, the Lagrangians depend on the position x and are continuous with respect to this variable. Conversely, in [141] the Lagrangians do not depend on the position but they are allowed to be discontinuous at the junction point. Even for discontinuous Lagrangians, the uniqueness of the viscosity solution has been established in [141].

Numerical schemes for Hamilton-Jacobi equations. Up to our knowledge, there are only two examples of numerical schemes for HJ equations on junctions : in [48], the authors introduce a convergent semi-Lagrangian scheme which is only dedicated to the Eikonal equation. In the very recent work [118], an adapted Lax-Friedrichs scheme is used to solve a traffic model but the junction condition is expressed in terms of density and implies conversions between Hamilton-Jacobi and conservation laws frameworks at each time steps (see our Section 4 for more details). On the contrary, there are a lot of schemes for HJ equations for problems without junctions. The majority of numerical schemes which were proposed to solve HJ equations are based on finite difference methods ; see for instance [74] for upwind and centered discretizations, and [91, 212] for ENO or WENO schemes. For finite elements methods, the reader could also refer to [138] and [243]. Explicit classical monotone schemes have convergence properties but they require to satisfy a CFL condition and they exhibit a viscous behaviour. We can also cite Semi-Lagrangian schemes [82, 90, 92, 93]. Anti-diffusive methods coming from numerical schemes adapted for conservation laws were thus introduced [31] [238]. Some other interesting numerical advances are done along the line of discontinuous Galerkin methods [30, 53, 54]. Notice that more generally, an important effort deals with Hamilton-Jacobi-Bellman equations and Optimal Control viewpoint. It is out of the scope here.

1.5 Organization of the paper

In Section 2, we point out our first main property, namely Theorem 1.3 about the time and space gradient estimates. Then in Section 3, we first recall the notion of viscosity solutions for HJ equations. We then prove the second main property of our numerical scheme, namely Theorem 1.5 and Theorem 1.8 about the convergence of the numerical solution toward a solution of HJ equations when the mesh grid goes to zero. In Section 4, we propose the interpretation of our numerical results to traffic flows problems on a junction. In particular, the numerical scheme for HJ equations (3.1.7) is derived and the junction condition is interpreted. Indeed, we recover the well-known junction condition of Lebacque (see [164]) or equivalently those for the Riemann solver at the junction as in the book of Garavello and Piccoli [106]. Finally, in Section 5 we illustrate the numerical behaviour of our scheme for a junction with two incoming and two outgoing branches.

2 Gradient estimates for the scheme

This section is devoted to the proofs of the first main result namely the time and space gradient estimates.

2.1 Proof of Proposition 1.2

We begin by proving the monotonicity of the numerical scheme.

Proof of Proposition 1.2 : We consider the numerical scheme given by (3.1.7) that we rewrite as follows for $n \geq 0$:

$$\begin{cases} U_i^{\alpha,n+1} = S_\alpha \left[U_{i-1}^{\alpha,n}, U_i^{\alpha,n}, U_{i+1}^{\alpha,n} \right] & \text{for} \quad i \geq 1, \quad \alpha = 1, ..., N, \\ U_0^{n+1} = S_0 \left[U_0^n, (U_1^{\beta,n})_{\beta=1,...,N} \right] & \text{for} \quad i = 0, \end{cases} \tag{3.2.23}$$

where

$$\begin{cases} S_\alpha \left[U_{i-1}^{\alpha,n}, U_i^{\alpha,n}, U_{i+1}^{\alpha,n} \right] & := U_i^{\alpha,n} - \Delta t \max \left\{ H_\alpha^+ \left(\dfrac{U_i^{\alpha,n} - U_{i-1}^{\alpha,n}}{\Delta x} \right), H_\alpha^- \left(\dfrac{U_{i+1}^{\alpha,n} - U_i^{\alpha,n}}{\Delta x} \right) \right\}, \\ S_0 \left[U_0^n, (U_1^{\beta,n})_{\beta=1,...,N} \right] & := U_0^n - \Delta t \max_{\beta=1,...,N} H_\beta^- \left(\dfrac{U_1^{\beta,n} - U_0^n}{\Delta x} \right). \end{cases} \tag{3.2.24}$$

Checking the monotonicity of the scheme means checking that S_α and S_0 are non-decreasing in all their variables.

Case 1 : $i \geq 1$

This case is very classical. It is straightforward to check that S_α for any $\alpha = 1, ..., N$ is non-decreasing in $U_{i-1}^{\alpha,n}$ and $U_{i+1}^{\alpha,n}$. We compute

$$\frac{\partial S_\alpha}{\partial U_i^{\alpha,n}} = \begin{cases} 1 - \dfrac{\Delta t}{\Delta x} (H_\alpha^+)'(p_{i,-}^{\alpha,n}) & \text{if} \quad \max \left\{ H_\alpha^+(p_{i,-}^{\alpha,n}), H_\alpha^-(p_{i,+}^{\alpha,n} \right\} = H_\alpha^+(p_{i,-}^{\alpha,n}), \\ 1 - \dfrac{\Delta t}{\Delta x} (H_\alpha^-)'(p_{i,+}^{\alpha,n}) & \text{if} \quad \max \left\{ H_\alpha^+(p_{i,-}^{\alpha,n}), H_\alpha^-(p_{i,+}^{\alpha,n} \right\} = H_\alpha^-(p_{i,+}^{\alpha,n}) \end{cases}$$

which is non-negative if the CFL condition (3.1.9) is satisfied.

Case 2 : $i = 0$

Similarly, it is straightforward to check that S_0 is non-decreasing in each $U_1^{\beta,n}$ for $\beta = 1, ..., N$. We compute

$$\frac{\partial S_0}{\partial U_0^n} = 1 - \frac{\Delta t}{\Delta x}(H_\alpha^-)'(p_{0,+}^{\alpha,n}) \quad \text{if} \quad H_\alpha^-(p_{0,+}^{\alpha,n}) > H_\beta^-(p_{0,+}^{\beta,n}) \quad \text{for all} \quad \beta \in \{1, ..., N\} \setminus \{\alpha\}$$

which is also non-negative due to the CFL condition (3.1.9).
From cases 1 and 2, we deduce that the scheme is monotone. □

2.2 Proof of Theorem 1.3

In this subsection, we prove the first main result Theorem 1.3 about time and space gradient estimates.

Let us first define for any $n \geq 0$

$$m^n := \inf_{\alpha,i} W_i^{\alpha,n} \quad \text{and} \quad M^n := \sup_{\alpha,i} W_i^{\alpha,n}, \tag{3.2.25}$$

where $W_i^{\alpha,n}$ represents the time gradient defined in (3.1.6).

We also define

$$I_{i,\sigma}^{\alpha,n} := \begin{cases} \left[p_{i,\sigma}^{\alpha,n}, p_{i,\sigma}^{\alpha,n+1}\right] & \text{if} \quad p_{i,\sigma}^{\alpha,n} \leq p_{i,\sigma}^{\alpha,n+1}, \\ \left[p_{i,\sigma}^{\alpha,n+1}, p_{i,\sigma}^{\alpha,n}\right] & \text{if} \quad p_{i,\sigma}^{\alpha,n} \geq p_{i,\sigma}^{\alpha,n+1}. \end{cases} \quad \text{for} \quad \sigma \in \{+,-\}, \tag{3.2.26}$$

with $p_{i,\sigma}^{\alpha,n}$ defined in (3.1.5) and we set

$$D_{i,+}^{\alpha,n} := \sup_{p_\alpha \in I_{i,+}^{\alpha,n}} |H_\alpha'(p_\alpha)|. \tag{3.2.27}$$

In order to establish Theorem 1.3, we need the two following results namely Proposition 2.1 and Lemma 2.2 :

Proposition 2.1. (Time derivative estimate)
Assume (A1). Let $n \geq 0$ fixed and Δx, $\Delta t > 0$. Let us consider $(U_i^{\alpha,n})_{\alpha,i}$ satisfying for some constant $C^n > 0$:

$$|p_{i,+}^{\alpha,n}| \leq C^n, \quad \text{for} \quad i \geq 0, \quad \alpha = 1, ...N. \tag{3.2.28}$$

We also consider $\left(U_i^{\alpha,n+1}\right)_{\alpha,i}$ and $\left(U_i^{\alpha,n+2}\right)_{\alpha,i}$ computed using the scheme (3.1.7).

If we have

$$D_{i,+}^{\alpha,n} \leq \frac{\Delta x}{\Delta t} \quad \text{for any} \quad i \geq 0 \quad \text{and} \quad \alpha = 1, ..., N, \tag{3.2.29}$$

Then it comes that

$$m^n \leq m^{n+1} \leq M^{n+1} \leq M^n.$$

Proof **Step 0 : Preliminaries.**
We introduce for any $n \geq 0$, $\alpha = 1, ..., N$ and for any $i \geq 1$, $\sigma \in \{+,-\}$ or for $i = 0$ and $\sigma = +$:

$$C_{i,\sigma}^{\alpha,n} := -\sigma \int_0^1 d\tau (H_\alpha^{-\sigma})'(p_{i,\sigma}^{\alpha,n+1} + \tau(p_{i,\sigma}^{\alpha,n} - p_{i,\sigma}^{\alpha,n+1})) \geq 0. \tag{3.2.30}$$

Notice that $C_{i,\sigma}^{\alpha,n}$ is defined as the integral of $(H_\alpha^{-\sigma})'$ over a convex combination of p with $p \in I_{i,\sigma}^{\alpha,n}$. Hence for any $n \geq 0$, $\alpha = 1, ..., N$ and for any $i \geq 1$, $\sigma \in \{+, -\}$ or for $i = 0$ and $\sigma = +$, we can check that

$$C_{i,\sigma}^{\alpha,n} \leq \sup_{\substack{\beta=1,...,N \\ j\geq 0}} D_{j,+}^{\beta,n}. \tag{3.2.31}$$

We also underline that for any $n \geq 0$, $\alpha = 1, ..., N$ and for any $i \geq 1$, $\sigma \in \{+, -\}$ or for $i = 0$ and $\sigma = +$, we have the following relationship :

$$\frac{p_{i,\sigma}^{\alpha,n} - p_{i,\sigma}^{\alpha,n+1}}{\Delta t} = -\sigma \frac{W_{i+\sigma}^{\alpha,n} - W_i^{\alpha,n}}{\Delta x}. \tag{3.2.32}$$

Let $n \geq 0$ be fixed and consider $(U_i^{\alpha,n})_{\alpha,i}$ with Δx, $\Delta t > 0$ given. We compute $\left(U_i^{\alpha,n+1}\right)_{\alpha,i}$ and $\left(U_i^{\alpha,n+2}\right)_{\alpha,i}$ using the scheme (3.1.7).

Step 1 : Estimate on m^n

We want to show that $W_i^{\alpha,n+1} \geq m^n$ for any $i \geq 0$ and $\alpha = 1, ..., N$. It is then sufficient to take the infimum over $i \geq 0$ and $\alpha = 1, ..., N$ to conclude that

$$m^{n+1} \geq m^n.$$

Let $i \geq 0$ be fixed and we distinguish two cases :

Case 1 : Proof of $W_i^{\alpha,n+1} \geq m^n$ for all $i \geq 1$

Let a branch α fixed. We assume that

$$\max\left\{H_\alpha^+(p_{i,-}^{\alpha,n+1}), H_\alpha^-(p_{i,+}^{\alpha,n+1})\right\} = H_\alpha^{-\sigma}(p_{i,\sigma}^{\alpha,n+1}) \quad \text{for one} \quad \sigma \in \{+, -\}. \tag{3.2.33}$$

We have

$$\begin{aligned}
\frac{W_i^{\alpha,n+1} - W_i^{\alpha,n}}{\Delta t} &= \frac{1}{\Delta t}\left(\max\left\{H_\alpha^+(p_{i,-}^{\alpha,n}), H_\alpha^-(p_{i,+}^{\alpha,n})\right\} - \max\left\{H_\alpha^+(p_{i,-}^{\alpha,n+1}), H_\alpha^-(p_{i,+}^{\alpha,n+1})\right\}\right) \\
&\geq \frac{1}{\Delta t}\left(H_\alpha^{-\sigma}(p_{i,\sigma}^{\alpha,n}) - H_\alpha^{-\sigma}(p_{i,\sigma}^{\alpha,n+1})\right) \\
&= \frac{1}{\Delta t}\int_0^1 d\tau (H_\alpha^{-\sigma})'(p_{i,\sigma}^{\alpha,n+1} + \tau p)p \qquad \text{with} \quad p = p_{i,\sigma}^{\alpha,n} - p_{i,\sigma}^{\alpha,n+1} \\
&= C_{i,\sigma}^{\alpha,n}\left(\frac{W_{i+\sigma}^{\alpha,n} - W_i^{\alpha,n}}{\Delta x}\right)
\end{aligned}$$

where we use (3.2.32) and (3.2.30) in the last line.

Using (3.2.31) and (3.2.29), we thus get

$$\begin{aligned}
W_i^{\alpha,n+1} &\geq \left(1 - C_{i,\sigma}^{\alpha,n}\frac{\Delta t}{\Delta x}\right)W_i^{\alpha,n} + C_{i,\sigma}^{\alpha,n}\frac{\Delta t}{\Delta x}W_{i+\sigma}^{\alpha,n} \\
&\geq \min(W_i^{\alpha,n}, W_{i+\sigma}^{\alpha,n}) \\
&\geq m^n.
\end{aligned}$$

Case 2 : Proof of $W_i^{n+1} \geq m^n$ for $i = 0$

We recall that in this case, we have $U_0^{\beta,n} =: U_0^n$ for any $\beta = 1, ..., N$. Let us denote $W_0^{\beta,n} =: W_0^n = \dfrac{U_0^{n+1} - U_0^n}{\Delta t}$ for any $\beta = 1, ..., N$. Then we define α_0 such that

$$H_{\alpha_0}^-(p_{0,+}^{\alpha_0,n+1}) = \max_{\alpha=1,...,N} H_\alpha^-(p_{0,+}^{\alpha,n+1}).$$

We argue like in Case 1 above and we get

$$\frac{W_0^{n+1}-W_0^n}{\Delta t} \geq C_{0,+}^{\alpha_0,n}\left(\frac{W_1^{\alpha_0,n}-W_0^n}{\Delta x}\right).$$

Then using (3.2.31) and (3.2.29) we conclude that :

$$W_0^{n+1} \geq m^n.$$

Step 2 : : Estimate on M^n
We recall that $n \geq 0$ is fixed. The proof for M^n is directly adapted from Part 1. We want to show that $W_i^{\alpha,n+1} \leq M^n$ for any $i \geq 0$ and $\alpha = 1, ..., N$. We distinguish the same two cases :

- If $i \geq 1$, instead of (3.2.33) we simply choose σ such that

$$\max\left\{H_\alpha^+(p_{i,-}^{\alpha,n}), H_\alpha^-(p_{i,+}^{\alpha,n})\right\} = H_\alpha^{-\sigma}(p_{i,\sigma}^{\alpha,n}) \quad \text{for one} \quad \sigma \in \{+,-\}.$$

- If $i = 0$, we define α_0 such that

$$H_{\alpha_0}^-(p_{0,+}^{\alpha_0,n}) = \max_{\alpha=1,...,N} H_\alpha^-(p_{0,+}^{\alpha,n}).$$

Then taking the supremum, we can easily prove that

$$M^{n+1} \leq M^n, \quad \text{for any} \quad n \geq 0.$$

By definition of m^n and M^n for a given $n \geq 0$, we recover the result

$$m^n \leq m^{n+1} \leq M^{n+1} \leq M^n.$$

□

The second important result needed for the proof of Theorem 1.3 is the following one :

Lemma 2.2. (Gradient estimate)
Assume (A1). Let $n \geq 0$ fixed and Δx, $\Delta t > 0$. We consider that $(U_i^{\alpha,n})_{\alpha,i}$ is given and we compute $\left(U_i^{\alpha,n+1}\right)_{\alpha,i}$ using the scheme (3.1.7).

If there exists a constant $K \in \mathbb{R}$ such that for any $i \geq 0$ and $\alpha = 1, ..., N$, we have

$$K \leq W_i^{\alpha,n} := \frac{U_i^{\alpha,n+1}-U_i^{\alpha,n}}{\Delta t}$$

Then it follows for any $i \geq 0$ and $\alpha = 1, ..., N$

$$(H_\alpha^-)^{-1}(-K) \leq p_{i,+}^{\alpha,n} \leq (H_\alpha^+)^{-1}(-K)$$

with $p_{i,+}^{\alpha,n}$ defined in (3.1.5) and $(H_\alpha^-)^{-1}$, $(H_\alpha^+)^{-1}$ defined in (3.1.10).

Proof Let $n \geq 0$ be fixed and consider $(U_i^{\alpha,n})_{\alpha,i}$ with Δx, $\Delta t > 0$ given. We compute $\left(U_i^{\alpha,n+1}\right)_{\alpha,i}$ using the scheme (3.1.7).

Let us consider any $i \geq 0$ and $\alpha = 1, ..., N$. We distinguish two cases according to the value of i.

Case 1 : $i \geq 1$
Assume that we have

$$K \leq W_i^{\alpha,n} = -\max_{\sigma\in\{+,-\}} H_\alpha^{-\sigma}(p_{i,\sigma}^{\alpha,n}).$$

It is then obvious that we get

$$-K \geq H_\alpha^{-\sigma}(p_{i,\sigma}^{\alpha,n}), \quad \text{for any} \quad \sigma \in \{+,-\}.$$

According to (A1) on the monotonicity of the Hamiltonians H_α, we obtain

$$\begin{cases} (H_\alpha^+)^{-1}(-K) \geq p_{i,-}^{\alpha,n} = p_{i-1,+}^{\alpha,n} \\ \\ (H_\alpha^-)^{-1}(-K) \leq p_{i,+}^{\alpha,n} \end{cases} \quad \text{for any} \quad i \geq 1, \quad n \geq 0 \quad \text{and} \quad \alpha = 1,\dots,N. \tag{3.2.34}$$

Case 2 : $i = 0$
The proof is similar to Case 1 because on the one hand we have

$$K \leq W_0^{\alpha,n} =: W_0^n = -\max_{\beta=1,\dots,N} H_\beta^-(p_{0,+}^{\beta,n})$$

which obviously leads to

$$(H_\alpha^-)^{-1}(-K) \leq p_{0,+}^{\alpha,n},$$

where we use the monotonicity of H_α^- from assumption (A1). On the other hand, from (3.2.34) we get

$$(H_\alpha^+)^{-1}(-K) \geq p_{1,-}^{\alpha,n} = p_{0,+}^{\alpha,n}.$$

We conclude

$$(H_\alpha^-)^{-1}(-K) \leq p_{i,+}^{\alpha,n} \leq (H_\alpha^+)^{-1}(-K), \quad \text{for any} \quad i, \quad n \geq 0 \quad \text{and} \quad \alpha = 1,...,N$$

which ends the proof. □

Proof of Theorem 1.3 : The idea of the proof is to introduce new continuous Hamiltonians $\tilde{H}_\alpha$ that satisfy the following properties :

(i) the new Hamiltonians $\tilde{H}_\alpha$ are equal to the old ones H^α on the segment $[\underline{p}_\alpha, \overline{p}_\alpha]$,

(ii) the derivative of the new Hamiltonians $|\tilde{H}'_\alpha|$ taken at any point is less or equal to $\sup_{p\in[\underline{p}_\alpha,\overline{p}_\alpha]} |H'_\alpha(p)|$.

This modification of the Hamiltonians is done in order to show that the gradient stays in the interval $[\underline{p}_\alpha, \overline{p}_\alpha]$.

Step 1 : Modification of the Hamiltonians
Let the new Hamiltonians $\tilde{H}_\alpha$ for all $\alpha = 1,...,N$ be defined as

$$\tilde{H}_\alpha(p) = \begin{cases} g_\alpha^l(p) & \text{for} \quad p \leq \underline{p}_\alpha \\ H_\alpha(p) & \text{for} \quad p \in [\underline{p}_\alpha, \overline{p}_\alpha] \\ g_\alpha^r(p) & \text{for} \quad p \geq \overline{p}_\alpha \end{cases} \tag{3.2.35}$$

with $\underline{p}_\alpha$, $\overline{p}_\alpha$ defined in (3.1.11) and g_α^l, g_α^r two functions such that

$$\begin{cases} g_\alpha^l \in C^1((-\infty, \underline{p}_\alpha]), \\ g_\alpha^l(\underline{p}_\alpha) = -m_0, \\ (g_\alpha^l)'(\underline{p}_\alpha) = H_\alpha'(\underline{p}_\alpha), \\ (g_\alpha^l)' < 0 \quad \text{on} \quad (-\infty, \underline{p}_\alpha), \\ |(g_\alpha^l)'(p)| < |H_\alpha'(\underline{p}_\alpha)| \quad \text{for} \quad p < \underline{p}_\alpha, \\ g_\alpha^l \to +\infty \quad \text{for} \quad p \to -\infty, \end{cases} \quad \text{and} \quad \begin{cases} g_\alpha^r \in C^1([\overline{p}_\alpha, +\infty)), \\ g_\alpha^r(\overline{p}_\alpha) = -m_0, \\ (g_\alpha^r)'(\overline{p}_\alpha) = H_\alpha'(\overline{p}_\alpha), \\ (g_\alpha^r)' > 0 \quad \text{on} \quad (\overline{p}_\alpha, +\infty), \\ |(g_\alpha^r)'(p)| < |H_\alpha'(\overline{p}_\alpha)| \quad \text{for} \quad p > \overline{p}_\alpha, \\ g_\alpha^r \to +\infty \quad \text{for} \quad p \to +\infty. \end{cases}$$

We can easily check that

$$0 < \tilde{H}_\alpha' < \sup_{p_\alpha \in [\underline{p}_\alpha, \overline{p}_\alpha]} |H_\alpha'(p_\alpha)|, \quad \text{on} \quad \mathbb{R} \setminus [\underline{p}_\alpha, \overline{p}_\alpha], \tag{3.2.36}$$

and

$$\tilde{H}_\alpha > -m_0 \quad \text{on} \quad \mathbb{R} \setminus [\underline{p}_\alpha, \overline{p}_\alpha]. \tag{3.2.37}$$

We can also check that $\tilde{H}_\alpha$ satisfies (A1). Then Proposition 2.1 and Lemma 2.2 hold true for the new Hamiltonians $\tilde{H}_\alpha$ (especially we can adapt (3.1.10) to the $\tilde{H}_\alpha$ for defining a sort of inverse).

Let $\tilde{H}_\alpha^+$ (resp. $\tilde{H}_\alpha^-$) denotes the non-decreasing (resp. non-increasing) part of $\tilde{H}_\alpha$.

We consider the new numerical scheme for any $n \geq 0$ that reads as :

$$\begin{cases} \dfrac{\tilde{U}_i^{\alpha,n+1} - \tilde{U}_i^{\alpha,n}}{\Delta t} + \max\left\{\tilde{H}_\alpha^+(\tilde{p}_{i,-}^{\alpha,n}), \tilde{H}_\alpha^-(\tilde{p}_{i,+}^{\alpha,n})\right\} = 0, \quad \text{for} \quad i \geq 1, \quad \alpha = 1, \dots, N, \\ \tilde{U}_0^{\beta,n} =: \tilde{U}_0^n, \quad \text{for all} \quad \beta = 1, \dots, N \\ \dfrac{\tilde{U}_0^{n+1} - \tilde{U}_0^n}{\Delta t} + \max\limits_{\beta=1,\dots,N} \tilde{H}_\beta^-(p_{0,+}^{\beta,n}) = 0 \end{cases} \quad \text{for} \quad i = 0, \tag{3.2.38}$$

subject to the initial condition

$$\tilde{U}_i^{\alpha,0} = U_i^{\alpha,0} = u_0^\alpha(i\Delta x), \quad i \geq 0, \quad \alpha = 1, \dots, N. \tag{3.2.39}$$

The discrete time and space gradients are defined such as :

$$\tilde{p}_{i,+}^{\alpha,n} := \frac{\tilde{U}_{i+1}^{\alpha,n} - \tilde{U}_i^{\alpha,n}}{\Delta x} \quad \text{and} \quad \tilde{W}_i^{\alpha,n} := \frac{\tilde{U}_i^{\alpha,n+1} - \tilde{U}_i^{\alpha,n}}{\Delta t}. \tag{3.2.40}$$

Let us consider

$$\tilde{m}^n := \inf_{i,\alpha} \tilde{W}_i^{\alpha,n} \quad \text{and} \quad \tilde{M}^n := \sup_{i,\alpha} \tilde{W}_i^{\alpha,n} \tag{3.2.41}$$

where $\tilde{W}_i^{\alpha,n}$ is defined in (3.2.40). We also set

$$\tilde{D}_{i,+}^{\alpha,n} := \sup_{p_\alpha \in \tilde{I}_{i,+}^{\alpha,n}} |\tilde{H}_\alpha'(p_\alpha)|, \tag{3.2.42}$$

where $\tilde{I}_{i,+}^{\alpha,n}$ is the analogue of $I_{i,+}^{\alpha,n}$ defined in (3.2.26) with $\tilde{p}_{i,+}^{\alpha,n}$ and $\tilde{p}_{i,+}^{\alpha,n+1}$ given in (3.2.40).

According to (3.2.36), the supremum of $|\tilde{H}_\alpha'|$ is reached on $[\underline{p}_\alpha, \overline{p}_\alpha]$. As $\tilde{H}_\alpha \equiv H_\alpha$ on $[\underline{p}_\alpha, \overline{p}_\alpha]$, the CFL condition (3.1.12) gives that for any $i \geq 0$, $n \geq 0$ and $\alpha = 1, ..., N$:

$$\tilde{D}_{i,+}^{\alpha,n} \leq \sup_{p_\alpha \in [\underline{p}_\alpha, \overline{p}_\alpha]} |H_\alpha'(p_\alpha)| \leq \frac{\Delta x}{\Delta t}. \tag{3.2.43}$$

Step 2 : First gradient bounds
Let $n \geq 0$ be fixed. By definition (3.2.41) and if $\tilde{m}^n$ is finite, we have

$$\tilde{m}^n \leq \tilde{W}_i^{\alpha,n}, \quad \text{for any} \quad i \geq 0, \quad \alpha = 1, ..., N.$$

Using Lemma 2.2, it follows that

$$(\tilde{H}_\alpha^-)^{-1}(-\tilde{m}^n) \leq \tilde{p}_{i,+}^{\alpha,n} \leq (\tilde{H}_\alpha^+)^{-1}(-\tilde{m}^n), \quad \text{for any} \quad i \geq 0 \quad \text{and} \quad \alpha = 1, ..., N. \tag{3.2.44}$$

We define

$$C^n = \max\left\{\left|(\tilde{H}_\alpha^-)^{-1}(-\tilde{m}^n)\right|, \left|(\tilde{H}_\alpha^+)^{-1}(-\tilde{m}^n)\right|\right\} > 0,$$

and we recover that

$$|\tilde{p}_{i,+}^{\alpha,n}| \leq C^n, \quad \text{for any} \quad i \geq 0, \quad \alpha = 1, ..., N.$$

Step 3 : Time derivative and gradient estimates
For any $n \geq 0$, (3.2.43) holds true. Moreover, if $\tilde{m}^n$ is finite, then there exists $C^n > 0$ such that

$$|\tilde{p}_{i,+}^{\alpha,n}| \leq C^n, \quad \text{for any} \quad i \geq 0, \quad \alpha = 1, ..., N.$$

Then using Proposition 2.1 we get

$$\tilde{m}^n \leq \tilde{m}^{n+1} \leq \tilde{M}^{n+1} \leq \tilde{M}^n \quad \text{for any} \quad n \geq 0. \tag{3.2.45}$$

In particular, $\tilde{m}^{n+1}$ is also finite.

Using the assumption that m^0 is finite and according to (3.1.11), Lemma 2.2 and the scheme (3.1.7), we can check that

$$\underline{p}_\alpha \leq p_{i,+}^{\alpha,0} \leq \overline{p}_\alpha \quad \text{for any} \quad i \geq 0 \quad \text{and} \quad \alpha = 1, ..., N. \tag{3.2.46}$$

From (3.2.39), we have $p_{i,+}^{\alpha,0} = \tilde{p}_{i,+}^{\alpha,0}$. Therefore, from (3.2.35), (3.1.7) and (3.2.46), we deduce that $\tilde{W}_i^{\alpha,0} = W_i^{\alpha,0}$ and we obtain that

$$\tilde{m}^0 = m^0.$$

According to (3.2.45), we deduce that $m^0 \leq \tilde{W}_i^{\alpha,n}$ for any $i \geq 0$, $n \geq 0$ and $\alpha = 1, ..., N$.

Then using Lemma 2.2 and (3.2.37), we conclude that for all $i \geq 0$, $n \geq 0$ and $\alpha = 1, ..., N$

$$\underline{p}_\alpha \leq \tilde{p}_{i,+}^{\alpha,n} \leq \overline{p}_\alpha. \tag{3.2.47}$$

Step 4 : Conclusion
If (3.2.47) holds true, then $\tilde{H}_\alpha(\tilde{p}_{i,+}^{\alpha,n}) = H_\alpha(\tilde{p}_{i,+}^{\alpha,n})$ for all $i \geq 0$, $n \geq 0$ and $\alpha = 1, ..., N$. Thus the modified scheme (3.2.38) is strictly equivalent to the original scheme (3.1.7) and $U_i^{\alpha,n} = \tilde{U}_i^{\alpha,n}$. We finally recover the results for all $i \geq 0$, $n \geq 0$ and $\alpha = 1, ..., N$:

(i) (Time derivative estimate)

$$m^n \leq m^{n+1} \leq M^{n+1} \leq M^n,$$

(ii) (Gradient estimate)

$$\underline{p}_\alpha \leq p_{i,+}^{\alpha,n} \leq \overline{p}_\alpha.$$

□

Remark 2.3. (Do the bounds (3.1.14) always give informations on the gradient ?)
We assume that the assumptions of Theorem 1.3 hold true.

(i) **(Bounds on m^n)** *From the scheme (3.1.7), we can rewrite*

$$m^n = \inf_{\alpha,i} \min_{\sigma\in\{+,-\}} \left\{-H_\alpha^{-\sigma}(p_{i,\sigma}^{\alpha,n})\right\}.$$

It is then obvious that

$$-m^0 \geq \min_{p_\alpha\in\mathbb{R}} H_\alpha(p_\alpha) \quad \text{for} \quad \alpha = 1, ..., N,$$

which ensures that the bound from below in (3.1.14) always gives an information on the gradient $(p_{i,+}^{\alpha,n})$.

(ii) **(Bounds on M^n)** *For the bounds from above in (3.1.14), we get*

$$H_\alpha\left(p_{i,+}^{\alpha,n}\right) \geq -M^0 \quad \text{for all} \quad \alpha = 1, ..., N, \quad i \geq 0 \quad \text{and} \quad n \leq n_T. \tag{3.2.48}$$

Then (3.2.48) is always true if $-M^0 \leq \min_{\mathbb{R}} H_\alpha$. Therefore for each $\alpha = 1, ..., N$, (3.2.48) gives an information on the $(p_{i,+}^{\alpha,n})$ only if

$$-M_0 > \min_{p_\alpha\in\mathbb{R}} H_\alpha(p_\alpha).$$

Remark 2.4. (Extension to weaker assumptions on H_α than (A1))
All the results of this paper can be extended if we consider weaker conditions than (A1) on the Hamiltonians H_α. Indeed, we can assume that the H_α for any $\alpha = 1, ..., N$ are locally Lipschitz instead of being C^1. This assumption is more adapted for our traffic application (see Section 4).

We now focus on what should be modified if we do so.

How to modify CFL condition (3.1.9) ?
The main new idea is then to consider the closed convex hull for the discrete gradient defined by

$$I^{\alpha,n} := \overline{Conv(p_{i,+}^{\alpha,n})}_{i\geq 0}.$$

Then the Lipschitz constant $L^{\alpha,n}$ of the considered H_α is a natural upper bound

$$|H_\alpha(p+q) - H_\alpha(p)| \leq L^{\alpha,n}|q| \quad \text{with} \quad p,\ p+q \in I^{\alpha,n}.$$

Then the natural CFL condition which replaces (3.1.9) is the following one :

$$\frac{\Delta x}{\Delta t} \geq \sup_{\substack{\alpha=1,...,N\\ n\leq n_T}} L^{\alpha,n}. \tag{3.2.49}$$

With such a condition, we can easily prove the monotonicity of the numerical scheme.

How to modify CFL condition (3.1.12) ?
Assume that CFL condition (3.1.12) is replaced by the following one

$$\frac{\Delta x}{\Delta t} \geq \operatorname*{ess\,sup}_{\substack{\alpha=1,...,N\\ p_\alpha\in[\underline{p}_\alpha,\overline{p}_\alpha]}} |H'_\alpha(p_\alpha)|, \tag{3.2.50}$$

where ess sup *denotes the essential supremum.*

In the proof of Theorem 1.3, the time derivative estimate uses the integral of H'_α which is defined almost everywhere if H_α is at least Lipschitz. The remaining of the main results of Section 1.3 do not use a definition of H'_α, except in the CFL condition. We just need to satisfy the new CFL condition (3.2.50).

3 Convergence result for the scheme

3.1 Viscosity solutions

We introduce the main definitions related to viscosity solutions for HJ equations that are used in the remaining. For a more general introduction to viscosity solutions, the reader could refer to Barles [19] and to Crandall, Ishii, Lions [72].

Let $T > 0$. We set $u := (u^\alpha)_{\alpha=1,\dots,N} \in C^1_*(J_T)$ where $C^1_*(J_T)$ is defined in (3.1.1) and we consider the additional condition

$$u^\alpha(t,0) = u^\beta(t,0) =: u(t,0) \quad \text{for any} \quad \alpha,\beta.$$

Remark 3.1. *Following [141], we recall that (3.1.2) can be rigorously rewritten as*

$$u_t + H(y,u_y) = 0, \quad \textit{for} \quad (t,y) \in [0,T) \times J, \tag{3.3.51}$$

with

$$H(y,p) := \begin{cases} H_\alpha(p), & \textit{for} \quad p \in \mathbb{R}, & \textit{if} \quad y \in J^*_\alpha, \\ \max\limits_{\alpha=1,\dots,N} H^-_\alpha(p_\alpha), & \textit{for} \quad p = (p_1,\dots,p_N) \in \mathbb{R}^{\mathbb{N}}, & \textit{if} \quad y = 0, \end{cases}$$

subject to the initial condition

$$u(0,y) = u_0(y) := (u_0^\alpha(x))_{\alpha=1,\dots,N}, \quad \textit{for} \quad y = xe_\alpha \in J \quad \textit{with} \quad x \in [0,+\infty). \tag{3.3.52}$$

Definition 4. (Upper and lower semi-continuous envelopes)
For any function $u : [0,T) \times J \to \mathbb{R}$, upper and lower semi-continuous envelopes are respectively defined as :

$$u^*(t,y) = \limsup_{(t',y') \to (t,y)} u(t',y') \quad \textit{and} \quad u_*(t,y) = \liminf_{(t',y') \to (t,y)} u(t',y').$$

Moreover, we recall

$$\begin{cases} u \quad \textit{is upper semi-continuous if and only if} \quad u = u^*, \\ u \quad \textit{is lower semi-continuous if and only if} \quad u = u_*, \\ u \quad \textit{is continuous if and only if} \quad u_* = u^*. \end{cases}$$

Definition 5. (Viscosity solutions)
i) Viscosity sub and super-solution on $J_T = (0,T) \times J$
A function $u : J_T \to \mathbb{R}$ is a viscosity subsolution (resp. supersolution) of (3.1.2) on J_T if it is an upper semi-continuous (resp. lower semi-continuous) function, and if for any $P = (t,y) \in J_T$ and any test function $\varphi := (\varphi^\alpha)_\alpha \in C^1_*(J_T)$ such that $u - \varphi \le 0$ (resp. $u - \varphi \ge 0$) at the point P, we have

$$\varphi^\alpha_t(t,x) + H_\alpha(\varphi^\alpha_x(t,x)) \le 0 \quad \textit{if} \quad y = xe_\alpha \in J^*_\alpha, \tag{3.3.53}$$

$$\Big(\textit{resp.} \quad \varphi^\alpha_t(t,x) + H_\alpha(\varphi^\alpha_x(t,x)) \ge 0 \quad \textit{if} \quad y = xe_\alpha \in J^*_\alpha\Big), \tag{3.3.54}$$

$$\varphi_t(t,0) + \max_{\alpha=1,\dots,N} H^-_\alpha(\varphi^\alpha_x(t,0)) \le 0 \quad \textit{if} \quad y = 0, \tag{3.3.55}$$

$$\Big(\textit{resp.} \quad \varphi_t(t,0) + \max_{\alpha=1,\dots,N} H_\alpha^-(\varphi_x^\alpha(t,0)) \geq 0 \quad \textit{if} \quad y=0\Big). \tag{3.3.56}$$

ii) Viscosity sub and super-solution on $[0,T)\times J$

A function $u : [0,T)\times J \to \mathbb{R}$ *is said to be a viscosity subsolution (resp. supersolution) of (3.1.2)-(3.1.3) on* $[0,T)\times J$*, if* u *is upper semi-continuous (resp. lower semi-continuous), if it is a viscosity subsolution (resp. supersolution) of (3.1.2) on* J_T *and if moreover it satisfies :*

$$\begin{cases} u(0,y) \leq u_0(y) & \textit{for all} \quad y \in J, \\ \\ \Big(\textit{resp.} \quad u(0,y) \geq u_0(y) & \textit{for all} \quad y \in J\Big), \end{cases}$$

when the initial data u_0 *is assumed to be continuous.*

iii) Viscosity solution on J_T ***and on*** $[0,T)\times J$

A function $u : [0,T)\times J \to \mathbb{R}$ *is said to be a viscosity solution of (3.1.2) on* J_T *(resp. of (3.1.2)-(3.1.3) on* $[0,T)\times J$*) if* u^* *is a viscosity subsolution and* u_* *is a viscosity supersolution of (3.1.2) on* J_T *(resp. of (3.1.2)-(3.1.3) on* $[0,T)\times J$*).*

Hereafter, we recall two properties of viscosity solutions on a junction that are extracted from [141] :

Proposition 3.2. (Comparison principle)
Assume (A0)-(A1') and let $T > 0$*. Assume that* $\overline{u}$ *and* $\underline{u}$ *are respectively a viscosity subsolution and a viscosity supersolution of (3.1.2)-(3.1.3) on* $[0,T)\times J$ *in the sense of Definition 5. We also assume that there exists a constant* $C_T > 0$ *such that for all* $(t,y) \in [0,T)\times J$

$$\overline{u}(t,y) \leq C_T(1+|y|) \quad (\textit{resp.} \quad \underline{u}(t,y) \geq -C_T(1+|y|)).$$

Then we have $\overline{u} \leq \underline{u}$ *on* J_T*.*

Proposition 3.3. (Equivalence with relaxed junction conditions)
Assume (A1') and let $T > 0$*. A function* $u : [0,T)\times J \to \mathbb{R}$ *is a viscosity subsolution (resp. a viscosity supersolution) of (3.1.2) on* J_T *if and only if for any function* $\varphi := (\varphi^\alpha)_\alpha \in C^1_*(J_T)$ *and for any* $P = (t,y) \in J_T$ *such that* $u-\varphi \leq 0$ *(resp.* $u-\varphi \geq 0$*) at the point* P*, we have the following properties*

- *if* $y = xe_\alpha \in J^*_\alpha$*, then*

$$\varphi_t^\alpha(t,x) + H_\alpha(\varphi_x^\alpha(t,x)) \leq 0 \quad (\textit{resp.} \geq 0)$$

- *if* $y = 0$*, then either there exists one index* $\alpha \in \{1,\dots,N\}$ *such that*

$$\varphi_t^\alpha(t,0) + H_\alpha(\varphi_x^\alpha(t,0)) \leq 0 \quad (\textit{resp.} \geq 0)$$

  or (3.3.55) (resp. (3.3.56)) holds true for $y = 0$*.*

We skip the proof of Proposition 3.2 and Proposition 3.3 which are directly available in [141].

3.2 Convergence of the numerical solution

We assume (A0), (A1') and we set

$$\varepsilon := (\Delta t, \Delta x)$$

satisfying the CFL condition (3.1.12). This section first deals with a technical result (see Lemma 3.5) that is very useful for the proof of Theorem 1.8 that is the convergence of the numerical solution of (3.1.7)-(3.1.8) towards a solution of (3.1.2)-(3.1.3) when ε goes to zero. According to Theorem 1.7, we know that the equation (3.1.2)-(3.1.3) admits a unique solution in the sense of Definition 5. For Theorem 1.5, we extend the convergence proof, assuming the weakest assumption (A1) instead of (A1'). We close this subsection with the proof of gradient estimates for the continuous solution (see Corollary 1.6).

For $\alpha = 1, ..., N$, $i \geq 0$ and $n \geq 0$, recall that $(U_i^{\alpha,n})$ solves the numerical scheme (3.1.7)-(3.1.8). This numerical solution $U_i^{\alpha,n}$ is expected to be a certain approximation of $u^\alpha(n\Delta t, i\Delta x)$ where u^α is the unique viscosity solution of (3.1.2)-(3.1.3) given by Theorem 1.7. For sake of clarity, we then denote our numerical solution as follows

$$u_\varepsilon^\alpha(n\Delta t, i\Delta x) := U_i^{\alpha,n}, \quad \text{for any} \quad \alpha = 1, ..., N \quad \text{and any} \quad i \geq 0, \ n \geq 0,$$

and we recall

$$u_\varepsilon^\alpha(n\Delta t, 0) =: u_\varepsilon(n\Delta t, 0), \quad \text{for any} \quad \alpha = 1, ..., N.$$

We also denote by G_ε^α the set of all grid points $(n\Delta t, i\Delta x)$ on $[0,T) \times J_\alpha$ for any branch $\alpha = 1, ..., N$, and we set

$$G_\varepsilon = \bigcup_{\alpha=1,...,N} G_\varepsilon^\alpha \tag{3.3.57}$$

the whole set of grid points on $[0,T) \times J$, with identification of the junction points $(n\Delta t, 0)$ of each grid G_ε^α.

We call u_ε the function defined by its restrictions to the grid points of the branches

$$u_\varepsilon = u_\varepsilon^\alpha \quad \text{on} \quad G_\varepsilon^\alpha.$$

For any point $(t,y) \in [0,T) \times J$, we define the half relaxed limits

$$\overline{u}(t,y) = \limsup_{\substack{\varepsilon \to 0 \\ G_\varepsilon \ni (t',y') \to (t,y)}} u_\varepsilon(t',y'), \tag{3.3.58}$$

$$\left(\text{resp.} \quad \underline{u}(t,y) = \liminf_{\substack{\varepsilon \to 0 \\ G_\varepsilon \ni (t',y') \to (t,y)}} u_\varepsilon(t',y') \right). \tag{3.3.59}$$

Thus we have that $\overline{u} := (\overline{u}^\alpha)_\alpha$ (resp. $\underline{u} := (\underline{u}^\alpha)_\alpha$) is upper semi-continuous (resp. lower semi-continuous).

Remark 3.4 (Upper semi-continuity of $\overline{u}$)**.** *It is classical to show that $\overline{u}$ is upper semi-continuous i.e. (we drop the dependence in time which is off interest here)*

$$\overline{u}(x) = \overline{u}^*(x) = \limsup_{y \to x} \overline{u}(y).$$

Step 1 : Proof of $\overline{u}^*(x) \leq \overline{u}(x)$
We take $x_k \to x$ and $\overline{u}(x_k) \to l$ when $k \to \infty$. Assume that for any $\delta > 0$ there exists k large enough ($k \geq k(\delta)$) such that

$$|\overline{u}(x_k) - l| \leq \delta.$$

Fix $k(\delta)$ such that

$$|u^\varepsilon(y_{\varepsilon,k}) - \overline{u}(x_k)| \leq \delta.$$

For ε small enough, we have

$$|u^\varepsilon(y_{\varepsilon,k}) - l| \leq 2\delta$$

such that

$$l \leq 2\delta + u^\varepsilon(y_{\varepsilon,k}). \tag{3.3.60}$$

In the same way, we can take $|x_k - x| \leq \delta$ and $|y_{\varepsilon,k} - x_k| \leq \delta$ such that

$$|x - y_{\varepsilon,k}| \leq 2\delta \tag{3.3.61}$$

We take $\delta \to 0$ in (3.3.60)

$$l \leq 0 + \limsup_{\delta \to 0} u^{\varepsilon_\delta}(y_{\varepsilon_\delta,k_\delta}) \leq \limsup_{\substack{\varepsilon \to 0 \\ y \to x}} u^\varepsilon(y) = \overline{u}(x),$$

where we use also (3.3.61). **Step 2 : Proof of $\overline{u}^*(x) \geq \overline{u}(x)$**
It is obvious since $\overline{u}^*(x) = \limsup_{y \to x} \overline{u}(y)$ then it suffices to take the sequence $y = x$.

Lemma 3.5. (ε-uniform space and time gradient bounds)
Assume (A0)-(A1). Let $T > 0$ and $\varepsilon = (\Delta t, \Delta x)$ such that the CFL condition (3.1.12) is satisfied. If $(U_i^{\alpha,n})$ is the numerical solution of (3.1.7)-(3.1.8), then for any $\alpha = 1, ..., N$, $i \geq 0$ and $n \geq 0$, we have

$$\underline{p}_\alpha^0 \leq \frac{U_{i+1}^{\alpha,n} - U_i^{\alpha,n}}{\Delta x} \leq \overline{p}_\alpha^0 \quad \text{and} \quad m_0^0 \leq \frac{U_i^{\alpha,n+1} - U_i^{\alpha,n}}{\Delta t} \leq M_0^0, \tag{3.3.62}$$

where the quantities (independent of ε) m_0^0, M_0^0, $\underline{p}_\alpha^0$ and $\overline{p}_\alpha^0$ are respectively defined in (3.1.17) and (3.1.18).

Proof of Lemma 3.5 :
Let $\varepsilon = (\Delta t, \Delta x)$ be fixed such that the CFL condition (3.1.12) is satisfied.
Step 1 : Proof of $m^0 \geq m_0^0$, $\underline{p}_\alpha^0 \leq \underline{p}_\alpha$ and $\overline{p}_\alpha \leq \overline{p}_\alpha^0$
We first show that

$$m^0 \geq m_0^0. \tag{3.3.63}$$

Indeed using (A1) and the fact that $H_\alpha(p) = \max\{H_\alpha^-(p), H_\alpha^+(p)\}$ for any $p \in \mathbb{R}$, we get

$$m^0 = \inf_{\alpha,i}\left\{-H_\alpha(p_i^{\alpha,0})\right\} \geq \inf_{\substack{\alpha \\ p_\alpha \in [L^{\alpha,-}, L^{\alpha,+}]}} \{-H_\alpha(p_\alpha)\} =: m_0^0,$$

where we recall that $L^{\alpha,-}$ and $L^{\alpha,+}$ are the best Lipschitz constants defined in (3.1.16) that implies

$$L^{\alpha,-} \leq p_{i,+}^{\alpha,0} \leq L^{\alpha,+}, \quad \text{for any} \quad i \geq 0. \tag{3.3.64}$$

From (3.1.18) and the monotonicity of $H_\alpha^\pm$, we deduce

$$\underline{p}_\alpha^0 \leq \underline{p}_\alpha \quad \text{and} \quad \overline{p}_\alpha \leq \overline{p}_\alpha^0, \quad \text{for any} \quad \alpha = 1, ..., N. \tag{3.3.65}$$

Step 2 : Proof of $M^0 \leq M_0^0$
Recall the definitions

$$M^0 := \sup_{\alpha,i} W_i^{\alpha,0} = \max\{A, B\}, \quad \text{with} \quad \begin{cases} A := \min\limits_{\alpha=1,\dots,N} \left\{-H_\alpha^-(p_{0,+}^{\alpha,0})\right\}, \\ B := \sup\limits_{\alpha,i\geq 1} \left(\min\limits_{\sigma\in\{+,-\}} \left\{-H_\alpha^{-\sigma}(p_{i,\sigma}^{\alpha,0})\right\}\right). \end{cases}$$

and

$$M_0^0 := \max\left[\max_{\alpha=1,\dots,N} \left(\min_{\sigma\in\{+,-\}} \{-H_\alpha^{-\sigma}(L^{\alpha,\sigma})\}\right), \min_{\alpha=1,\dots,N} \left\{-H_\alpha^-(L^{\alpha,+})\right\}\right].$$

Let us show that

$$M^0 \leq M_0^0. \tag{3.3.66}$$

We distinguish two cases according to the value of M^0 :

- If $M^0 = A$, then

$$M_0^0 \geq \min_{\alpha=1,\dots,N}(-H_\alpha^-(L^{\alpha,+})) \geq \min_{\alpha=1,\dots,N}(-H_\alpha^-(p_{0,+}^{\alpha,0})) = A = M^0,$$

  where we use (3.3.64) and the monotonicity of H_α^-.

- If $M^0 = B$, then

$$M_0^0 \geq \max_{\alpha=1,\dots,N} \left(\min_{\sigma\in\{+,-\}} (-H_\alpha^{-\sigma}(L^{\alpha,\sigma}))\right) \geq \sup_{\alpha,i\geq 1} \left(\min_{\sigma\in\{+,-\}} (-H_\alpha^{-\sigma}(p_{i,\sigma}^{\alpha,0}))\right) = B = M^0.$$

  which comes from (3.3.64) and the following inequality (due to (3.3.64))

$$\min_{\sigma\in\{+,-\}} (-H_\alpha^{-\sigma}(L^{\alpha,\sigma})) \geq \min_{\sigma\in\{+,-\}} (-H_\alpha^{-\sigma}(p_{i,\sigma}^{\alpha,0})), \quad \text{for any} \quad i \geq 1.$$

Step 3 : Conclusion
The estimates (3.3.62) directly follow from (3.3.63), (3.3.66) and (3.3.65) and Theorem 1.3.
□

Proof of Theorem 1.8 :
Step 0 : Preliminaries
Let $T > 0$ be fixed and let $\varepsilon := (\Delta t, \Delta x)$ satisfy the CFL condition (3.1.12).

Assume that u_ε is the numerical solution of (3.1.7)-(3.1.8). We consider $\overline{u}$ and $\underline{u}$ respectively defined in (3.3.58) and (3.3.59). By construction, we have

$$\underline{u} \leq \overline{u}.$$

We will show in the following steps that $\underline{u}$ (resp. $\overline{u}$) is a viscosity supersolution (resp. viscosity subsolution) of equation (3.1.2)-(3.1.3), such that there exists a constant $C_T > 0$ such that for all $(t, y) \in [0, T) \times J$

$$\underline{u}(t, y) \geq -C_T(1 + |y|) \quad (\text{resp.} \quad \overline{u}(t, y) \leq C_T(1 + |y|)),$$

and such that

$$\underline{u}(0, y) \geq u_0(y) \quad (\text{resp.} \quad \overline{u}(0, y) \leq u_0(y)) \quad \text{for all} \quad y \in J.$$

Using the comparison principle (Proposition 3.2), we obtain

$$\overline{u} \leq u \leq \underline{u}.$$

Thus from Definition 5, we can conclude that $\overline{u} = u = \underline{u}$. This implies the statement of Theorem 1.8.

Step 1 : First bounds on the half relaxed limits
From Lemma 3.5, we deduce that for any $\alpha = 1, ..., N$, any $i \geq 0$ and any $n \geq 0$, we have

$$m_0^0 n\Delta t \leq U_i^{\alpha,n} - U_i^{\alpha,0} \leq M_0^0 n\Delta t.$$

Passing to the limit with $\varepsilon \to 0$ (always satisfying CFL condition (3.1.12)), we get

$$u_0(y) + m_0^0 t \leq \underline{u}(t,y) \leq \overline{u}(t,y) \leq u_0(y) + M_0^0 t, \quad \text{for} \quad (t,y) \in [0,T) \times J.$$

This implies that

$$\overline{u}(0,y) \leq u_0(y) \leq \underline{u}(0,y), \quad \text{for all} \quad y \in J, \tag{3.3.67}$$

and

$$\overline{u}(t,y) \leq C_T(1+|y|) \quad \text{and} \quad \underline{u}(t,y) \geq -C_T(1+|y|),$$

with $C_T = \max\{|m_0^0|T, |M_0^0|T\} + |u_0(0)| + L$ and $L = \max\limits_{\alpha,\sigma\in\{\pm\}} |L^{\alpha,\sigma}|$.

In next step, we show that $\underline{u}$ is a supersolution of (3.1.2)-(3.1.3) in the viscosity sense. We skip the proof that $\overline{u}$ is a viscosity subsolution because it is similar.

Step 2 : Proof of $\underline{u}$ being a viscosity supersolution
Let us consider $\underline{u} = (\underline{u}^\alpha)_{\alpha=1,...,N}$ as defined in (3.3.59) and a test function $\varphi := (\varphi^\alpha)_\alpha \in \mathcal{C}^1_*([0,T) \times J)$ satisfying

$$\begin{cases} \underline{u} \geq \varphi & \text{on} \quad [0,T) \times J, \\ \underline{u} = \varphi & \text{at} \quad P_0 = (t_0, y_0) \in [0,T) \times J, \quad \text{with} \quad t_0 > 0. \end{cases}$$

Thus up to replacing $\varphi(P)$ by $\hat{\varphi}(P) = \varphi(P) + |P - P_0|^2$, we can assume that

$$\begin{cases} \underline{u} > \varphi & \text{on} \quad \overline{B_r(P_0)} \setminus \{P_0\}, \\ \underline{u} = \varphi & \text{at} \quad P_0. \end{cases}$$

We set $B_r(P_0)$ the open ball in $[0,T) \times J$ centred at P_0 with fixed radius $r > 0$ i.e.

$$B_r(P_0) := \Big\{(t,y) \in [0,T) \times J, \quad (t-t_0)^2 + d(y,y_0)^2 < r\Big\}$$

where $d(\cdot,\cdot)$ denotes the natural distance on J. We also set Ω_ε defined as the intersection between the closed ball centred on P_0 and the grid points G_ε (defined in (3.3.57)), i.e.

$$\Omega_\varepsilon := \overline{B_r(P_0)} \cap G_\varepsilon.$$

Note that for ε small enough, we have $\Omega_\varepsilon \neq \emptyset$. Up to decreasing r, we can assume that $B_r(P_0) \subset [0, T-r) \times J$.

Define also

$$M_\varepsilon = \inf_{\Omega_\varepsilon} (u_\varepsilon - \varphi) = (u_\varepsilon - \varphi)(P_\varepsilon),$$

where

$$P_\varepsilon = (t_\varepsilon, y_\varepsilon) \in [0,T) \times J_{\alpha_\varepsilon} \quad \text{with} \quad y_\varepsilon = x_\varepsilon e_{\alpha_\varepsilon} \quad \text{and} \quad \begin{cases} t_\varepsilon := n_\varepsilon \Delta t \\ x_\varepsilon := i_\varepsilon \Delta x \end{cases}.$$

By the definition of $\underline{u}$ in (3.3.59), it is classical to show that if $\varepsilon \to 0$ we get the following (at least for a subsequence)

$$\begin{cases} M_\varepsilon = (u_\varepsilon - \varphi)(P_\varepsilon) \to M_0 = \inf\limits_{\overline{B_r(P_0)}} (\underline{u} - \varphi) = 0, \\ P_\varepsilon \to P_0. \end{cases} \tag{3.3.68}$$

Remark 3.6 (Proof of $P_{\varepsilon'} \to P_0$ when $\varepsilon' \to 0$)**.** *We argue by contradiction, assuming that for a subsequence $\varepsilon_k \to 0$ (when $k \to \infty$) we have $P_{\varepsilon_k} \to \tilde{P}_0$ with $\tilde{P}_0 \neq P_0$. We consider $M_{\varepsilon_k} = \inf\limits_{\Omega_{\varepsilon_k}} (u_{\varepsilon_k} - \varphi) = (u_{\varepsilon_k} - \varphi)(P_{\varepsilon_k})$. As for any k, we have $P_0 \in \Omega_{\varepsilon_k}$ then we get*

$$\liminf_{k\to\infty} M_{\varepsilon_k} \leq \liminf_{k\to\infty} u^{\varepsilon_k}(P_0) - \varphi(P_0).$$

The right part of the inequality is equal to

$$\underline{u}(P_0) - \varphi(P_0) = 0,$$

while the left part is such that

$$\liminf_{k\to\infty} M_{\varepsilon_k} = \liminf_{k\to\infty} (u_{\varepsilon_k} - \varphi)(P_{\varepsilon_k}) = (\underline{u} - \varphi)(\tilde{P}_0) > 0,$$

where we use that $\underline{u} > \varphi$ on $\overline{B_r(P_0)} \setminus \{P_0\}$. We thus get a contradiction.

Let us now check that $\underline{u}$ is a viscosity supersolution of (3.1.2). To this end, using Proposition 3.3 we want to show that

- if $y_0 = x_0 e_{\alpha_0} \in J^*_{\alpha_0}$ for a given α_0, then
$$\varphi_t^{\alpha_0} + H_{\alpha_0}(\varphi_x^{\alpha_0}) \geq 0 \quad \text{at} \quad (t_0, x_0),$$
- if $y_0 = 0$, then either there exists one index α_0 such that
$$\varphi_t^{\alpha_0} + H_{\alpha_0}(\varphi_x^{\alpha_0}) \geq 0 \quad \text{at} \quad (t_0, 0),$$
or we have
$$\varphi_t + \sup_{\alpha=1,\dots,N} \{H_\alpha^-(\varphi_x^\alpha)\} \geq 0 \quad \text{at} \quad (t_0, 0).$$

Because $t_0 > 0$ and $P_\varepsilon \to P_0$, this implies in particular that $n_\varepsilon \geq 1$ for ε small enough. We have to distinguish two cases according to the value of y_0.

Case 1 : $P_0 = (t_0, y_0)$ with $y_0 = 0$

We distinguish two subcases, up to subsequences.

Subcase 1.1 : $P_\varepsilon = (t_\varepsilon, y_\varepsilon)$ with $y_\varepsilon = y_0 = 0$

Using the definitions (3.2.23), (3.2.24) and the numerical scheme (3.1.7), we recall that for all $n \geq 0$ and for any $\alpha = 1, ..., N$

$$\begin{aligned} U_0^{\alpha,n+1} =: U_0^{n+1} &= U_0^n - \Delta t \max_{\alpha=1,\dots,N} H_\alpha^- \left(\frac{U_1^{\alpha,n} - U_0^n}{\Delta x} \right) \\ &= S_0 \left[U_0^n, (U_1^{\alpha,n})_{\alpha=1,\dots,N} \right] \end{aligned}$$

where S_0 is monotone under the CFL condition (3.1.12) (see Proposition 1.2).

Let $\varphi_\varepsilon := M_\varepsilon + \varphi$ such that

$$\begin{aligned}\varphi_\varepsilon(P_\varepsilon) = u_\varepsilon(P_\varepsilon) &= U_0^{n_\varepsilon} \\ &= S_0\left[U_0^{n_\varepsilon-1}, \left(U_1^{\alpha,n_\varepsilon-1}\right)_{\alpha=1,\dots,N}\right] \\ &\geq S_0\left[\varphi_\varepsilon((n_\varepsilon-1)\Delta t, 0), (\varphi_\varepsilon^\alpha((n_\varepsilon-1)\Delta t, \Delta x))_{\alpha=1,\dots,N}\right]\end{aligned}$$

where we use the monotonicity of the scheme in the last line and the fact that $u_\varepsilon \geq \varphi_\varepsilon$ on Ω_ε.

Thus we have

$$\frac{\varphi_\varepsilon(n_\varepsilon\Delta t, 0) - \varphi_\varepsilon((n_\varepsilon-1)\Delta t, 0)}{\Delta t} + \max_{\alpha=1,\dots,N} H_\alpha^-\left(\frac{\varphi_\varepsilon^\alpha((n_\varepsilon-1)\Delta t, \Delta x) - \varphi_\varepsilon^\alpha((n_\varepsilon-1)\Delta t, 0)}{\Delta x}\right) \geq 0.$$

This implies

$$(\varphi_\varepsilon)_t + \max_{\alpha=1,\dots,N} H_\alpha^-((\varphi_\varepsilon^\alpha)_x) + o_\varepsilon(1) \geq 0 \quad \text{at} \quad (t_\varepsilon, 0)$$

and passing to the limit with $\varepsilon \to 0$, we get the supersolution condition at the junction point

$$\varphi_t + \max_{\alpha=1,\dots,N} H_\alpha^-(\varphi_x^\alpha) \geq 0 \quad \text{at} \quad (t_0, 0). \tag{3.3.69}$$

Subcase 1.2 : $P_\varepsilon = (t_\varepsilon, y_\varepsilon)$ **with** $y_\varepsilon \in J_{\alpha_\varepsilon}^*$

In this case, the infimum M_ε is reached for a point on the branch α_ε which is different from the junction point. Thus the definitions (3.2.23), (3.2.24) and the numerical scheme (3.1.7) give us that for all $n \geq 0$ and $i \geq 1$

$$\begin{aligned}U_i^{\alpha_\varepsilon,n+1} &= U_i^{\alpha_\varepsilon,n} + \Delta t \min\left\{-H_{\alpha_\varepsilon}^-(p_{i,+}^{\alpha_\varepsilon,n}), -H_{\alpha_\varepsilon}^+(p_{i,-}^{\alpha_\varepsilon,n})\right\} \\ &= S_{\alpha_\varepsilon}[U_{i-1}^{\alpha_\varepsilon,n}, U_i^{\alpha_\varepsilon,n}, U_{i+1}^{\alpha_\varepsilon,n}].\end{aligned}$$

Let $\varphi_\varepsilon^{\alpha_\varepsilon} := M_\varepsilon + \varphi^{\alpha_\varepsilon}$ such that

$$\begin{aligned}\varphi_\varepsilon^{\alpha_\varepsilon}(P_\varepsilon) = u_\varepsilon^{\alpha_\varepsilon}(P_\varepsilon) &= U_{i_\varepsilon}^{\alpha_\varepsilon,n_\varepsilon} \\ &= S_{\alpha_\varepsilon}[U_{i_\varepsilon-1}^{\alpha_\varepsilon,n_\varepsilon-1}, U_{i_\varepsilon}^{\alpha_\varepsilon,n_\varepsilon-1}, U_{i_\varepsilon+1}^{\alpha_\varepsilon,n_\varepsilon-1}] \\ &\geq S_{\alpha_\varepsilon}[\varphi_\varepsilon^{\alpha_\varepsilon}((n_\varepsilon-1)\Delta t, (i_\varepsilon-1)\Delta x), \varphi_\varepsilon^{\alpha_\varepsilon}((n_\varepsilon-1)\Delta t, i_\varepsilon\Delta x), \varphi_\varepsilon^{\alpha_\varepsilon}((n_\varepsilon-1)\Delta t, (i_\varepsilon+1)\Delta x\end{aligned}$$

where we use the monotonicity of the scheme and the fact that $u_\varepsilon^{\alpha_\varepsilon} \geq \varphi_\varepsilon^{\alpha_\varepsilon}$ in the neighbourhood of $(t_\varepsilon, x_\varepsilon)$.

Thus we have that for any $\varepsilon = (\Delta t, \Delta x)$

$$\begin{aligned}0 \leq &\frac{\varphi_\varepsilon^{\alpha_\varepsilon}(n_\varepsilon\Delta t, i_\varepsilon\Delta x) - \varphi_\varepsilon^{\alpha_\varepsilon}((n_\varepsilon-1)\Delta t, i_\varepsilon\Delta x)}{\Delta t} \\ &+ \max\left\{H_{\alpha_\varepsilon}^+\left(\frac{\varphi_\varepsilon^{\alpha_\varepsilon}(n_\varepsilon\Delta t, i_\varepsilon\Delta x) - \varphi_\varepsilon^{\alpha_\varepsilon}(n_\varepsilon\Delta t, (i_\varepsilon-1)\Delta x)}{\Delta x}\right),\right. \\ &\left. H_{\alpha_\varepsilon}^-\left(\frac{\varphi_\varepsilon^{\alpha_\varepsilon}(n_\varepsilon\Delta t, (i_\varepsilon+1)\Delta x) - \varphi_\varepsilon^{\alpha_\varepsilon}(n_\varepsilon\Delta t, i_\varepsilon\Delta x)}{\Delta x}\right)\right\}.\end{aligned}$$

Since $H_\alpha(p) = \max\{H_\alpha^+(p), H_\alpha^-(p)\}$, this implies

$$(\varphi^{\alpha_\varepsilon})_t + H_{\alpha_\varepsilon}((\varphi^{\alpha_\varepsilon})_x) + o_\varepsilon(1) \geq 0 \quad \text{at} \quad (t_\varepsilon, x_\varepsilon).$$

Up to a subsequence, we can assume that α_ε is independent of ε and equal to α_0. Thus passing to the limit with $\varepsilon \to 0$, we obtain

$$\varphi_t^{\alpha_0} + H_{\alpha_0}(\varphi_x^{\alpha_0}) \geq 0 \quad \text{at} \quad (t_0, 0). \tag{3.3.70}$$

Case 2 : $P_0 = (t_0, y_0)$ with $y_0 = x_0 e_{\alpha_0} \in J^*_{\alpha_0}$

As $P_\varepsilon \to P_0$ from (3.3.68), we can always consider that for ε small enough, we can write $P_\varepsilon = (t_\varepsilon, y_\varepsilon)$ with $y_\varepsilon \in J^*_{\alpha_\varepsilon}$. Thus the proof for this case is similar to the one in Subcase 1.2. We then conclude

$$\varphi_t^{\alpha_0} + H_{\alpha_0}(\varphi_x^{\alpha_0}) \geq 0 \quad \text{at} \quad (t_0, x_0). \tag{3.3.71}$$

Step 3 : Conclusion

The results (3.3.67), (3.3.69), (3.3.70) and (3.3.71) imply that $\underline{u}$ is a viscosity supersolution of (3.1.2)-(3.1.3). This ends the proof of Theorem 1.8. □

Lemma 3.7 (From point to point convergence to uniform convergence)**.** *If $\underline{u} = u = \overline{u}$, then $u_\varepsilon \to u$ locally uniformly on $\mathbb{R}$ i.e. for any any compact set $K \subset \mathbb{R}$*

$$\lim_{\varepsilon \to 0} \|u_\varepsilon - u\|_{L^\infty(K)} = 0. \tag{3.3.72}$$

Proof We argue by contradiction. Assume that (3.3.72) is false. There exists a compact set $K \subset \mathbb{R}$, there exists $\delta > 0$ small enough and there exists a sequence (ε_k) such that $\varepsilon_k \to 0$ when $k \to \infty$, such that

$$\|u_{\varepsilon_k} - u\|_{L^\infty(K)} \geq \delta > 0.$$

Thus there exists a subsequence $x_{\varepsilon_k} \in K$ such that

$$|u_{\varepsilon_k}(x_{\varepsilon_k}) - u(x_{\varepsilon_k})| \geq \frac{\delta}{2},$$

which implies in particular that

$$u_{\varepsilon_k}(x_{\varepsilon_k}) \geq \frac{\delta}{2} + u(x_{\varepsilon_k}).$$

We pass to the limit for $\varepsilon_k \to 0$ and we assume that $x_{\varepsilon_k} \to x_0$. We get

$$u(x_0) = \overline{u}(x_0) \geq \frac{\delta}{2} + u_*(x_0),$$

where we use that

$$\limsup_{(\varepsilon, y) \to (0, x)} u_\varepsilon(y) \leq \limsup_{\varepsilon \to 0} u_\varepsilon(x_\varepsilon)$$

and the definition of u_*. However we also have that $u_*(x_0) = u(x_0)$ because u is necesseraly continuous ($\underline{u} = u = \overline{u}$ with $\underline{u}$ lower semi-continuous and $\overline{u}$ upper semi-continuous). Then we get a contradiction. □

Proof of Theorem 1.5 : The proof is quite similar to the proof of Theorem 1.8. However it differs on some points mainly because we do not know if the comparison principle from Proposition 3.2 holds for (3.1.2).

- We recall from Lemma 3.5 that $u_\varepsilon^\alpha(n\Delta t, i\Delta x) := U_i^{\alpha,n}$ with $\varepsilon = (\Delta t, \Delta x)$ enjoys some discrete Lipschitz bounds in time and space, independent of ε.

- It is then possible to extend the discrete function u_ε, defined only on the grid points, into a continuous function $\tilde{u}_\varepsilon$, with the $\mathcal{Q}_1$ quadrilateral finite elements approximation for which we have the same Lipschitz bounds. We recall that the approximation is the following : consider a map $(t,x) \mapsto u(t,x)$ that takes values only on the vertex of a rectangle $ABCD$ with $A=(0,0)$, $B=(0,1)$, $C=(1,1)$ and $D=(1,0)$ (for sake of simplicity we take $\Delta t = 1 = \Delta x$). Then we extend the map u to any point (t,x) of the rectangle such that

$$u(t,x) = [u_A + x(u_B - u_A)](1-t) + [u_D + x(u_C - u_D)]t.$$

- In this way we can apply the Ascoli theorem which shows that there exists a subsequence $\tilde{u}_{\varepsilon'}$ which converges towards a function u, uniformly on every compact set (in time and space).

- We can then conclude that u is a viscosity super and subsolution of (3.1.2)-(3.1.3) repeating the proof of Theorem 1.8.

This ends the proof. □

Proof of Corollary 1.6 : The proof combines the gradient and time derivative estimates from Lemma 3.5 and the results of convergence from Theorem 1.5. Indeed, passing to the limit in (3.3.62) for a subsequence ε', using the convergence result of Theorem 1.5, we finally get (3.1.19). □

4 Application to traffic flow

As our motivation comes from traffic flow modelling, this section is devoted to the traffic interpretation of the model and the scheme. Notice that [141] has already focused on the meaning of the junction condition in this framework.

4.1 Settings

We first recall the main variables adapted for road traffic modelling as they are already defined in [141]. We consider a junction with $N_I \geq 1$ incoming roads and $N_O \geq 1$ outgoing ones. We also set that $N_I + N_O =: N$.

Densities and scalar conservation law. We assume that the vehicles densities denoted by $(\rho^\alpha)_\alpha$ solve the following scalar conservation laws (also called LWR model for Lighthill, Whitham [184] and Richards [221]) :

$$\begin{cases} \rho^\alpha_t + (f^\alpha(\rho^\alpha))_X = 0, & \text{for} \quad (t,X) \in [0,+\infty) \times (-\infty,0), \quad \alpha = 1,...,N_I, \\ \rho^\alpha_t + (f^\alpha(\rho^\alpha))_X = 0, & \text{for} \quad (t,X) \in [0,+\infty) \times (0,+\infty), \quad \alpha = N_I+1,...,N_I+N_O, \end{cases} \tag{3.4.73}$$

where we assume that the junction point is located at the origin $X=0$.

We assume that for any α the flux function $f^\alpha : \mathbb{R} \to \mathbb{R}$ reaches its unique maximum value for a critical density $\rho = \rho^\alpha_c > 0$ and it is non decreasing on $(-\infty, \rho^\alpha_c)$ and non-increasing on $(\rho^\alpha_c, +\infty)$. In traffic modelling, $\rho^\alpha \mapsto f^\alpha(\rho^\alpha)$ is usually called the *fundamental diagram*.

Let us define for any $\alpha = 1, ..., N$ the Demand function f_D^α (resp. the Supply function f_S^α) such that

$$f_D^\alpha(p) = \begin{cases} f^\alpha(p) & \text{for} \quad p \le \rho_c^\alpha \\ f^\alpha(\rho_c^\alpha) & \text{for} \quad p \ge \rho_c^\alpha \end{cases} \qquad \left(\text{resp.} \quad f_S^\alpha(p) = \begin{cases} f^\alpha(\rho_c^\alpha) & \text{for} \quad p \le \rho_c^\alpha \\ f^\alpha(p) & \text{for} \quad p \ge \rho_c^\alpha \end{cases} \right). \quad (3.4.74)$$

We assume that we have a set of fixed coefficients $0 \le (\gamma^\alpha)_\alpha \le 1$ that denote :

- either the proportion of the flow from the branch $\alpha = 1, ..., N_I$ which enters in the junction,
- or the proportion of the flow on the branch $\alpha = N_I + 1, ..., N$ exiting from the junction.

We also assume the natural relations

$$\sum_{\alpha=1}^{N_I} \gamma^\alpha = 1 \quad \text{and} \quad \sum_{\beta=N_I+1}^{N_I+N_O} \gamma^\beta = 1.$$

Remark 4.1. *We consider that the coefficients $(\gamma^\alpha)_{\alpha=1,...,N}$ are fixed and known at the beginning of the simulations. Such framework is particularly relevant for "quasi stationary" traffic flows.*

Vehicles labels and Hamilton-Jacobi equations. Extending for any $N_I \ge 1$ the interpretation and the notations given in [141] for a single incoming road, let us consider the *continuous* analogue u^α of the discrete vehicles labels (in the present paper with labels increasing in the backward direction with respect to the flow)

$$\begin{cases} u^\alpha(t,x) = u(t,0) - \dfrac{1}{\gamma^\alpha} \displaystyle\int_0^{-x} \rho^\alpha(t,y)dy, \quad \text{for} \quad x := -X > 0, \quad \text{if} \quad \alpha = 1, ..., N_I, \\ \\ u^\beta(t,x) = u(t,0) - \dfrac{1}{\gamma^\beta} \displaystyle\int_0^{x} \rho^\beta(t,y)dy, \quad \text{for} \quad x := X > 0, \quad \text{if} \quad \beta = N_I + 1, ..., N, \end{cases} \quad (3.4.75)$$

with equality of the functions at the junction point ($x = 0$), i.e.

$$u^\alpha(t,0) = u^\beta(t,0) =: u(t,0) \quad \text{for any} \quad \alpha, \beta. \quad (3.4.76)$$

where the common value $u(t,0)$ is nothing else than the (continuous) label of the vehicle at the junction point.

Following [141], for a suitable choice of the function $u(t,0)$, it is possible to check that the vehicles labels u^α satisfy the following Hamilton-Jacobi equation :

$$u_t^\alpha + H_\alpha(u_x^\alpha) = 0, \quad \text{for} \quad (t,x) \in [0, +\infty) \times (0, +\infty), \quad \alpha = 1, ..., N \quad (3.4.77)$$

where

$$H_\alpha(p) := \begin{cases} -\dfrac{1}{\gamma^\alpha} f^\alpha(\gamma^\alpha p) & \text{for} \quad \alpha = 1, ..., N_I, \\ \\ -\dfrac{1}{\gamma^\alpha} f^\alpha(-\gamma^\alpha p) & \text{for} \quad \alpha = N_I + 1, ..., N_I + N_O. \end{cases} \quad (3.4.78)$$

Following definitions of H_α^- and H_α^+ in (3.1.4) we get

$$H_\alpha^-(p) = \begin{cases} -\frac{1}{\gamma^\alpha} f_D^\alpha(\gamma^\alpha p) & \text{for} \quad \alpha \leq N_I, \\ -\frac{1}{\gamma^\alpha} f_S^\alpha(-\gamma^\alpha p) & \text{for} \quad \alpha \geq N_I + 1, \end{cases} \quad \text{and} \quad H_\alpha^+(p) = \begin{cases} -\frac{1}{\gamma^\alpha} f_S^\alpha(\gamma^\alpha p) & \text{for} \quad \alpha \leq N_I, \\ -\frac{1}{\gamma^\alpha} f_D^\alpha(-\gamma^\alpha p) & \text{for} \quad \alpha \geq N_I + 1. \end{cases} \tag{3.4.79}$$

The junction condition in (3.1.2) that reads

$$u_t(t,0) + \max_{\alpha=1,\dots,N} H_\alpha^-(u_x(t,0^+)) = 0. \tag{3.4.80}$$

is a natural condition from the traffic point of view. Indeed condition (3.4.80) can be rewritten as

$$u_t(t,0) = \min\left(\min_{\alpha=1,\dots,N_I} \frac{1}{\gamma^\alpha} f_D^\alpha(\rho^\alpha(t,0^-)), \min_{\beta=N_I+1,\dots,N} \frac{1}{\gamma^\beta} f_S^\beta(\rho^\beta(t,0^+)) \right). \tag{3.4.81}$$

The condition (3.4.81) claims that the passing flux is equal to the minimum between the upstream demand and the downstream supply functions as they were presented by Lebacque in [163] and [164] (also for the case of junctions). This condition maximizes the flow through the junction. This is also related to the Riemann solver *RS2* in [107] for junctions.

4.2 Review of the literature with application to traffic

Junction modelling. There is an important and fast growing literature about junction modeling from a traffic engineering viewpoint : see [97,148,225] for a critical review of junction models. The literature mainly refers to *pointwise junction* models [148,170,171]. Pointwise models are commonly restated in many instances as optimization problems.

Scalar one dimensional conservation laws and networks. Classically, macroscopic traffic flow models are based on a scalar one dimensional conservation law, e.g. the so-called LWR model (Lighthill, Whitham [184] and Richards [221]). The literature is also quite important concerning hyperbolic systems of conversation laws (see for example [36,75,160,222] and references therein) but these books also propose a large description of the scalar case. It is well-known that under suitable assumptions there exists a unique weak entropy solution for scalar conservation laws without junction.

Until now, existence of weak entropy solutions for a Cauchy problem on a network has been proved for general junctions in [107]. See also Garavello and Piccoli's book [106]. Uniqueness for scalar conservation laws for a junction with two branches has been proved first in [105] and then in [4] under suitable assumptions. Indeed [4] introduces a general framework with the notion of L^1-*dissipative admissibility germ* that is a selected family of elementary solutions. To the best authors' knowledge, there is no uniqueness result for general junctions with $N \geq 3$ branches and a differential characterization of the solution.

The conservation law counterpart of model (3.4.77),(3.4.76),(3.4.80) has been studied in [107] as a Riemann solver called *RS2*. In [107] an existence result is presented for concave flux functions, using the Wave Front Tracking (WFT) method. Moreover the Lipschitz continuous dependence of the solution with respect to the initial data is proven. This shows that the process of construction of a solution (here the WFT method) creates

a unique solution. Nevertheless, up to our knowledge, there is no differential characterization of this solution. Therefore the uniqueness of this solution is still an open problem.

Numerical schemes for conservation laws. According to [116] and [181], the numerical treatment of scalar conservation laws mainly deals with first order numerical schemes based on upwind finite difference method, such as the Godunov scheme [117] which is well-adapted for the LWR model [164].

As finite difference methods introduce numerical viscosity, other techniques were developed such as kinetic schemes that derive from the kinetic formulation of hyperbolic equations [215]. Such kinetic schemes are presented in [5] and they are applied to the traffic case in [41–43].

In [118] the authors apply a semidiscrete central numerical scheme to the Hamilton-Jacobi formulation of the LWR model. The equivalent scheme for densities recovers the classical Lax-Friedrichs scheme. Notice that the authors need to introduce at least two *ghost-cells* on each branch near the junction point to counterstrike the dispersion effects when computing the densities at the junction.

4.3 Derived scheme for the densities

The aim of this subsection is to properly express the numerical scheme satisfied by the densities in the traffic modelling framework. Let us recall that the density denoted by ρ^α is a solution of (3.4.73).

Let us consider a discretization with time step Δt and space step Δx. Then we define the discrete car density $\rho_i^{\alpha,n} \geq 0$ for $n \geq 0$ and $i \in \mathbb{Z}$ (see Figure 3.2) by

$$\rho_i^{\alpha,n} := \begin{cases} \gamma^\alpha p_{|i|-1,+}^{\alpha,n}, & \text{for} \quad i \leq -1, \quad \alpha = 1, ..., N_I, \\ -\gamma^\alpha p_{i,+}^{\alpha,n}, & \text{for} \quad i \geq 0, \quad \alpha = N_I + 1, ..., N_I + N_O, \end{cases} \tag{3.4.82}$$

where we recall

$$p_{j,+}^{\alpha,n} := \frac{U_{j+1}^{\alpha,n} - U_j^{\alpha,n}}{\Delta x}, \quad \text{for} \quad j \in \mathbb{N}, \quad \alpha = 1, ..., N.$$

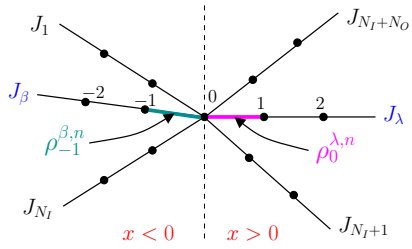

FIGURE 3.2 – Discretization of the branches with the nodes for $\left(U_{|i|}^{\alpha,n}\right)_{i\in\mathbb{Z}}$ and the segments for $(\rho_i^{\alpha,n})_{i\in\mathbb{Z}}$.

We have the following result :

Lemma 4.2 (Derived numerical scheme for the density)**.**
If $(U_i^{\alpha,n})$ stands for the solution of (3.1.7)-(3.1.8), then the density $(\rho_i^{\alpha,n})$ defined in (3.4.82)

is a solution of the following numerical scheme for $\alpha = 1, ..., N$

$$\frac{\Delta x}{\Delta t}\{\rho_i^{\alpha,n+1} - \rho_i^{\alpha,n}\} = \begin{cases} F^\alpha(\rho_{i-1}^{\alpha,n}, \rho_i^{\alpha,n}) - F^\alpha(\rho_i^{\alpha,n}, \rho_{i+1}^{\alpha,n}) & \text{for } \begin{cases} i \le -1 & \text{if } \alpha \le N_I, \\ i \ge 1 & \text{if } \alpha \ge N_I + 1, \end{cases} \\ F_0^\alpha\left((\rho_{-1}^{\beta,n})_{\beta \le N_I}, (\rho_0^{\lambda,n})_{\lambda \ge N_I+1}\right) - F^\alpha(\rho_i^{\alpha,n}, \rho_{i+1}^{\alpha,n}) & \text{for } i = 0, \quad \alpha \ge N_I + 1, \\ F^\alpha(\rho_{i-1}^{\alpha,n}, \rho_i^{\alpha,n}) - F_0^\alpha\left((\rho_{-1}^{\beta,n})_{\beta \le N_I}, (\rho_0^{\lambda,n})_{\lambda \ge N_I+1}\right) & \text{for } i = -1, \quad \alpha \le N_I, \end{cases} \tag{3.4.83}$$

where we define the fluxes by

$$\begin{cases} F^\alpha(\rho_{i-1}^{\alpha,n}, \rho_i^{\alpha,n}) := \min\left\{f_D^\alpha(\rho_{i-1}^{\alpha,n}),\ f_S^\alpha(\rho_i^{\alpha,n})\right\} & \text{for } \begin{cases} i \le -1 & \text{if } \alpha \le N_I, \\ i \ge 1 & \text{if } \alpha \ge N_I + 1, \end{cases} \\ F_0^\alpha\left((\rho_{-1}^{\beta,n})_{\beta \le N_I}, (\rho_0^{\lambda,n})_{\lambda \ge N_I+1}\right) := \gamma^\alpha F_0 & \text{for } \alpha = 1, ..., N, \\ F_0 := \min\left\{\min_{\beta \le N_I} \frac{1}{\gamma^\beta} f_D^\beta(\rho_{-1}^{\beta,n}),\ \min_{\lambda \ge N_I+1} \frac{1}{\gamma^\lambda} f_S^\lambda(\rho_0^{\lambda,n})\right\}. \end{cases} \tag{3.4.84}$$

and f_S^α, f_D^α *are defined in (3.4.74).*

The initial condition is given by

$$\rho_i^{\alpha,0} := \begin{cases} \gamma^\alpha \dfrac{u_0^\alpha(|i|\Delta x) - u_0^\alpha((|i|-1)\Delta x)}{\Delta x}, & \text{for } i \le -1, \quad \alpha = 1, ..., N_I, \\ \gamma^\alpha \dfrac{u_0^\alpha(i\Delta x) - u_0^\alpha((i+1)\Delta x)}{\Delta x}, & \text{for } i \ge 0, \quad \alpha = N_I + 1, ..., N_I + N_O. \end{cases} \tag{3.4.85}$$

Remark 4.3. *Notice that (3.4.83) recovers the classical Godunov scheme [117] for* $i \neq 0, -1$ *while it is not standard for the two other cases* $i = 0, -1$*. Moreover we can check that independently of the chosen CFL condition, the scheme (3.4.83) is not monotone (at the junction,* $i = 0$ *or* $i = -1$*) if the total number of branches* $N \ge 3$ *and is monotone if* $N = 2$ *for a suitable CFL condition.*

Remark 4.4. *From (3.1.11), (3.1.7) and (3.4.79), we can easily show that*

$$\begin{aligned} m^0 = \min\Bigg\{ & \min_{\substack{\alpha \le N_I \\ i \le -1}} \min\left(\frac{1}{\gamma^\alpha} f_D^\alpha(\rho_{i-1}^{\alpha,0}), \frac{1}{\gamma^\alpha} f_S^\alpha(\rho_i^{\alpha,0})\right), \\ & \min_{\substack{\alpha \ge N_I+1 \\ i \ge 1}} \min\left(\frac{1}{\gamma^\alpha} f_D^\alpha(\rho_{i-1}^{\alpha,0}), \frac{1}{\gamma^\alpha} f_S^\alpha(\rho_i^{\alpha,0})\right), \\ & \min\left(\min_{\alpha \le N_I} \frac{1}{\gamma^\alpha} f_D^\alpha(\rho_{-1}^{\alpha,0}), \min_{\alpha \ge N_I+1} \frac{1}{\gamma^\alpha} f_S^\alpha(\rho_0^{\alpha,0})\right)\Bigg\}, \end{aligned}$$

with the first part dealing with incoming branches, the second with outgoing branches and the third with the junction point. As $f^\alpha(p) = \min\{f_S^\alpha(p), f_D^\alpha(p)\}$ *for any* p*, the latter can be rewritten as the minimal initial flux*

$$m^0 = \min\left\{\min_{\substack{\alpha \le N_I \\ i \le -1}} \left(\frac{1}{\gamma^\alpha} f^\alpha(\rho_i^{\alpha,0})\right), \min_{\substack{\alpha \ge N_I+1 \\ i \ge 0}} \left(\frac{1}{\gamma^\alpha} f^\alpha(\rho_i^{\alpha,0})\right)\right\}.$$

We set for any $\alpha = 1, ..., N$

$$\begin{cases} \rho_\alpha^- := (f_D^\alpha)^{-1}(\gamma^\alpha m^0), \\ \rho_\alpha^+ := (f_S^\alpha)^{-1}(\gamma^\alpha m^0), \end{cases}$$

From Theorem 1.3 and Remark 1.4, if (3.1.12) is satisfied then it is easy to check that

$$\rho_\alpha^- \le \rho_i^{\alpha,n} \le \rho_\alpha^+, \quad \text{for all} \quad n \ge 0.$$

Then the CFL condition (3.1.12) can be rewritten for the densities as

$$\frac{\Delta x}{\Delta t} \ge \sup_{\substack{\alpha=1,...,N \\ \rho^\alpha \in [\rho_\alpha^-, \rho_\alpha^+]}} \left| (f^\alpha)'(\rho^\alpha) \right|. \tag{3.4.86}$$

Proof of Lemma 4.2 : We distinguish two cases according to if we are either on an incoming or an outgoing branch. We investigate the incoming case. The outgoing case can be done similarly.

Let us consider any $\alpha = 1, ..., N_I$, $n \ge 0$ and $i \le -1$.

According to (3.4.82), for $i \le -2$ we have that :

$$\begin{aligned} \frac{\rho_i^{\alpha,n+1} - \rho_i^{\alpha,n}}{\Delta t} &= \frac{\gamma^\alpha}{\Delta x \Delta t} \left\{ \left(U_{|i|}^{\alpha,n+1} - U_{|i|-1}^{\alpha,n+1} \right) - \left(U_{|i|}^{\alpha,n} - U_{|i|-1}^{\alpha,n} \right) \right\} \\ &= \frac{\gamma^\alpha}{\Delta x} \left\{ \min\left(-H_\alpha^-(p_{|i|,+}^{\alpha,n}), -H_\alpha^+(p_{|i|,-}^{\alpha,n}) \right) - \min\left(-H_\alpha^-(p_{|i|-1,+}^{\alpha,n}), -H_\alpha^+(p_{|i|-1,-}^{\alpha,n}) \right) \right\} \\ &= \frac{1}{\Delta x} \left\{ \min\left(f_D^\alpha(\rho_{i-1}^{\alpha,n}), f_S^\alpha(\rho_i^{\alpha,n}) \right) - \min\left(f_D^\alpha(\rho_i^{\alpha,n}), f_S^\alpha(\rho_{i+1}^{\alpha,n}) \right) \right\} \end{aligned}$$

where we use the numerical scheme (3.1.7) in the second line and (3.4.79) in the last line.

We then recover the result if we set the fluxes functions F^α as defined in (3.4.84).

For the special case of $i = -1$, we have

$$\begin{aligned} \frac{\rho_{-1}^{\alpha,n+1} - \rho_{-1}^{\alpha,n}}{\Delta t} &= \frac{\gamma^\alpha}{\Delta x} \left\{ \left(\frac{U_1^{\alpha,n+1} - U_1^{\alpha,n}}{\Delta t} \right) - \left(\frac{U_0^{\alpha,n+1} - U_0^{\alpha,n}}{\Delta t} \right) \right\} \\ &= \frac{\gamma^\alpha}{\Delta x} \left\{ \min\left(-H_\alpha^-(p_{1,+}^{\alpha,n}), -H_\alpha^+(p_{1,-}^{\alpha,n}) \right) - \min_{\beta=1,...,N} \left(-H_\beta^-(p_{0,+}^{\beta,n}) \right) \right\} \\ &= \frac{1}{\Delta x} \left\{ \min\left(f_D^\alpha(\rho_{-2}^{\alpha,n}), f_S^\alpha(\rho_{-1}^{\alpha,n}) \right) - \gamma^\alpha \min\left(\min_{\beta=1,...,N_I} \frac{1}{\gamma^\beta} f_D^\beta(\rho_{-1}^{\beta,n}), \min_{\lambda=N_I+1,...,N} \frac{1}{\gamma^\lambda} f_S^\lambda(\rho_0^{\lambda,n}) \right) \right\} \end{aligned}$$

where in the last line we have used (3.4.79). Setting the flux function F_0^α for $i = 0$ as defined in (3.4.84), we also recover the result in that case. □

4.4 Numerical extension for non-fixed coefficients (γ^α)

Up to now, we were considering fixed coefficients $\gamma := (\gamma^\alpha)_\alpha$ and the flux of the scheme at the junction point at time step $n \ge 0$ was

$$F_0(\gamma) := \min\left\{ \min_{\beta \le N_I} \frac{1}{\gamma^\beta} f_D^\beta(\rho_{-1}^{\beta,n}), \min_{\lambda \ge N_I+1} \frac{1}{\gamma^\lambda} f_S^\lambda(\rho_0^{\lambda,n}) \right\}.$$

In certain situations, we want to maximize the flux $F_0(\gamma)$ for γ belonging to an admissible set Γ. Indeed we can consider the set

$$A := \operatorname*{argmax}_{\gamma \in \Gamma} F_0(\gamma).$$

In the case where this set is not a singleton, we can also use a priority rule to select a single element $\gamma^{*,n}$ of A. This defines a map

$$\left((\rho_{-1}^{\beta,n})_{\beta\leq N_I}, (\rho_0^{\lambda,n})_{\lambda\geq N_I+1}\right) \mapsto \gamma^{*,n}.$$

At each time step $n \geq 0$ we can then choose this value $\gamma = \gamma^{*,n}$ in the numerical scheme (3.4.83), (3.4.84).

5 Simulation

In this section, we present a numerical experiment. The main goal is to check if the numerical scheme (3.1.7),(3.1.8) (or equivalently the scheme (3.4.83),(3.4.85)) is able to illustrate the propagation of shock or rarefaction waves for densities on a junction.

5.1 Settings

We consider the case of a junction with $N_I = 2 = N_O$, that is two incoming roads denoted $\alpha = 1$ and 2 and two outgoing roads denoted $\alpha = 3$ and 4.

For the simulation, we consider that the flow functions are equal on each branch $f^\alpha =: f$ for any $\alpha = 1, ..., 4$. Moreover the function f is bi-parabolic (and only Lipschitz) as depicted on Figure 3.3. It is defined as follows

$$f(\rho) = \begin{cases} \dfrac{(1-k)f_{max}}{\rho_c^2}\rho^2 + \dfrac{k f_{\max}}{\rho_c}\rho, & \text{for} \quad \rho \leq \rho_c, \\ \dfrac{(1-k)f_{max}}{(\rho_{max}-\rho_c)^2}\rho^2 + \dfrac{(k\rho_c + (k-2)\rho_{max})f_{max}}{(\rho_{max}-\rho_c)^2}\rho - \dfrac{\rho_{max}(k\rho_c - \rho_{max})f_{max}}{(\rho_{max}-\rho_c)^2}, & \text{for} \quad \rho > \rho_c, \end{cases} \tag{3.5.87}$$

with the jam density $\rho_c = 20\ veh/km$, the maximal $\rho_{max} = 160\ veh/km$, the maximal flow $f_{max} = 1000\ veh/h$ and $k = 1.5$.

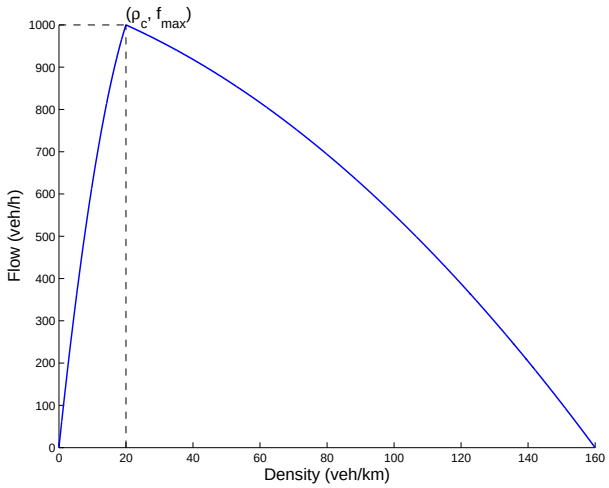

FIGURE 3.3 – Graph of the function f

The Hamiltonians H^α for $\alpha = 1, ..., 4$ are defined in (3.4.78) according to the flow function f given in (3.5.87). Because f is not C^1 at ρ_c, the Hamiltonians H_α do not satisfy assumption (A1). Nevertheless, we can use Remark 2.4 and the fact that f is Lipschitz to

extend our results for those Hamiltonians. We also assume that the coefficients (γ^α) are all identical

$$\gamma^\alpha = \frac{1}{2} \quad \text{for any} \quad \alpha = 1, ..., 4.$$

Notice that the computations are carried out for different Δx. In each case the time step Δt is set to the maximal possible value satisfying the CFL condition (3.1.12). We consider branches of length $L = 200\ m$ and we have $N_b := \left\lfloor \frac{L}{\Delta x} \right\rfloor$ points on each branch such that $i \in \{0, ..., N_b\}$.

5.2 Initial and boundary conditions

Initial conditions. In traffic flow simulations it is classical to consider Riemann problems for the vehicles densities at the junction point. We not only consider a Riemann problem at the junction but we also choose the initial data to be discontinuous (with two values of the densities (left and right)) on the outgoing branch number 3 (see Table 3.1 where *left* (resp. *right*) stands for the left (resp. right) section of branch 3). We then consider initial conditions $(u_0^\alpha(x))_{\alpha=1,...,N}$ corresponding to the primitive of the densities depicted on Figure 3.6 (a). We also take the initial label at the junction point such that

$$u_0^\alpha(0) =: u_0(0) = 0, \quad \text{for any} \quad \alpha.$$

We can check that the initial data $(u_0^\alpha(x))_{\alpha=1,...,N}$ satisfy (A0).

We are interested in the evolution of the densities. We stop to compute once we get a stationary final state as shown on Figure 3.6 (f). The values of densities and flows are summarized in Table 3.1.

	Initial state		Final state	
Branch	Density (veh/km)	Flow (veh/h)	Density (veh/km)	Flow (veh/h)
1	15	*844*	90	*625*
2	15	*844*	90	*625*
3 (left)	30	*962*	90	*625*
3 (right)	90	*625*	90	*625*
4	5	*344*	10	*625*

TABLE 3.1 – Values of densities and flows for initial and final states on each branch

Boundary conditions. For any $i \leq N_b$ we use the numerical scheme (3.1.7) for computing $(U_i^{\alpha,n})$. Nevertheless at the last grid point $i = N_b$, we have

$$\frac{U_{N_b}^{\alpha,n+1} - U_{N_b}^{\alpha,n}}{\Delta t} + \max\left\{H_\alpha^+(p_{N_b,-}^{\alpha,n}), H_\alpha^-(p_{N_b,+}^{\alpha,n})\right\} = 0, \quad \text{for} \quad \alpha = 1, \dots, N,$$

where $p_{N_b,-}^{\alpha,n}$ is defined in (3.1.5) and we set the boundary gradient as follows

$$p_{N_b,+}^{\alpha,n} = \begin{cases} \dfrac{\rho_0^\alpha}{\gamma^\alpha}, & \text{if} \quad \alpha \leq N_I, \\ p_{N_b,-}^{\alpha,n} = p_{N_b-1,+}^{\alpha,n}, & \text{if} \quad \alpha \geq N_I + 1. \end{cases}$$

These boundary conditions are motivated by our traffic application. Indeed while they are presented for the scheme (3.1.7) on $(U_i^{\alpha,n})$, the boundary conditions are easily translatable to the scheme (3.4.83) for the densities. For incoming roads, the flow that can enter

the branch is given by the minimum between the supply of the first cell and the demand of the virtual previous cell which correspond to the value of f evaluated for the initial density on the branch ρ_0^α (see Table 3.1). For outgoing roads, the flow that can exit the branch is given by the minimum between the demand of the last cell $H_\alpha^+(p_{N_b,-}^{\alpha,n})$ and the supply of the virtual next cell $H_\alpha^-(p_{N_b,+}^{\alpha,n})$ which is the same than the supply of the last cell $H_\alpha^-(p_{N_b-1,+}^{\alpha,n})$.

5.3 Simulation results

Vehicles labels and trajectories. Notice that here the computations are carried out for the discrete variables $(U_i^{\alpha,n})$ while the densities $(\rho_i^{\alpha,n})$ are computed in a post-treatment using (3.4.82). It is also possible to compute directly the densities $(\rho_i^{\alpha,n})$ according to the numerical scheme (3.4.83). Hereafter we consider $\Delta x = 5m$ (that corresponds to the average size of a vehicle) and $\Delta t = 0.16s$.

The numerical solution $(U_i^{\alpha,n})$ is depicted on Figure 3.4 (a). The vehicles trajectories are deduced by considering the iso-values of the labels surface $(U_i^{\alpha,n})$ (see Figure 3.4 (b)). In this case, one can observe that the congestion (described in the next part) induces a break in the velocities of the vehicles when going through the shock waves. The same is true when passing through the junction.

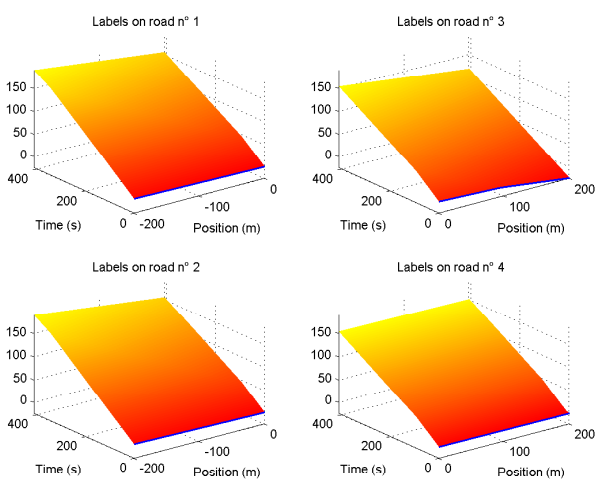

(a) Discrete labels $(U_i^{\alpha,n})_{i,n}$

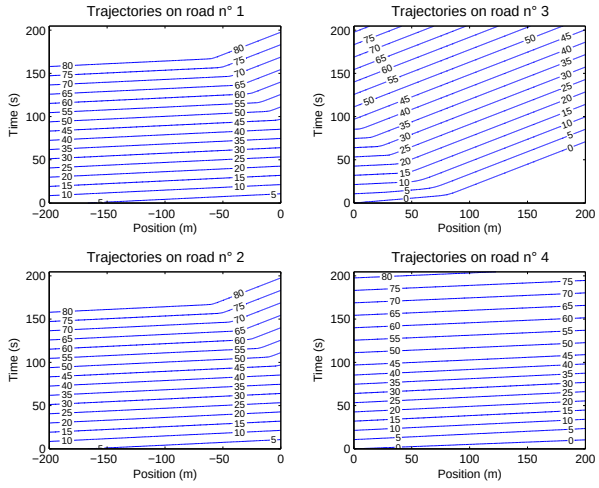

(b) Trajectories of some vehicles

FIGURE 3.4 – Numerical solution and vehicles trajectories

We can also recover the gradient properties of Theorem 1.3. On Figure 3.5, the gradients $\left(p_{i,+}^{\alpha,n}\right)$ are plotted as a function of time. We numerically check that the gradients stay between the bounds $\overline{p}^\alpha$ and $\underline{p}^\alpha$.

Propagation of waves. We describe hereafter the shock and rarefaction waves that appear from the considered initial data (see Figure 3.6). At the initial state (Figure 3.6 (a)), the traffic situation on roads 1, 2 and 4 is fluid $(\rho_0^{\{1,2,4\}} \leq \rho_c)$ while the road 3 is congested $(\rho_0^3 \geq \rho_c)$. Nevertheless the demands at the junction point are fully satisfied. As we can see on Figure 3.6 (b), there is the apparition of a rarefaction wave on road 4 and a shock wave on road 3, just downstream the junction point. At the same time, there is a shock wave propagating from the middle of the section on road 3 due to the initial discontinuous data there. This shock wave should propagate backward at the Rankine-Hugoniot speed $\tilde{v}_1 = -6$ km/h. A while later (Figure 3.6 (c)), the shock wave coming from the junction point and the shock wave coming from the middle of road 3 generate

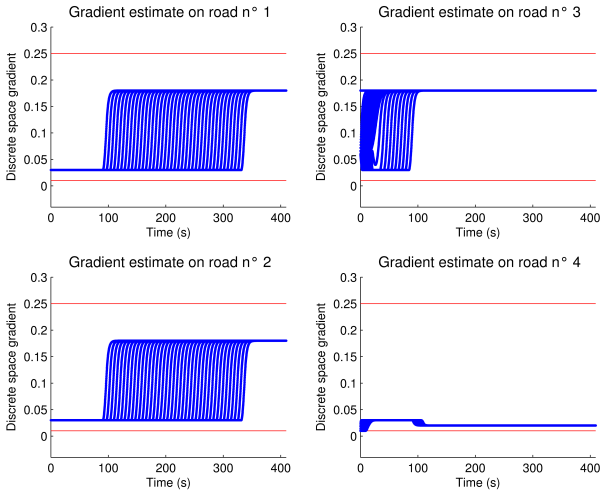

FIGURE 3.5 – Bounds $\overline{p}^{\alpha}$ and $\underline{p}^{\alpha}$ on the gradient

a new shock wave propagating backward at the speed of $\tilde{v}_2 = -3$ km/h. The congestion spreads all over the branch 3 and reaches the junction point. At that moment (Figure 3.6 (d)), the supply on road 3 (immediately downstream the junction point) collapses. The demand for road 3 cannot be satisfied. Then it generates a congestion on both incoming roads. The shock wave continues to propagate backward in a similar way on roads 1 and 2 at speed $\tilde{v}_2$ (Figure 3.6 (e)). This congestion creates a shock wave on road 4 (see Figure 3.6 (d)) and then decreases also the possible passing flow from the incoming roads to the road 4. However road 3 is still congested while the traffic situation on road 4 is fluid (see Figures 3.6 (e) and (f)).

Figure 3.6 numerically illustrates the convergence of the numerical solution $(\rho_i^{\alpha,n})$ when the grid size $(\Delta x, \Delta t)$ goes to zero. The rate of convergence is let to further research.

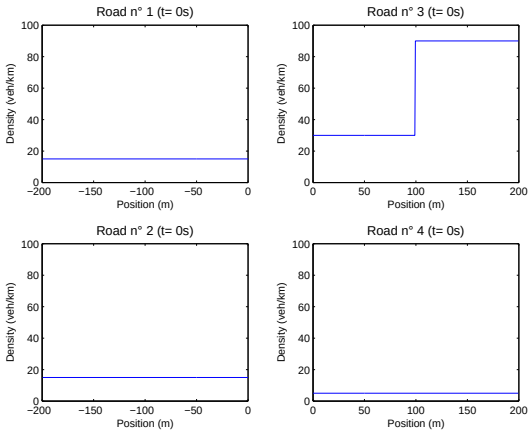

(a) Initial conditions for densities

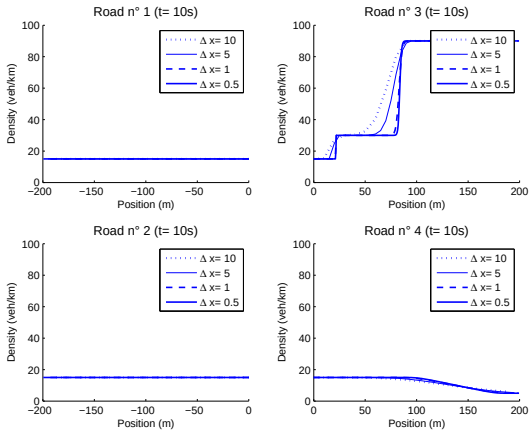

(b) Densities at $t = 10$ s

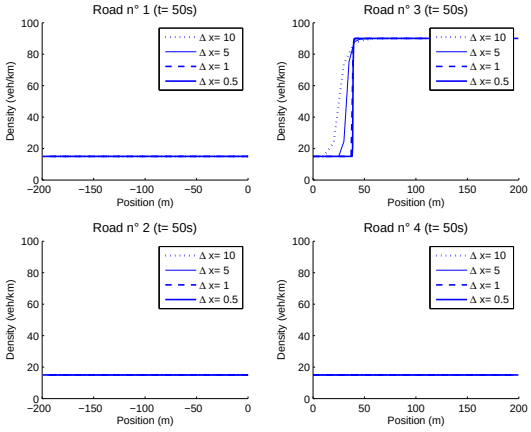

(c) Densities at $t = 50$ s

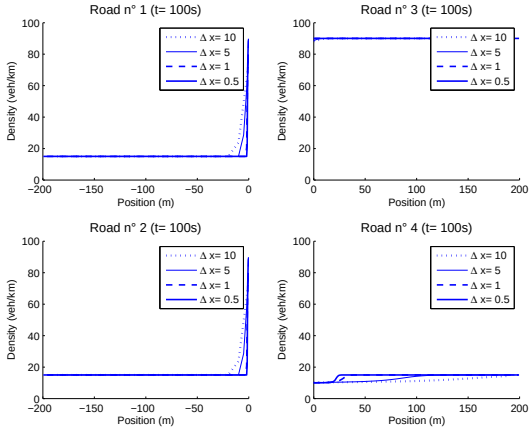

(d) Densities at $t = 100$ s

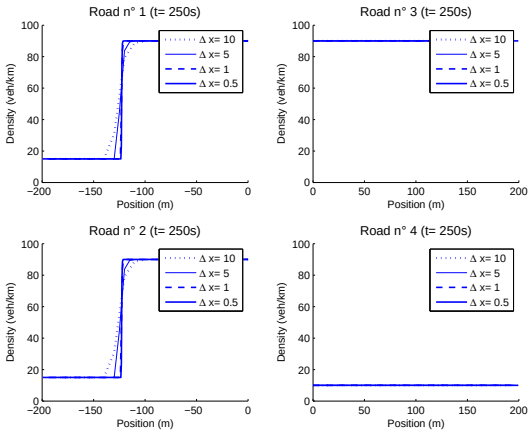

(e) Densities at $t = 250$ s

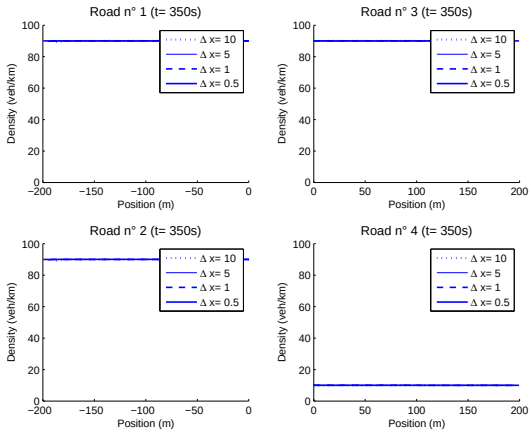

(f) Densities at $t = 350$ s

FIGURE 3.6 – Time evolution of vehicle densities for different Δx

Chapitre 4

Discussion about traffic junction modelling : conservation laws VS Hamilton-Jacobi equations

This chapter 4 is an adapted version of the published article [67], written in collaboration with Jean-Patrick Lebacque.

Sommaire

Abstract

In this chapter, we consider a numerical scheme to solve first order Hamilton-Jacobi (HJ) equations posed on a junction. The main mathematical properties of the scheme are first recalled and then we give a traffic flow interpretation of the key elements. The scheme formulation is also adapted to compute the vehicles densities on a junction. The equivalent scheme for densities recovers the well-known Godunov scheme outside the junction point. We give two numerical illustrations for a merge and a diverge which are the two main types of traffic junctions. Some extensions to the junction model are finally discussed.

1 Introduction

There exist many mathematical methods to deal with road traffic modelling, including Hamilton-Jacobi (HJ) equations. However HJ theory has been mainly used up to now in the frame of an infinite one-directional road [58, 80, 199–201]. Hamilton-Jacobi equations have been introduced in [141] for modelling junction problems. The approach was very recently completed in [140]. To the best authors' knowledge, they are the only works which model the flow on a junction as a unique function. The works [118, 122] introduce also an Hamilton-Jacobi formulation for networks but they need to deal with tedious coupling conditions at each junction. Here the goal of this paper is to introduce a numerical scheme to solve the model from [141] and to give a traffic interpretation of this scheme. We mainly refer hereafter to [69] in which the mathematical properties of the numerical scheme have been deeply studied. Our scheme (4.3.17) is related to the Godunov scheme for conservation laws in one space dimension, as it is explained in our application to traffic in Section 4.

The outline of the paper is the following : in Section 3 we recall the main elements of the HJ model on junction and we introduce the numerical scheme for solving such equations. The main mathematical results from [69] are also recalled. In Section 4, we propose the traffic flow interpretation of our numerical results. In particular, the numerical scheme for HJ equations (4.3.17) is derived and the junction condition is interpreted in terms of traffic flow modelling. Indeed, we recover the well-known junction condition of Lebacque (see [164]) or equivalently those for the Riemann solver at the junction as in the book of Garavello and Piccoli [106]. Then in Section 5 we illustrate the numerical behaviour of our scheme for two cases of junctions : a diverge (one incoming and two outgoing branches) and a merge (two incoming and one outgoing branches) which are classical junction configurations for arterial traffic. Finally, we discuss some possible extensions for the HJ model in Section 6.

2 Conservation laws framework

We are interested in macroscopic junction models that do not consider the individual behavior of drivers through the junction. However we need to take into account the specificity of the microscopic conflicts to build a model as realistic as possible.

2.1 Notations

We assume that the vehicles density denoted by ρ^α on each road α solves the following scalar conservation law (also called LWR model for Lighthill, Whitham [184] and Richards [221]) :

$$\rho_t^\alpha + (f^\alpha(\rho^\alpha))_X = 0, \quad \text{for} \quad (t, X) \in [0, +\infty) \times J^\alpha \tag{4.2.1}$$

where we assume that the junction point is located at the origin $X = 0$ such that J^α denotes the branch α of the junction. We have

$$J^\alpha := \begin{cases} (-\infty, 0), & \text{for an incoming branch,} \\ (0, +\infty), & \text{for an outgoing branch.} \end{cases}$$

We assume that for any α the flux function $f^\alpha : \mathbb{R} \to \mathbb{R}$ reaches its unique maximum value for a critical density $\rho = \rho_c^\alpha > 0$ and it is non decreasing on $(-\infty, \rho_c^\alpha]$ and non-increasing on $[\rho_c^\alpha, +\infty)$. In traffic modeling, $\rho^\alpha \mapsto f^\alpha(\rho^\alpha)$ is usually called the *fundamental diagram* and the vehicles density is bounded in $[0, \rho_{max}^\alpha]$ where ρ_{max}^α denotes the maximal density on branch α.

Let us define for any $\alpha = 1, ..., N$ the Demand function f_D^α (resp. the Supply function f_S^α) such that

$$f_D^\alpha(p) = \begin{cases} f^\alpha(p) & \text{for} \quad p \le \rho_c^\alpha \\ f^\alpha(\rho_c^\alpha) & \text{for} \quad p \ge \rho_c^\alpha \end{cases} \qquad \left(\text{resp.} \quad f_S^\alpha(p) = \begin{cases} f^\alpha(\rho_c^\alpha) & \text{for} \quad p \le \rho_c^\alpha \\ f^\alpha(p) & \text{for} \quad p \ge \rho_c^\alpha \end{cases} \right). \quad (4.2.2)$$

These functions are illustrated on Figure 4.1.

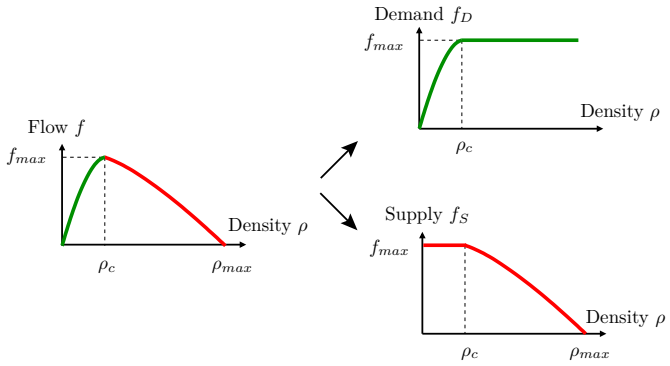

FIGURE 4.1 – Supply and demand functions

Remark 2.1. *Following [164], one can notice that the flow f^α is supposed to be at an equilibrium state at any point in space and time. The flow is given by the so-called Min formula that reads as the minimum between the immediate upstream demand and the immediate downstream supply*

$$f^\alpha(p(x,t)) = \min\left\{ f_D^\alpha(p(x^-,t)), f_S^\alpha(p(x^+,t)) \right\}. \quad (4.2.3)$$

This formula could be interpreted as the result of the competition between users wills (which form the demand) for the limited resource which is the available space in front of each driver (which forms the supply).

2.2 General optimization problem

We consider a general junction with $i \in \mathcal{I}$ incoming roads and $j \in \mathcal{J}$ outgoing ones. A general model for describing traffic flow at this junction consists in computing the incoming flows denoted by q_i on each incoming road indexed by i and the outgoing flows r_j on each outgoing road indexed by j. In this aim, we consider a optimization problem (originally

given in [171]) with a quadratic objective function to be maximized on a convex set of linear constraints :

$$\begin{array}{rl} \max & \sum_i \phi_i(q_i) + \sum_j \psi_j(r_j) \\ \text{s.t.} & \left| \begin{array}{ll} 0 \le q_i \le \delta_i & \forall i \\ 0 \le r_j \le \sigma_j & \forall j \\ 0 = r_j - \sum_i \gamma_{ij} q_i & \forall j \end{array} \right. \end{array} \tag{4.2.4}$$

where we have defined the demand on each incoming roads and respectively the supply on each outgoing ones such that :

$$\begin{cases} \delta_i := f_D^i(\rho_i(a-,t)) \\ \sigma_j := f_S^j(\rho_j(a+,t)) \end{cases} \tag{4.2.5}$$

Notice that γ_{ij} are the proportion of flow coming from road i which exits the junction point on road j.

As the objective function needs to be strictly concave to insure that there exists a unique maximum of (4.2.4), then the functions ϕ_i for each i and ψ_j for each j need to be increasing and strictly concave.

Remark 2.2. *Many models of the literature could be recast under the form of an optimization model. For example, the Daganzo's merge model in [77] is strictly equivalent to solve the optimization problem (4.2.4) with the following functions*

$$\phi_i(q_i) = N_{max}\left(q_i - \frac{q_i^2}{2p_i q_{i,max}}\right)$$

where p_i is the priority of flow coming from road i and $N_{max} = \phi_i'(0)$.

Other examples encompass the models of Herty and Klar [132], Holden and Risebro [133] and Coclite, Garavello, Piccoli [60].

At the optimal point, the Karush-Kuhn-Tucker optimality conditions give that :

- For any incoming road i

$$\phi_i'(q_i) + \sum_k s_k \gamma_{ik} - \lambda_i = 0, \quad \lambda_i \ge 0, \quad q_i \le \delta_i \quad \text{and} \quad \lambda_i(q_i - \delta_i) = 0,$$

  where (s_k, λ_i) are the Karush-Kuhn-Tucker coefficients (or Lagrange multipliers).

- and for any outgoing road j

$$\psi_j'(r_j) - s_j - \lambda_j = 0, \quad \lambda_j \ge 0, \quad r_i \le \sigma_j \quad \text{and} \quad \lambda_j(r_j - \sigma_j) = 0,$$

  where (s_j, λ_j) are the Karush-Kuhn-Tucker coefficients (or Lagrange multipliers).

Let us consider the first case of incoming roads. We can deal with outgoing roads in the same way. Let i be fixed. We have to distinguish two cases :

- Either $q_i < \delta_i$ and then it implies that $\lambda_i = 0$ (because of $\lambda_i(q_i - \delta_i) = 0$). If ϕ_i' is invertible, then we get

$$q_i = (\phi_i')^{-1}\left(-\sum_k s_k \gamma_{ik}\right).$$

- Or $q_i = \delta_i$. In this case, we notice that as $\lambda_i \geq 0$ and $(\phi_i')^{-1}$ is non-increasing, then we get

$$(\phi_i')^{-1}\left(-\sum_k s_k\gamma_{ik} + \lambda_i\right) \leq (\phi_i')^{-1}\left(-\sum_k s_k\gamma_{ik}\right).$$

Then we can deduce that the incoming and outgoing flows are given by the following relationships

$$\begin{cases} q_i = \min\left\{\delta_i, (\phi_i')^{-1}\left(-\sum_k \gamma_{ik}s_k\right)\right\}, & \text{for any} \quad i, \\ \\ r_j = \min\left\{(\psi_j')^{-1}(s_j), \sigma_j\right\}, & \text{for any} \quad j, \end{cases} \tag{4.2.6}$$

or equivalently by

$$\begin{cases} q_i = \Gamma_{[0,\delta_i]}\left((\phi_i')^{-1}\left(-\sum_k \gamma_{ik}s_k\right)\right), & \text{for any} \quad i, \\ \\ r_j = \Gamma_{[0,\sigma_j]}\left((\psi_j')^{-1}(s_j)\right), & \text{for any} \quad j, \end{cases} \tag{4.2.7}$$

where $\Gamma_{\mathcal{K}}$ is the projection operator on the set $\mathcal{K}$ and s_j are the Karush-Kuhn-Tucker coefficients which can be determined from the condition $0 = r_j - \sum_i \gamma_{ij}q_i$ for all j.

Remark 2.3. *Notice that (4.2.6) gives the flows under the form of a min formula between supply and demand. Then it is clear that such a model satisfies the invariance principle stated in [171].*

Remark 2.4. *We could be a little bit more general in (4.2.4) by considering another objective function denoted by $J((q_i)_i, (r_j)_j)$ which is such that J is strictly concave on each of its variables. The calculus are the same than before and we just need to replace ϕ_i' by $\dfrac{\partial S}{\partial q_i}$ for any i and ϕ_j' by $\dfrac{\partial S}{\partial r_j}$ for any j.*

2.3 Boundary conditions

From [171], we recall that to prescribe some supply/demand conditions at the boundaries of a link $\mathcal{D}$ (see Figure 4.2) such that

$$\begin{cases} f^{\mathcal{D}}(a,t) = \min\left\{f_D^u(t), f_S(a^+,t)\right\} \\ \\ f^{\mathcal{D}}(b,t) = \min\left\{f_D(b^-,t), f_S^d(t)\right\} \end{cases}$$

is strictly equivalent to respect Bardos-LeRoux-Nédélec conditions [18] (also equivalent to Dubois-LeFloch conditions [86] in the scalar case)

$$\left\{\text{sgn}[\rho(x,t)-\kappa] - \text{sgn}[A(c,t)-\kappa]\right\}\left[f(\rho(c,t)) - f(\kappa)\right]n(c) \geq 0, \quad \forall c \in \{a,b\} = \partial\mathcal{D}, \quad \text{and} \quad \forall \kappa \geq 0,$$

where $A(c,t)$ and $n(c)$ for $c \in \{a,b\}$ are respectively the boundary data and the normal to the boundary.

To prescribe the upstream boundary data $A(a,.)$ (resp. the downstream boundary data $A(b,.)$) in the BLN sense is equivalent to prescribe the boundary data $f_D^u(.)$ (resp. $f_S^d(.)$). Notice that basically A represents a density, while f is a flow but both are closely related.

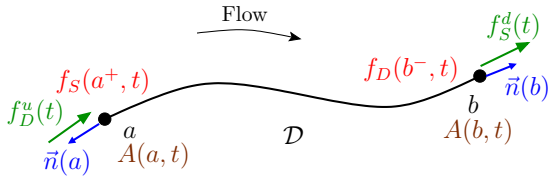

FIGURE 4.2 – Boundary conditions on a road $\mathcal{D} = [a, b]$

Remark 2.5 (Internal node supplies)**.** *We simply mention here that one can find in the literature (see for instance [45–47, 55, 104, 162]), models with specific internal boundary conditions, namely* internal node supplies*. The interested reader could refer to [64] for an extensive review of the literature. The idea is quite simple at the macroscopic viewpoint. Starting from engineering aspects of traffic flowing through a real junction, some authors have considered point-wise junctions with a constraint on the node supply (which may depend on the number of vehicles that could be contained in the node). This constraint stands for the sub-optimality of the flow through the junction point, due to interactions between vehicles (gap acceptance, yielding rules, etc.).*

2.4 A bird's eye on Garavello-Piccoli's solvers

The main mathematical interest is in the resolution of Cauchy problem on network. The classical approach in conservation laws framework (see [106]) is to consider a Riemann problem at junction points, that is to say specific Cauchy problems with initial discontinuous data on each branch of the junction.

The hyperbolic approach [106] focuses on the three following assumptions :

(i) The conservation of vehicles is available at the junction point, that can be written as the Rankine-Hugoniot condition :

$$\sum_{i=1}^{n} f(\rho_i(t,0^-)) = \sum_{j=n+1}^{n+m} f(\rho_j(t,0^+))$$

where ρ_i, $i = 1,...,n$ are the vehicles densities on incoming roads and ρ_j, $j = n+1,...,n+m$ are the vehicles density on the outgoing roads.

(ii) The prescribed preferences of drivers are known ; we determine a traffic distribution matrix A according to each proportion of drivers coming from the denoted i incoming road and who go through the indexed j outgoing road.

$$A = \{\alpha_{ji}\}_{\substack{j=n+1,...,n+m \\ i=1,...,n}} \in \mathbb{R}^{m\times n}$$

and

$$0 < \alpha_{ji} < 1, \quad \sum_{j=n+1}^{n+m} \alpha_{ji} = 1$$

(iii) The drivers behave in order to maximize the through-flow at the junction point. We recover a kind of optimization model described in Section 2.2 with $\varphi_i = 1$ and $\phi_j = 0$ or equivalently $\varphi_i = 0$ and $\phi_j = 1$ since $\sum_{i=1}^{n} q_i = \sum_{j=n+1}^{m} r_j$ where we recall that

$q_i := f(\rho_i(t,0^-))$ (resp. $r_j := f(\rho_j(t,0^+))$).

In the case where all the cars cannot go through the junction, there will be a loss of the uniqueness for the solutions. It is the reason why it is necessary to consider a fourth assumption :

(iv) A yielding rule has to be introduced in the case of the case of junctions where the number of incoming roads is greater than the number of outgoing ones. It is generally expressed as percentages γ_i of flux on incoming roads $i \in \{1, ..., n\}$ which can effectively enter the junction point. These coefficients satisfy

$$0 < \gamma_i < 1, \quad \sum_{i=1}^{n} \gamma_i = 1.$$

This priority condition affects only the upstream links.

Remark 2.6 (Riemann solvers)**.** *The above description matches the Riemann solver* RS1 *presented by Garavello and Piccoli in [106]. The Riemann solver* RS2 *use the maximization of the flux through the junction point but it doesn't consider the distribution matrix A. Instead, it introduces a separate distribution over incoming and outgoing branches through coefficients γ_i, γ_j which are close to our approach.*

3 Hamilton-Jacobi framework

3.1 Setting of the PDE problem

In this subsection, we first define the junction, then the space of functions on the junction and finally the Hamilton-Jacobi Partial Differential Equation (HJ-PDE). We follow [141].

The junction. Let us consider $N \geq 1$ different unit vectors $e_\alpha \in \mathbb{R}^2$ for $\alpha = 1, \dots, N$. We define the branches as the half-lines generated by these unit vectors

$$J_\alpha = [0, +\infty)e_\alpha \quad \text{and} \quad J_\alpha^* = J_\alpha \setminus \{0\}, \quad \text{for all} \quad \alpha = 1, \dots, N,$$

and the whole *junction* (see Figure 4.3) as

$$J = \bigcup_{\alpha=1,\dots,N} J_\alpha.$$

The origin $y = 0$ is called the *junction point*. For a time $T > 0$, we also consider the time-space domain defined as

$$J_T = (0, T) \times J.$$

HJ equation on the junction. We are interested in continuous functions $u : [0, T) \times J \to \mathbb{R}$ which are *viscosity solutions* (see Definition 3.3 in [69]) on J_T of

$$\begin{cases} u_t^\alpha + H_\alpha(u_x^\alpha) = 0 & \text{on} \quad (0,T) \times (0, +\infty), \quad \text{for} \quad \alpha = 1, \dots, N, \\ u^\beta =: \overline{u}, \quad \text{for all} \quad \beta = 1, \dots, N \\ \overline{u}_t + \max\limits_{\beta=1,\dots,N} H_\beta^-(u_x^\beta) = 0 & \text{on} \quad (0,T) \times \{0\}, \end{cases} \tag{4.3.8}$$

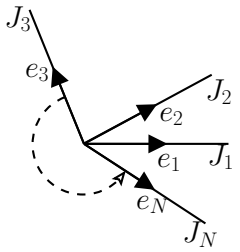

FIGURE 4.3 – Junction model

for functions H_α and H_α^- that will be defined below in assumption (A1).

We consider an initial condition

$$u^\alpha(0,x) = u_0^\alpha(x), \quad \text{with} \quad x \in [0,+\infty) \quad \text{for} \quad \alpha = 1,\dots,N. \tag{4.3.9}$$

Remark 3.1. *Following [141], we recall that (4.3.8) can be rigorously rewritten as*

$$u_t + H(y,u_y) = 0, \quad \textit{for} \quad (t,y) \in [0,T) \times J, \tag{4.3.10}$$

with

$$H(y,p) := \begin{cases} H_\alpha(p), & \textit{for} \quad p \in \mathbb{R}, & \textit{if} \quad y \in J_\alpha^*, \\ \max\limits_{\alpha=1,\dots,N} H_\alpha^-(p_\alpha), & \textit{for} \quad p = (p_1,\dots,p_N) \in \mathbb{R}^{\mathbb{N}}, & \textit{if} \quad y = 0, \end{cases}$$

subject to the initial condition

$$u(0,y) = u_0(y) := \left(u_0^\alpha(x)\right)_{\alpha=1,\dots,N}, \quad \textit{for} \quad y = xe_\alpha \in J \quad \textit{with} \quad x \in [0,+\infty). \tag{4.3.11}$$

This formulation highlights that HJ equation (4.3.10) subsumes all branches incident to the junction, making the state variable u a vector. This approach is very new compared to what is done in traffic literature (see Subsection 4.3).

We make the following assumptions :

(A0) **Initial data**

The initial data $u_0 := (u_0^\alpha)_\alpha$ is globally Lipschitz continuous on J, i.e. each associated u_0^α is Lipschitz continuous on $[0,+\infty)$ and $u_0^\alpha(0) = u_0^\beta(0)$ for any $\alpha \neq \beta$.

(A1) **Strong convexity of the Hamiltonians**

We assume that there exists a constant $\gamma > 0$, such that for each $\alpha = 1,...,N$, there exists a lagrangian function $L_\alpha \in C^2(\mathbb{R};\mathbb{R})$ satisfying $L_\alpha'' \geq \gamma > 0$ such that H_α is the Legendre-Fenchel transform of L_α i.e.

$$H_\alpha(p) = L_\alpha^*(p) = \sup_{q\in\mathbb{R}} (pq - L_\alpha(q)). \tag{4.3.12}$$

The assumption (A1) implies that

- the functions $H_\alpha \in C^1(\mathbb{R};\mathbb{R})$ are coercive, i.e. $\lim\limits_{|p|\to+\infty} H_\alpha(p) = +\infty$;

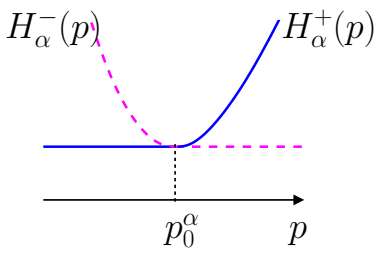

FIGURE 4.4 – Illustration of Hamiltonian function

- there exists a unique $p_0^\alpha \in \mathbb{R}$ such that H_α is non-increasing on $(-\infty, p_0^\alpha]$ and non-decreasing on $[p_0^\alpha, +\infty)$, and we set :

$$H_\alpha^-(p) = \begin{cases} H_\alpha(p) & \text{for} \quad p \le p_0^\alpha \\ \\ H_\alpha(p_0^\alpha) & \text{for} \quad p \ge p_0^\alpha \end{cases}$$

and (4.3.13)

$$H_\alpha^+(p) = \begin{cases} H_\alpha(p_0^\alpha) & \text{for} \quad p \le p_0^\alpha \\ \\ H_\alpha(p) & \text{for} \quad p \ge p_0^\alpha \end{cases}$$

where H_α^- is non-increasing and H_α^+ is non-decreasing (see Figure 4.4). Moreover, we have the following relationships

$$H_\alpha^-(p) = \sup_{q \le 0} (pq - L_\alpha(q)) \quad \text{and} \quad H_\alpha^+(p) = \sup_{q \ge 0} (pq - L_\alpha(q)). \tag{4.3.14}$$

3.2 Presentation of the scheme

We denote by Δx the space step and by Δt the time step. We denote by $U_i^{\alpha,n}$ an approximation of $u^\alpha(n\Delta t, i\Delta x)$ for $n \in \mathbb{N}$, $i \in \mathbb{N}$, where α stands for the index of the considered branch, as illustrated on Figure 4.5.

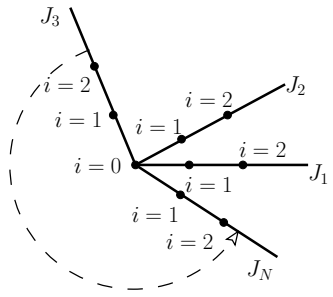

FIGURE 4.5 – Discretization of the junction model

We define the discrete space derivatives

$$p_{i,+}^{\alpha,n} := \frac{U_{i+1}^{\alpha,n} - U_i^{\alpha,n}}{\Delta x} \quad \text{and} \quad p_{i,-}^{\alpha,n} := \frac{U_i^{\alpha,n} - U_{i-1}^{\alpha,n}}{\Delta x}, \tag{4.3.15}$$

and similarly the discrete time derivative

$$W_i^{\alpha,n} := \frac{U_i^{\alpha,n+1} - U_i^{\alpha,n}}{\Delta t}. \tag{4.3.16}$$

Then we consider the following numerical scheme corresponding to the discretization of the HJ equation (4.3.8) for $n \geq 0$:

$$\begin{cases} \dfrac{U_i^{\alpha,n+1} - U_i^{\alpha,n}}{\Delta t} + \max\left\{H_\alpha^+(p_{i,-}^{\alpha,n}), H_\alpha^-(p_{i,+}^{\alpha,n})\right\} = 0, & \text{for} \quad i \geq 1, \quad \alpha = 1, \dots, N, \\ U_0^{\beta,n} =: U_0^n, \quad \text{for all} \quad \beta = 1, \dots, N \\ \dfrac{U_0^{n+1} - U_0^n}{\Delta t} + \max\limits_{\beta=1,\dots,N} H_\beta^-(p_{0,+}^{\beta,n}) = 0 \end{cases} \quad \text{for} \quad i = 0, \tag{4.3.17}$$

with the initial condition

$$U_i^{\alpha,0} = u_0^\alpha(i\Delta x) \quad \text{for} \quad i \geq 1, \quad \alpha = 1, \dots, N. \tag{4.3.18}$$

As usual, it is natural to introduce a Courant-Friedrichs-Lewy (CFL) condition [70]

$$\frac{\Delta x}{\Delta t} \geq \sup_{\substack{\alpha=1,\dots,N \\ p_\alpha \in [\underline{p}_\alpha, \overline{p}_\alpha]}} |H'_\alpha(p_\alpha)|. \tag{4.3.19}$$

It is easy to check that if the CFL condition (4.3.19) is satisfied, then the numerical scheme (4.3.17) is monotone.

3.3 Main result : convergence of the numerical solution

Hereafter is recalled one of the main results extracted from [69]. We particularly skip gradient and time derivatives estimates and also convergence property under weaker assumption than (A1) on the Hamiltonians. Interested readers are refered to [69].

Recall that under (A1), it is possible to recover the uniqueness of the solution (see [141]) :

Theorem 3.2. (Existence and uniqueness for a solution of the HJ-PDE)
Assume (A0)-(A1) and let $T > 0$. Then there exists a unique viscosity solution u of (4.3.8)-(4.3.9) on J_T in the viscosity sense, satisfying for some constant $C_T > 0$

$$|u(t,y) - u_0(y)| \leq C_T \quad \textit{for all} \quad (t,y) \in J_T.$$

Moreover the function u is Lipschitz continuous with respect to (t,y) on J_T.

Then from [69], we recover the following convergence result :

Theorem 3.3. (Convergence of the numerical solution)
Assume (A0)-(A1). Let $T > 0$ and $\varepsilon = (\Delta t, \Delta x)$ such that the CFL condition (4.3.19) is satisfied. If the function $u := (u^\alpha)_\alpha$ is the unique solution of (4.3.8)-(4.3.9) in the viscosity sense, then the numerical solution $(U_i^{\alpha,n})$ of (4.3.17)-(4.3.18) converges locally uniformly to u when $\varepsilon \to 0$ on any compact set $\mathcal{K} \subset [0,T) \times J$, i.e.

$$\limsup_{\varepsilon \to 0} \sup_{(n\Delta t, i\Delta x) \in \mathcal{K}} |u^\alpha(n\Delta t, i\Delta x) - U_i^{\alpha,n}| = 0 \tag{4.3.20}$$

where the index α in (4.3.20) is chosen such that $(n\Delta t, i\Delta x) \in \mathcal{K} \cap [0,T) \times J_\alpha$.

Remark 3.4. (Extension to weaker assumptions on H_α than (A1))
All the results above can be extended if we consider some weaker conditions than (A1) on the Hamiltonians H_α. Indeed, we can assume that u_0 and H_α for any $\alpha = 1, ..., N$ are at least locally Lipschitz. Such definitions are more accurate for our traffic application (see Section 4).

We need to consider that CFL condition (4.3.19) is replaced by the following one

$$\frac{\Delta x}{\Delta t} \geq \operatorname*{ess\,sup}_{\substack{\alpha=1,...,N \\ p_\alpha \in [\underline{p}_\alpha, \overline{p}_\alpha]}} |H'_\alpha(p_\alpha)|, \tag{4.3.21}$$

where ess sup *denotes the essential supremum defined such as the smallest number c for which the function H'_α only exceeds c on a set of measure zero.*

Using our scheme (4.3.17), we will present in Section 5 illustrations by numerical simulations with application to traffic.

4 Application to traffic flow

As our motivation comes from traffic flow modelling, this section is devoted to the traffic interpretation of the model and the scheme. Notice that [141] has already focused on the meaning of the junction condition in this framework.

4.1 Settings

We first recall the main variables adapted for road traffic modelling as they are already defined in [141]. We consider a junction with $N_I \geq 1$ incoming roads and $N_O \geq 1$ outgoing ones, such that $N_I + N_O =: N$.

Densities and scalar conservation law. We assume that the vehicles densities denoted by $(\rho^\alpha)_\alpha$ solve the following scalar conservation laws (also called LWR model for Lighthill, Whitham [184] and Richards [221]) :

$$\begin{cases} \rho^\alpha_t + (f^\alpha(\rho^\alpha))_X = 0, & \text{for} \quad (t, X) \in [0, +\infty) \times (-\infty, 0), \quad \alpha = 1, ..., N_I, \\ \rho^\alpha_t + (f^\alpha(\rho^\alpha))_X = 0, & \text{for} \quad (t, X) \in [0, +\infty) \times (0, +\infty), \quad \alpha = N_I + 1, ..., N_I + N_O, \end{cases} \tag{4.4.22}$$

where we assume that the junction point is located at the origin $X = 0$.

We assume that for any α the flux function $f^\alpha : \mathbb{R} \to \mathbb{R}$ reaches its unique maximum value for a critical density $\rho = \rho^\alpha_c > 0$ and it is non decreasing on $(-\infty, \rho^\alpha_c)$ and non-increasing on $(\rho^\alpha_c, +\infty)$. In traffic modelling, $\rho^\alpha \mapsto f^\alpha(\rho^\alpha)$ is usually called the *fundamental diagram*.

Let us define for any $\alpha = 1, ..., N$ the Demand function f^α_D (resp. the Supply function f^α_S) as in (4.2.2).

These functions are illustrated on Figure 4.1.

We assume that we have a set of fixed coefficients $0 \leq (\gamma^\alpha)_\alpha \leq 1$ that denote :

- either the proportion of the flow from the branch $\alpha = 1, ..., N_I$ which enters in the junction,
- or the proportion of the flow on the branch $\alpha = N_I + 1, ..., N$ exiting from the junction.

We also assume the natural relations

$$\sum_{\alpha=1}^{N_I} \gamma^\alpha = 1 \quad \text{and} \quad \sum_{\beta=N_I+1}^{N_I+N_O} \gamma^\beta = 1.$$

Remark 4.1. *We consider that the coefficients $(\gamma^\alpha)_{\alpha=1,\dots,N}$ are fixed and known at the beginning of the simulations. Such framework is particularly relevant for "quasi stationary" traffic flows.*

Vehicles labels and Hamilton-Jacobi equations. Extending for any $N_I \geq 1$ the interpretation and the notations given in [141] for a single incoming road, let us consider the *continuous* analogue u^α of the discrete vehicles labels (in the present paper with labels increasing in the backward direction with respect to the flow)

$$\begin{cases} u^\alpha(t,x) = u(t,0) - \dfrac{1}{\gamma^\alpha}\displaystyle\int_0^{-x} \rho^\alpha(t,y)dy, & \text{for } x := -X > 0, \quad \text{if } \alpha \leq N_I, \\ \\ u^\beta(t,x) = u(t,0) - \dfrac{1}{\gamma^\beta}\displaystyle\int_0^{x} \rho^\beta(t,y)dy, & \text{for } x := X > 0, \quad \text{if } \beta \geq N_I + 1, \end{cases} \tag{4.4.23}$$

with equality of the functions at the junction point ($x = 0$), i.e.

$$u^\alpha(t,0) = u^\beta(t,0) =: u(t,0) \quad \text{for any} \quad \alpha, \beta. \tag{4.4.24}$$

where the common value $u(t,0)$ is nothing else than the (continuous) label of the vehicle at the junction point.

Remark 4.2. *The vehicles labels are actually very useful for traffic management because on the one hand they are more reliable than flow and densities in-situ measurements and on the other hand, they give birth to the so-called Moskowitz function (or the Cumulative Vehicles Curves) of the labels on (t,x) which is very tractable. See [158] for a complete review.*

Following [141], for a suitable choice of the function $u(t,0)$, it is possible to check that the vehicles labels u^α satisfy the following Hamilton-Jacobi equation :

$$u_t^\alpha + H_\alpha(u_x^\alpha) = 0, \quad \text{for} \quad (t,x) \in [0,+\infty) \times (0,+\infty), \quad \alpha = 1, ..., N \tag{4.4.25}$$

where

$$H_\alpha(p) := \begin{cases} -\dfrac{1}{\gamma^\alpha} f^\alpha(\gamma^\alpha p) & \text{for} \quad \alpha = 1, ..., N_I, \\ \\ -\dfrac{1}{\gamma^\alpha} f^\alpha(-\gamma^\alpha p) & \text{for} \quad \alpha = N_I + 1, ..., N_I + N_O. \end{cases} \tag{4.4.26}$$

Remark 4.3. *It is worth noticing that the Hamiltonian H_α and the flow function f^α differ from a sign because flow function is classically assumed to be non-decreasing on $[0, \rho_c]$ and non-increasing on $[\rho_c, \rho_{max}]$ while it is the opposite for H_α according to (A1). The convexity of H_α is a key element for the uniqueness of the HJ solution as it is explained in [141].*

Following definitions of H_α^- and H_α^+ in (4.3.13) we get

$$H_\alpha^-(p) = \begin{cases} -\dfrac{1}{\gamma^\alpha} f_D^\alpha(\gamma^\alpha p) & \text{for} \quad \alpha \leq N_I, \\ -\dfrac{1}{\gamma^\alpha} f_S^\alpha(-\gamma^\alpha p) & \text{for} \quad \alpha \geq N_I + 1, \end{cases}$$

and (4.4.27)

$$H_\alpha^+(p) = \begin{cases} -\dfrac{1}{\gamma^\alpha} f_S^\alpha(\gamma^\alpha p) & \text{for} \quad \alpha \leq N_I, \\ -\dfrac{1}{\gamma^\alpha} f_D^\alpha(-\gamma^\alpha p) & \text{for} \quad \alpha \geq N_I + 1. \end{cases}$$

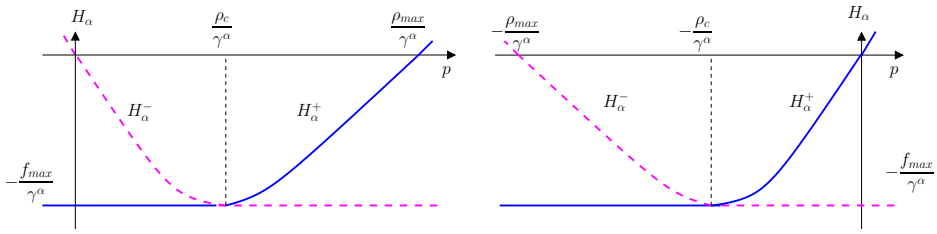

(a) Incoming branches (b) Outgoing branches

FIGURE 4.6 – Graphs of the Hamiltonians

4.2 Derived scheme for the densities

The aim of this subsection is to properly express the numerical scheme satisfied by the densities in the traffic modelling framework. Let us recall that the density denoted by ρ^α is a solution of (4.4.22).

Let us consider a discretization with time step Δt and space step Δx. Then we define the discrete car density $\rho_i^{\alpha,n} \geq 0$ for $n \geq 0$ and $i \in \mathbb{Z}$ (see Figure 4.7) by

$$\rho_i^{\alpha,n} := \begin{cases} \gamma^\alpha p_{|i|-1,+}^{\alpha,n}, & \text{for} \quad i \leq -1, \quad \alpha = 1, ..., N_I, \\ -\gamma^\alpha p_{i,+}^{\alpha,n}, & \text{for} \quad i \geq 0, \quad \alpha = N_I + 1, ..., N_I + N_O, \end{cases} \tag{4.4.28}$$

where we recall

$$p_{j,+}^{\alpha,n} := \frac{U_{j+1}^{\alpha,n} - U_j^{\alpha,n}}{\Delta x}, \quad \text{for} \quad j \in \mathbb{N}, \quad \alpha = 1, ..., N.$$

We have the following result :

Lemma 4.4 (Derived numerical scheme for the density)**.**
If $(U_i^{\alpha,n})$ stands for the solution of (4.3.17)-(4.3.18), then the density $(\rho_i^{\alpha,n})$ defined

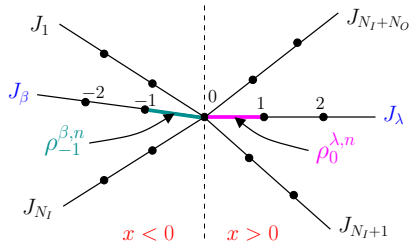

FIGURE 4.7 – Discretization of the branches with the nodes for $(U_i^{\alpha,n})$ and the segments for $(\rho_i^{\alpha,n})$

in (4.4.28) is a solution of the following numerical scheme for $\alpha = 1, ..., N$

$$\frac{\Delta x}{\Delta t}\{\rho_i^{\alpha,n+1} - \rho_i^{\alpha,n}\} = \begin{cases} F^\alpha(\rho_{i-1}^{\alpha,n}, \rho_i^{\alpha,n}) - F^\alpha(\rho_i^{\alpha,n}, \rho_{i+1}^{\alpha,n}) & \text{for } \begin{cases} i \le -1 & \text{if } \alpha \le N_I, \\ i \ge 1 & \text{else,} \end{cases} \\ F_0^\alpha\left((\rho_{-1}^{\beta,n})_{\beta\le N_I}, (\rho_0^{\lambda,n})_{\lambda \ge N_I+1}\right) - F^\alpha(\rho_i^{\alpha,n}, \rho_{i+1}^{\alpha,n}) & \text{for } i = 0, \quad \alpha \ge N_I + 1, \\ F^\alpha(\rho_{i-1}^{\alpha,n}, \rho_i^{\alpha,n}) - F_0^\alpha\left((\rho_{-1}^{\beta,n})_{\beta\le N_I}, (\rho_0^{\lambda,n})_{\lambda \ge N_I+1}\right) & \text{for } i = -1, \quad \alpha \le N_I, \end{cases} \tag{4.4.29}$$

where we define the fluxes by

$$\begin{cases} F^\alpha(\rho_{i-1}^{\alpha,n}, \rho_i^{\alpha,n}) := \min\left\{f_D^\alpha(\rho_{i-1}^{\alpha,n}),\ f_S^\alpha(\rho_i^{\alpha,n})\right\} & \text{for } \begin{cases} i \le -1 & \text{if } \alpha \le N_I, \\ i \ge 1 & \text{else,} \end{cases} \\ F_0^\alpha\left((\rho_{-1}^{\beta,n})_{\beta\le N_I}, (\rho_0^{\lambda,n})_{\lambda \ge N_I+1}\right) := \gamma^\alpha F_0 & \text{for } \alpha = 1, ..., N, \\ F_0 := \min\left\{\min_{\beta\le N_I} \frac{1}{\gamma^\beta} f_D^\beta(\rho_{-1}^{\beta,n}),\ \min_{\lambda \ge N_I+1} \frac{1}{\gamma^\lambda} f_S^\lambda(\rho_0^{\lambda,n})\right\}. \end{cases} \tag{4.4.30}$$

and f_S^α, f_D^α *are defined in (4.2.2).*

The initial condition is given by

$$\rho_i^{\alpha,0} := \begin{cases} \gamma^\alpha \dfrac{u_0^\alpha(|i|\Delta x) - u_0^\alpha((|i|-1)\Delta x)}{\Delta x}, & \text{for } i \le -1, \quad \alpha \le N_I, \\ \gamma^\alpha \dfrac{u_0^\alpha(i\Delta x) - u_0^\alpha((i+1)\Delta x)}{\Delta x}, & \text{for } i \ge 0, \quad \alpha \ge N_I + 1. \end{cases} \tag{4.4.31}$$

The proof of Lemma 4.4 is available in [69].

Remark 4.5. *Notice that (4.4.29) recovers the classical Godunov scheme [117] for* $i \neq 0, -1$ *while it is not standard for the two other cases* $i = 0, -1$*. Moreover we can check that independently of the chosen CFL condition, the scheme (4.4.29) is not monotone (at the junction,* $i = 0$ *or* $i = -1$*) if the total number of branches* $N \ge 3$ *and is monotone if* $N = 2$ *for a suitable CFL condition.*

Remark 4.6 (Non-monotonicity of (4.4.29))**.** *Let us recast the numerical scheme such as*

$$\rho_i^{\alpha,n+1} = \rho_i^{\alpha,n} + \frac{\Delta t}{\Delta x}\begin{cases} \left\{F^\alpha(\rho_{i-1}^{\alpha,n},\rho_i^{\alpha,n}) - F^\alpha(\rho_i^{\alpha,n},\rho_{i+1}^{\alpha,n})\right\}, & \text{for} \quad i\neq 0,-1,\\ \left\{F_0^\alpha\left((\rho_0^{\delta,n})_\delta\right) - F^\alpha(\rho_i^{\alpha,n},\rho_{i+1}^{\alpha,n})\right\}, & \text{for} \quad i=0,\\ \left\{F^\alpha(\rho_{i-1}^{\alpha,n},\rho_i^{\alpha,n}) - F_0^\alpha\left((\rho_0^{\delta,n})_\delta\right)\right\}, & \text{for} \quad i=-1, \end{cases}$$

so that we can set

$$\rho_i^{\alpha,n+1} = \begin{cases} S_i(\rho_{i-1}^{\alpha,n},\rho_i^{\alpha,n},\rho_{i+1}^{\alpha,n}) & \text{for} \quad i\neq 0,-1,\\ S_0\left((\rho_0^{\delta,n})_\delta,\rho_i^{\alpha,n},\rho_{i+1}^{\alpha,n}\right) & \text{for} \quad i=0,\\ S_{-1}\left(\rho_{i-1}^{\alpha,n},\rho_i^{\alpha,n},(\rho_0^{\delta,n})_\delta\right) & \text{for} \quad i=-1. \end{cases}$$

By definition, the scheme is monotone if and only if

$$\begin{cases} \dfrac{\partial S_i}{\partial \rho_j^{\alpha,n}} \geq 0, \quad \text{for} \quad i\neq 0,-1, \quad j\in\{i-1,i,i+1\},\\ \dfrac{\partial S_i}{\partial \rho_j^{\alpha,n}} \geq 0, \quad \text{for} \quad i=0, \quad j\in\{0,1\},\\ \dfrac{\partial S_i}{\partial \rho_j^{\alpha,n}} \geq 0, \quad \text{for} \quad i=-1, \quad j\in\{-2,-1\}. \end{cases}$$

It works pretty well for $i\neq 0,-1$ under the very classical CFL condition

$$\frac{\Delta x}{\Delta t} \geq \sup_{\substack{\alpha=1,\dots,N\\ p\in\mathbb{R}}} \left|(f^\alpha)'(p)\right|,$$

but we get counterexample for $i=0$ and as well for $i=-1$.

Indeed if we choose $i=0$ and if we assume that the flow through the junction is given by the supply of one outgoing branch i.e.

$$F_0^\alpha\left((\rho_0^{\delta,n})_\delta\right) := \frac{\gamma^\alpha}{\gamma^\lambda} f_S^\lambda(\rho_0^{\lambda,n}) \quad \text{for a certain} \quad \lambda \geq N_I.$$

Then

$$\frac{\partial S_{i=0}}{\partial \rho_0^{\lambda,n}} = \frac{\Delta t}{\Delta x}\frac{\gamma^\alpha}{\gamma^\lambda}(f_S^\lambda)'(\rho_0^{\lambda,n}) \leq 0,$$

because f_S^λ is a non-increasing function for any λ. Hence, for any condition on $\Delta t,\Delta x\geq 0$, it is not obvious to check that the scheme is monotone (as it is non-increasing for some $\rho_0^{\lambda,n}$).

Junction condition. The junction condition in (4.3.8) reads

$$u_t(t,0) + \max_{\alpha=1,\dots,N} H_\alpha^-(u_x(t,0^+)) = 0. \tag{4.4.32}$$

It is a natural condition from the traffic point of view. Indeed condition (4.4.32) can be rewritten as

$$\begin{aligned} u_t(t,0) &= \sum_{1\leq\alpha\leq N_I} f^\alpha(\rho^\alpha(t,0^-)) \\ &= \min\left(\min_{\alpha=1,\dots,N_I} \frac{1}{\gamma^\alpha} f_D^\alpha(\rho^\alpha(t,0^-)), \min_{\beta=N_I+1,\dots,N} \frac{1}{\gamma^\beta} f_S^\beta(\rho^\beta(t,0^+)) \right). \end{aligned} \tag{4.4.33}$$

The condition (4.4.33) claims that the passing flux is equal to the minimum between the upstream demand and the downstream supply functions as they were presented by Lebacque in [164] (also for the case of junctions). This condition maximizes the flow through the junction (also equal to the sum of all incoming flows or equivalently to the sum of all outgoing flows). Condition (4.4.33) could be recast as a linear optimization problem. Indeed if the densities $(\rho^\alpha(t,0^-))_{\alpha\leq N_I}$ and $\left(\rho^\beta(t,0^+)\right)_{\beta\geq N_I+1}$ at the boundaries of the junction point are known at time $t\geq 0$, we then can compute the densities at time t^+ by solving

$$\begin{aligned} &\max \sum_{1\leq\alpha\leq N_I} f^\alpha(\rho^\alpha(t^+,0^-)) \\ &\text{s.t.} \left| \begin{array}{ll} 0\leq f^\alpha(\rho^\alpha(t^+,0^-)) \leq f_D^\alpha(\rho^\alpha(t,0^-)), & \forall \alpha\leq N_I, \\ 0\leq f^\beta(\rho^\beta(t^+,0^+)) \leq f_S^\beta(\rho^\beta(t,0^+)), & \forall \beta\geq N_I+1, \\ 0 = f^\beta(\rho^\beta(t^+,0^+)) - \dfrac{\gamma^\beta}{\gamma^\alpha} f^\alpha(\rho^\alpha(t^+,0^-)), & \forall \alpha,\ \beta. \end{array} \right. \end{aligned} \tag{4.4.34}$$

where the constraints respectively express demand constraints on the incoming branches, supply constraints on outgoing branches and conservation of flows through the junction.

Remark 4.7. *The supply and demand conditions in (4.4.34) prescribe the values of densities at the boundaries of the junction point. For instance, consider the demand constraint*

$$f^\alpha(\rho^\alpha(t,0^-)\leq f_D^\alpha(\rho^\alpha(t,0^-)), \quad \textit{for any} \quad \alpha\leq N_I. \tag{4.4.35}$$

We have to distinguish two cases :

- *either there is equality in (4.4.35) and then the density at time t^+ is given by*

$$\rho^\alpha(t^+,0^-) = (f_D^\alpha)^{-1}\left(f^\alpha(\rho^\alpha(t,0^-))\right),$$

- *or we have the strict inequality in (4.4.35) and then the density at time t^+ becomes*

$$\rho^\alpha(t^+,0^-) = (f_S^\alpha)^{-1}\left(f^\alpha(\rho^\alpha(t,0^-))\right).$$

Notice that we need to properly define the inverse of $q_m^\alpha ax$ by f_D^α and f_S^α such that both functions are correctly invertible.

4.3 Review of the literature about junction modelling

Junction modelling has recently attracted an increasing interest but it was considered a long time ago by traffic engineers. In first papers (see Chapters 8 and 9 of [108]) the approaches were mainly built on microscopic description of vehicles. In the present work we adopt a macroscopic point of view in which individual cars behaviors are not taken into account.

Modelling approach. Intersections models can be classified into two categories : pointwise models and spatial extended models. On the one hand, spatial extended models consider the junction in its true space dimensions and analyze each conflicts between flows. These models offer a higher precision but also a greater complexity [46, 162]. On the other hand, pointwise models neglect the spatial dimension of the junction. Pointwise models are commonly restated in many instances as optimization problems [170, 171]. For sake of accuracy, some pointwise models take into account the node dynamics. The junction is seen as a buffer where incoming vehicles wait to be assigned on the outgoing roads. The literature often refers to internal state junction models [148]. The junction has an internal dynamics and it could be characterized by internal variables like the number of encompassed vehicles (denoted by N) or internal demand and supply constraints (respectively denoted by $\Delta(N)$ and $\Sigma(N)$ on Figure 4.8 (b)).

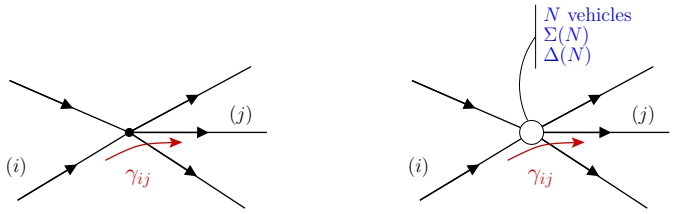

(a) Without internal dynamics (b) With internal dynamics

FIGURE 4.8 – Pointwise junction models

Lebacque's works [170, 171] have shown that in case of vehicles equilibrium inside the junction (for which the time scale of internal dynamics is infinitely small in regard to the variation of upstream demand and downstream supply), internal state models and optimization pointwise models are strictly equivalent for merges (two incoming and one outgoing roads) and FIFO diverges (one incoming and two outgoing roads).

General requirements. Formalizing the ideas expressed in [148], the authors in [225] propose a list of seven generic requirements that should be verified by every first order macroscopic junction model :

- General applicability to any kind of junction, regardless to the number of incoming and outgoing roads : merge and diverge models which are not applicable for general junctions, are then totally excluded.

  Maximization of the flows from an user point of view : road users try to maximize their own velocity whenever it is possible. In practice each flow would increase until be restricted by some constraint. Then the through-flow is not necessarily the maximum possible according to the difference between system optimum and user optimum.

- Non-negativity of flows since traffic flow only propagates forward.

- Satisfaction of supply and demand constraints : the outflow from an incoming road (resp. the inflow into a outgoing road) can never exceed the demand (resp. the supply) at the boundary of the road.

- Conservation of vehicles : no vehicle appears or disappears at the junction.

- Conservation if turning fractions : the model has to consider the users route choices and it should not maximize the flows without considering the turning fractions of

vehicles.

- Satisfaction of the invariance principle : stated first in [171] this principle expresses that the flows through the junction have to stay unchanged if the initial conditions (demand on incoming roads or supply on outgoing roads) are changed to the maximal capacity. Then (a) as long as a flow is limited by a capacity, a variation of its arriving demand cannot change the flow and (b) as long as a flow is not limited by a capacity, a variation of this capacity cannot change the flow.

In [97] and in [113], the authors consider an additional requirement :

- Internal supply constraints : such constraints are mainly justified for urban and regional junctions because they represent supply constraints due to vehicles interactions inside the junction. Such conflicts could be neglected for highways merges and diverges. However, [65] highlights that the uniqueness of the solution is not guaranteed with these additional constraints.

5 Simulations

In this section, we present two numerical experiments. The main goal is to check if the numerical scheme (4.3.17)-(4.3.18) (or equivalently the scheme (4.4.29)-(4.4.31)) is able to illustrate the propagation of shock or rarefaction waves for densities through a junction. We propose to apply the scheme for some special configurations of junctions that is (i) a diverge for which the scheme was originally designed (see [141]) and (ii) a simple merge. The scheme has been also applied to a more complex junction in [69].

Notice that here the computations are carried out for the discrete variables $(U_i^{\alpha,n})$ while the densities $(\rho_i^{\alpha,n})$ are computed in a post-treatment using (4.4.28). It is also possible to compute directly the densities $(\rho_i^{\alpha,n})$ according to the numerical scheme (4.4.29).

5.1 Settings

For the simulation, we consider that the flow functions are bi-parabolic (and only Lipschitz continuous) and defined as follows

$$f^\alpha(\rho) = \begin{cases} \dfrac{v^\alpha_{max}}{\rho^\alpha_c}\rho\left[(1-k)\rho + k\rho_{\max}\right], & \text{for} \quad \rho \le \rho^\alpha_c, \\ \dfrac{v^\alpha_{max}\rho^\alpha_c}{(\rho^\alpha_{max}-\rho^\alpha_c)^2}[(1-k)\rho^2 + (k\rho^\alpha_c + (k-2)\rho^\alpha_{max})\rho \\ \qquad\qquad -\rho^\alpha_{max}(k\rho^\alpha_c - \rho^\alpha_{max})], & \text{for} \quad \rho > \rho^\alpha_c, \end{cases}$$

where $k = 1.5$. The jam density ρ^α_c (resp. the maximal density ρ^α_{max}) on branch α is obtained as the product of the nominal jam density $\rho_c = 20\ veh/km$ (resp. the nominal maximal density $\rho_{max} = 160\ veh/km$) times the number of lanes on the branch. The maximal flow (or capacity) f^α_{max} is given by $v^\alpha_{max}\rho^\alpha_c$ where v^α_{max} is the maximal speed on branch α.

The Hamiltonians H^α are defined in (4.4.26) according to the flow function f^α. See also Remark 3.4 on weaker assumptions than (A1) on the Hamiltonians. We consider branches of length $L = 200\ m$ and we have $N_b := \left\lfloor \dfrac{L}{\Delta x} \right\rfloor$ points on each branch such that $i \in \{0, ..., N_b\}$.

5.2 Initial and boundary conditions

Initial conditions. In traffic flow simulations it is classical to consider Riemann problems for the vehicles densities (ρ_0^α) at the junction point. We then consider initial conditions $(u_0^\alpha(x))_{\alpha=1,\dots,N}$ corresponding to the primitive of the densities according to (4.4.31). We also take the initial label at the junction point such that

$$u_0^\alpha(0) =: u_0(0) = 0, \quad \text{for any} \quad \alpha.$$

We can check that if the initial densities (ρ_0^α) are piecewise constant, then the initial data $(u_0^\alpha(x))_{\alpha=1,\dots,N}$ satisfy (A0).

We are interested in the time evolution of the densities. We stop to compute once we get a stationary final state.

Boundary conditions. For any $i \leq N_b$ we use the numerical scheme (4.3.17) for computing $(U_i^{\alpha,n})$. Nevertheless at the last grid point $i = N_b$, we have

$$\frac{U_{N_b}^{\alpha,n+1} - U_{N_b}^{\alpha,n}}{\Delta t} + \max\left\{H_\alpha^+(p_{N_b,-}^{\alpha,n}), H_\alpha^-(p_{N_b,+}^{\alpha,n})\right\} = 0, \quad \text{for} \quad \alpha = 1,\dots,N,$$

where $p_{N_b,-}^{\alpha,n}$ is defined in (4.3.15) and we set the boundary gradient as follows

$$p_{N_b,+}^{\alpha,n} = \begin{cases} \dfrac{\rho_0^\alpha}{\gamma^\alpha}, & \text{if} \quad \alpha \leq N_I, \\ p_{N_b,-}^{\alpha,n}, & \text{if} \quad \alpha \geq N_I + 1. \end{cases}$$

These boundary conditions are motivated by our traffic application. Indeed while they are presented for the scheme (4.3.17) on $(U_i^{\alpha,n})$, the boundary conditions are easily translatable to the scheme (4.4.29) for the densities. For incoming roads, the flow that can enter the branch is given by the minimum between the supply of the first cell and the demand of the virtual previous cell which correspond to the value of f evaluated for the initial density on the branch ρ_0^α (see Table 4.1). For outgoing roads, the flow that can exit the branch is given by the minimum between the demand of the last cell and the supply of the virtual next cell which is the same than the supply of the last cell.

Remark 5.1. *From [171], we recall that to prescribe some supply/demand conditions at the boundaries of a branch is strictly equivalent to respect Bardos-LeRoux-Nédélec conditions [18].*

5.3 Simulation results for a diverge

We consider the case of a *diverge* : one incoming road denoted $\alpha = 1$ dividing into two outgoing roads respectively denoted 2 and 3 (see Figure 4.9). This case could illustrate the case of an off-ramp on a beltway. We introduce γ^α which represents the proportion of vehicles which exit the junction point on the branch indexed by α, with $\alpha = 2, 3$. These coefficients γ^2 and γ^3 are defined such as :

$$\gamma^2 + \gamma^3 = 1 \quad \text{and} \quad 0 \leq \gamma^2, \gamma^3 \leq 1.$$

For the simulation, let us consider that roads 1 and 2 have both two lanes and that the maximal speed on both roads is supposed to be $v_{max}^{\{1,2\}} = 90$ km/h. Roads 1 and 2 represent the main section of the beltway. Road 3, corresponding to the off-ramp, has a single lane and its maximal speed is $v_{max}^3 = 50$ km/h. We assume that 80 percent of the

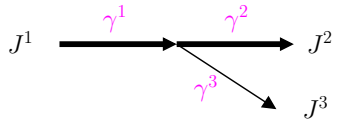

FIGURE 4.9 – Diverge junction model

Branch	Number of lanes	Maximal speed (km/h)	γ^α
1	2	90	1
2	2	90	0.80
3	1	50	0.20

TABLE 4.1 – Traffic flow characteristics of each branch

vehicles coming from road 1 wish to continue on the main section while the remaining 20 percent exit the beltway. These values are recalled in Table 4.1.

We then consider the flow functions f^α according to the values of Table 4.1 (see Figure 4.10). The values of densities and flows for initial and final states are summarized in Table 4.2. They are respectively plotted on (a) and (d) of Figure 4.13.

	Initial state		Final state	
Branch	Density (veh/km)	Flow (veh/h)	Density (veh/km)	Flow (veh/h)
1	50	*3533*	40	*3600*
2	20	*2250*	28	*2880*
3	30	*962*	12	*720*

TABLE 4.2 – Values of densities and flows for initial and final states on each branch. The 'final' state is obtained after some simulation time when a steady state is reached.

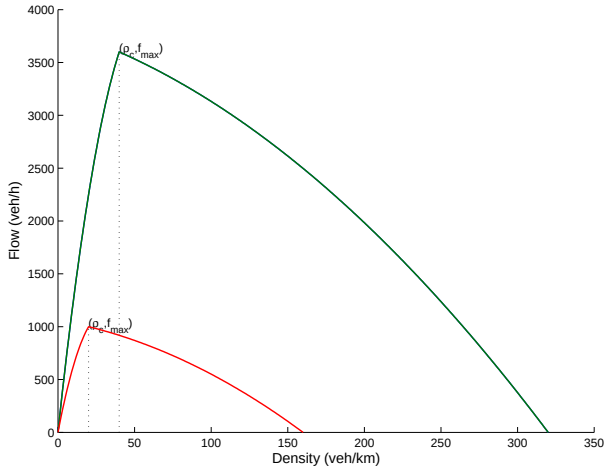

FIGURE 4.10 – Graphs of the functions f^α

Vehicles labels and trajectories. Hereafter we consider $\Delta x = 5m$ (that corresponds

to the average size of a vehicle) and $\Delta t = 0.16s$.

The numerical solution $(U_i^{\alpha,n})$ is depicted on Figure 4.11. The vehicles trajectories are deduced by considering the iso-values of the labels surface $(U_i^{\alpha,n})$ (see Figure 4.12). In this case, one can observe that the congestion (described in the next part) induces a break in the velocities of the vehicles when going through the shock waves. It is still true through the junction point.

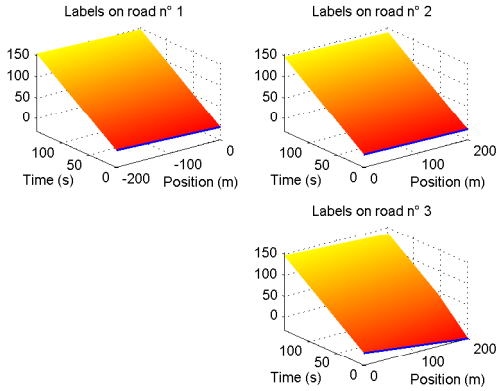

FIGURE 4.11 – Numerical solution on each branch for the diverge

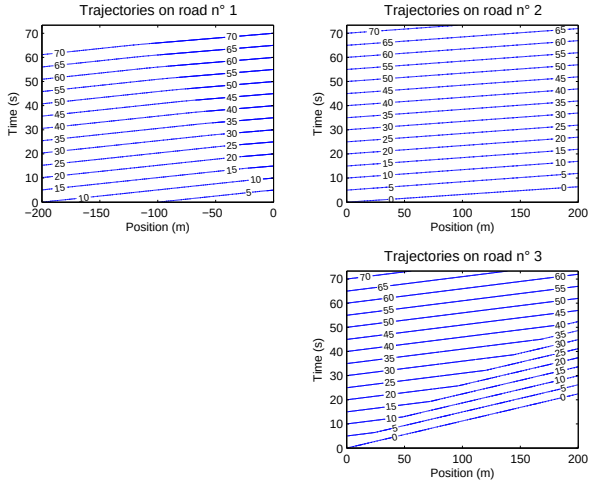

FIGURE 4.12 – Trajectories of some vehicles on each branch for the diverge

Propagation of waves. Let us describe in detail the shock and rarefaction waves that appear from the considered initial Riemann problem (see Figure 4.13). We first notice that at the initial time, roads 1 and 3 are congested (see Figure 4.13 (a)). The incoming road has a demand of $3600veh/h$ splitted into $2880veh/h$ toward road 2 and $720veh/h$ toward road 3. The supplies on roads 2 and 3 are respectively $3600veh/h$ and $962veh/h$. Thus the partial demands are totally satisfied on both outgoing roads. On road 1 (see the Figure 4.13 (b) and (c)), the vehicles density decreases from $50veh/km$ to the critical density $40veh/km$ and thus the flow increases to $3600veh/h$. There is the apparition of a rarefaction wave which propagates backward. Road 3 is no longer congested because the demand is fully satisfied and the vehicles can go freely on the branch (see the Figure 4.13

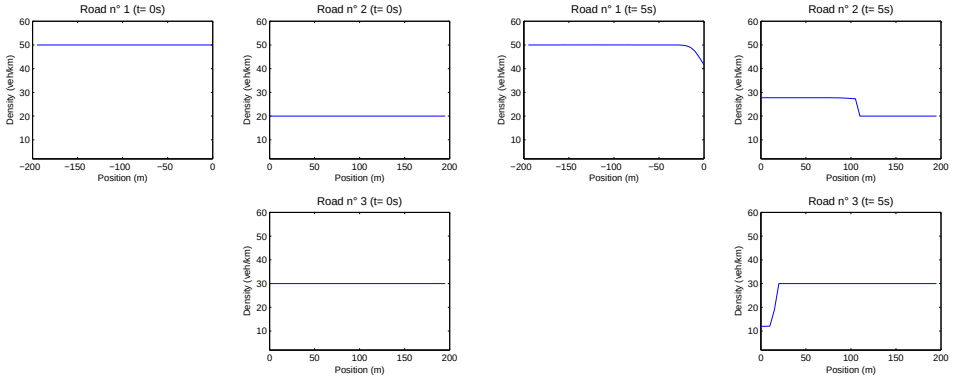

(a) Initial conditions for densities (b) Densities at $t = 5$ s

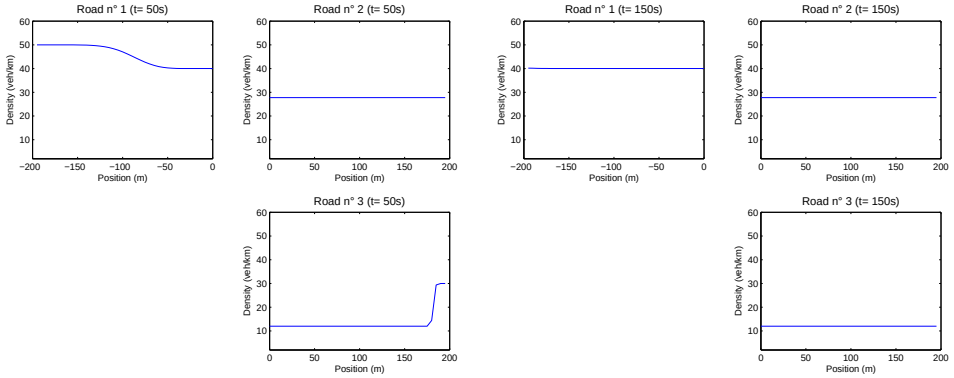

(c) Densities at $t = 50$ s (d) Densities at $t = 150$ s

FIGURE 4.13 – Time evolution of vehicles densities on a diverge

(b) and (c)). The flow goes from $962veh/h$ to $720veh/h$ and the density collapses from $30veh/km$ to $12veh/km$. Then a shock wave propagates forward at the speed $v^3 = 13km/h$ which matches to the Rankine-Hugoniot speed. On road 2, a rarefaction wave appears and propagates forward. The flow increases from $2250veh/h$ to $2880veh/h$ and the density goes from $20veh/km$ to $28veh/km$ (see the Figure 4.13 (b) and (c)).

5.4 Simulation results for a merge

We consider the case of a *merge* : two incoming roads denoted $\alpha = 1$ and 2 merging into a single outgoing road denoted 3 (see Figure 4.14). This case could illustrate the case of an on-ramp on a beltway.

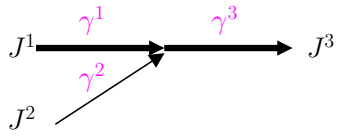

FIGURE 4.14 – Merge model

For the numerical simulation, let us consider the characteristics summarized in Table 4.3. We assume that 80 percent of the through-flow comes from road 1 while the remaining 20 percent comes from the on-ramp 2.

Remark 5.2. *Notice that for $N_I \geq 2$ incoming roads, a realistic choice of coefficients $(\gamma^\alpha)_{\alpha=1,\dots,N}$ is not obvious. We discuss that point in Section 6. Here we assume that the mix coefficients $(\gamma^\alpha)_{\alpha\leq N_I}$ are capacity proportional that is the ratio of the maximal flows that each incoming road could send to the junction point. This choice is motivated by what it was already established by empirical data sets in [15, 51] for which the merge ratios were closely related to the number of lanes per incoming branches.*

Branch	Number of lanes	Maximal speed (km/h)	γ^α
1	3	90	0.80
2	1	70	0.20
3	3	90	1

TABLE 4.3 – Traffic flow characteristics of each branch

We then consider the flow functions f^α according to the values of Table 4.3 (see Figure 4.15). The values of densities and flows for initial and final states are summarized in Table 4.4. They are respectively plotted on (a) and (d) of Figure 4.19.

	Initial state		Final state	
Branch	Density (veh/km)	Flow (veh/h)	Density (veh/km)	Flow (veh/h)
1	50	*4875*	189	*4320*
2	20	*1400*	68	*1080*
3	30	*3375*	60	*5400*

TABLE 4.4 – Values of densities and flows for initial and final states on each branch. The 'final' state is obtained after some simulation time when a steady state is reached.

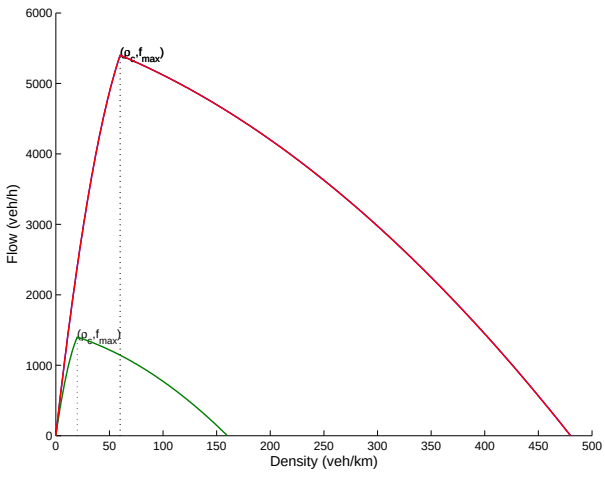

FIGURE 4.15 – Graphs of the functions f^α

Vehicles labels and trajectories. Hereafter we consider $\Delta x = 5m$ (that corresponds to the average size of a vehicle) and $\Delta t = 0.09s$.

The numerical solution $(U_i^{\alpha,n})$ is depicted on Figure 4.16. The vehicles trajectories are deduced by considering the iso-values of the labels surface $(U_i^{\alpha,n})$ (see Figure 4.17). Once

again, we can notice that the congestion spillback (described in the next part) induces a break in the velocity of the vehicles when going through the shock waves. It is still true through the junction point.

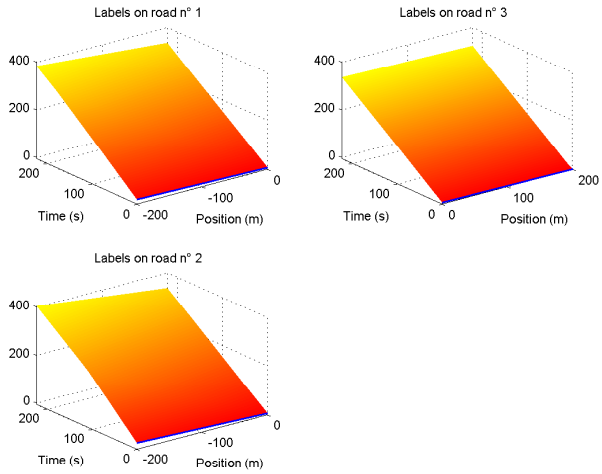

FIGURE 4.16 – Numerical solution on each branch for the merge

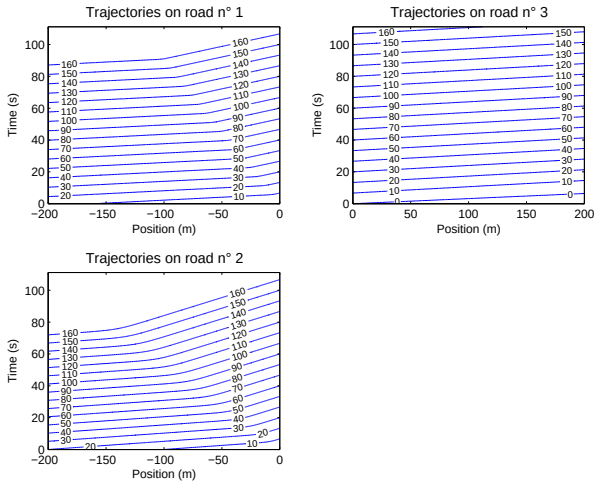

FIGURE 4.17 – Trajectories of some vehicles on each branch for the merge

Propagation of waves. Let us describe in detail the shock and rarefaction waves that appear from the considered initial Riemann problem (see Figure 4.19). At the initial state (see Figure 4.19 (a)) all the branches are not congested. At the initial state the supply on road 3 is $5400veh/h$ while the demands on roads 1 and 2 are respectively $4900veh/h$ and $1400veh/h$, that to say a total demand of $6300veh/h$. Thus all the demand can not be satisfied through the junction point. The junction is thus supply constrained and the flows are regulated by a priority share between both competitive roads.

To understand the behaviour of the flows at the junction point, we adopt the optimization viewpoint (see Figure 4.18). The share is given by the fixed mix coefficients γ^α with $\alpha = \{1, 2\}$. The supply of road 3 is divided into roads 1 and 2 such that $f_S^{\{1\to3\}} = 0.8 f_S^3$ and $f_S^{\{2\to3\}} = 0.2 f_S^3$ that is $f_S^{\{1\to3\}} = 4320veh/h$ and $f_S^{\{2\to3\}} = 1080veh/h$.

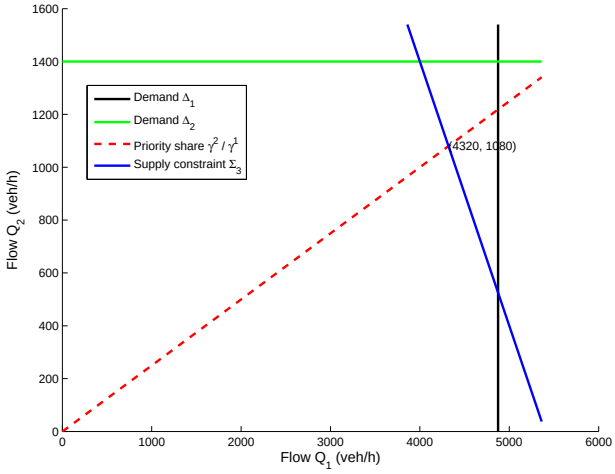

FIGURE 4.18 – Flows distribution at merge

The flow through the junction is limited by the supply and it is weaker than the demands on both incoming roads (see Figure 4.18). Then there are shock waves that propagate backward on each incoming road (see Figure 4.19 (b) and (c)). The waves speeds should match the Rankine-Hugoniot speeds, that is $-4km/h$ on road 1 and $-7km/h$ on road 2. Moreover a rarefaction wave appears on the outgoing road 3 and it propagates forward (see Figure 4.19 (b)). The flux on road 3 reaches the capacity.

6 Extensions

We discuss hereafter some possible extensions for the model (4.3.8)-(4.3.9) and the numerical scheme (4.3.17)-(4.3.18). We recall that our numerical scheme allows to find an approximate solution which converges to the exact solution of (4.3.8)-(4.3.9) when the time and space steps go to zero. However, we can improve the realism of the HJ model by considering a more general law (even sub optimal) for the junction condition or to numerically deal with time dependent coefficients $\gamma^\alpha(t)$.

Junction condition. Up to now, we have only considered the maximization of the total amount of incoming flows in the perspective of a system optimum. However it is classical to observe that the passing flow through the junction is often (if not always) sub-optimal. It is particularly the case when the number of incoming branches is strictly greater than 1, due to competitive aspects of the merging. That is the reason why it should be interesting to consider another condition F which is less than the function F_0 (the maximal theoretical flow that could pass through the junction) given by

$$F_0(\gamma) := \min\left\{\min_{\beta\leq N_I}\frac{1}{\gamma^\beta}f_D^\beta(\rho_{-1}^{\beta,n}),\ \min_{\lambda\geq N_I+1}\frac{1}{\gamma^\lambda}f_S^\lambda(\rho_0^{\lambda,n})\right\}. \tag{4.6.36}$$

The condition $F \leq F_0$ could be obtained by considering a simple penalization of the optimal flow according to the load of competitive flows at the junction. The very recent paper [140] extends the mathematical results of [141] to more general junction conditions considering a flux limiter. The uniqueness of the solution to HJ equations still holds.

Fixed coefficients. The reader can notice that the flux coefficients γ^α for any $\alpha = 1, ..., n+m$ are already considered known at the beginning of the simulations. Moreover

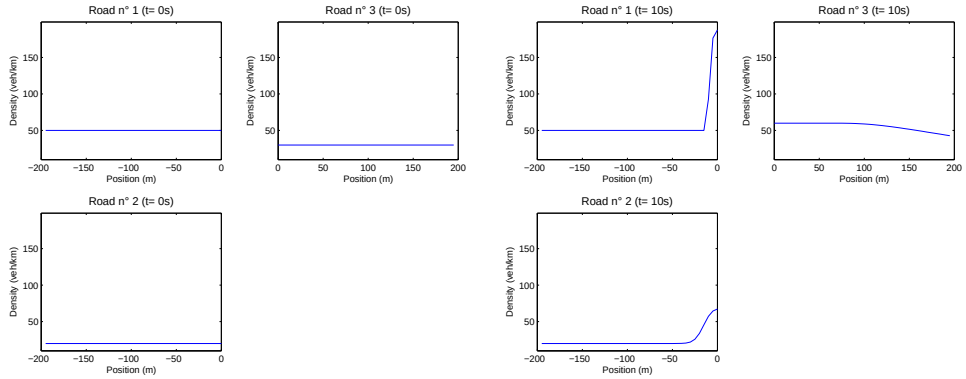

(a) Initial conditions for densities

(b) Densities at $t = 10$ s

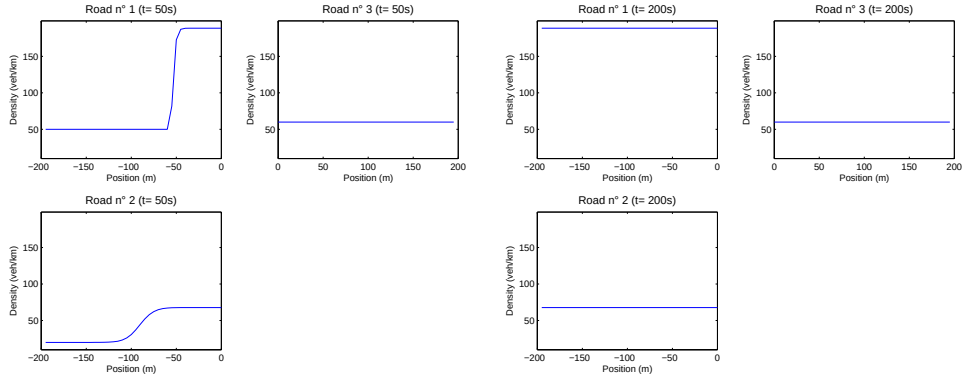

(c) Densities at $t = 50$ s

(d) Densities at $t = 200$ s

FIGURE 4.19 – Time evolution of vehicles densities on a merge

we suppose that these coefficients are given constant during the whole duration of the simulations. Both assumptions are not so realistic in a strict traffic context. Indeed for the incoming roads, the coefficients γ^α could be interpreted as *mixing coefficients* of the incoming flows through the junction point. For instance, consider a junction with two incoming roads for which the *mixing* coefficients depend on time and on the state of traffic. If the coefficients are chosen such that the road with the higher flow has the weakest mixing coefficient, then the main flow will be restricted in the junction model. In reality, the mixing coefficients are time dependent. It is obvious in the case of a signalized junction with priority rules or stop lights management. Fixed coefficients are only justified for a stationary traffic flow.

Numerical extension for non-fixed coefficients (γ^α). Up to now, we were considering fixed coefficients $\gamma := (\gamma^\alpha)_\alpha$ and the flux of the scheme at the junction point at time step $n \geq 0$ was (4.6.36).

In certain situations, we want to maximize the flux $F_0(\gamma)$ for γ belonging to an admissible set Γ. Indeed we can consider the set

$$A := \underset{\gamma \in \Gamma}{\operatorname{argmax}}\ F_0(\gamma).$$

In the case where this set is not a singleton, we can also use a priority rule to select a single element $\gamma^{*,n}$ of A. This defines a map

$$\left((\rho_{-1}^{\beta,n})_{\beta \leq N_I}, (\rho_0^{\lambda,n})_{\lambda \geq N_I+1}\right) \mapsto \gamma^{*,n}.$$

At each time step $n \geq 0$ we can then choose this value $\gamma = \gamma^{*,n}$ in the numerical scheme (4.4.29)-(4.4.30).

Towards a new model for non-fixed coefficients ? Both previous parts about junction condition and fixed coefficients point out some rigidity of the framework given by the model (4.3.8). This model is particularly convenient to treat the flows on a junction in a unified approach, i.e. without considering incoming or outgoing roads. However it has the drawback of introducing fixed coefficients (γ^α) which are hard to use in traffic modelling.

As a first extension, we can introduce non-fixed coefficients for the traffic flow model (4.4.22), (4.4.32). However, the vehicles labels u^α are defined in (4.4.23) according to the vehicles densities ρ^α and up to the coefficients γ^α. It is not obvious that in this case (with non-fixed coefficients $\gamma^\alpha(t)$), the vehicles labels still satisfy the model (4.3.8).

Another extension could be to introduce assignment coefficients γ_{ij} which stand for the percentage of vehicles coming from branch i and going on branch j. It is not suitable with the model (4.3.8) even if we sort incoming and outgoing branches.

Remark 6.1. *In traffic flow litterature, [46] already introduces junction models with dependent coefficients $\gamma^\alpha(\rho)$. However the developed methods are no longer satisfactory because these models do not comply the invariance principle of [171].*

7 Conclusion

In this article, we provide a discussion about traffic flow modelling on junctions. Using the well-known links between scalar conservation laws and Hamilton-Jacobi equations of the first order on a simple section, a new framework has been built to model junctions [140, 141]. This framework based on Hamilton-Jacobi equations allows to overpass certain shortcuts of the classical approach [106], yielding e.g. the uniqueness of the solution

whatever the number of incoming or outgoing branches. Thus we can built a numerical scheme that converges to that unique solution. The mathematical properties of the numerical scheme are deeply investigated in a companion article [69].

The numerical scheme we propose for Hamilton-Jacobi equations is strictly equivalent to the Godunov scheme for conservation laws. The numerical tests performed in this paper attempt to illustrate the ability of the scheme to reproduce kinematic waves such as shocks or rarefaction fans. For a deeper numerical comparison between numerical schemes (in the conservation laws framework), the interested reader is referred to [40, 41]. It is out of the scope here.

Chapitre 5

Numerical homogenization of Hamilton-Jacobi equations on networks

Warning. The reader is kindly warned that this chapter is based on a still ongoing research. This means in particular that some of the results and the companion proofs below are only proposed in a formal way. The work has greatly benefited of discussions with Amin Ghorbel, University of Sfax, Tunisia, and Régis Monneau, Université Paris-Est, as well.

Sommaire

Abstract

This chapter is concerned with the numerical homogenization of Hamilton-Jacobi (HJ) equations posed on a periodic network in $\mathbb{R}^d$ with $d = 2$. For this continuous HJ problem, we propose a finite difference scheme which was previously designed for HJ equations on a single junction. We are interested in providing some qualitative properties of the effective Hamiltonian. We also apply a derived scheme to compute the densities of vehicles for a traffic flow model on the network and we recover some macroscopic features of traffic flow such as the Macroscopic Fundamental Diagram. We finally provide numerical computations of the effective Hamiltonian in different "realistic" configurations, as for instance fixed traffic signals.

1 Introduction

In this paper, we study the homogenization of Hamilton-Jacobi (HJ) equations posed on a simple periodic network generated in $\mathbb{R}^2$. We propose an adapted numerical scheme and we provide several numerical simulations.

1.1 Setting of the PDE problem

In this subsection, we first define the junction, then the space of functions on the junction and finally the Hamilton-Jacobi equations. We follow [139, 140].

The network. Let us consider a road network $\mathcal{N}$ made of edges and vertices and naturally embedded in $\mathbb{R}^2$. Edges e are defined by segments generated by space unit vectors. We set e^*, the set of spatial points that are on the edge e and which are not at a vertex. We define by $\mathcal{E}$ the set of edges and by $\mathcal{V}$ the set of vertices.

HJ equation on the network. We consider the following "oscillating" Hamilton-Jacobi equations

$$\begin{cases} u_t^\varepsilon + H_{\frac{e}{\varepsilon}}\left(u_x^\varepsilon\right) = 0, & \text{for} \quad t > 0,\ x \in e^*,\ e^* \in \mathcal{E}, \\ u_t^\varepsilon + F_A\left(\dfrac{x}{\varepsilon}, u_x^\varepsilon\right) = 0, & \text{for} \quad t > 0,\ x \in \mathcal{V}_\varepsilon, \end{cases} \tag{5.1.1}$$

submitted to the initial condition

$$u^\varepsilon(0, x) = u_0(x), \quad \text{for any} \quad x. \tag{5.1.2}$$

We set the flux through vertices

$$F_A(y, p) = \max\left[A, \max_\alpha H^-(p_\alpha)\right], \quad \text{for any} \quad y \in \mathcal{V} \quad \text{and} \quad p := (p_\alpha)_\alpha \in \mathbb{R}^n,$$

n being the number of edges that connect at vertex $y \in \mathcal{V}$ and for some flux limiter $A \in \mathbb{R}$ (independent on the vertex y).

We are interested in the homogenization of the equation (5.1.1) when the size ε of the branches goes to zero.

We make the following assumptions :

(A0) **Initial data**

The initial data u_0 is globally Lipschitz continuous.

(A1) **Hamiltonians**

For any $e \in \mathcal{E}$,

- we consider functions $H_e \in C^1(\mathbb{R})$ which are coercive, i.e. $\lim_{|p| \to +\infty} H_e(p) = +\infty$;

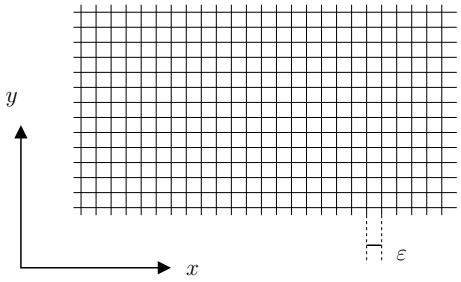

FIGURE 5.1 – Homogenization of the bi-dimensional network

- we assume that there exists a $p_0^e \in \mathbb{R}$ such that H_e is non-increasing on $(-\infty, p_0^e]$ and non-decreasing on $[p_0^e, +\infty)$, and we set :

$$H_e^-(p) = \begin{cases} H_e(p) & \text{for} \quad p \leq p_0^e \\ \\ H_e(p_0^e) & \text{for} \quad p \geq p_0^e \end{cases} \quad \text{and} \quad H_e^+(p) = \begin{cases} H_e(p_0^e) & \text{for} \quad p \leq p_0^e \\ \\ H_e(p) & \text{for} \quad p \geq p_0^e \end{cases} \tag{5.1.3}$$

  where H_e^- is non-increasing and H_e^+ is non-decreasing.

(A2) Periodicity : For all $m \in \mathbb{Z}^d$ and for any p, $H_{e+m}(p) = H_e(p)$.

Theorem 1.1 (Homogenization of Hamilton-Jacobi equations on a periodic network)**.** *Assume (A0)-(A1)-(A2). Then the solution* $u^\varepsilon(x,t) := \varepsilon u\left(\frac{x}{\varepsilon}, \frac{t}{\varepsilon}\right)$ *of (5.1.1)-(5.1.2) converges locally uniformly, when* ε *goes to zero, towards the solution* u^0 *of the following homogenized problem*

$$\begin{cases} u_t^0 + \bar{H}(\nabla u^0) = 0, & \text{for} \quad t > 0, \ x \in \mathbb{R}^d, \\ u^0(0,x) = u_0(x), & \text{for} \quad x \in \mathbb{R}^d, \end{cases} \tag{5.1.4}$$

where $\bar{H}$ *is the effective Hamiltonian and* $\nabla u = (p_\alpha)_\alpha \in \mathbb{R}^n$ *the macroscopic density of vehicles in* $\mathbb{R}^d$ *with* $d = 2$.

Proof See Theorem 8.1 in [139]. □

We also have that

$$\bar{H}(P) = \pm\lambda(P), \quad \text{with} \quad P := (p_\alpha)_\alpha \in \mathbb{R}^n$$

and we know from [140, 141] that there exists a unique λ such that

$$u(t,X) = \pm\lambda t + X.P + v(t,X)$$

with $X = (x,y)$ and v is a k-periodic function ($k \in \mathbb{Z}^2$ and we assume that v is independent of time t.

We set

$$w(t,X) := \lambda t + v(X)$$

which satisfies the new HJ problem

$$\left| \begin{array}{l} w_t + H_{\mathcal{N}}(P + Dw) = 0 \\ w \mid_{t=0} = 0 \end{array} \right. \tag{5.1.5}$$

or equivalently

$$\left| \begin{array}{l} w_t + \tilde{H}(Dw) = 0 \\ w \mid_{t=0} = 0 \end{array} \right. \tag{5.1.6}$$

where we have set $\tilde{H}(Dw) := H_{\mathcal{N}}(P + Dw)$.

We will see later that the problem on the whole network can be recast as a simplest cell problem in which we only deal with a single junction.

The junction. $N \geq 1$ different unit vectors $e_\alpha \in \mathbb{R}^2$ for $\alpha = 1, \dots, N$. We define the branches as the half-lines generated by these unit vectors

$$J_\alpha = [0, +\infty) e_\alpha \quad \text{and} \quad J_\alpha^* = J_\alpha \setminus \{0_{\mathbb{R}^2}\}, \quad \text{for all} \quad \alpha = 1, \dots, N,$$

and the whole *junction* (see Figure 5.2) as

$$J = \bigcup_{\alpha=1,\dots,N} J_\alpha.$$

The origin $y = 0_{\mathbb{R}^2}$ (we just call it "$y = 0$" in the following) is called the *junction point*. For a time $T > 0$, we also consider the time-space domain defined as

$$J_T = (0, T) \times J.$$

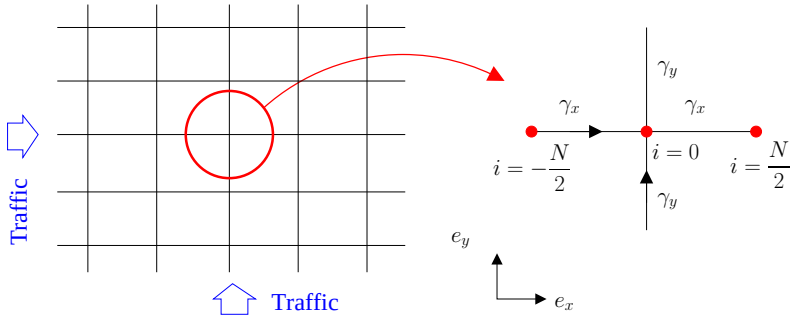

FIGURE 5.2 – Network and junction model

HJ equation on the junction. We are interested in continuous functions $u : [0, T) \times J \to \mathbb{R}$ which are *viscosity solutions* on J_T of

$$\left\{ \begin{array}{ll} u_t^\alpha + H_\alpha(u_x^\alpha) = 0 & \text{on} \quad (0,T) \times (0, +\infty), \quad \text{for} \quad \alpha = 1, \dots, N, \\ \\ u^\beta =: u, \quad \text{for all} \quad \beta = 1, \dots, N & \\ \\ u_t + \max\left[A, \max\limits_{\beta=1,\dots,N} H_\beta^-(u_x^\beta)\right] = 0 & \text{on} \quad (0,T) \times \{0\}, \end{array} \right. \tag{5.1.7}$$

for functions H_α and H_α^- that will be defined below in assumption (A1).

We consider an initial condition

$$u^\alpha(0, x) = u_0^\alpha(x), \quad \text{with} \quad x \in [0, +\infty) \quad \text{for} \quad \alpha = 1, \dots, N. \tag{5.1.8}$$

1.2 Presentation of the scheme for the cell problem

We follow [69]. We denote by Δx the space step and by Δt the time step. We denote by $U_i^{\alpha,n}$ an approximation of $u^\alpha(n\Delta t, i\Delta x)$ for $n \in \mathbb{N},\ i \in \mathbb{N}$, where α stands for the index of the considered branch.

We define the discrete space derivatives

$$p_{i,+}^{\alpha,n} := \frac{U_{i+1}^{\alpha,n} - U_i^{\alpha,n}}{\Delta x} \quad \text{and} \quad p_{i,-}^{\alpha,n} := \frac{U_i^{\alpha,n} - U_{i-1}^{\alpha,n}}{\Delta x}, \tag{5.1.9}$$

and similarly the discrete time derivative

$$W_i^{\alpha,n} := \frac{U_i^{\alpha,n+1} - U_i^{\alpha,n}}{\Delta t}. \tag{5.1.10}$$

Then we consider the following numerical scheme corresponding to the discretization of the HJ equation (5.1.7) for $n \geq 0$:

$$\begin{cases} \dfrac{U_i^{\alpha,n+1} - U_i^{\alpha,n}}{\Delta t} + \max\left\{H_\alpha^+(p_{i,-}^{\alpha,n}), H_\alpha^-(p_{i,+}^{\alpha,n})\right\} = 0, & \text{for} \quad i \geq 1, \quad \alpha = 1, \dots, N, \\ U_0^{\beta,n} =: U_0^n, \quad \text{for all} \quad \beta = 1, \dots, N \\ \dfrac{U_0^{n+1} - U_0^n}{\Delta t} + \max\limits_{\beta=1,\dots,N} H_\beta^-(p_{0,+}^{\beta,n}) = 0 \end{cases} \quad \text{for} \quad i = 0, \tag{5.1.11}$$

with the initial condition

$$U_i^{\alpha,0} = u_0^\alpha(i\Delta x) \quad \text{for} \quad i \geq 0, \quad \alpha = 1, \dots, N. \tag{5.1.12}$$

It is natural to introduce the following Courant-Friedrichs-Lewy (CFL) condition :

$$\frac{\Delta x}{\Delta t} \geq \sup_{\substack{\alpha=1,\dots,N \\ i\geq 0,\ 0\leq n\leq n_T}} |H'_\alpha(p_{i,+}^{\alpha,n})| \tag{5.1.13}$$

where the integer n_T is assumed to be defined as $n_T = \left\lfloor \dfrac{T}{\Delta t} \right\rfloor$ for a given $T > 0$.

1.3 Brief review of the literature

We mainly refer here to the results and comments provided in [140] and references therein. There is a huge literature dealing with HJ equations and mainly with equations with discontinuous Hamiltonians. However, concerning the study of HJ equation on a network, there exist a few works. The reader is referred to [140] for a general definition of viscosity solutions on a network, a uniqueness result, a presentation of numerical schemes and the homogenization result under specific assumptions. In the present work, we will try to numerically relax some of these assumptions and to study the homogenization of HJ equations on a network.

1.4 Organization of the paper

In Section 2, we present the application of the numerical scheme to traffic flow modeling. In particular, we define the *assignment* coefficients $(\gamma^\alpha)_\alpha$ which will be used in the

remaining part of the paper. In Section 4, we deal with numerical homogenization with different type of networks on which we consider the Hamilton-Jacobi model (5.4.25) with fixed coefficients $(\gamma^\alpha)_\alpha$. We recall that these cases are fully covered by the theory developed in [139, 140]. In Section 5, we consider numerical homogenization of Hamilton-Jacobi equations on an orthotropic network, taking into account that assignment coefficients are time-varying and that we select the optimal set of coefficients such that the passing flux is maximized at the junction. Section 6 is concerned with the study of traffic signals and the homogenization of traffic flow through such signals. Last, in Section 7 we review the cases that could be interesting to deal with in future researches.

2 Application to traffic flow

As our motivation comes from traffic flow modelling, this section is devoted to the traffic interpretation of the model and the scheme. Notice that [141] has already focused on the meaning of the junction condition in this framework.

2.1 Settings

We first recall the main variables adapted for road traffic modelling as they are already defined in [141]. We consider a junction with $N_I \geq 1$ incoming roads and $N_O \geq 1$ outgoing ones. We also set that $N_I + N_O =: N$.

Densities and scalar conservation law. We assume that the vehicles densities denoted by $(\rho^\alpha)_\alpha$ solve the following scalar conservation laws (also called LWR model for Lighthill, Whitham [184] and Richards [221]) :

$$\begin{cases} \rho_t^\alpha + (f^\alpha(\rho^\alpha))_X = 0, & \text{for} \quad (t,X) \in [0,+\infty) \times (-\infty, 0), \quad \alpha = 1, ..., N_I, \\ \rho_t^\alpha + (f^\alpha(\rho^\alpha))_X = 0, & \text{for} \quad (t,X) \in [0,+\infty) \times (0, +\infty), \quad \alpha = N_I+1, ..., N_I+N_O, \end{cases} \tag{5.2.14}$$

where we assume that the junction point is located at the origin $X = 0$.

We assume that for any α the flux function $f^\alpha : \mathbb{R} \to \mathbb{R}$ reaches its unique maximum value for a critical density $\rho = \rho_c^\alpha > 0$ and it is non decreasing on $(-\infty, \rho_c^\alpha)$ and non-increasing on $(\rho_c^\alpha, +\infty)$. In traffic modelling, $\rho^\alpha \mapsto f^\alpha(\rho^\alpha)$ is usually called the *fundamental diagram*.

Let us define for any $\alpha = 1, ..., N$ the Demand function f_D^α (resp. the Supply function f_S^α) such that

$$f_D^\alpha(p) = \begin{cases} f^\alpha(p) & \text{for} \quad p \leq \rho_c^\alpha \\ f^\alpha(\rho_c^\alpha) & \text{for} \quad p \geq \rho_c^\alpha \end{cases} \qquad \left(\text{resp.} \quad f_S^\alpha(p) = \begin{cases} f^\alpha(\rho_c^\alpha) & \text{for} \quad p \leq \rho_c^\alpha \\ f^\alpha(p) & \text{for} \quad p \geq \rho_c^\alpha \end{cases} \right).$$

We assume that we have a set of fixed coefficients $0 \leq (\gamma^\alpha)_\alpha \leq 1$ that denote :

- either the proportion of the flow from the branch $\alpha = 1, ..., N_I$ which enters in the junction,
- or the proportion of the flow on the branch $\alpha = N_I + 1, ..., N$ exiting from the junction.

We also assume the natural relations

$$\sum_{\alpha=1}^{N_I} \gamma^\alpha = 1 \quad \text{and} \quad \sum_{\beta=N_I+1}^{N_I+N_O} \gamma^\beta = 1.$$

Remark 2.1. *We consider that the coefficients $(\gamma^\alpha)_{\alpha=1,...,N}$ are fixed and known at the beginning of the simulations. Such framework is particularly relevant for "quasi stationary" traffic flows.*

Vehicles labels and Hamilton-Jacobi equations. Extending for any $N_I \geq 1$ the interpretation and the notations given in [141] for a single incoming road, let us consider the *continuous* analogue u^α of the discrete vehicles labels (in the present paper with labels increasing in the backward direction with respect to the flow)

$$\begin{cases} u^\alpha(t,x) = u(t,0) - \dfrac{1}{\gamma^\alpha}\displaystyle\int_0^{-x} \rho^\alpha(t,y)dy, \quad \text{for} \quad x := -X > 0, \quad \text{if} \quad \alpha = 1, ..., N_I, \\ \\ u^\beta(t,x) = u(t,0) - \dfrac{1}{\gamma^\beta}\displaystyle\int_0^{x} \rho^\beta(t,y)dy, \quad \text{for} \quad x := X > 0, \quad \text{if} \quad \beta = N_I+1, ..., N, \end{cases} \tag{5.2.15}$$

with equality of the functions at the junction point ($x = 0$), i.e.

$$u^\alpha(t,0) = u^\beta(t,0) =: u(t,0) \quad \text{for any} \quad \alpha, \beta. \tag{5.2.16}$$

where the common value $u(t,0)$ is nothing else than the (continuous) label of the vehicle at the junction point.

Following [141], for a suitable choice of the function $u(t,0)$, it is possible to check that the vehicles labels u^α satisfy the following Hamilton-Jacobi equation :

$$u_t^\alpha + H_\alpha(u_x^\alpha) = 0, \quad \text{for} \quad (t,x) \in [0,+\infty) \times (0,+\infty), \quad \alpha = 1, ..., N \tag{5.2.17}$$

where

$$H_\alpha(p) := \begin{cases} -\dfrac{1}{\gamma^\alpha} f^\alpha(\gamma^\alpha p) & \text{for} \quad \alpha = 1, ..., N_I, \\ \\ -\dfrac{1}{\gamma^\alpha} f^\alpha(-\gamma^\alpha p) & \text{for} \quad \alpha = N_I+1, ..., N_I+N_O. \end{cases} \tag{5.2.18}$$

2.2 Review of the literature with application to traffic

Macroscopic Fundamental Diagram. The existence of Macroscopic Fundamental Diagrams (MFDs) have been proved in large urban networks in which traffic conditions are homogeneous. They allow an inflow-outflow mapping on a (sub-) network. They can be used for estimation of the level of service on road networks, perimeter control, and macroscopic traffic modeling [81,110]. This notion of network FD could be also an adequate tool for determining the optimal timings of traffic signals.

Network or Macroscopic Fundamental Diagram (MFD) serves to asset the macroscopic performance of an urban road infrastructure. The MFD connects the total number of vehicles N on a road network at any time (or the total cumulative amount of vehicles also linked to traffic density given by the average number of vehicles per length unit $\rho := -\partial_x N$) with the rate at which trips reach their destinations, that is either traffic flow or traffic speed. According to [81], the MFD should be only dependent on the network infrastructure (e.g. link length and number of lanes) and on control parameters (mainly traffic signal timings). Helbing shows [125] that the MFD depends on the spatial distribution of demand. The dependency is corroborated by Geroliminis and Sun [111]. As we can expect it, the aggregated values are highly dependent to the measurements means (e.g. loop detectors) [44] and it can lead to hysteresis effect.

Simulations [110] in the case of San Francisco (and also Yokohama, Japan) show that adapted traffic signal timings in the periphery of the considered network allow to restrict

the number of entering vehicles at the sweet-spot of vehicle accumulation and then to maintain a high output without dropping towards zero when entering the system gridlock.

Traffic signals. The paper of Wen-Long Jin and Yifeng Yu [145] is a theoretical work on the asymptotic solutions of more general 1D conservation laws

$$\begin{cases} \rho_t + (\chi f(x))_x = 0, & \text{for} \quad (x,t) \in [0,L] \times (0,+\infty), \\ \rho(x,0) = \rho_0(x), \end{cases}$$

with periodic flow constraints (e.g. traffic signals)

$$\chi(x,t) = \begin{cases} 0 & \text{if} \quad (x,t) \in \Gamma_T, \\ 1 & \text{otherwise.} \end{cases}$$

The set Γ_T is defined such that

$$\Gamma_T := \left\{ (l,s) \;\middle|\; l \in \mathbb{Z},\ s \in \left[kT, kT + \frac{T}{2} \right] \quad \text{for some } k \in \mathbb{Z} \right\}.$$

They recast the problem into its Hamilton-Jacobi (HJ) form due to the classical relation between 1D conservation law and first order HJ equation. Indeed by setting

$$u(x,t) := -\int_0^x \rho(y,t)dy, \quad \text{for} \quad x \in [0,L],$$

we recover that u solves

$$\begin{cases} u_t + H(u_x,x,t) = 0, & \text{for} \quad (x,t) \in [0,L] \times (0,+\infty), \\ u(x,0) = ax + w(x) = -\int_0^x \rho_0(y)dy, & \text{for} \quad t = 0, \end{cases}$$

with $H(p,x,t) := \chi(x,t)f(p)$ and f is (strictly) concave, or equivalently

$$\begin{cases} u_t + f(u_x) = 0, & \text{for} \quad (x,t) \in [0,L] \times (0,+\infty) \setminus \Gamma_T, \\ u(x,t) = u(x,kT), & \text{for} \quad k \in \mathbb{N}, \quad t \in \Gamma_T, \\ u(x,0) = ax + w(x) = -\int_0^x \rho_0(y)dy, & \text{for} \quad t = 0, \end{cases}$$

with $-a := \displaystyle\int_0^L \rho_0(y)dy$ the average density of vehicles on the road section, at initial time ($0 \le -a \le 1$).

Moreover we ask u to satisfy

$$u(x+l,t) = u(x,t) + al, \quad \text{for all} \quad l \in \mathbb{Z} \quad \text{and} \quad t > 0.$$

The paper exhibits two main results :

- The existence (and uniqueness) of the effective Hamiltonian (long time average of the flux) and its dependence on the initial average density $-a$ (concave w.r.t. $-a$) and on the cycle length T

  $$\bar{f}(a,T) = \lim_{t \to \infty} \frac{1}{t} \int_0^t f(u_x(x,t))dt$$

  By the way, they prove also the existence and uniqueness of the L-periodic continuous viscosity solution to the aforementioned problem. The effective Hamiltonian $c := \bar{f}(a,T)$ is selected such that the cell problem

  $$\begin{cases} v_t + f(a + v_x) = c, & \text{if green light} \\ v(x,t) - v(x,kT) = (t - kT)c, & \text{if red light} \end{cases}$$

  has a unique $(L-T)$-periodic continuous viscosity solution.

- The expression of the asymptotic limit of $u(x,t)$ as $t \to +\infty$ for the steady state in density and flow and the period of the steady state (which is a integer multiple of T).

It is worth noting that the maximum average flux is obtained for a cycle length $T = 0$ and that larger cycle length result in smaller average flows in steady states. Therefore one needs to decrease the cycle length. However for realistic application, the cycle length should be large enough because significant part of the green time is lost due to reaction times and finite acceleration rate. On the contrary, the LWR model assumes vehicles have an infinite acceleration rate and a zero reaction time, which is obviously not satisfactory.

2.3 Derived scheme for conservation laws

Our aim is to properly express the numerical scheme satisfied by the densities in the traffic modelling framework. Let us consider a discretization of space and time domains with time and space steps denoted by Δt and Δx. The discrete car density $\rho_i^{\alpha,n} \geq 0$ with $n \geq 0$ and $i \in \mathbb{Z}$ is defined such that :

$$\rho_i^{\alpha,n} := \begin{cases} \gamma^\alpha p_{|i|-1,+}^{\alpha,n} & \text{for} \quad i \leq -1, \quad \alpha = 1, ..., N_I, \\ \\ -\gamma^\alpha p_{i,+}^{\alpha,n} & \text{for} \quad i \geq 0, \quad \alpha = N_I + 1, ..., N, \end{cases} \tag{5.2.19}$$

where $p_{j,+}^{\alpha,n}$ is the upwind space gradient for $j \in \mathbb{N}$.

Let us define for any $\alpha = 1, ..., N$ the Demand function f_D^α (resp. the Supply function f_S^α) such that

$$f_D^\alpha(p) = \begin{cases} f^\alpha(p) & \text{for} \quad p \leq \rho_c^\alpha \\ f^\alpha(\rho_c^\alpha) & \text{for} \quad p \geq \rho_c^\alpha \end{cases} \qquad \left(\text{resp.} \quad f_S^\alpha(p) = \begin{cases} f^\alpha(\rho_c^\alpha) & \text{for} \quad p \leq \rho_c^\alpha \\ f^\alpha(p) & \text{for} \quad p \geq \rho_c^\alpha \end{cases} \right). \tag{5.2.20}$$

Lemma 2.2 (Derived numerical scheme for the density)**.** *If $U_i^{\alpha,n}$ stands for the solution of the HJ numerical scheme (+ initial conditions), then the density $\rho_i^{\alpha,n}$ defined in (5.2.19) is a solution of the following numerical scheme :*

$$\frac{\Delta x}{\Delta t}\{\rho_i^{\alpha,n+1} - \rho_i^{\alpha,n}\} = \begin{cases} F^\alpha(\rho_{i-1}^{\alpha,n}, \rho_i^{\alpha,n}) - F^\alpha(\rho_i^{\alpha,n}, \rho_{i+1}^{\alpha,n}) & \textit{for} \quad i \neq 0, -1, \\ \\ F_0^\alpha\left((\rho_0^{\delta,n})_\delta\right) - F^\alpha(\rho_i^{\alpha,n}, \rho_{i+1}^{\alpha,n}) & \textit{for} \quad i = 0, \\ \\ F^\alpha(\rho_{i-1}^{\alpha,n}, \rho_i^{\alpha,n}) - F_0^\alpha\left((\rho_0^{\delta,n})_\delta\right) & \textit{for} \quad i = -1, \end{cases} \tag{5.2.21}$$

where we define the fluxes by

$$\begin{cases} F^\alpha(\rho_{i-1}^{\alpha,n}, \rho_i^{\alpha,n}) := \min\left\{f_D^\alpha(\rho_{i-1}^{\alpha,n}),\ f_S^\alpha(\rho_i^{\alpha,n})\right\} & \textit{for} \quad i \neq 0, \\ \\ F_0^\alpha\left((\rho_0^{\delta,n})_\delta\right) := \gamma^\alpha \min\left\{\min\limits_{\beta \leq N_I} \dfrac{1}{\gamma^\beta} f_D^\beta(\rho_0^{\beta,n}),\ \min\limits_{\lambda > N_I} \dfrac{1}{\gamma^\lambda} f_S^\lambda(\rho_0^{\lambda,n})\right\} & \textit{for} \quad i = 0. \end{cases} \tag{5.2.22}$$

We recall that f_S^α and f_D^α for any α are defined in (5.2.20).

Remark 2.3. *Notice that (5.2.21) recovers the seminal Godunov scheme for $i \neq 0, -1$ while it is not standard for the two other cases $i = 0, -1$. Moreover we can check that the natural CFL condition for (5.2.21) which reads as*

$$\frac{\Delta x}{\Delta t} \geq \sup_{\substack{\alpha=1,\dots,N \\ p\in\mathbb{R}}} \left|(f^\alpha)'(p)\right|$$

is not sufficient to recover the monotonicity of the scheme due to the expression of F_0^α for $i = 0, -1$.

3 Setting of the simulations

The steps of the algorithm are the following ones :

(i) Consider the function v given for time $t = 0$ since $w(0, X) = v(X)$.

(ii) Assume a grid in time and space on the junction. Set $W_i^{\alpha,n}$ the discrete value of w at the grid points.

(iii) Apply the numerical scheme (5.1.11) for the case of a junction with four branches (two incoming and two outgoing) for solving the equation (5.1.6).

(iv) We stop the computations for large time once $\tilde{H}$ is constant or at least does not oscillate too much (tolerance factor). We then consider that the effective hamiltonian $\bar{H}$ is reached.

(v) The last step consists in computing λ by $\lambda(P) = \pm\bar{H}(P)$.

Modified scheme for "physical" sense of flowing

Consider the junction represented on Figure 5.2 with two incoming and two outgoing roads. The HJ equations are given by (5.1.7), (5.1.8).

Then the adequate numerical scheme corresponding to the discretization of these HJ equations is the following one :

$$\left\{\begin{array}{ll} \dfrac{U_i^{\alpha,n+1} - U_i^{\alpha,n}}{\Delta t} + \max\left\{H_\alpha^-\left(p_{i,+}^{\alpha,n}\right), H_\alpha^+\left(p_{i,-}^{\alpha,n}\right)\right\} = 0, & \text{for} \quad i \neq 0, \quad \alpha = 1,\dots,N, \\ U_0^{\beta,n} =: U_0^n, \quad \text{for all} \quad \beta = 1,\dots,N & \\ \dfrac{U_0^{n+1} - U_0^n}{\Delta t} + \max\left\{A, \max\limits_{\beta\leq N_I} H_\beta^-\left(p_{0,+}^{\beta,n}\right), \max\limits_{\beta\geq N_I+1} H_\beta^+\left(p_{0,-}^{\beta,n}\right)\right\} = 0 & \text{for} \quad i = 0, \end{array}\right. \tag{5.3.23}$$

with the initial condition

$$U_i^{\alpha,0} = u_0^\alpha(i\Delta x) \quad \text{for} \quad i \geq 0, \quad \alpha = 1,\dots,N. \tag{5.3.24}$$

In this section, we present some numerical experiments based on the derived scheme (5.2.21).

3.1 List of considered cases

Below is the list of the possibilities we have to numerically explore :

- Consider fixed coefficients and a flux through the junction point equal to the minimum between the upstream demand (on incoming branches) and the downstream supply (on outgoing branches)

$$F^0 = \min\left(\min\left\{\frac{1}{\gamma^1} f_D(\rho_{-1}^{1,n}), \frac{1}{\gamma^2} f_D(\rho_{-1}^{2,n})\right\}, \min\left\{\frac{1}{\gamma^3} f_S(\rho_0^{3,n}), \frac{1}{\gamma^4} f_S(\rho_0^{4,n})\right\}\right)$$

- Consider assignment coefficients "à la Garavello-Piccoli" and a flux which is locally maximized with eventually an additional priority rule if there exists more than one solution to the optimization problem. For instance, it could be yielding priority to the right (which is translated as selecting the lowest γ^1) ;

- Consider time-varying coefficients $(\gamma^{\alpha,n})_\alpha$ and a flux limiter L through the junction point (which could depend itself on time) such that the flux is given by

$$F^0 = \min\left(\min\left\{\frac{1}{\gamma^{1,n}} f_D(\rho_{-1}^{1,n}), \frac{1}{\gamma^{2,n}} f_D(\rho_{-1}^{2,n})\right\}, \min\left\{\frac{1}{\gamma^{3,n}} f_S(\rho_0^{3,n}), \frac{1}{\gamma^{4,n}} f_S(\rho_0^{4,n})\right\}, A(n\Delta t)\right)$$

- Consider turning coefficients $\mathcal{A} = (a_{\alpha\beta})$ such that $\sum_\alpha a_{\alpha\beta} = 1$ and $1 \geq a_{\alpha\beta} \geq 0$ for any α, β. Notice that in such a case, we have

$$\gamma_\alpha = \sum_{\beta=2}^{3} a_{\alpha\beta}\gamma_\beta, \quad \text{for} \quad \alpha = 1,\ 2.$$

  Thus there is only one parameter for the optimization problem. We can also consider a priority rule to select just one solution if there exists many solutions.

- **Traffic signals :** consider traffic signals such that the coefficients are given by

$$\begin{cases}\gamma^{1,n} = 1\\ \gamma^{2,n} = 0\end{cases} \quad \text{alternating over time period with} \quad \begin{cases}\gamma^{1,n} = 0\\ \gamma^{2,n} = 1\end{cases}$$

  We can distinguish different cases :

  1. First step : time independent coefficients $\Gamma = (\gamma^\alpha)_\alpha$
  2. Second step : time dependent coefficients $\Gamma^n = (\gamma^{\alpha,n})_\alpha$ and optimization problem according to upstream demands (the coefficients for outgoing branches are prescribed)

$$F^n = \min\left(\min\left\{\frac{1}{\gamma^{1,n}} f_D(\rho_{-1}^{1,n}), \frac{1}{1-\gamma^{1,n}} f_D(\rho_{-1}^{2,n})\right\}, \min\left\{\frac{1}{\gamma^3} f_S(\rho_0^{3,n}), \frac{1}{\gamma^4} f_S(\rho_0^{4,n})\right\}\right)$$

     and then the optimal set of coefficients is given by

$$\Gamma^\star = \text{argmax } F^n$$

  3. Third step : time dependent coefficients and optimization problem if and only if the "cost" for user is over a given threshold i.e. the users are willing to change their minds if the waiting time is at least equal or superior to the traveling time on the reroute.

3.2 Numerical instantiation

The stopping criterion is selected to be the 1-norm of the instantaneous numerical flow vector

$$C := \frac{1}{\Delta t} \left\| \rho^{n+1} - \rho^n \right\|_{L^1},$$

where $\rho^n := (\rho_i^{\alpha,n})_{i,\alpha}$ denotes the vector of densities over all the numerical cells on each branch at time $n\Delta t$. Let ε be the selected threshold. If $C \leq \varepsilon$, then we consider that we have reached a stationary state and we stop the computations. By homogenization, at the stationary state we have $\partial_t \rho = 0$. From the conservation law satisfied by the density on each branch (outside the junction point)

$$\partial_t \rho + \partial_x f(\rho) = 0,$$

we deduce that $\partial_x f(\rho) = 0$. Hence, we consider that the flow obtained at the junction point is equal to the homogenized flow in the whole cell.

In the case of numerical homogenization on a cell with traffic signals, we need to introduce a new stopping criterion. Indeed the numerical homogenization needs to be run for (many) full cycles of green and red phases. We then compare traffic states during the whole cycles to determine if we get a steady state or not. If yes, we stop the computations and we consider that the effective Hamiltonian is given by the mean value of flow during the full cycle.

4 Fixed assignment coefficients

4.1 Explicit bound on the effective Hamiltonian for fixed coefficients

Consider the junction described on Figure 5.2 and the associated Hamilton-Jacobi equations (5.1.7), (5.1.8) with an infinite flux limiter $A(t) = \infty$ for any time $t > 0$, that is

$$\begin{cases} u_t + H_\gamma(u_x) = 0, & x \neq 0, \\ u_t + \max\left\{H^-(u_x(0^+,t), H^+(u_x(0^-,t), H^-(u_y(0^+,t), H^+(u_y(0^-,t)\right\} = 0, & x = 0. \end{cases} \tag{5.4.25}$$

We search for a solution of the form

$$u(t,x) = -\lambda t + px + v(x) \tag{5.4.26}$$

where $-\lambda$ is the homogenized flux such that $\bar{H} : p \mapsto -\lambda$ describes the effective Hamiltonian. We have $p = p^\alpha$ with $\alpha = \{H, V\}$ where p^H (resp. p^V) is the density on the horizontal (resp. vertical) axis and $v = v^\alpha$ with $\alpha = \{H, V\}$ is a corrector term. We assume that v is a periodic function.

Proposition 4.1 ((Formal) Bound by above on the Hamiltonian)**.**
Assume (A1)-(A2)-(A3). If u defined in (5.4.26) is a periodic solution of (5.4.25), then we have a bound by above on the effective Hamiltonian $\bar{H}$ given by

$$\bar{H}\left(p^H, p^V\right) \leq \max\left\{A, H\left(p^H\right), H\left(p^V\right)\right\}.$$

Proof If we plug the solution (5.4.26) in (5.4.25) and if we consider the periodicity of the solution u i.e. $u^\alpha(t,L) = u^\alpha(t,-L)$, then we get

$$\begin{cases} \lambda = H(p + v_x^\alpha(x)), & x \neq 0, \\ \lambda = \max\left\{H^-(v_x^H(0^+) + p^H), H^+(v_x^H(L^-) + p^H), H^-(v_x^V(0^+) + p^V), H^+(v_x^V(L^-) + p^V)\right\}, & x = 0. \end{cases} \tag{5.4.27}$$

Let first assume that $v = K$ with a constant $K \in \mathbb{R}$. Then we have $u(t,x) = -\lambda t + px + K$ and we can easily deduce from (5.4.27) that

$$\lambda = \max\left\{H(p^H), H(p^V)\right\} = H(p^\alpha).$$

We define $p^- := (H^-)^{-1}(p^\alpha)$ and $p^+ := (H^+)^{-1}(p^\alpha)$ such that $p^- \leq p^+$. We can also show that

$$p^- = (H^-)^{-1}(p^+).$$

If we consider $v = K = 0$, and if we set $\lambda^\star = H(p^H) \geq H(p^V)$ then we can show that $u^\star(t,x) = -\lambda^\star t + p^\alpha x$ (with $\alpha \in \{H, V\}$) is a (viscosity) subsolution of (5.4.25) since we have

$$\begin{cases} -\lambda^\star + H(p^H) = 0, \\ -\lambda^\star + H(p^V) \leq 0, \\ -\lambda^\star + \max\left\{H(p^H), H(p^V)\right\} = 0. \end{cases}$$

and $u^\star \leq -\lambda t + p^\alpha x + v^\alpha(x)$ at $t = 0$. The comparison principle leads to

$$-\lambda^\star t \leq -\lambda t, \quad \text{for} \quad t \gg 1$$

and then we get a natural bound by above on the *true* homogenized flux λ that is

$$\lambda^\star = \max\left\{H(p^H), H(p^V)\right\} \geq \lambda.$$

□

Remark 4.2 (Particular case of the parabola for traffic Fundamental Diagram)**.** *Going back to traffic, since* $H(p) = -\dfrac{1}{\gamma} f(\gamma p)$ *for any* p*, we have a bound by below on the vehicle flux* f*.*

Moreover, in the particular case of the parabola (known as the Greenshields flow function in traffic literature) that is

$$f(x) = 4x(1-x),$$

we have

$$\begin{cases} p^- = \dfrac{1-\sqrt{1-\lambda}}{2}, \\ \\ p^+ = \dfrac{1+\sqrt{1-\lambda}}{2} \end{cases}$$

Remark 4.3 (Strict equality)**.** *It has been demonstrated by Imbert and Monneau, see Proposition 8.6 in [139] that we have in reality the equality*

$$\bar{H}\left(p^H, p^V\right) = \max\left\{A, H\left(p^H\right), H\left(p^V\right)\right\}.$$

The proof uses the definition of adequate test functions developed in [140].

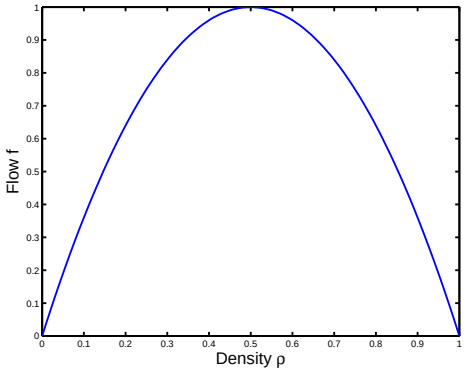

FIGURE 5.3 – Flow function f

4.2 Case of a concave fundamental diagram

Let us consider the classical Greenshields Fundamental Diagram that reads

$$f(\rho) = \rho(1-\rho) \tag{5.4.28}$$

where the density ρ ranges from 0 to $\rho_{\max} = 1$. For sake of simplicity, up to multiplying f, we normalize the maximal flow to 1 (see Figure 5.3).

We now study the cell problem of a simple crossing with two incoming and two outgoing roads. Assume that the roads are labeled from 1 to 4 such that 1 and 3 are respectively the incoming and outgoing roads on the horizontal axis, and 2 and 4 the incoming and outgoing roads on the vertical axis.

Below we will consider different values of *fixed* assignments coefficients γ^α for $\alpha \in \{1, 4\}$.

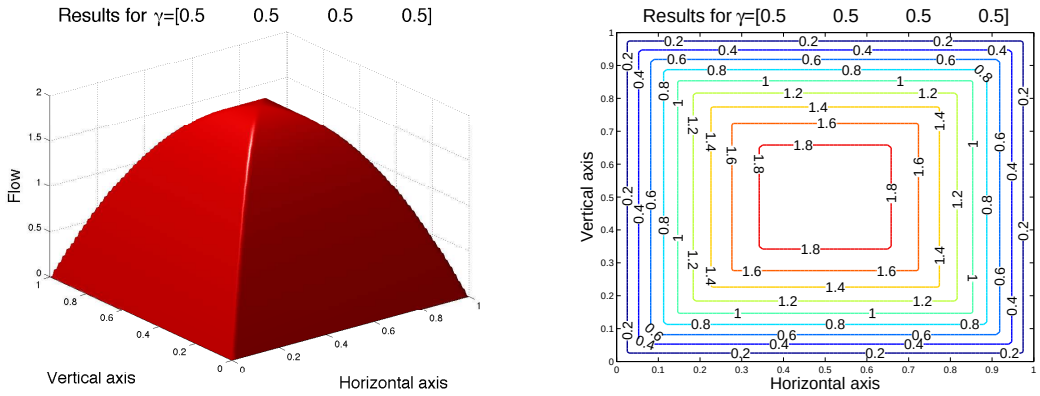

(a) Effective Hamiltonian (b) Isolines for the effective Hamiltonian

FIGURE 5.4 – Case of parabola, without flux limiter $A = \infty$. Tolerance $= 10^-3$, step of density $= 0.01$

In the case of

$$\begin{cases} \gamma^1 = 0.5, \\ \gamma^2 = 0.5, \end{cases} \quad \text{and} \quad \begin{cases} \gamma^3 = 0.5, \\ \gamma^4 = 0.5, \end{cases}$$

we can note that the effective Hamiltonian is strictly symmetric with respect to vertical and horizontal axis (see Figure 5.4). Moreover the flux limiter A does not impose any plateau at the top of the macroscopic flow function (see Figure 5.5).

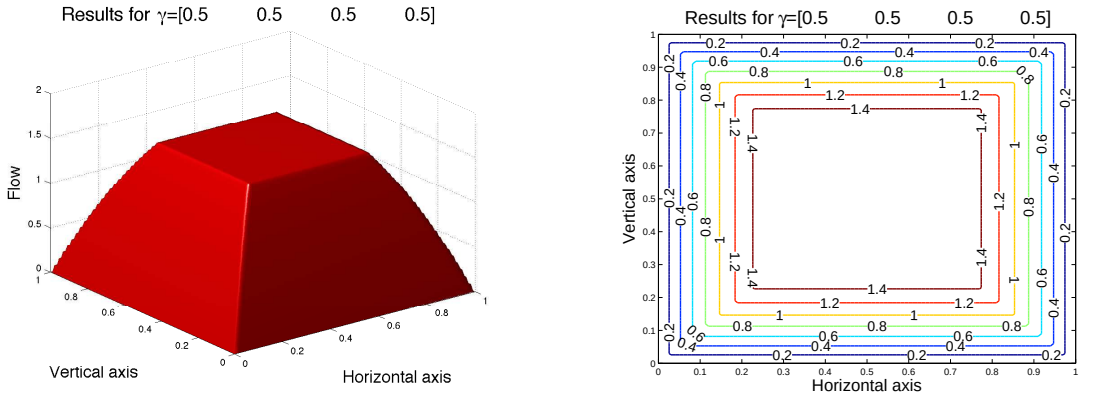

(a) Effective Hamiltonian (b) Isolines for the effective Hamiltonian

FIGURE 5.5 – Case with flux limiter $A = 1.5$. Tolerance $= 10^{-}3$, step of density $= 0.01$

In the following case (see Figure 5.6) we have chosen

$$\begin{cases} \gamma^1 = 0.7, \\ \gamma^2 = 0.3, \end{cases} \quad \text{and} \quad \begin{cases} \gamma^3 = 0.7, \\ \gamma^4 = 0.3. \end{cases}$$

Thus the coefficient are the same on horizontal (resp. vertical) branches. We observe that the maximal flow through the junction is lower than the previous case (Figure 5.4) and the shape of the effective Hamiltonian is notably different. To ease the comparisons with Figures 5.4 and 5.5, the flow axis on Figure 5.6 is rescaled between 0 and 2.

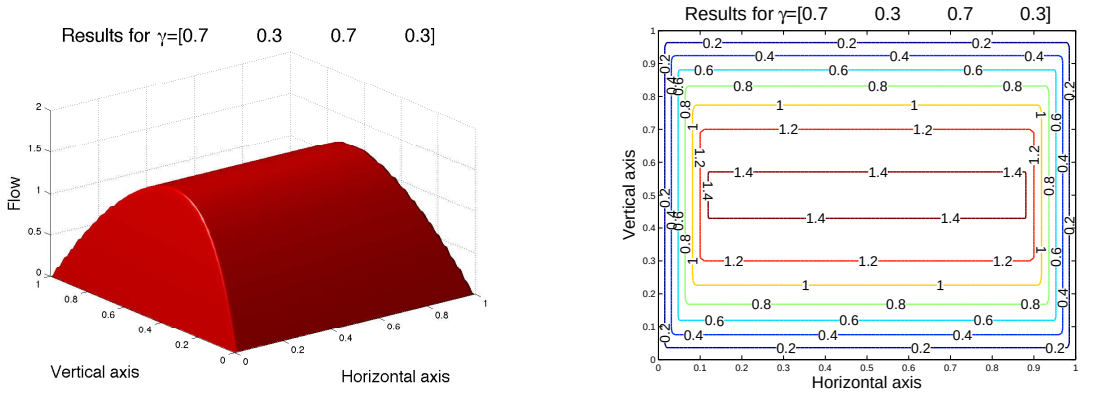

(a) Effective Hamiltonian (b) Isolines for the effective Hamiltonian

FIGURE 5.6 – Case of the parabola, without flux limiter $A = \infty$. Tolerance $= 10^{-3}$, step of density $= 0.01$

In the following case (see Figure 5.7) we have chosen

$$\begin{cases} \gamma^1 = 0.8, \\ \gamma^2 = 0.2, \end{cases} \quad \text{and} \quad \begin{cases} \gamma^3 = 0.2, \\ \gamma^4 = 0.8. \end{cases}$$

One can observe that in that case the effective Hamiltonian goes to zero for every value of density. Indeed due to the fact that the coefficients are not strictly equal on the same axis (i.e. $\gamma^1 \neq \gamma^3$ and $\gamma^2 \neq \gamma^4$), the long time behavior of flows in the cell tends to a gridlock and a null flow through the junction.

It seems to be true (up to now, we have only checked it numerically) as soon as we have $\gamma^1 \neq \gamma^3$ and $\gamma^2 \neq \gamma^4$. By the way, the closer to the equality, the longer (in computation time) the homogenization to zero. Without loss of generality, the phenomenon is illustrated on Figure 5.8 for a particular setting of densities on the branches.

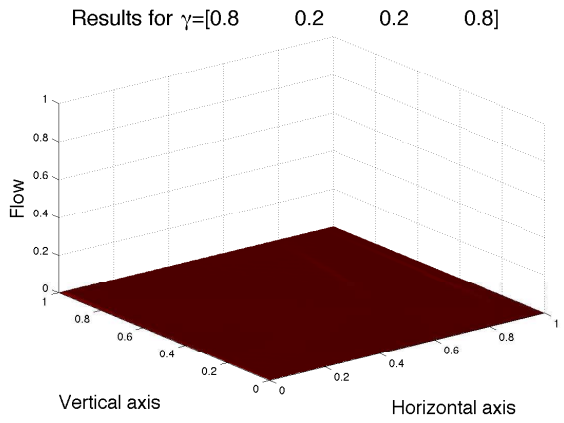

FIGURE 5.7 – Effective Hamiltonian. Case of the parabola, without flux limiter $A = \infty$. Tolerance $= 10^{-3}$, step of density $= 0.01$. The flow axis is rescaled between 0 and 1.

As our tolerance threshold is not set to zero, the effective Hamiltonian is not rigorously equal to zero but it is just a numerical matter and we can assume that the flow is strictly null in very long time behavior for a tighter threshold.

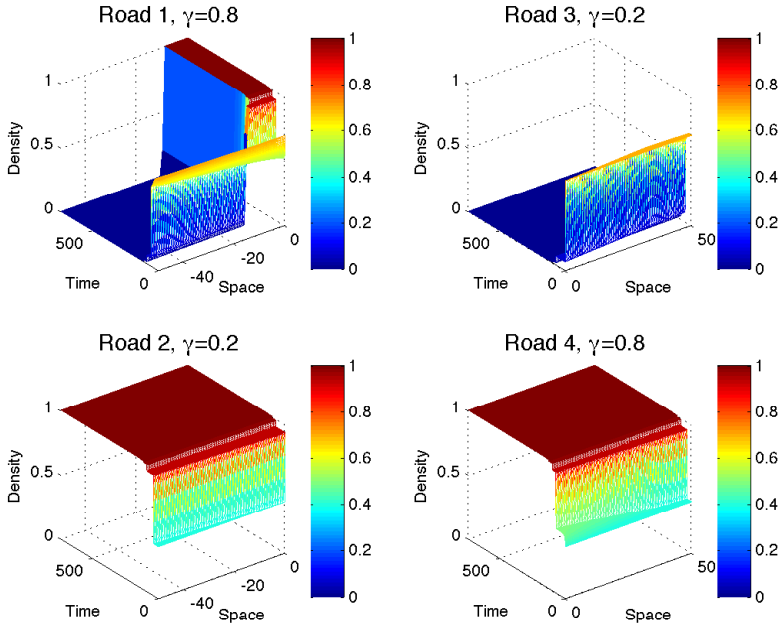

FIGURE 5.8 – Evolution of density on each road. Case of the parabola, without flux limiter. Tolerance $= 0$.

In that case (which is generalizable to other configurations of initial densities), we will concentrate vehicles on the vertical axis (roads 2 and 4) until the roads are saturated. At that moment, the supply on road 4 is equal (or very close) to zero and thus the possible

passing flow through the junction collapses to zero. Any vehicle cannot go by anymore and there is an accumulation (queue) of vehicles upstream the junction, on road 1.

Remark 4.4 (Critical case)**.** *If we consider the degenerated case given by*

$$\begin{cases}\gamma^1 = 1,\\ \gamma^2 = 0,\end{cases} \quad \text{and} \quad \begin{cases}\gamma^3 = 1,\\ \gamma^4 = 0,\end{cases}$$

we naturally observe that the homogenized flow through the junction is never influenced by the densities on the roads for which the coefficients are null i.e. the horizontal axis here (see Figure 5.9).

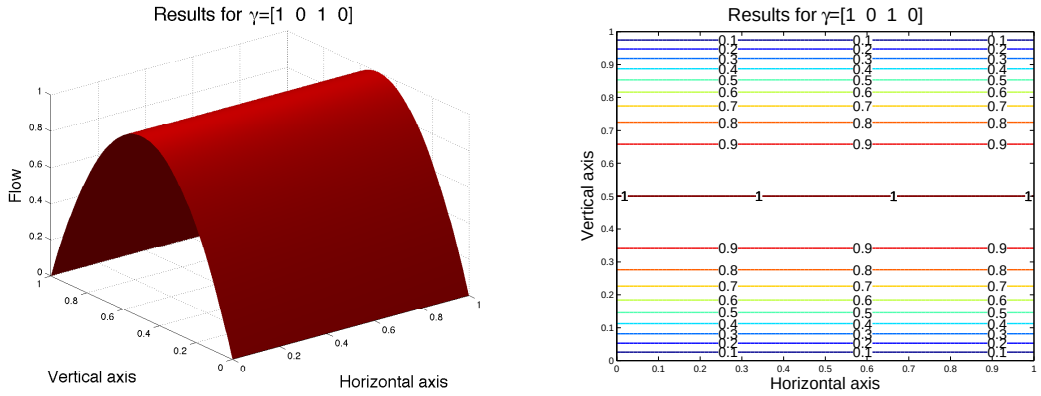

(a) Effective Hamiltonian (b) Isolines for the effective Hamiltonian

FIGURE 5.9 – Critical case (without flux limiter)

As the passing flux through the junction comes only from road 1*, whatever the density on the horizontal axis is, the shape of the effective Hamiltonian is simply the flow function f with respect to the density on the vertical axis, and it is invariant by translation on the horizontal axis.*

4.3 Case of an exponential fundamental diagram

We now consider an exponential fundamental diagram given by

$$f(\rho) = \rho \exp\left(\frac{1}{\rho - 1}\right), \tag{5.4.29}$$

with the density ranging from 0 to 1. We can also modify the flow function such that the maximal flow is equal to 1 (see Figure 5.10).

For our reference case, we do not consider a flux limiter A (which is equivalent to consider an infinite flux limiter) and we choose

$$\begin{cases}\gamma^1 = 0.5,\\ \gamma^2 = 0.5,\end{cases} \quad \text{and} \quad \begin{cases}\gamma^3 = 0.5,\\ \gamma^4 = 0.5.\end{cases}$$

The effective Hamiltonian is plotted on Figure 5.11.

In the second case (see Figure 5.12) we conserve the coefficients of our reference case but we introduce a flux limiter $A = 1.5$.

In the following case (see Figure 5.13) we have chosen

$$\begin{cases}\gamma^1 = 0.8,\\ \gamma^2 = 0.2,\end{cases} \quad \text{and} \quad \begin{cases}\gamma^3 = 0.8,\\ \gamma^4 = 0.2.\end{cases}$$

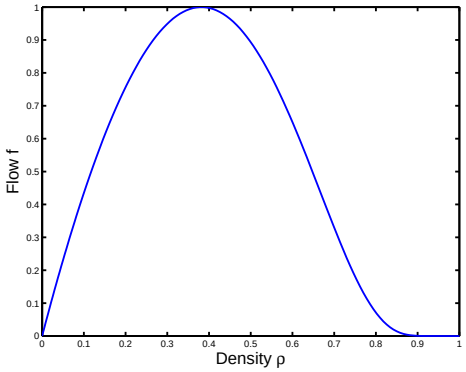

FIGURE 5.10 – Flow function f

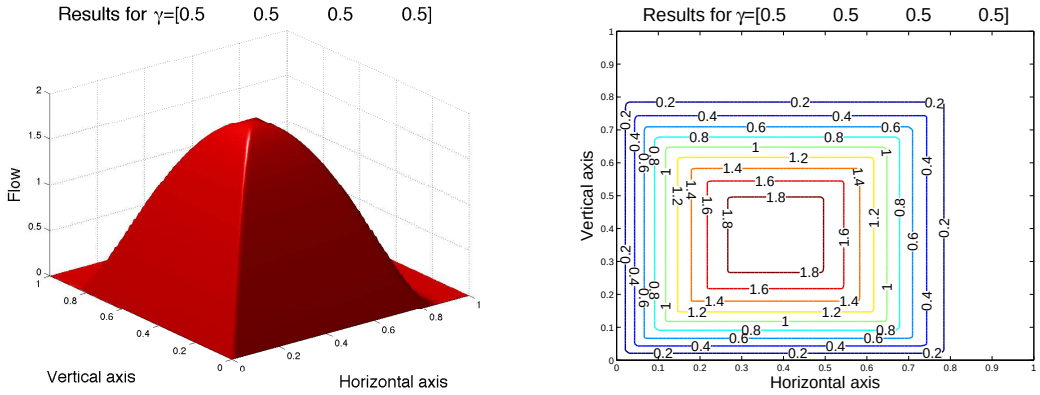

(a) Effective Hamiltonian (b) Isolines for the effective Hamiltonian

FIGURE 5.11 – Reference case for exponential flow function (without flux limiter)

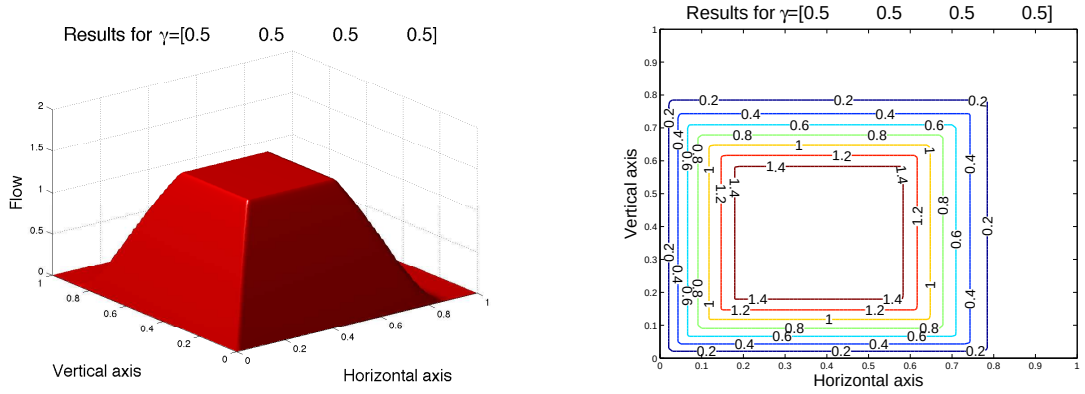

(a) Effective Hamiltonian (b) Isolines for the effective Hamiltonian

FIGURE 5.12 – Case of the exponential function, with flux limiter $A = 1.5$. Tolerance $= 10^{-3}$, step of density $= 0.01$

Remark 4.5 (Critical case)**.** *If we consider*

$$\begin{cases} \gamma^1 = 1, \\ \gamma^2 = 0, \end{cases} \quad \text{and} \quad \begin{cases} \gamma^3 = 1, \\ \gamma^4 = 0, \end{cases}$$

we naturally observe that the flow through the junction is never influenced by the densities

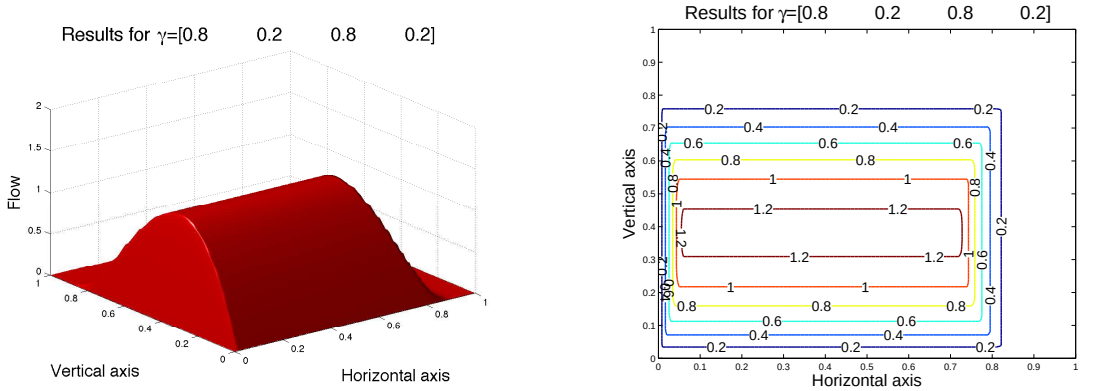

(a) Effective Hamiltonian (b) Isolines for the effective Hamiltonian

FIGURE 5.13 – Case of the exponential function, without flux limiter. Tolerance $= 10^{-3}$, step of density $= 0.01$

on the roads for which the coefficients are null i.e. the vertical axis here (see Figure 5.14).

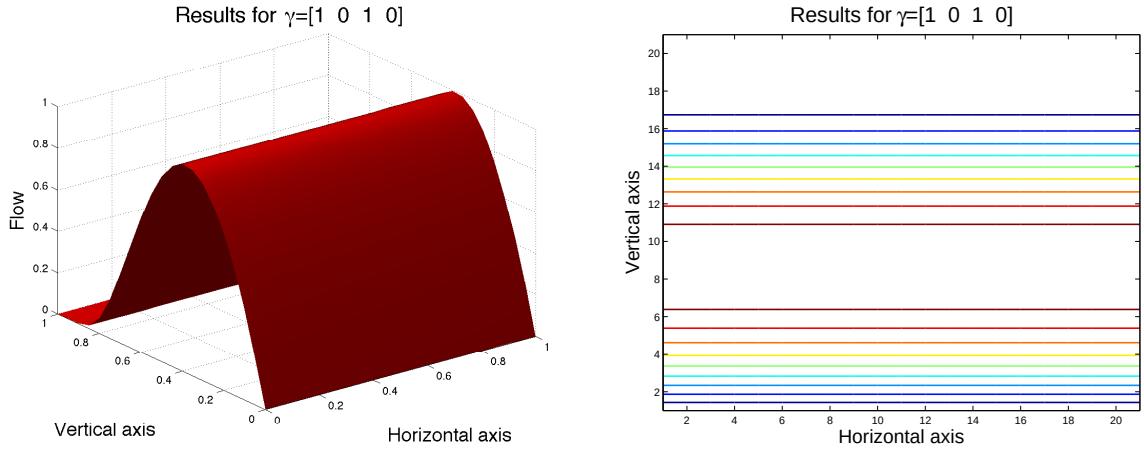

(a) Effective Hamiltonian (b) Isolines for the effective Hamiltonian

FIGURE 5.14 – Critical case for the exponential function, without flux limiter. Tolerance $= 10^{-3}$, step of density $= 0.01$

4.4 Different network shapes : a triangular mesh

If we make the particular choice of $\rho_j = \dfrac{\rho_1 + \rho_{j^2}}{2}$ (see Figure 5.15), which is a compatibility condition for the primitive, then it is possible to get theoretical results on the homogenization and the analytic expression of the effective Hamiltonian. By the way, we can forget this condition on the densities for numerical homogenization.

In the particular setting of the triangular shape (see Figure 5.15), without loss of generality, we consider a single junction with three incoming and three outgoing branches, with the following settings

$$\gamma^i = \frac{1}{3}, \quad \text{for any} \quad i \in \{1, 6\}\,.$$

The effective flow that we obtain for this particular choice is plotted on Figure 5.16.

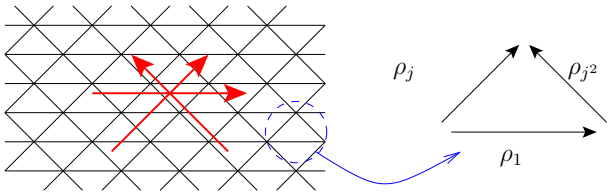

FIGURE 5.15 – Representation of the use case of a triangular shaped network.

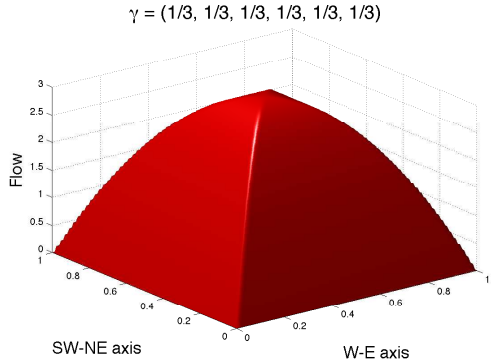

(a) Effective Hamiltonian

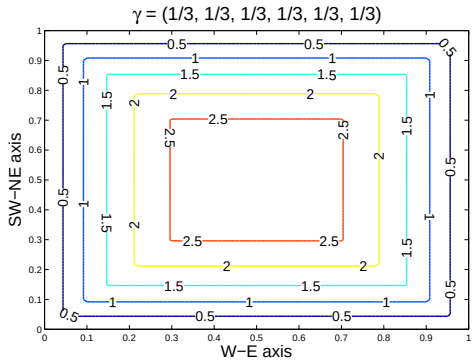

(b) Isolines for the effective Hamiltonian

FIGURE 5.16 – Case of the parabola, without flux limiter $A = \infty$. Tolerance $= 10^{-3}$, step of density $= 0.01$

We have also tested another values for (γ^α) as follows

$$\begin{cases} \gamma^1 = \gamma^2 = \gamma^4 = \gamma^5 = 0.3, \\ \gamma^3 = \gamma^6 = 0.4. \end{cases}$$

The results are displayed on Figure 5.17.

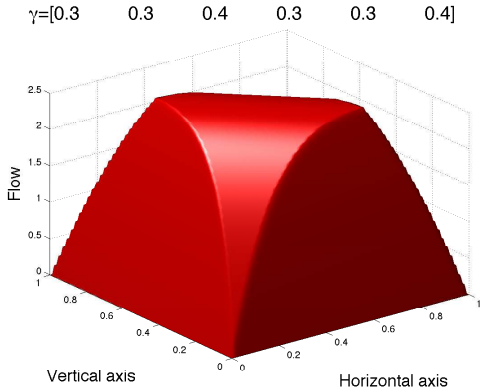

(a) Effective Hamiltonian

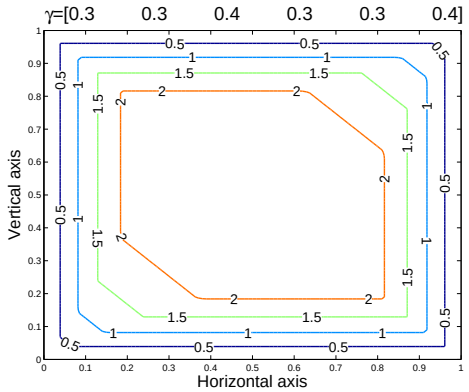

(b) Isolines for the effective Hamiltonian

FIGURE 5.17 – Case of the parabola, without flux limiter $A = \infty$. Tolerance $= 10^{-3}$, step of density $= 0.01$

One can remark that we recover the characterization of the effective Hamiltonian given for any number of branches $d \in \mathbb{N}$, say

$$\bar{H}(P) = \max\left\{A, \max_\alpha H_\alpha(p_\alpha)\right\}, \quad \text{for any} \quad P = (p_\alpha)_\alpha \in \mathbb{R}^d.$$

5 Optimized assignment coefficients

We simply search the optimal set of assignment coefficients $\gamma_\star := (\gamma_\star^\alpha)_\alpha$ such that the passing flow through the junction point F_0 is maximized. We can split the nonlinear optimization problem under constraints between incoming and outgoing roads. At this level, we simply focus on the case of a junction with two incoming and two outgoing branches. The associated optimization problem reads

$$\max_{\gamma=(\gamma^\alpha)_\alpha} F_0(\gamma) \quad s.t. \left| \begin{array}{l} 0 \leq \gamma^\alpha \leq 1, \quad \alpha = 1, ..., N \\ \sum_{\alpha=1}^N \gamma^\alpha = 1. \end{array} \right.$$

where the flow through the junction is given by

$$F_0(\gamma) := \min \left\{ \min_{1\leq\alpha\leq N_I} \left(\frac{1}{\gamma^\alpha} f_D^\alpha \right), \min_{N_I+1\leq\beta\leq N} \left(\frac{1}{\gamma^\beta} f_S^\beta \right) \right\}.$$

In the case of two incoming and two outgoing roads, we can consider two cases

- either the coefficients for the outgoing branches are fixed once for all, such that $\gamma^3 + \gamma^4 = 1$ and we only search the optimal values of $(\gamma_\star^1, \gamma_\star^2)$ that maximize the flow passing through the junction ;
- or all the coefficients $(\gamma^\alpha)_{\alpha=1,...,4}$ are variable. The optimal set $(\gamma_\star^\alpha)_{\alpha=1,...,4}$ is computed at each time step $n\Delta t$, with $n \in \mathbb{N}$ such that the flow through the junction F_0 is maximized. We also need to satisfy at each time step that $\gamma_\star^1 + \gamma_\star^2 = 1$ and $\gamma_\star^3 + \gamma_\star^4 = 1$.

Optimization of coefficients on incoming branches only

In the first case, as $\gamma^2 = 1 - \gamma^1$, the problem can be recast as follows

$$\gamma_\star^1 = \text{argmax } F_0(\gamma^1)$$

with $0 \leq \gamma_\star^1 \leq 1$ and

$$F_0(\gamma^1) := \min \left\{ \min \left(\frac{1}{\gamma^1} f_D^1, \frac{1}{1-\gamma^1} f_D^2 \right), \min \left(\frac{1}{\gamma^3} f_S^3, \frac{1}{\gamma^4} f_S^4 \right) \right\}.$$

We have voluntarily split the flow expression between upstream demands which are dependent on the parameter γ^1 and the downstream supplies which do not depend on it. Thus we can easily deduce the value of $\gamma_\star^1$, according to the values of demands (f_D^1 and f_D^2) and supplies ($\min \left(\frac{1}{\gamma^3} f_S^3, \frac{1}{\gamma^4} f_S^4 \right)$), as illustrated on Figure 5.18.

By the way, one can notice that if F_0 is reached for a downstream supply, we have many possibilities for $\gamma_\star^1 = \text{argmax } F_0$. Thus we need to introduce a priority law to choose one of the possible values. For instance, we impose $\gamma_\star^1$ to be the closest of 1 (and so $\gamma_\star^2 = 1 - \gamma_\star^1$ is the closest to 0).

Proposition 5.1 ((Formal) Convergence to a fixed coefficients situation)**.** *Assume (H0), (H1). If the function u (we define the density such that $u_x^\alpha = \rho^\alpha$) which solves (5.1.1) converges to U solution of (5.1.4) with the optimization of the coefficients (γ^1, γ^2) with fixed coefficients on outgoing branches (γ^3, γ^4), and if we assume that there exists a time*

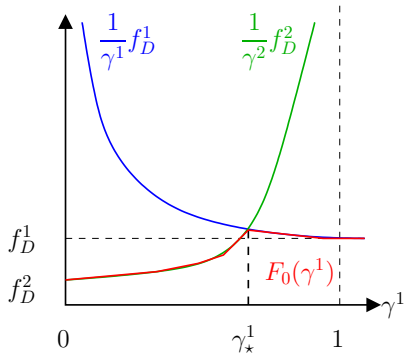

FIGURE 5.18 – Optimal solution $\gamma_\star^1$ in the particular case of $f_D^1 \geq f_D^2$ and $\min\left(\frac{1}{\gamma^3} f_S^3, \frac{1}{\gamma^4} f_S^4\right) > \frac{f_D^1}{\gamma_\star^1}$.

$T > 0$ such that the set $(\gamma^\alpha(t))_\alpha$ converges to a stationary set $(\gamma_\star^\alpha)_\alpha$ for $t \leq T$ then at the homogenized state, we have

$$\gamma_\star^1 = \gamma^3, \quad \textit{and} \quad \gamma_\star^2 = \gamma^4.$$

Obviously, we have also $\gamma_\star^3 = \gamma^3$ and $\gamma_\star^4 = \gamma^4$.

Proof **(Formal)** The proof is really simple. We work with densities (traffic framework). Let T be the first time such that we got the homogenization of flows over the cell. First, we argue that as soon as $t \geq T$, we have $\partial_t \rho^\alpha = 0$ for any branch α (stationary state). As the vehicle density ρ^α solves the conservation law

$$\partial_t \rho^\alpha + \partial_x f(\rho^\alpha) = 0,$$

on each branch $\alpha = 1, ..., 4$, then we obtain $f(\rho^\alpha(x,t)) = K^\alpha$ for any $(x,t) \in \mathbb{R} \times [T, +\infty)$, with $0 < K^\alpha \leq 1$ a constant. By definition of the flow near the junction, we get $K^\alpha = \gamma^\alpha F_0$ for any $\alpha = 1, ..., 4$. Moreover, from Periodicity assumption (H2) and if $F_0 \neq 0$, we deduce

$$K^1 = K^3, \quad \text{and} \quad K^2 = K^4.$$

This ends the proof. □

Case of the concave flow function

On figures 5.19 and 5.22, we have plotted the effective Hamiltonian obtained by optimizing the coefficients on the incoming roads in order to maximize the flow through the junction. The assignment coefficients are fixed on both outgoing branches.

On Figure 5.19 we have chosen $\gamma^3 = \gamma^4 = 0.5$.

On Figure 5.21 we have chosen $\gamma^3 = 0.7$ (and so $\gamma^4 = 1 - \gamma^3 = 0.3$) that is to say that 70 percent of the passing vehicles go on road 3, whatever is the proportion of vehicles coming from branch 1 or 2.

One can notice on Figure 5.22 that the flow reaches a maximal value of 1.4 which corresponds to the product $2\gamma^3 f_{max}$. Moreover, as the coefficients are fixed on the outgoing roads, we recover that if the density is too high, the supply of (one or both) outgoing roads decreases, tending to diminishing the flow through the junction. By homogenization (under the periodicity assumption), the effective Hamiltonian goes to zero if the density is too much important.

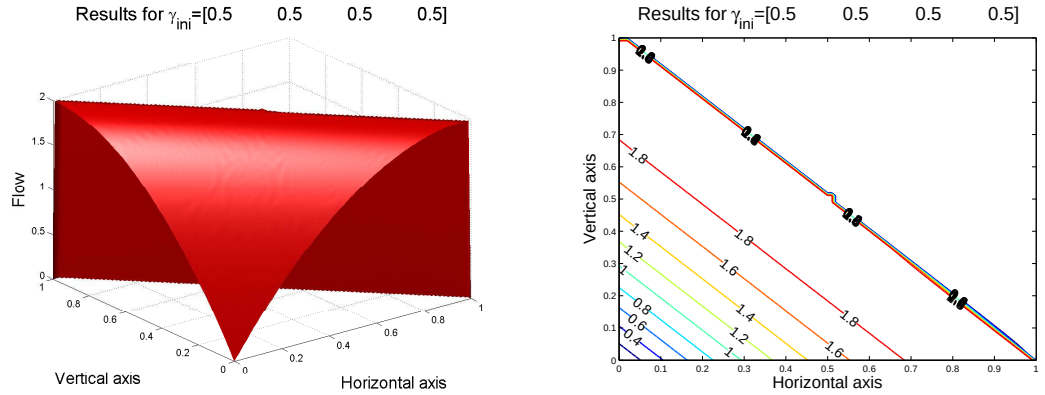

(a) Effective Hamiltonian (b) Isolines for the effective Hamiltonian

FIGURE 5.19 – Optimization case, for incoming roads only, without flux limiter ($A = \infty$). Tolerance $= 10^{-3}$, step of density $= 0.01$

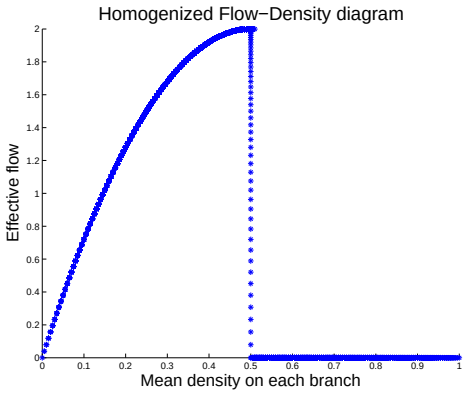

FIGURE 5.20 – Effective Hamiltonian as a function of the mean density in the cell

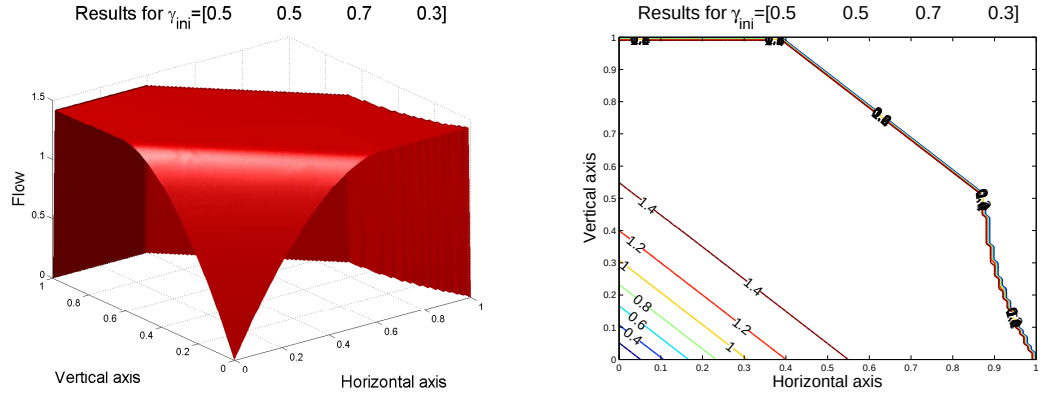

(a) Effective Hamiltonian (b) Isolines for the effective Hamiltonian

FIGURE 5.21 – Optimization case, for incoming roads only, without flux limiter ($A = \infty$). Tolerance $= 10^{-3}$, step of density $= 0.01$

One can also plot the value of the homogenized flow according to the value of densities (or the mean value of density) on the branches at the stationary state (see Figure 5.22).

Remark 5.2 (Critical case)**.** *In the "critical" case (i.e. choosing* $\gamma^3 = 1$ *and* $\gamma^4 = 0$ *for*

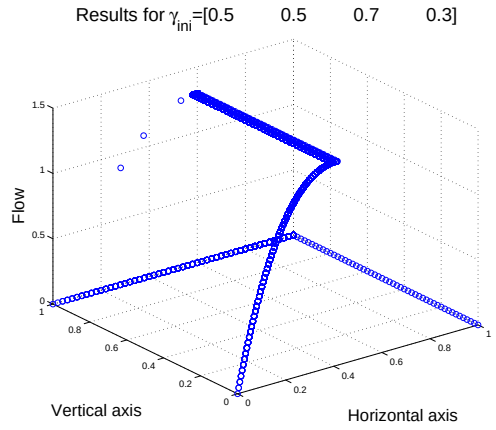

(a) Hamiltonian w.r.t. *equivalent* densities

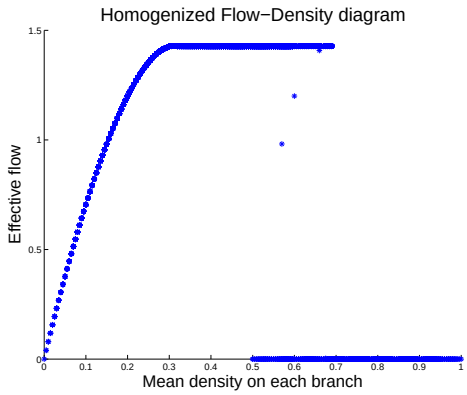

(b) Hamiltonian w.r.t. the mean density in the cell

FIGURE 5.22 – Optimization case, for incoming roads only, without flux limiter ($A = \infty$). Tolerance $= 10^{-3}$, step of density $= 0.01$

instance) plotted on Figure 5.23, we recover an effective Hamiltonian which highly looks like to the case of Figure 5.9 with fixed coefficients on incoming and outgoing roads.

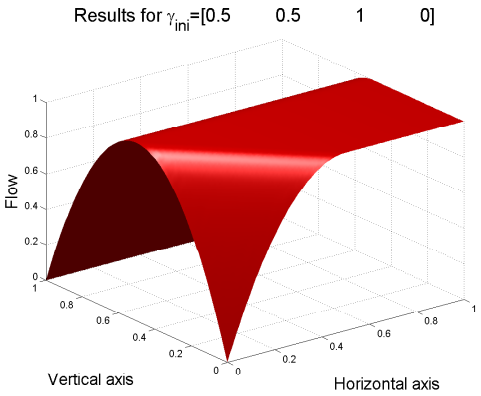

(a) Effective Hamiltonian

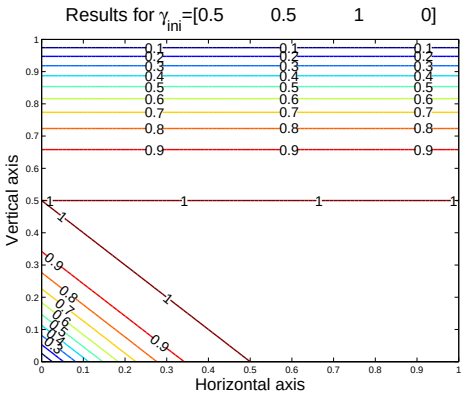

(b) Isolines for the effective Hamiltonian

FIGURE 5.23 – Optimization case, for incoming roads only, without flux limiter ($A = \infty$). Tolerance $= 10^{-3}$, step of density $= 0.01$

We have a plateau at maximal flow 1. *The flow is naturally limited by the supply on road* 3 *which has to absorb all the passing vehicular flux. This supply is upper bounded by* 1.

Remark 5.3 (Vehicle conservation in the cell)**.** *One can notice that starting from an initial condition where densities are constant on the same axis (ρ_0^H for horizontal and ρ_0^V for vertical), we get a new equivalent initial condition (say ρ_{eq}^H and ρ_{eq}^V) after some time iterations (some ε).*

Of course, density on a branch can be non-constant at the stationary state. We define ρ_{eq}^H and ρ_{eq}^V as the mean value of density on horizontal and vertical axis. We only know that

$$\rho_0^H + \rho_0^V = \rho_{eq}^H + \rho_{eq}^V.$$

Assume that we can define the equivalent set of densities as the densities at the stationary state. We consider the function that maps the initial densities to their equivalent den-

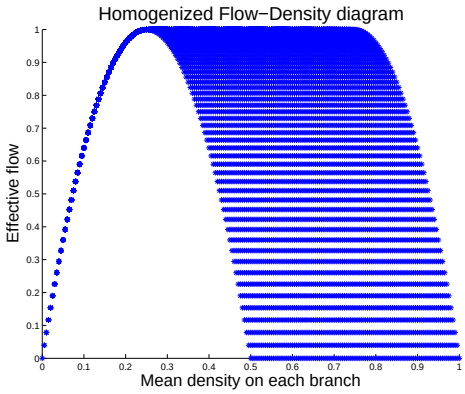

FIGURE 5.24 – Effective Hamiltonian as a function of the mean density in the cell

sities. If we consider two different sets of initial densities $\left(\rho_0^H, \rho_0^V\right)_1$ *and* $\left(\rho_0^H, \rho_0^V\right)_2$ *such that the number of vehicles in the cell is the same, say* $\left(\rho_0^H\right)_1 + \left(\rho_0^V\right)_1 = \left(\rho_0^H\right)_2 + \left(\rho_0^V\right)_2$*, then do we get the same set of equivalent densities ?*

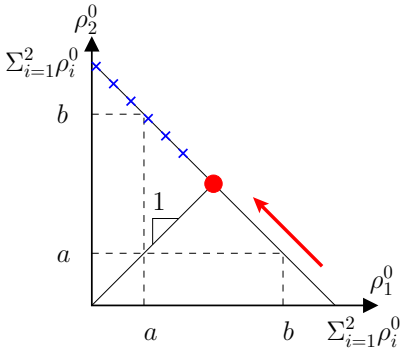

FIGURE 5.25 – Map between initial densities and *equivalent* densities for a given number of vehicles in the cell, say $2\Sigma_{i=1}^2\rho_0^i$. It is only true in case of $\gamma^1 \neq \gamma^2 (\neq 0.5)$ because if $\gamma^1 = \gamma^2 = 0.5$, everything converges to the point at the intersection with the first diagonal.

It seems not possible due to the priority law that we consider in our optimization case. Indeed vehicles will be assigned in priority on the horizontal axis. Thus, considering $\rho_0^H = a$, $\rho_0^V = b$ *with* $a \neq b$, *is different of considering* $\rho_0^H = b$, $\rho_0^V = a$ *(see Figure 5.25).*

Comparison between the optimization case and the case with fixed coefficients

In this part, we assume that we consider an initial state in density $\left(\rho_0^H, \rho_0^V\right)$ on the horizontal and vertical axis and we are interested in the comparison between the effective Hamiltonian for fixed coefficients (and we select $\gamma^1 = \gamma^3 = \gamma^H$ and $\gamma^2 = \gamma^4 = \gamma^V$) say $\bar{H}\left(\rho_0^H, \rho_0^V\right)$, and the effective Hamiltonian $\bar{H}\left(\rho_{eq}^H, \rho_{eq}^V\right)$ obtained when optimizing the flow by selecting the most adequate incoming coefficients (γ^1, γ^2) and knowing that γ^3, γ^4 are fixed.

We recall that $\bar{H}\left(\rho_0^H, \rho_0^V\right)$ is simply obtained as follows

$$\bar{H}\left(\rho_0^H, \rho_0^V\right) = \max\left\{A, H(\rho_0^H), H(\rho_0^V)\right\}.$$

It is worth noticing also that in our traffic application, the coefficients $(\gamma^\alpha)_\alpha$ are implicitly embedded in the Hamiltonian H. Thus in terms of traffic flow, we have

$$\bar{H}\left(\rho_0^H, \rho_0^V\right) = \min\left\{A, \frac{1}{\gamma^H} f(\rho_0^H), \frac{1}{\gamma^V} f(\rho_0^V)\right\}.$$

In the first example, we consider $\gamma^3 = \gamma^4 = \frac{1}{2}$. Graphical results are shown on Figure 5.26.

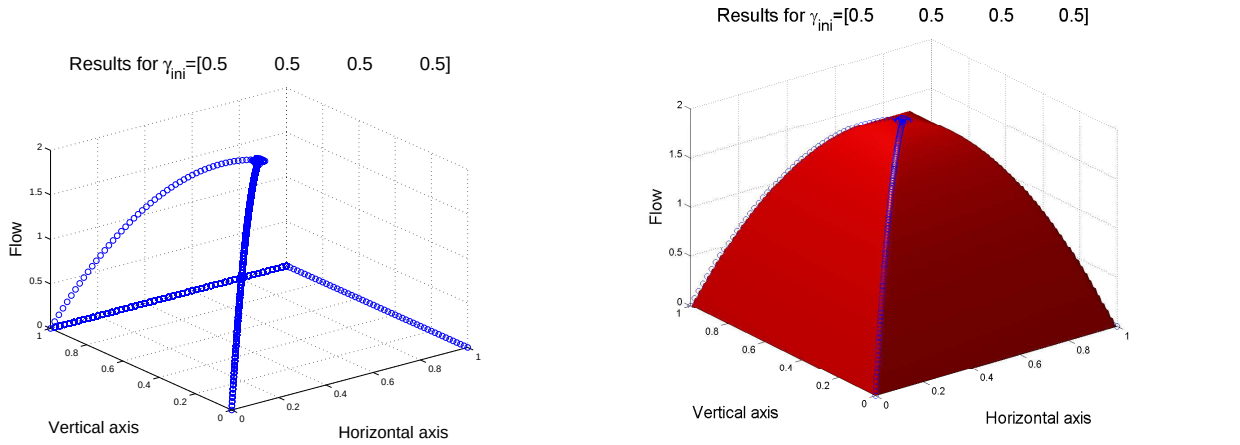

(a) Effective Hamiltonian $\bar{H}\left(\rho_{eq}^H, \rho_{eq}^V\right)$ (b) Comparison between $\bar{H}\left(\rho_0^H, \rho_0^V\right)$ and $\bar{H}\left(\rho_{eq}^H, \rho_{eq}^V\right)$

FIGURE 5.26 – Optimization case, for incoming roads only, without flux limiter ($A = \infty$). Tolerance $= 10^{-3}$, step of density $= 0.01$

In the second example, we consider $(\gamma^H =)\gamma^3 = 0.3$ and $(\gamma^V =)\gamma^4 = 1 - \gamma^3 = 0.7$. The numerical results are shown on Figure 5.27.

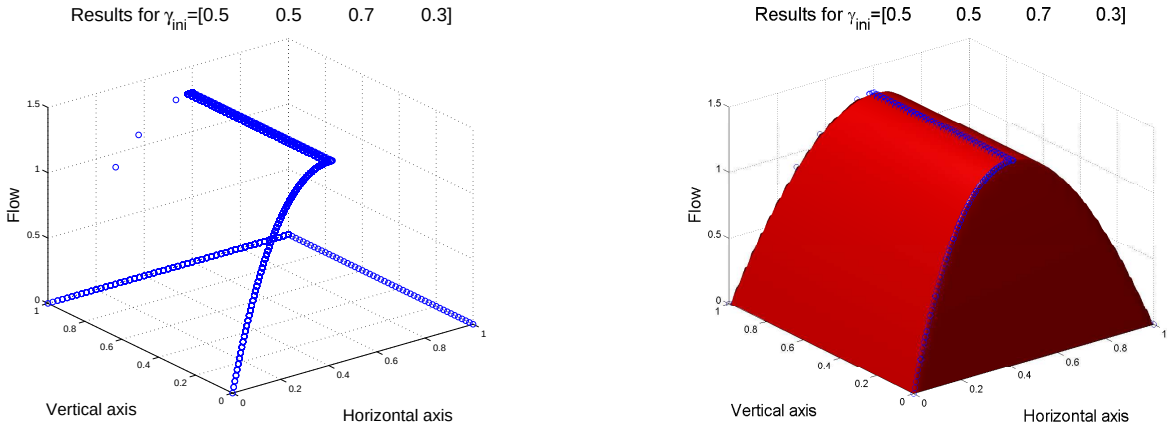

(a) Effective Hamiltonian $\bar{H}\left(\rho_{eq}^H, \rho_{eq}^V\right)$ (b) Comparison between $\bar{H}\left(\rho_0^H, \rho_0^V\right)$ and $\bar{H}\left(\rho_{eq}^H, \rho_{eq}^V\right)$

FIGURE 5.27 – Optimization case, for incoming roads only, without flux limiter ($A = \infty$). Tolerance $= 10^{-3}$, step of density $= 0.01$

Remark 5.4 (Equivalence between fixed coefficients case and optimization case, in large time behavior)**.** *It needs to be properly establish but simulations let us think that in large time behavior (homogenization), the junction model with fixed coefficients and the one with optimized incoming coefficients are strictly equivalent.*

By the way, it is not really so surprising because as we have already observed it, in large time, we have that $\gamma^1_\star \to \gamma^3 = \gamma^H$ *and* $\gamma^2_\star \to \gamma^4 = \gamma^V$ *(see Proposition 5.1).*

Optimization of coefficients on incoming and outgoing branches

In the second case ((γ^3, γ^4) are also time varying, the optimization problem boils down ta two-parameters problem by noticing that $\gamma^2 = 1-\gamma^1$ and $\gamma^4 = 1-\gamma^3$. Thus, the optimal set $\gamma_\star$ is given by

$$\left(\gamma^1_\star, \gamma^1_\star\right) = \text{argmax } F_0(\gamma^1)$$

with $0 \leq \gamma^1_\star \leq 1$ and the flow through the junction reads

$$F_0(\gamma^1, \gamma^3) := \min\left\{\min\left(\frac{1}{\gamma^1} f^1_D, \frac{1}{1-\gamma^1} f^2_D\right), \min\left(\frac{1}{\gamma^3} f^3_S, \frac{1}{1-\gamma^3} f^4_S\right)\right\}.$$

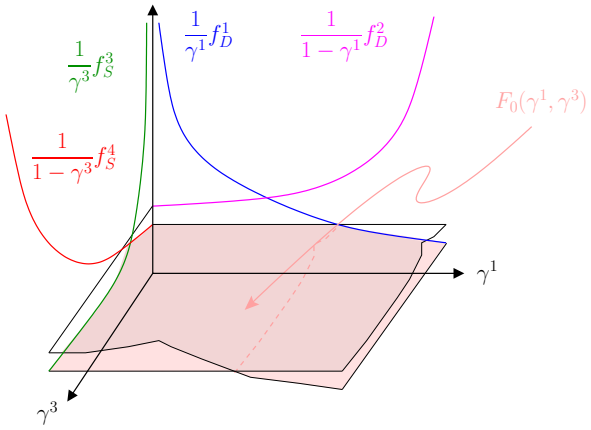

FIGURE 5.28 – Representation of the flow through the junction as a function of (γ^1, γ^3).

Proposition 5.5 ((Formal) Convergence to a fixed coefficients situation)**.** *Assume (H0), (H1). If the function* u *(we define the density such that* $u^\alpha_x = \rho^\alpha$*) which solves (5.1.1) converges to* U *solution of (5.1.4) with the optimization of the coefficients* $(\gamma^\alpha)_\alpha$*, then at the homogenized state, we have*

$$\gamma^1_\star = \gamma^3_\star = \gamma^2_\star = \gamma^4_\star = \frac{1}{2}.$$

Proof **(Formal)** In a first step, thanks to Proof of Proposition 5.1, we can easily show that

$$\gamma^1_\star = \gamma^3_\star, \quad \text{and} \quad \gamma^2_\star = \gamma^4_\star.$$

In a second step, let argue by contradiction. Assume that $(\gamma^\alpha_\star)_\alpha$ is the optimal set of parameters for which we have the homogenization, such that

$$\left(\gamma^1_\star = \gamma^3_\star\right) \neq \left(\gamma^2_\star = \gamma^4_\star\right).$$

We can rewrite the (homogenized) flow at the junction as follows

$$F_0 = \min\left[\frac{1}{\gamma^1_\star} f^H, \frac{1}{\gamma^2_\star} f^V\right],$$

with $f^H := \min\left(f_D^1, f_S^3\right)$ and $f^V := \min\left(f_D^2, f_S^4\right)$. We can assume that $F_0 = \dfrac{1}{\gamma_\star^1} f^H$ (the reasoning is perfectly reversible for $F_0 = \dfrac{1}{\gamma_\star^2} f^V$). If $\gamma_\star^1 \neq \gamma_\star^2$, then it follows that the flow outgoing on branch 4 reads

$$f^4 = \frac{\gamma_\star^2}{\gamma_\star^1} f^H \neq f^H.$$

In particular it means that at the following time step, the flow $F_0(\gamma_\star^1, \gamma_\star^3)$ will be sub-optimal (either the demand on one incoming road, or the supply on one outgoing road is not satisfied). Hence we will compute a new set of parameters which is in contradiction with the assumption of homogenization (stationary state). This ends the proof. □

Remark 5.6. *One can notice that the optimization process tends to equally share vehicles among all the branches until the homogenization of the whole system. Thus, even optimized time varying coefficients boil down to a homogenized fixed coefficients model of junction.*

Case of the concave fundamental diagram

We consider the Greenshields concave flow function (5.4.28). See Figure 5.29 for the results.

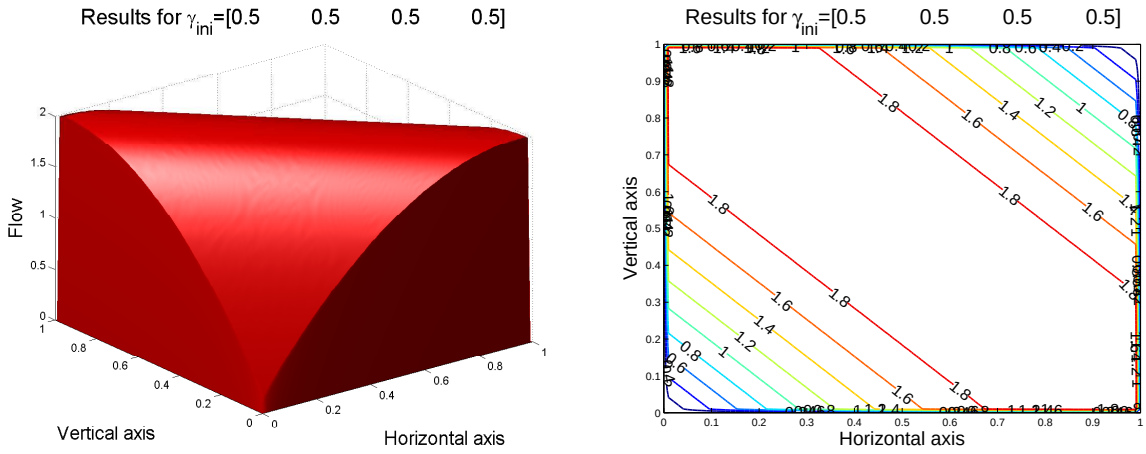

(a) Effective Hamiltonian (b) Isolines for the effective Hamiltonian

FIGURE 5.29 – Optimization case, without flux limiter ($A = \infty$). Tolerance $= 10^{-3}$, step of density $= 0.01$

One can notice that the effective Hamiltonian is only a function of the total density in the cell i.e. $\rho^H + \rho^V$ if ρ^H (resp. ρ^V) denotes the density on the horizontal (resp. vertical) axis (see Figure 5.30 where the density axis is resized between 0 and 1). It agrees the concept of (Network or) Macroscopic Fundamental Diagram (MFD) in traffic which only matches the entering density of vehicles (whichever the sense) to the total outflow on a determined urban area.

By the way, the values of null flow on Figure 5.30 are due to the discrete step in density. The reader can also see on Figure 5.29 (b), that the isolines do not perfectly fit the boundaries while they should with a numerical step going to zero.

Remark 5.7 (Computational cost)**.** *The computation of the effective Hamiltonian plotted on Figure 5.29 lasts more than 40 hours on a Dell computer, Intel Xeon 2.49 GHz, with 3,25 Go RAM and 8 cores.*

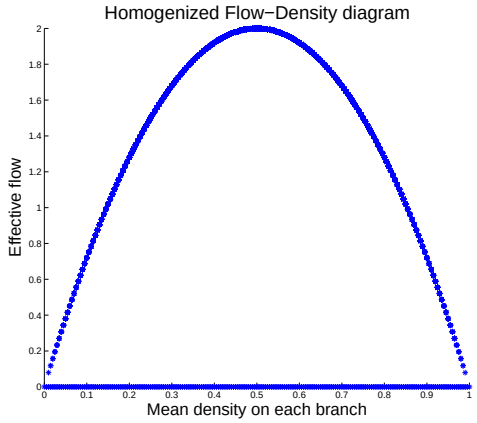

FIGURE 5.30 – Effective Hamiltonian as a function of the mean density in the cell

Case of the exponential fundamental diagram

Here we consider the exponential fundamental diagram given in (5.4.29). See Figure 5.31 for the numerical results.

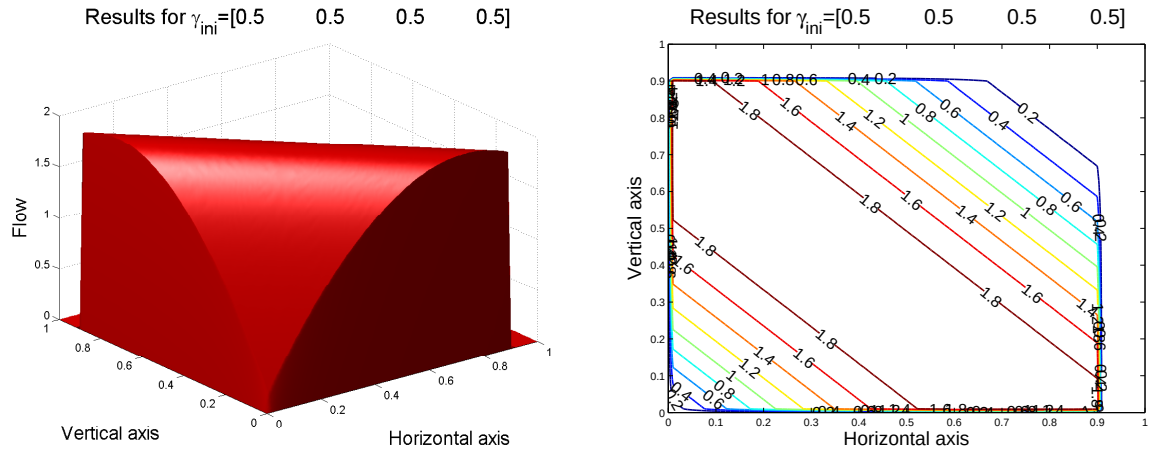

(a) Effective Hamiltonian (b) Isolines for the effective Hamiltonian

FIGURE 5.31 – Optimization case, without flux limiter ($A = \infty$). Tolerance $= 10^{-3}$, step of density $= 0.01$

6 Traffic signals

6.1 Formal results

Let consider a one-dimensional road with a traffic signal situated at $x = 0$. We assume that the traffic signal timings are fixed once for all and we set δ_R and δ_G respectively the time of red and green phases. On each arc we consider that vehicles density $\rho(t, x)$ satisfies the classical LWR model (standing for Lighthill-Whitham and Richards) that reads

$$\rho_t + (f(\rho))_x = 0, \quad \text{for any} \quad x \neq 0, \quad t \geq 0, \tag{5.6.30}$$

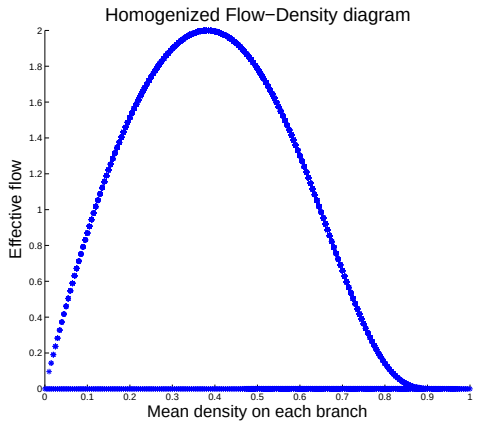

FIGURE 5.32 – Effective Hamiltonian as a function of the mean density in the cell

where f describes the flow-density function, known as the *fundamental diagram* in traffic flow literature. This function is assumed to be strictly concave such that there exists a unique density σ such that f is maximal and we take $f(0) = f(1) = 0$.

We can recast the LWR model (5.6.30) into Hamilton-Jacobi framework

$$u_t + H(u_x) = 0, \tag{5.6.31}$$

where $\rho = -u_x$ and the Hamiltonian H is chosen such that $H(p) = -f(-p)$ for any $p \in \mathbb{R}$. Thus the Hamiltonian is strictly convex. At the junction point $x = 0$, we assume

$$u_t + \max\left[-A(t), H^-(u_x(0^+, t)), H^+(u_x(0^-, t))\right] = 0 \tag{5.6.32}$$

which stands for Lebacque's rule of demand and supply. Moreover we have a flux limiter A which depends on time t. This flux limiter accounts for the period of traffic signals

$$A(t) = \begin{cases} 0 & \text{if} \quad t \text{ is within a period } \delta_R, \\ 1 & \text{if} \quad t \text{ is within a period } \delta_G. \end{cases}$$

The flux limiter will only act during the red phase of the traffic signals i.e. when we set $A = 0$. Indeed the Hamiltonian is non-positive so the max form in (5.6.32) will only capture the value of A and set the passing flow to zero. Note also that we consider a "normalized" Hamiltonian such that $\sup_{p\in\mathbb{R}} |H(p)| = 1 \, (= \|H\|_{L^\infty})$.

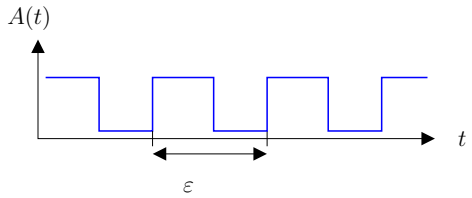

FIGURE 5.33 – On-and-off traffic signal as a flux limiter

Up to a rescaling, we get the following homogenization problem (outside the junction point)

$$u_t^\varepsilon + H(u_x^\varepsilon) = 0 \tag{5.6.33}$$

where we have defined the homogenized variable

$$u^\varepsilon(x,t) = \varepsilon u\left(\frac{x}{\varepsilon}, \frac{t}{\varepsilon}\right).$$

At the junction point ($x = 0$), we obtain

$$u_t^\varepsilon + \max\left(H^-(u_x^\varepsilon(0^+,t)), H^+(u_x^\varepsilon(0^-,t)), A(t/\varepsilon)\right) = 0. \tag{5.6.34}$$

We set

$$F_A := \max\left(H^-(u_x^\varepsilon(0^+,t)), H^+(u_x^\varepsilon(0^-,t)), A(t/\varepsilon)\right).$$

From [140], if H is convex, we have that u^ε converges towards u^0 when $\varepsilon \to 0$ where u^0 is a solution to the following problem

$$\begin{cases} u_t^0 + H(u_x^0) = 0, & \text{outside the junction point} \\ u_t^0 + F_{\bar{A}}(u_x^0(0^+,t), u_x^0(0^-,t)) = 0, & \text{at the junctuon point} \end{cases}$$

where

$$\bar{A} =< A(0) >= \frac{0\delta_R + (\min H)\delta_G}{\delta_R + \delta_G} = \eta \min H,$$

with $\eta := \dfrac{\delta_G}{\delta_R + \delta_G}$ is the proportion of green time on the total signal period.

We can show that the flow function through the junction point $F_{\bar{A}}$ is equivalent to the minimum between upstream demands, downstream supplies and a flux limiter ηf_{max}.

Lax-Hopf formula : If we set the Lagrangian L as the Fenchel transform of the Hamiltonian H i.e. $L = H^* = \sup_{q\in\mathbb{R}}\{pq - H(q)\}$ then we have that the solution of the previous problem is given by the Lax-Hopf formula

$$u(x,t) = \inf_{\substack{X(.) \\ X(0)=y \\ X(t)=x}} \left\{u_0(y) + \int_0^t \mathcal{L}\left(X(\tau), \dot{X}(\tau)\right) d\tau\right\} \tag{5.6.35}$$

where

$$\mathcal{L}(x,p) = \begin{cases} L(p) & \text{if} \quad x \neq 0, \\ -A(t) & \text{if} \quad x = 0. \end{cases}$$

One can notice that we have

$$L(0) = \sup(-H) = -\min H > 0,$$

and

$$-A(t) \in [0, -\min H].$$

Assume that the trajectory from $X(0) = y < 0$ to $X(t) = x > 0$ stays at the junction point between times t_1 and t_2 (see Figure 5.34) with

$$< \mathcal{L}(x,p) >= - < A >, \quad \text{for any} \quad t_1 \leq t \leq t_2.$$

Thus the equation (5.6.35) could be recast as follows

$$u(x,t) = u_0(y) + t_1 v^- + (t - t_2)L(v^+) - (t_2 - t_1) < A > .$$

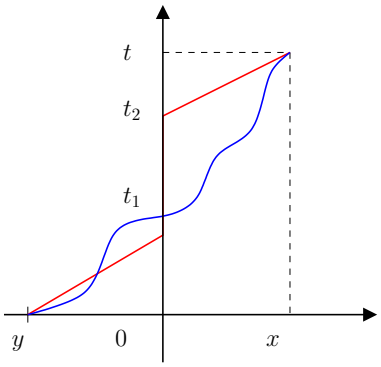

FIGURE 5.34 – Trajectories through the junction point

where $v^{\pm}$ denotes either the speed on the incoming ($x < 0$) or the outgoing branch ($x > 0$). The solution is then computed as the initial cost plus the "classical" cost outside the junction point, plus the cost to stay at the junction point.

The flow at the junction given by (5.6.32) can be recast according to Lebacque's rule

$$F_A \Leftrightarrow \min\left(f_D^-, f_S^+, - < A >\right)$$

with

$$-A = \begin{cases} 0, & \delta_R, \\ \min\left(\max f^-, \max f^+\right), & \delta_G. \end{cases}$$

6.2 Homogenization result for two traffic signals on a one-directional road

We now consider the following case : assume that we have two traffic signals which are set on a one-directional road, respectively at x_1 and x_2, with $x_1 < x_2$. These two consecutive signals are separated by length $x_2 - x_1 =: l > 0$. We consider that traffic is injected at a point E located at $x_E = x_1 - L$ and traffic flow exits the section at a point S located at $x_S = x_2 + L$, with $L > l > 0$.

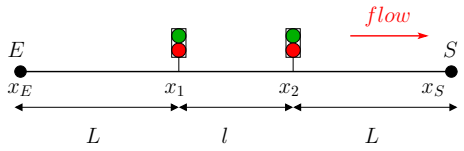

FIGURE 5.35 – Case of two consecutive signals on a one-dimensional network.

On this particular network (which a simple one-dimensional road), we plug Hamilton-Jacobi equations as follows

$$\begin{cases} u_t + H(u_x) = 0, & \text{if} \quad x \neq \{x_E, x_1, x_2, x_S\}, \\ u_t + F_{a_i(t)}\left(u_x(x^-), u_x(x^+)\right) = 0, & \text{if} \quad x = x_i, \quad \text{with} \quad x_i \in \{x_1, x_2\}, \\ u_t + H^-(u_x(x^+)) = 0, & \text{if} \quad x = x_E, \\ u_t + H^+(u_x(x^-)) = 0, & \text{if} \quad x = x_S. \end{cases} \tag{5.6.36}$$

It is worth noticing that the third and fourth equations in (5.6.36) implicitly say that the upstream demand of the link and the downstream supply are infinite.

We recall that the Hamiltonian H is convex or level-set convex and that H^- (resp. H^+) is the non-increasing (resp. non-decreasing) part of the Hamiltonian. According to [140], we define F_A as follows

$$F_A(p,q) = \max\{A, H(p), H(q)\}, \quad \text{for any} \quad (p,q) \in \mathbb{R}^2.$$

We also set (for some fixed $A_R \geq A_G$)

$$a_1(t) := \begin{cases} A_G, & \text{if} \quad kT \geq t > k\tau, \\ A_R, & \text{if} \quad k\tau \geq t \geq (k+1)T \end{cases} \quad \text{and} \quad a_2(t) := \begin{cases} A_R, & \text{if} \quad kT \geq t > k\tau, \\ A_G, & \text{if} \quad k\tau \geq t \geq (k+1)T \end{cases}$$

for some $k \in \mathbb{Z}$, and T the traffic cycle length, and let $0 < \dfrac{\tau}{T} \leq 1$ be the proportion of green light (for second traffic signal) over the full cycle length. One can notice that both traffic signals are in opposition of phase (when one turns red, the other one turns green and so on).

Looking for homogenization of time and space homogenization (re-scaling effect with scale factor ε going to zero), we will converge to the case of a single traffic signal which will impose a new flux limiter $\bar{A}$ and the flow will be regulated by the following model

$$\begin{cases} u_t + H(u_x) = 0, & \text{if} \quad x \neq x_i, \\ u_t + F_{\bar{A}}(u_x(x^-), u_x(x^+)) = 0 & \text{if} \quad x = x_i, \end{cases} \quad \text{with} \quad x_i \in \{x_1, x_2\}.$$

The question is then to compute the new (mean) flux limiter $\bar{A}$ as a function of different parameters :

- Length l between both signals ;
- Length L separating signals from entry and exit points ;
- Time τ as a measure of green over red light times.

In the particular case of a single traffic signal with

$$a_0(t) := \begin{cases} A_G, & \text{if} \quad kT \geq t > k\tau, \\ A_R, & \text{if} \quad k\tau \geq t \geq (k+1)T \end{cases}, \quad \text{for any} \quad k \in \mathbb{Z}, \quad \text{and} \quad 0 < \tau \leq T,$$

it has been already demonstrated [103] that $\bar{A}_0 =< a_0 >= \dfrac{A_G\tau + A_R(T-\tau)}{\tau}$.

Remark 6.1 (Physical intuition on the equivalent flux limiter)**.** *Some intuition from shock and rarefaction waves obtained in the conservation laws framework for vehicle densities is given by Figure 5.36.*

As one can see on Figure 5.36, the behavior of traffic flows through both consecutive traffic signals is very dependent on the phase offset φ, on the length of green phase over the red one and also it depends on the distance l separating both traffic signals.

The length L has *a priori* no impact on the form of $\bar{A}$. It strongly supports the fact that $\bar{A}$ is only dependent on a short-distance phenomenon. Numerical results obtained for the Hamiltonian

$$H(p) = 4p(p-1),$$

and $L = 100$, $\Delta x = 1$, $\Delta t = 0.25$, are plotted on Figure 5.37.

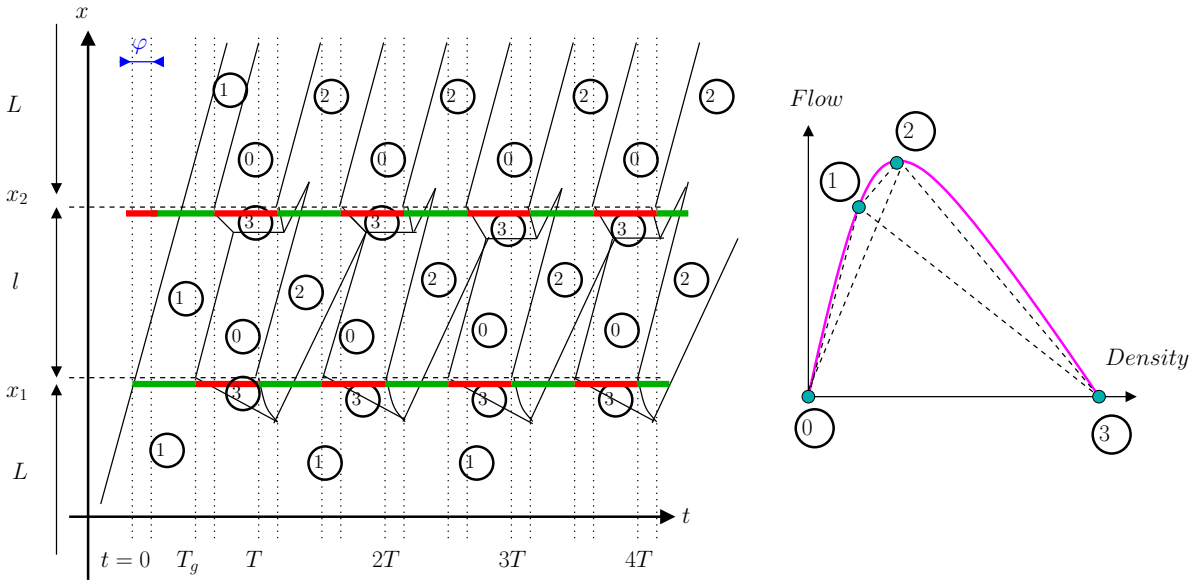

FIGURE 5.36 – Kinematic waves induced from two consecutive traffic signals with a phase offset $\varphi > 0$.

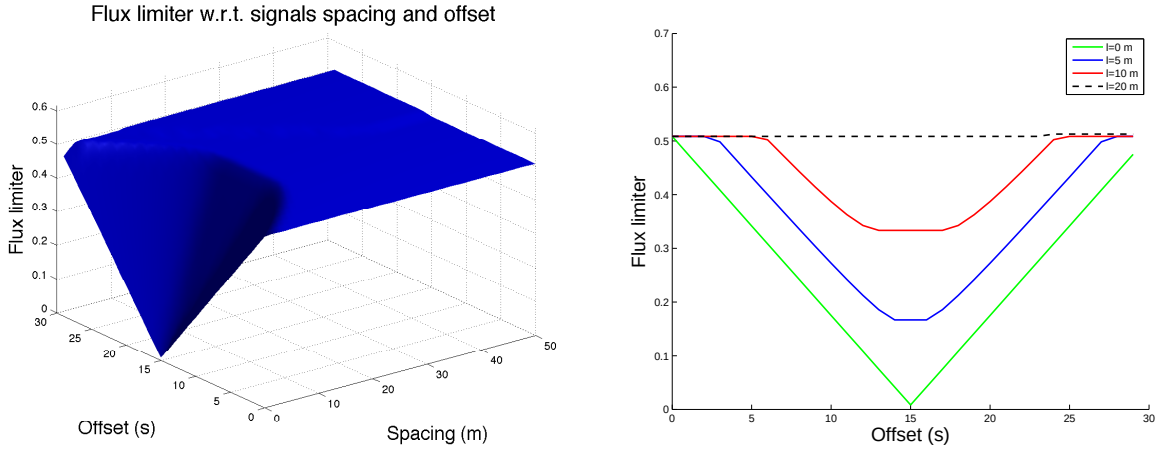

(a) Flux limiter (b) Some cuts for fixed spacing

FIGURE 5.37 – Flux limiter $\bar{A}$ for the effective Hamiltonian, in case of two traffic signals, with respect to the spacing l and the offset φ between both signals.

7 Perspectives

Below is a list of possible cases that we have to (or can) consider in our numerical simulations.

- Lane changing : let consider a one dimensional road with periodic "junctions" between right and left lanes (see Figure 5.38). We assume fixed constant coefficients $(\gamma^\alpha)_\alpha$.

  We also need to impose some periodicity conditions on the solutions (for instance exiting flows are incoming demands). It is worth noticing that theory is possible in that case.

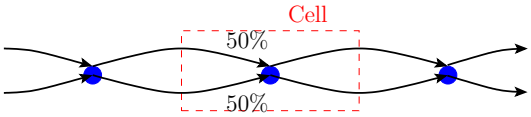

FIGURE 5.38 – Representation of the use case of lane changing.

It is also possible to define different velocity functions on right and left lanes (to take into consideration that vehicles go faster on one of lanes).

- Exchanging zones : this case is quite similar to the previous one, except that sense of flowing are opposed on one lane (see Figure 5.39). By the way, this case seems to be identical to the simplest crossing studied as the first case above. However, there is a topological difference with this latter case. Indeed, at the level of densities, there is no difference but it is hard to define primitives. We also assume that the coefficients $(\gamma^\alpha)_\alpha$ are fixed once for all.

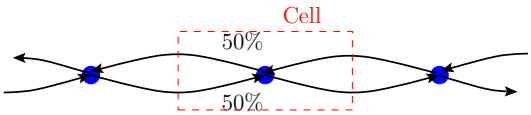

FIGURE 5.39 – Representation of the use case of exchanging zones.

- Realistic model of urban junction : if we want to model a realistic urban junction, we need to take into consideration four incoming and four outgoing branches. We have two possibilities to model junction behavior : either we consider that the junction is point-wise and that we have fixed coefficients $(\gamma^\alpha)_\alpha$ (then we do not need to introduce traffic lights), or we consider the physical dimension of the junction with different *internal* links (see Figure 5.40). We then need to introduce traffic lights to avoid as much as possible conflicts between turning flows. We also consider fixed coefficients $(\gamma^\alpha)_\alpha$, which is clearly the drawback for the realism of the model.

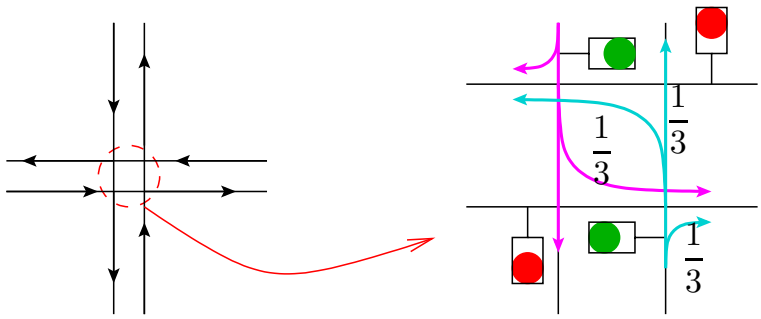

FIGURE 5.40 – Representation of the use case of a realistic junction.

By the way, on Figure 5.40, the revolving movements are not plotted but can be also take into account (even if the coefficients devoted to that movements are very negligible compared to the other ones).

To improve the modeling, it could be convenient to introduce turning fraction coefficients $(\alpha_{ij})_{i,j}$ which state the proportion of vehicles coming from branch (i) that

exits on branch (j), with the obvious relations

$$\begin{cases} \sum_j \alpha_{ij} = 1, \\ \\ f_j = \displaystyle\sum_i \alpha_{ij} f_i = \sum_i \frac{\alpha_{ij}}{\gamma_i} F_0, \\ \\ \dfrac{1}{\gamma_j} = \displaystyle\sum_i \frac{\alpha_{ij}}{\gamma_i}. \end{cases}$$

Troisième partie

Formules de représentation et modèles GSOM de trafic

Chapitre 6

A variational formulation for higher order macroscopic traffic flow models : numerical investigation

This chapter is an adaptation of paper [68] written in collaboration with Jean-Patrick Lebacque and accepted pending minor revisions, in *Transportation Research Part B : Methodological*.

Sommaire

Abstract

This paper deals with numerical methods providing semi-analytic solutions to a wide class of macroscopic traffic flow models for piecewise affine initial and boundary conditions. In [172], a variational principle has been proved for models of the Generic Second Order Modeling (GSOM) family, yielding an adequate framework for effective numerical methods. Any model of the GSOM family can be recast into its Lagrangian form as a Hamilton-Jacobi equation (HJ) for which the solution is interpreted as the position of vehicles. This solution can be computed thanks to Lax-Hopf like formulas and a generalization of the inf-morphism property [58]. The efficiency of this computational method is illustrated through a numerical example and finally a discussion about future developments is provided.

1 Introduction

1.1 General background

In order to get a realistic estimation of the real-time traffic states on networks, traffic operators and managers need macroscopic traffic flow models. These models must be simple, robust, allowing to get solutions at a low computational cost. The main macroscopic models are based on conservation laws or hyperbolic systems (see [135] or Chapter in [108] for traffic aspects and [106] for mathematical aspects). The seminal LWR model (for Lighthill-Whitham and Richards) was proposed in [184, 221] as a single conservation law with unknown the vehicle density. This model based on a first order Partial Differential Equation (PDE) is very simple and robust but it fails to recapture some empirical features of traffic. In particular, it does not allow to take into account non-equilibrium traffic states mainly in congested situation. More sophisticated models referred to as *higher order* models were developed to encompass kinematic constraints of real vehicles or also the wide variety of driver behaviors, even at the macroscopic level. In this paper we deal with models of the Generic Second Order Modeling (GSOM) family. Even if these models are more complicated to deal with, they permit to reproduce traffic instabilities (such as the so-called *stop-and-go* waves, the hysteresis phenomenon or capacity drop) which move at the traffic speed and differ from kinematic waves [241] (see also [174] and references therein).

Before the wide propagation of internet handsets, traffic monitoring has mainly been built on dedicated infrastructure which imply quite important installation and maintenance costs. Traffic flow monitoring and management has been deeply modified with the development of new technologies in mobile sensing aiming to provide a quite important quantity of floating car data. Traffic flow models are needed to be well suited such that managers could use both Eulerian and Lagrangian data for improving traffic state estimation. The term *Eulerian* refers to "classical" fixed equipment giving records of occupancy or flow of vehicles on a freeway section. This kind of measurements come from e.g. fixed inductive loop detectors, Radio Frequency Identification (RFID) transponders, radars or video cameras. By opposite, the term *Lagrangian* is used to characterize data coming from sensors which move within the measured field of interest. Lagrangian data are provided by on board mobile sensors such as *Global Positioning Systems* (GPS) or GPS-enabled *smartphones*.

While the idea of monitoring traffic using mobile sensors appeared less than ten years ago with the popularization of the mobile internet devices, there exists a fast growing literature about how to integrate Lagrangian data into classical macroscopic traffic flow

models. The process of incorporating Eulerian and Lagrangian data into a mathematical model to improve the modeling is called *data estimation* or equivalently *inverse modeling*. According to the major UC Berkeley field experiment named *Mobile Century* and then *Mobile Millennium* investigating Lagrangian sensing, it has been shown that even a 2% to 5% penetration rate of probe vehicles into the driver population provides sufficient and accurate data for estimating traffic velocity or density on highways [129, 130, 237]. Nevertheless, it has been demonstrated in [216] that the quality of estimation for *higher-order traffic quantities* including vehicle acceleration/deceleration, emission and fuel consumption rates is dramatically affected when the penetration rate of probe vehicles or the sampling frequency of the current mobile sensors decrease. However on board devices propose a real breakthrough in traffic monitoring by providing a very cheap and efficient way to collect traffic data.

1.2 Motivation

In order to improve traffic states estimation from Lagrangian data, we propose to deal with macroscopic traffic flow models of the GSOM family. As these models combine the simplicity of the LWR model with the dynamics of driver specific attributes, we are able to recapture more specific phenomenon with a higher accuracy. While methods of data assimilation have been mainly developed for first order models up to now (except [29] which is dedicated to phase transition model), this work presents a new algorithm to reconstruct traffic states from both Eulerian and Lagrangian data. We take advantage of a very recent article [172] in which a variational principle has been proved for models of the GSOM family.

1.3 Organization of the paper

The rest of this paper is structured as follows. Section 2 presents more in detail the GSOM models and sheds a specific light on the LWR model which is widely used in traffic engineering. The variational principles for the GSOM models including LWR model are briefly recalled in Section 3. Section 4 is devoted to the presentation of the main elements of our computational method. Finally, Section 5 proposes a numerical example of our method.

2 GSOM traffic flow models

2.1 Formulation of GSOM models

In [169, 174], the authors introduce a general class of macroscopic traffic flow models called the Generic Second Order Models (GSOM) family. Any model of the GSOM family can be stated in conservation form as follows

$$\begin{cases} \partial_t \rho + \partial_x(\rho v) = 0 & \text{Conservation of vehicles,} \\ \partial_t(\rho I) + \partial_x(\rho v I) = \rho\varphi(I) & \text{Dynamics of the driver attribute } I, \\ v = \mathfrak{I}(\rho, I) & \text{Fundamental diagram,} \end{cases} \tag{6.2.1}$$

where ρ stands for the density of vehicles, v for the flow speed (equal to the mean spatial velocity of vehicles), x and t for position and time. The variable I is a specific driver attribute which can represent for example the driver aggressiveness, the driver destination or the vehicle class. The flow-density fundamental diagram (FD) is defined by

$$\mathfrak{F} : (\rho, I) \mapsto \rho\mathfrak{I}(\rho, I).$$

Notice moreover that it was shown in [174] that the notions of Supply and Demand functions defined in [164] for the classical LWR model could be extended to the GSOM family. The GSOM models admit two kinds of waves :

- Kinematic waves or 1-waves as in the seminal LWR model : a wave propagates density variations at speed $\nu_1 = \partial_\rho \mathfrak{F}(\rho, I)$ while the driver attribute I is continuous across such a wave.
- Contact discontinuities or 2-waves : a wave propagates variations of driver attribute I at speed $\nu_2 = \mathfrak{I}(\rho, I)$ while the flow speed is constant across such a wave.

2.2 Examples

The GSOM family recovers a wide range of existing models :

- The LWR model [184, 221] itself is simply a GSOM model with no specific driver attribute, expressed as follows

$$\begin{cases} \partial_t \rho + \partial_x(\rho v) = 0 & \text{Conservation of vehicles,} \\ v = \mathfrak{I}(\rho, x) & \text{Fundamental diagram.} \end{cases} \tag{6.2.2}$$

  The fundamental diagram (FD) for the LWR model states that traffic flow is always at an equilibrium state. It is commonly assumed that the flow is an increasing function of density between zero (corresponding to an empty section) and a critical density and then the flow decreases until the maximal density (corresponding to a bumper-to-bumper situation). However the FD shape is always a subject of debates (see for instance [95]) and there exists a wide variety in the literature encompassing concave and triangular flow functions (see Figure 6.1 and also Chapter 3 of [106] for additional examples).

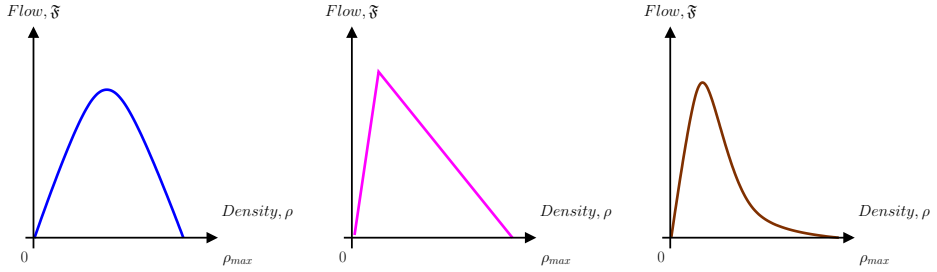

FIGURE 6.1 – Illustrations of some flow functions $\mathfrak{F}$ for the LWR model : Greenshields (left), triangular (center) and exponential (right).

- The LWR model with bounded acceleration proposed in [165, 166, 175] is also a GSOM model in which the propagated driver attribute is simply the speed of vehicles.
- The ARZ model (standing for Aw, Rascle [11] and Zhang [241]) for which the driver attribute is taken as $I = v - V_e(\rho)$ that is $\mathfrak{I}(\rho, I) = I + V_e(\rho)$.
- The Generalized ARZ model proposed in [94] that can be also seen as a particular case of the model described in [242]. These models introduce an interaction mechanism between two different FDs for distinguish equilibrium and non-equilibrium states.

- Multi-commodity models (multi-class, multi-lanes) of Jin and Zhang [143], Bagnerini and Rascle [12] or Herty, Kirchner, Moutari and Rascle [131]. It encompasses also the model of Klar, Greenberg and Rascle [150].
- The Colombo 1-phase model deduced in [174] from the 2-phase model of Colombo [61]. In this case, the driver attribute I is a scalar which is non-trivial in congested situation. In fluid area, the model follows the classical LWR model.
- The stochastic GSOM model of Khoshyaran and Lebacque [149]. The driver attribute I is a random variable depending on the vehicle index N and on the random event ω such that $I = I(N, t, \omega)$. The random perturbations do not affect the vehicle dynamics but affect the driver perception and its behavior.

The interested reader is referred to [172] and references therein for more details on examples.

3 Variational principles in traffic flow modeling

In traffic flow literature, the variational formulation was first conjectured by Newell in [199–201] for the LWR first-order traffic flow model. It was then properly established and generalized by Daganzo in [78–80]. In this section, we first present the variational formulation of the GSOM family lead by the ideas developed for the LWR model. Then the numerical methods for solving these variational formulations are introduced.

3.1 Variational formulation of the GSOM family

Guided by the ideas developed for the LWR model, variational formulations have been recently developed and proved for models of the GSOM family in both Eulerian [183] and Lagrangian frameworks [172].

Lagrangian setting

In [172], the authors prove the existence of a variational principle for the GSOM models family expressed under its Lagrangian form, introducing $r := 1/\rho$ the spacing and N the vehicle label

$$\begin{cases} \partial_t r + \partial_N v = 0 & \text{Conservation of vehicles,} \\ \partial_t I = \varphi(N, I, t) & \text{Dynamics of the driver attribute } I, \\ v = \mathcal{V}(r, I) = \mathfrak{I}(1/r, I) & \text{Fundamental diagram.} \end{cases} \tag{6.3.3}$$

Remark 3.1 (Vehicle labeling)**.** *Note that vehicles are labeled in the classical traffic sense, according to their passing time through a reference spatial point. Thus, the label axis is in the opposite sense that the spatial axis.*

Considering the position $\mathcal{X}(N, t) = \int_{-\infty}^{t} v(N, \tau) d\tau$, we obviously have that

$$v = \partial_t \mathcal{X} \quad \text{and} \quad r = -\partial_N \mathcal{X}. \tag{6.3.4}$$

Hence the system (6.3.3) could be written as a Hamilton-Jacobi equation satisfied by $\mathcal{X}$:

$$\partial_t \mathcal{X} - \mathcal{W}(N, -\partial_N \mathcal{X}, t) = 0, \tag{6.3.5}$$

where $\mathcal{W}$ denotes the speed-spacing fundamental diagram of vehicle N at time t. It is defined such that

$$\mathcal{W}(N, r, t) := \mathcal{V}(r, I(N, t)) = \mathfrak{I}(1/r, I(N, t)),$$

where the driver attribute $I(N,t)$ solves the following nonlinear first order ODE

$$\left|\begin{array}{ll} \partial_t I(N,t) = \varphi(N,I,t), & \\ I(N,0) = i_0(N), & \text{for any} \quad N. \end{array}\right.$$

By classical results on optimal control problems i.e. dynamic programming on Hamilton-Jacobi-Bellman equations, we can check that :

$$\begin{aligned} \mathcal{X}(N_T,T) = \min_{u,(N_0,t_0)} & \int_{t_0}^{T} \mathcal{M}(N,u,t)dt + \xi(N_0,t_0), \\ & \left|\begin{array}{l} \dot{N} = u \\ N(t_0) = N_0, \quad N(T) = N_T \\ (N_0,t_0) \in \mathcal{J} \end{array}\right. \end{aligned} \tag{6.3.6}$$

where $\mathcal{M}$ is the Legendre-Fenchel transform of $\mathcal{W}$ according to its second variable (see Figure 6.2 for an illustration of the Legendre-Fenchel transform), defined such that

$$\mathcal{M}(N,u,t) = \sup_{r\in\mathbb{R}} \{\mathcal{W}(N,r,t) - ur\}. \tag{6.3.7}$$

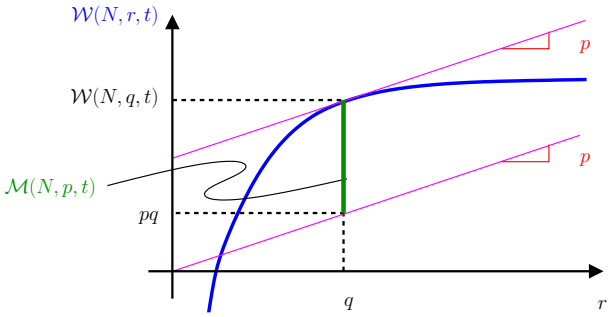

FIGURE 6.2 – Legendre transform $\mathcal{M}$ of function $\mathcal{W}$.

Notice that the variational formulation of GSOM models (6.3.6) is only available if and only if $r \mapsto \mathcal{W}(N,r,t)$ is concave such that the Legendre-Fenchel transform of $\mathcal{M}$ gives back the function $\mathcal{W}$.

In the previous formulation (6.3.6), $\mathcal{J}$ is the locus of initial and boundary conditions and $\xi(N_0,t_0)$ is the initial data of the position of vehicle N_0 at time t_0 for any $(N_0,t_0) \in \mathcal{J}$.

The optimal trajectories are given by the characteristics (Eulerian and Lagrangian characteristics are equal) described by the following coupled ODEs

$$\begin{cases} \dot{N} = \partial_r \mathcal{W}(N,r,t), \\ \dot{r} = -\partial_N \mathcal{W}(N,r,t), \end{cases} \tag{6.3.8}$$

where $u = \dot{N}$ is the command of the optimal control problem (6.3.6). The system (6.3.8) is a simple system of ODEs in the (N,r) plane.

Eulerian setting

In [183], the authors prove the existence of a variational formulation of a class of models from the GSOM family. Unlike the paper of Lebacque and Khoshyaran [172], these models are expressed from the Eulerian viewpoint as a system of two conservation laws

$$\begin{cases} \partial_t \rho + \partial_x f(\rho,s) = 0 & \text{Conservation of vehicles,} \\ \partial_t s + \partial_x g(\rho,s) = 0 & \text{Dynamics around the equilibrium.} \end{cases} \tag{6.3.9}$$

The first conservation law is obviously satisfied by the vehicle density ρ and the corresponding flux f is the product of density times speed $f(\rho, v) = \rho v$. The second conservation law is satisfied by a variable s (a non-equilibrium measure) which can be replaced by $s = \rho I$ yielding the GSOM family without source terms $\varphi(I) = 0$. The corresponding flux g needs to satisfy some specific conditions to ensure that the wave speed is less or equal to traffic speed.

The paper [183] highlights that taking $\varphi(I) = 0$ is equivalent to say that the driver attribute I is invariant along vehicle trajectories which seems to be corroborated for instance by the work of Duret *et al.* [87] on the NGSIM I-80 trajectories data-set (in congested situation). For the models (6.3.9), the authors show in [183] a variational formulation based on Lax-Hopf like formulas for both N_ρ and N_s defined as the cumulative quantity of respectively ρ and s.

When taking into account a non trivial relaxation term ($\varphi(I) \neq 0$), the authors assume that the problem reduces to solving a LWR model in large time because the relaxation term induces an exponential decay in time of the difference between (6.3.9) and a regular LWR model (6.2.2).

Remark 3.2 (Variational formulations of the LWR model)**.** *The variational theory for the LWR relies on the three dimensional representation of traffic flow or the so-called Moskowitz function [186, 196] yielding Hamilton-Jacobi formulations in Eulerian and Lagrangian coordinates (see also [158] and references therein).*

Under suitable assumptions, the solutions to the HJ equations could be determined thanks to a variational formulation, known as Lax-Hopf formula in the mathematics literature [89]. There exist different methods to obtain the variational formulation of these problems, including calculus of variations, dynamic programming [78, 79] and viability theory [58, 123].

Notice that from a mathematical point of view it was rigorously established in [123] that the (viscosity) solutions of HJ equations in Eulerian and Lagrangian coordinates are strictly equivalent.

3.2 Computational methods for GSOM models

Lax-Hopf algorithms in LWR case

Up to our best knowledge, existing numerical procedures for data assimilation use the seminal paper [58] which proposes a semi-explicit form of the solution to Hamilton-Jacobi equations with concave flow-density fundamental diagrams and with any piecewise affine (PWA) initial and boundary conditions. They introduce a generalized Lax-Hopf formula and the inf-morphism property [8, 9] to compute the solution by taking the infimum of all solutions associated with simpler partial problems. It follows computational methods that are commonly referenced as "grid free" schemes [59, 190]. Unlike dynamic programming methods [79], Lax-Hopf algorithms have been proved to be exact in general cases of concave flow-density fundamental diagrams (i.e. for convex Hamiltonians) [58]. Some elements of comparison are given in [190] between dynamic programming, Lax-Hopf algorithm and more classical methods such as Godunov scheme [77, 164] and wave tracking algorithm [128, 134].

The Lax-Hopf algorithm has been extended to the Lagrangian version of the LWR problem in [123] for a triangular flow-density FD and for piecewise affine initial and boundary conditions.

Review of computational methods for GSOM models

There already exists some works on computational methods for models of the GSOM family [183,188,220]. However these existing methods are developed in the Eulerian framework which does not seem to be the best one to deal with Lagrangian data. Moreover the paper [220] deals with the LWR model with bounded acceleration which is a very specific GSOM model. The algorithm is very similar to the ones developed in [59, 190] but it is not applicable to general models of the GSOM family.

In [183] the authors present a numerical scheme that is based on a discretization of Eulerian time and space domain. The idea of the scheme (close to dynamic programming) is then to update the cumulative quantities

$$N_\rho := \int_x^{+\infty} \rho(y,t)dy \quad \text{and} \quad N_s := \int_x^{+\infty} s(y,t)dy,$$

on the vertexes of a mesh (whatever its shape if this mesh is dense enough) following the optimal paths in an iterative way because of the coupling of the equations to solve. The values of ρ (resp. s) are deduced from a first order approximation of the derivative of N_ρ (resp. N_s). Notice that this computational method is not exact in general.

A finite difference scheme

A numerical scheme based on a uniform grid of the Lagrangian domain with steps Δt and Δn, was presented in [172].

We define for any n, $t \geq 0$

$$\mathcal{X}_n^t := \mathcal{X}(n\Delta n, t\delta t).$$

As usual with finite difference scheme, we need to introduce a Courant-Friedrichs-Lewy (CFL) condition [70] to ensure the scheme to be monotone and convergent

$$\frac{\Delta n}{\Delta t} \geq \sup_{N,r,t} \left|\partial_r \mathcal{W}\left(N,r,t\right)\right|.$$

Then we consider the classical first order finite difference scheme as follows

$$\mathcal{X}_n^{t+1} = \mathcal{X}_n^t + \Delta t\ \mathcal{W}\left(n\Delta n, \frac{\mathcal{X}_{n-1}^t - \mathcal{X}_n^t}{\Delta n}, t\Delta t\right). \tag{6.3.10}$$

By construction the above scheme can be interpreted as the seminal Godunov (finite volume) scheme (6.3.11) for the Lagrangian formulation of the GSOM model (see [69])

$$r_n^{t+1} = r_n^t + \frac{\Delta t}{\Delta n}\left[\mathcal{W}_{n-1}^t - \mathcal{W}_n^t\right], \tag{6.3.11}$$

where we have defined the discrete spacing and respectively the numerical speed as follows

$$\begin{cases} r_n^t := \dfrac{\mathcal{X}_{n-1}^t - \mathcal{X}_n^t}{\Delta n}, \\ \\ \mathcal{W}_n^t := \mathcal{W}\left(n\Delta n, r_n^t, t\Delta t\right). \end{cases}$$

The upstream and downstream boundary conditions for the finite difference scheme (6.3.10) are fully described in [172]. They match the Bardos-LeRoux-Nédélec [18] or Dubois-LeFloch [86] boundary conditions and it was already shown that such conditions are

equivalent to prescribe supply and demand conditions (see [172] and references therein).

Up to our best knowledge, there is no other existing work on computational methods for models of the GSOM family in the Lagrangian framework. The method of finite differences does not enjoy the semi-analytical expression of the solution of the HJ equation (6.3.5) thanks to Lax-Hopf formula (6.3.6). In the next section, we provide a semi-analytical algorithm to compute the solution based on that representation formula.

4 A "grid free" scheme

We are now interested in numerical methods to efficiently recover the solution of the Hamilton-Jacobi problem (6.3.5). The computation of numerical solutions of the HJ equation has already attracted an important interest in the mathematical community. The majority of numerical schemes which were proposed to solve HJ equations are based on finite difference methods, Semi-Lagrangian schemes and discontinuous Galerkin methods (the interested reader is referred to [59, 69] and references therein).

4.1 Computational strategy

The idea to compute the solution of the Eulerian GSOM model (6.2.1) is to recast it under its Lagrangian form (6.3.3). As it was shown in the previous section, the position $\mathcal{X}$ of vehicle N at time t solves the Hamilton-Jacobi equation (6.3.5). As explained in [172], the HJ equation (6.3.5) admits a quite simple representation formula (6.3.6), very similar to the Hopf-Lax formula presented for the LWR model.

The Hopf-Lax formula (6.3.6) can be simplified because it is well-known from optimal control theory, that the optimal trajectories for which the minimum is attained are the characteristics (6.3.8). Hence we have to solve the following system of coupled ODEs (6.3.8). Then the generalized Hopf-Lax formulation (6.3.6) can be recast as follows

$$\begin{aligned} \mathcal{X}(N_T,T) = \min_{(N_0,r_0,t_0)} & \int_{t_0}^{T} \mathcal{M}(N,\partial_r\mathcal{W}(N,r,t),t)dt + \xi(N_0,t_0), \\ & \left| \begin{array}{l} \dot{N}(t) = \partial_r\mathcal{W}(N,r,t) \\ \dot{r}(t) = -\partial_N\mathcal{W}(N,r,t) \\ N(t_0) = N_0, \quad r(t_0) = r_0, \quad N(T) = N_T \\ (N_0,r_0,t_0) \in \mathcal{K} \end{array} \right. \end{aligned} \tag{6.4.12}$$

where $\mathcal{K}$ is the set of initial/boundary values obtained by combining the initial values of $\mathcal{J}$ with the initial/boundary value r_0 deduced from the initial values $\xi(N_0,t_0)$.

According to the principle of inf-morphism property [8,9,58,59], if the initial/boundary condition data ξ are located on a union (non necessarily disjoint) of sets

$$\mathcal{K} = \bigcup_l \mathcal{K}_l,$$

it suffices to solve partial problems on each set $\mathcal{K}_l$ and to compute the minimum of the solutions to these sub-problems

$$\mathcal{X}(N_T,T) = \min_l \mathcal{X}_l(N_T,T), \tag{6.4.13}$$

with

$$\mathcal{X}_l(N_T,T) := \min_{(N_0,r_0,t_0)} \int_{t_0}^{T} \mathcal{M}(N_l,\partial_r\mathcal{W}(N_l,r_l,t),t)dt + \xi(N_0,t_0). \\ \left| \begin{array}{l} \dot{N}_l(t) = \partial_r\mathcal{W}(N_l,r_l,t) \\ \dot{r}_l(t) = -\partial_N\mathcal{W}(N_l,r_l,t) \\ N_l(t_0) = N_0, \quad r_l(t_0) = r_0, \quad N_l(T) = N_T \\ (N_0,r_0,t_0) \in \mathcal{K}_l \end{array} \right. \tag{6.4.14}$$

In the remaining of this article, we will apply the inf-morphism property by considering initial and boundary conditions which are piecewise affine (PWA). Thus we will calculate the solution generated by each piece using (6.4.14) and then apply (6.4.13) in order to obtain the solution of (6.3.6).

4.2 Algorithm for piecewise affine value conditions

Hereafter, we study separately the different elements which contribute to the value of the solution of (6.3.5) in its Lagrangian setting. We distinguish

- the initial condition at time $t = t_0$ describing the initial position of vehicles $\xi(N, t_0)$ for any considered N,
- the "upstream" boundary condition that is the trajectory of the first vehicle $N = N_0$ traveling on the section $\xi(N_0, t)$ for any considered t,
- and internal boundary conditions given for instance by cumulative vehicle counts at fixed location $\mathcal{X} = x_0$.

Note that Lagrangian data which are individual vehicle trajectories are considered as a particular case of "upstream" boundary condition for a given $N \geq N_0$ (see Remark 4.4).

While the Lax-Hopf algorithm can handle infinite horizon problems either in the Eulerian or in the Lagrangian framework, we restrict ourselves to finite values for a convenient numerical implementation. Without loss of generality, we assume that $N \in [N_0, N_{max}]$ with $N_{max} < +\infty$ and similarly $t \in [t_0, t_{max}]$ with $t_{max} < +\infty$.

We recall that according to Remark 3.1, in all the following figures, the N-axis and x-axis are increasing in opposite directions. Hence, the highest labels actually match vehicles that are located further upstream.

Initial conditions

In this case, at $t = t_0$, the positions $\xi(n, t_0)$ of vehicles n are given. We have that

$$r_0(N) = -\partial_N\xi(N, t_0), \quad \text{for any} \quad N.$$

The initial conditions for the characteristics are the couples $(N, r_0(N))$.

First, we need to discretize the set of vehicle labels into intervals $[n_p, n_{p+1}]$ of length Δn, for $p = 1, ..., P$, with the additional convention

$$n_1 := N_0 \quad \text{and} \quad n_{P+1} := N_{max},$$

in such a way that the dynamics φ of the driver attribute I can be approximated by φ_p in the interval $[n_p, n_{p+1}]$

$$\varphi(N, I, t) = \varphi_p(I, t), \quad \text{for any} \quad N \in [n_p, n_{p+1}].$$

If the discrete step Δn is small enough, we could also assume that the initial data are piecewise constant, say

$$\begin{cases} I(N,t_0) = I_{0,p}, \\ r(N,t_0) = r_{0,p}. \end{cases} \quad , \quad \text{for any} \quad N \in [n_p, n_{p+1}],$$

or equivalently we define

$$\begin{cases} I_{0,p} := \dfrac{1}{\Delta n}\displaystyle\int_{n_p}^{n_{p+1}} I(N,t_0)dN, \\ r_{0,p} := \dfrac{1}{\Delta n}\displaystyle\int_{n_p}^{n_{p+1}} r(N,t_0)dN, \end{cases} \quad , \quad \text{for any} \quad p = 1, ..., P.$$

We will now first define properly the initial condition and then we calculate the solution generated by the p^{th} component $(p = 1, ..., P)$.

Definition 6 (PWA initial condition)**.**
Let $t_0 \geq 0$ be fixed. Then the p^{th} component of the initial condition $(p = 1, ..., P)$ is given by

$$\mathcal{X}^{ini}(N,t_0) = r_{0,p}\,(N - n_p) + \alpha_p, \quad \textit{for any} \quad N \in [n_p, n_{p+1}].$$

Without loss of generality, we state that

$$\alpha_1 = \mathcal{X}^{ini}(N_0,t_0) = 0.$$

To ensure continuity of the initial data $\mathcal{X}^{ini}$ on $[N_0, N_{max}]$, we require that

$$\alpha_p = \sum_{l=1}^{p-1} r_{0,l}\Delta n, \quad \textit{for any} \quad p = 2, ..., P.$$

In a first step, we want to compute the characteristics generated by the initial conditions ($I(N,t_0) = i_{0,p}$ and $r(N,t_0) = r_{0,p}$ given on the interval $[n_p, n_{p+1}]$ at time t_0). In the general case, we would have

$$I(N,t) = I_p(t) \quad \text{for any} \quad N \in [n_p, n_{p+1}].$$

In the following, we consider a characteristic denoted by $N(t)$ for $t \in [t_0, t_{max}]$ and we distinguish two cases according to the location of this characteristic.

On the interval $\mathbf{N} \in]\mathbf{n_p}, \mathbf{n_{p+1}}[$.
Consider $\Omega_p := \{t \mid N(t) \in]n_p, n_{p+1}[\}$ for any $p = 1, ..., P$. We then have to solve the following nonlinear first order ODE

$$\begin{cases} \dot{I}_p(t) = \varphi_p(I_p(t)), \quad \text{for} \quad t \in \Omega_p, \\ I_p(t_0) = I_{0,p}. \end{cases}$$

On the interval $]n_p, n_{p+1}[$, we have that $I(N,t) = I_p(t)$ is independent of N i.e. $\partial_N I = 0$. Then from (6.3.8), we deduce

$$\begin{aligned} \dot{r} &= -\partial_N \mathcal{W}(N,r,t) \\ &= -\partial_I \mathcal{V}(N, I(N,t))\ \partial_N I(N,t) \\ &= 0. \end{aligned}$$

Thus $r(N,t)$ is constant along any characteristic in Ω_p. Hence it simply suffices to solve the second ODE in (6.3.8) that is

$$\dot{N} = \partial_r \mathcal{W}(N,r,t)$$

to get the equation of the characteristic on the interval $]n_p, n_{p+1}[$. We finally get

$$N(t) = \int_u^t \partial_r \mathcal{W}(N, r, \tau) d\tau + N(u), \quad \text{for any} \quad t, u \in \Omega_p. \tag{6.4.15}$$

To considerably simplify the presentation, we will restrict ourselves to the case of systems with no relaxation that is the dynamics of driver attributes $\varphi_p(I, t) = 0$ at any time $t \geq t_0$ and for any interval $[n_p, n_{p+1}]$ with $p = 1, ..., P$.

If we assume that the dynamics is null, then it obviously follows that $\dot{I}_p = 0$ which leads to

$$I_p(t) = I_{0,p} \quad \text{for any} \quad t \in \Omega_p. \tag{6.4.16}$$

In traffic modeling, this choice is relevant if the driver attribute I represents for example some origin-destination (OD) information or if it characterizes the vehicle kind. The driver attribute is conserved at any time and along any characteristic inside each "strip" $[n_p, n_{p+1}] \times [t_0, t_{max}]$ of width Δn.

By the way, the simplification (6.4.16) allows to consider characteristics which are straight lines while there are not in the general case.

At the edge $\mathbf{N = n_p}$.

The edge $N = n_p$ separates two different traffic states that exhibit two different speed-spacing fundamental diagrams. We need to take care of the kinematic waves that can appear at this locus. As illustrated on Figure 6.3, we set the characteristic speed related to the spacing $r_{0,p}$ as follows

$$\nu_p := \partial_r \mathcal{V}\left(r_{0,p}, I_{0,p}\right),$$

and we also define the speed of the "refracted" characteristic wave through the discontinuity of I such that

$$\nu_p^* := \partial_r \mathcal{V}\left(r_{0,p}^*, I_{0,p}\right). \tag{6.4.17}$$

This characteristic speed is related to a new spacing value $r_{0,p}^*$ defined as follows

$$r_{0,p}^* = \begin{cases} \mathcal{V}^{-1}\left(\mathcal{V}\left(r_{0,p-1}, I_{0,p-1}\right), I_{0,p}\right) & \text{if} \quad \mathcal{V}\left(r_{0,p-1}, I_{0,p-1}\right) < \sup\limits_{r \in \mathbb{R}} \mathcal{V}\left(r, I_{0,p}\right), \\ +\infty & \text{else.} \end{cases} \tag{6.4.18}$$

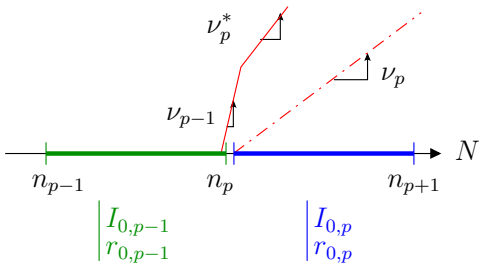

FIGURE 6.3 – Schematic view of what happens for the characteristic wave generated from the edge $N = n_p$ and passing through a discontinuity of I.

Remark 4.1 (Transported spacing value along a characteristic)**.**
We extend the idea of what happens at each discontinuity of I by introducing a function

$$\tau : (r_{0,p}, q) \mapsto r_{0,p}^q \tag{6.4.19}$$

that maps a given (initial) spacing $r_{0,p}$ *to its projection* $r^q_{0,p}$ *(which is the spacing value transported along the corresponding characteristic) in a strip* $[n_q, n_{q+1}] \times [t_0, t_{max}]$*, with any* $q \geq p$ *and* $p \in \{1, ..., P\}$*. The transported value can be computed thanks to a recursive composition of function* τ *on consecutive strips*

$$r^p_{0,q} := \tau\left(r_{0,p}, q\right) = \tau\left(\tau\left(\ldots\tau\left(r_{0,p}, p+1\right), \ldots, q-1\right), q\right),$$

where $r^{p+1}_{0,p} := \tau\left(r_{0,p}, p+1\right) = r^*_{0,p+1}$ *can be easily computed according to (6.4.18), for any* $p \in \{1, ..., P\}$*. Indeed, the speed is conserved through a discontinuity of* I *i.e.*

$$\mathcal{V}\left(r^q_{0,p}, I_{0,q}\right) = \mathcal{V}\left(r^{q+1}_{0,p}, I_{0,q+1}\right), \quad \textit{for any} \quad q \geq p.$$

Obviously we also have that $r^p_{0,p} := \tau\left(r_{0,p}, p\right) = r_{0,p}$*.*

Regarding the values of the initial spacing $r_{0,p}$ and $r_{0,p-1}$, we can distinguish two cases that could occur starting to an edge $N = n_p$:

- either $\nu^*_p > \nu_p$ and in this case there will be a shock wave. The characteristics carrying respectively the initial states $r_{0,p-1}$ and $r_{0,p}$ will cross each other, offering a partial superposition of both characteristics domains (see (a) on Figure 6.4). The solution is then simply computed thanks to the inf-morphism property. Hence we only consider the two characteristics (indicated as ① and ② on Figures 6.6, 6.7 and 6.9) that encompass the domain of influence generated by the initial spacing $r_{0,p}$.

- or $\nu^*_p < \nu_p$ and in this case there will be a rarefaction fan. The characteristics waves carrying the initial states $r_{0,p-1}$ and $r_{0,p}$ diverge (see (b) on Figure 6.4). The solution on the area between both extreme characteristics may not be computed and even the inf-morphism property will not be able to recover it. That is why we need to consider the first two characteristics (as above) and a third wave corresponding to the first characteristic matching with the initial state $r_{0,p-1}$ (labeled ⓪ on Figures 6.6, 6.7 and 6.9).

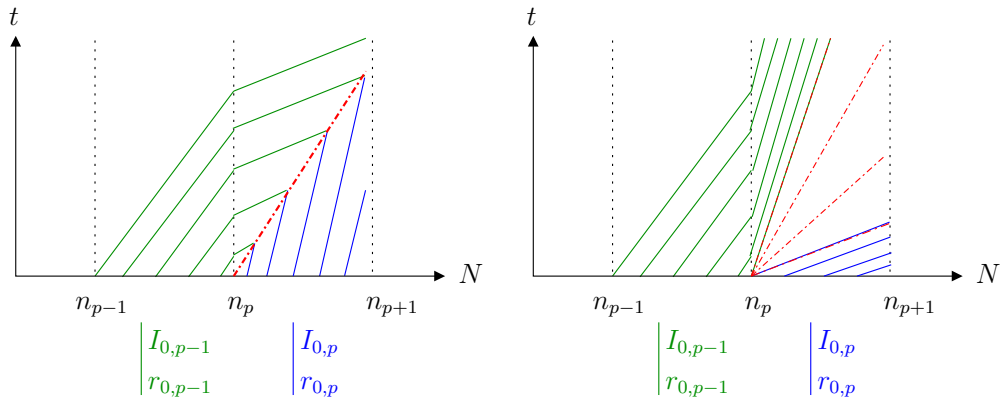

(a) Case of a shock wave (b) Case of a rarefaction fan

FIGURE 6.4 – Characteristics through a discontinuity of I of r.

Notice that by convention, for a given $p = 1, ..., P$, we add the rarefaction wave ⓪ separating the two states at $N = n_p$ (if any) to the solution generated by the initial condition on $[n_p, n_{p+1}]$.

Remark 4.2 (Degenerate case for characteristics through a discontinuity of I)**.**
When passing through a discontinuity of I (assume (a) and (b) the states on both sides of the discontinuity as illustrated on Figure 6.5), the characteristics speed may be changed. Nevertheless it is well known (Rankine-Hugoniot jump condition) that through such a discontinuity, the traffic speed should be unmodified

$$v^{(a)} := \mathcal{V}(r^{(a)}, I^{(a)}) = \mathcal{V}(r^{(b)}, I^{(b)}) =: v^{(b)}.$$

In case of $v^{(a)} > v_{max}^{(b)} := \sup_{r\in\mathbb{R}} \mathcal{V}(r, I^{(b)})$, it is obvious that the equality between these two speeds cannot be complied. In an Eulerian setting, it means that the group of upstream vehicles (b) cannot accelerate enough (even increasing their speeds to $v_{max}^{(b)}$) to catch up with the downstream vehicles (a). This induces the apparition of a vacuum area between both groups of vehicles. There is a rarefaction wave as vehicles (b) accelerate to attain their top speed and a shock wave following the last vehicle of type (a).

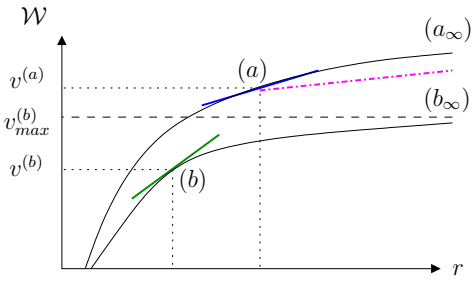

(a) Speed-spacing fundamental diagram

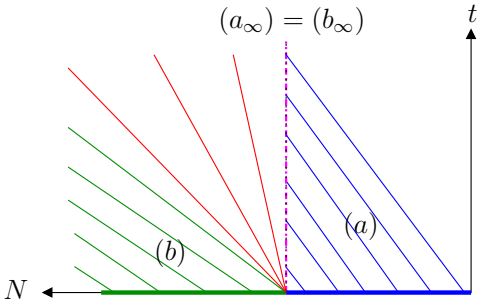

(b) Some characteristics in Lagrangian viewpoint

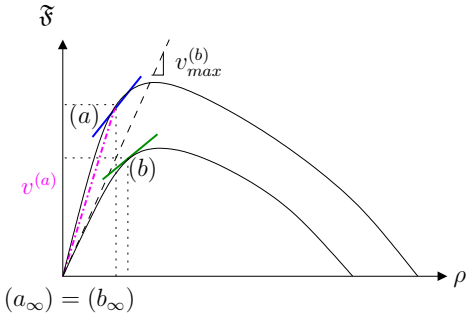

(c) Flow-density fundamental diagram

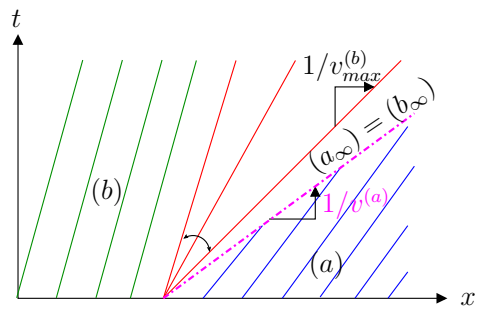

(d) Some characteristics in Eulerian viewpoint

FIGURE 6.5 – Critical "vacuum" case appearing from special condition values.

Notice that the vacuum *states (a_∞) and (b_∞) defined on Figure 6.5 coincide for $r = +\infty$ (or equivalently at $\rho = 0$). It is noteworthy that the vacuum area is not visible in Lagrangian viewpoint (see Figure 6.5 (b)) while it matches the rarefaction fan and characteristics of type (a) in Eulerian viewpoint (see the area delimited by characteristic with speed $v_{max}^{(b)}$ and dash-dotted characteristic with speed $v^{(a)}$ on Figure 6.5 (d)).*

Remark 4.3 (Some examples of functions φ_p)**.** *It is possible to consider a non-zero source term $\varphi_p \neq 0$. Below are some examples describing how to compute the value of I_p.*
Example 1 : case of φ_p constant for any $p \in \mathbb{Z}$
Assume that $\varphi_p = C_p$. Then it follows that

$$I_p(t) = C_p t + I_{0,p} \quad \text{for any} \quad t \in \Omega_p.$$

Example 2 : case of φ_p linear for any $p \in \mathbb{Z}$
Let p be fixed. Assume that $\varphi_p(I) = A_p.(I - I_{ref,p})$ where A_p is a diagonalizable matrix with non negative eigenvalues. This dynamics represents a relaxation phenomenon of the driver attribute I towards a reference value $I_{ref,p}$. In this case, we obtain

$$I_p(t) = (I_{0,p} - I_{ref,p})e^{A.(t-t_0)} + I_{ref,p}, \quad \text{for any} \quad t \in \Omega_p.$$

Notice that one can consider for example $\varphi_p(I) = -\dfrac{I}{\tau}$ where τ is a relaxation time. Then we have

$$I_p(t) = I_{0,p}e^{-\frac{t}{\tau}},$$

which means that the mean variations in initial data of I are dampened out exponentially fast.

The contribution $\mathcal{X}_p$ of the initial condition defined on $[n_p, n_{p+1}] \times \{t_0\}$ for any $p \in \{1, ..., P\}$ is then computed as follows :

(i) Initialize the partial solution $\mathcal{X}_p$ at $+\infty$ on the whole computational domain $[N_0, N_{max}] \times [t_0, t_{max}]$.

(ii) Determine the number of characteristics to compute (two or three) according to what could occur at the edge $N = n_p$.

(iii) Compute the equation $N(t)$ of each characteristic while $t \leq t_{max}$ and $N \leq N_{max}$.

(iv) Calculate the (exact) solution $\mathcal{X}_p$ all along each computed characteristic generated by the interval $[n_p, n_{p+1}] \times \{t_0\}$, namely characteristics ① and ②, and ⓪ whenever it appears (see Figure 6.6). To this aim, we use the generalized Lax-Hopf formula (6.4.14) which gives that

$$\dot{\mathcal{X}}_p(t) = \mathcal{M}\left(N(t), \dot{N}(t), t\right).$$

The interested reader is referred to [35, 63, 185] for additional information about the Legendre-Fenchel transform and fast algorithms for its numerical computation.

(v) Compute the exact value at any point within the characteristics strip (delimited by characteristics ① and ② on Figure 6.6) using the fact that for any point (N, t) belonging to the characteristic strip, the position at this point can be deduced by a simple translation of the position on characteristic ① (see Figure 6.6). Indeed we have for any $N \in [n_q, n_{q+1}]$ with $q \geq p$ and any $t \in \left[t_N^{(2)}, t_N^{(1)}\right]$

$$\begin{aligned} \mathcal{X}_p(N,t) &= \mathcal{X}_p\left(N, t_N^{(1)}\right) + \int_{t_N^{(1)}}^{t} \mathcal{V}\left(r(N,\tau), I(N,\tau)\right) d\tau \\ &= \mathcal{X}_p\left(N, t_N^{(1)}\right) + \mathcal{V}\left(r_{0,p}^q, I_{0,q}\right)\left(t - t_N^{(1)}\right), \end{aligned} \tag{6.4.20}$$

where we recall that $\varphi_p(I, t) = 0$ for any couple (I, t) and $r_{0,p}^q$ is computed according to (6.4.19). The time $t_N^{(i)}$, $i = 1, 2$ corresponds to the time when the characteristic ① crosses the line $\{N\} \times [t_0, t_{max}]$.

(vi) In the case of a rarefaction fan, evaluate the value of $\mathcal{X}_p$ at each point within the influence domain of the considered initial condition (illustrated on Figure 6.6) by an interpolation technique based on triangular meshes (the value at each triangle vertex is exact).

Algorithm 1 Pseudo-code for the computation of $\mathcal{X}_p$ on the computational domain $[N_0, N_{max}] \times [t_0, t_{max}]$, under the initial condition $\mathcal{X}^{ini}$.

Input: N_0, N_{max}, t_0, t_{max}, Δn, N_p and $r_{0,p}$ {Input label domain, time domain and initial condition}

$\mathcal{X}_p \leftarrow +\infty$ {Initialization of the position function to infinity}
Compute μ_p^* and $r_{0,p}^*$ according to (6.4.17)-(6.4.18)
if $\mu_p^* > \mu_p$ **then** {Determination of the number of characteristic curves to compute}
    $n_{charac} = 2$
else
    $n_{charac} = 3$
end if
for $j = 1$ to n_{charac} **do** {Iteration on the characteristics}
    for $t = t_0$ to t_{max} **do** {Iteration on time}
        Compute $N^{(j)}(t)$ using (6.4.15) {Computation of the characteristic equation}
        Compute $\mathcal{X}_p(N^{(j)}(t), t)$ using (6.4.14) {Computation of the position along the characteristic}
    end for
end for
for $N = N_p$ to N_{max} **do** {Iteration on greater labels}
    for $t = t_N^{(2)}$ to $t_N^{(1)}$ **do** {Iteration on time}
        Compute $\mathcal{X}(N, t)$ using (6.4.20) {Computation of the position within the characteristics strip}
    end for
end for
if $n_{charac} = 3$ **then** {Case of the rarefaction fan}
    for $N = N_p$ to N_{max} **do** {Iteration on greater labels}
        for $t = t_N^{(1)}$ to $t_N^{(0)}$ **do** {Iteration on time}
            Compute $\mathcal{X}(N, t)$ using interpolation on the three closest exact values {Computation of the position within the rarefaction fan}
        end for
    end for
end if

Output: $\mathcal{X}_p(.,.)$ over $[N_0, N_{max}] \times [t_0, t_{max}]$

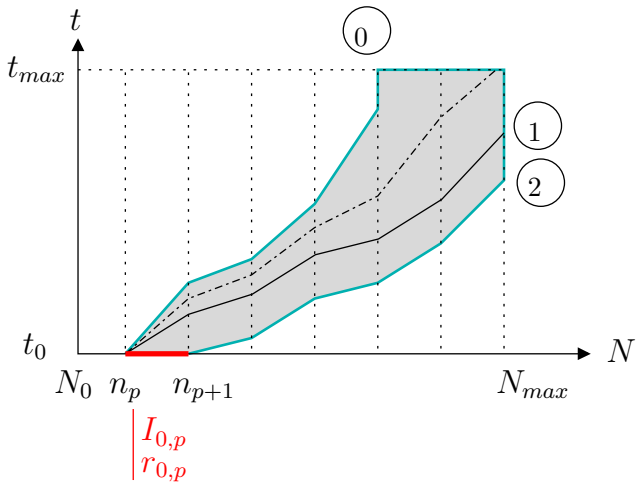

FIGURE 6.6 – Domain of influence of the initial data $[n_p, n_{p+1}] \times \{t_0\}$.

"Upstream" boundary conditions

In the Lagrangian setting, boundary conditions describe floating vehicle conditions in Eulerian setting. Indeed such a condition is equivalent to consider the trajectory $t \mapsto \xi(N_0, t)$ of a given vehicle N_0. Then we have that

$$v_0(t) := \partial_t \xi(N_0, t) = \mathcal{V}(r_0(N_0, t), I(N_0, t)), \quad \text{for any} \quad t \geq t_0,$$

which can be solved and yields a unique solution (because $\mathcal{V}$ is strictly increasing)

$$r_0(t) = \mathcal{V}^{-1}(v_0(t), I(N_0, t)), \quad \text{for any} \quad t \geq t_0.$$

The initial conditions for the characteristics are the couples $(N_0, r_0(t))$.

As for initial condition, we introduce a discrete time step Δt and we consider a full discretization of the time domain $[t_0, t_{max}]$ into segments $[t_q, t_{q+1}]$ of length Δt with $q = 1, ..., Q$. We have by convention

$$t_{q=1} := t_0 \quad \text{and} \quad t_{Q+1} := t_{max}.$$

We still consider that $I(N, t)$ is piecewise constant w.r.t. N and constant w.r.t. time t ($\varphi = 0$) such that $I(N_0, t) = I_{0,p=1}$. If Δt is small enough, we can consider that for any $q \in \{1, ..., Q\}$, we have

$$\begin{cases} v_0(t) =: v_{0,q}, \\ r_0(t) = \mathcal{V}^{-1}(v_{0,q}, I_{0,p=1}) =: r_{0,q}, \end{cases} \quad \text{for any} \quad t \in [t_q, t_{q+1}].$$

Definition 7 (PWA upstream boundary condition)**.**
Let $N_0 \in \mathbb{Z}$ be fixed. Then the q^{th} component of the upstream boundary condition ($q = 1, ..., Q$) is given by

$$\mathcal{X}^{up}(N_0, t) = v_{0,q}\,(t - t_q) + \beta_q, \quad \textit{for any} \quad t \in [t_q, t_{q+1}].$$

Without loss of generality, we set β_1 such that

$$\beta_1 := \mathcal{X}^{up}(N_0, t_0) = 0.$$

To ensure continuity of the upstream boundary data $\mathcal{X}^{ini}$ *on* $[t_0, t_{max}]$*, we require that*

$$\beta_q = \sum_{l=1}^{q-1} v_{0,l}\Delta t, \quad \textit{for any} \quad q = 2, ..., Q.$$

The contributions of upstream boundary conditions are computed in a similar way than those of initial condition described in the previous subsection. The domain of influence of upstream boundary conditions is simply separated into what happens on each interval $]t_q, t_{q+1}[$ and at the edge t_q for any $q \in \{1, ..., Q\}$ (see Figure 6.7).

It is worth noting that we have a rarefaction wave at $t = t_q$ for any $q \in \{1, ..., Q\}$ if and only if $v_{0,q-1} < v_{0,q}$ (or equivalently $r_{0,q-1} < r_{0,q}$). Note that in this case, the rarefaction wave denoted ⓪ separating the two states at $t = t_q$ (see Figure 6.7) is added by convention, to the solution computed from the boundary condition on $[t_q, t_{q+1}]$.

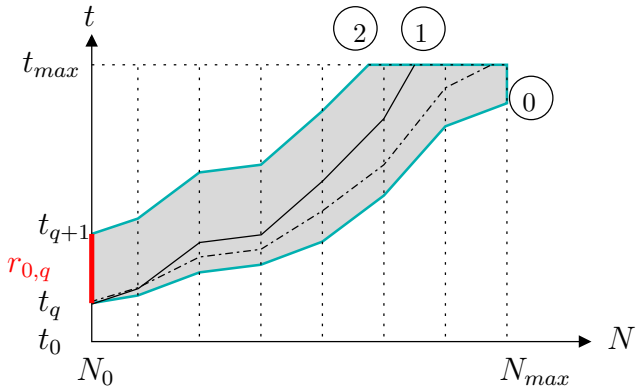

FIGURE 6.7 – Domain of influence of the upstream boundary data $\{N = N_0\} \times [t_q, t_{q+1}]$.

Remark 4.4 (Extension to any individual trajectory condition)**.** *Any Lagrangian data giving the trajectory of a vehicle* N^* *with* $N^* \in [N_0, N_{max}]$ *will strictly generate the same type of calculations than the ones described for the upstream boundary condition. It is then easy to deal with data coming from mobile sensors moving within the traffic stream.*

Internal boundary conditions

Note that *internal boundary condition* is here understood in the Lagrangian framework. It does not correspond to internal vehicle trajectories which can also be incorporated in the algorithm (see the previous subsection and Remark 4.4). Notice that internal boundary condition is called *mixed condition* in [172] to avoid any misunderstanding.

We assume that the data comes from vehicles $N(t)$ located at a point $\xi(N(t), t)$ at time t. Thus we get

$$\frac{d}{dt}\xi(N(t), t) = -\dot{N}(t)r_0(t) + \mathcal{W}(N(t), r_0(t), t). \tag{6.4.21}$$

As not all data are compatible (in the sense that they need to comply to the traffic dynamics laws), we need to introduce compatibility conditions. From Legendre-Fenchel transform, we have

$$\sup_{r\in\mathbb{R}} \Big\{ -\dot{N}(t)r + \mathcal{W}(N(t), r, t) \Big\} = \mathcal{M}(N(t), \dot{N}(t), t),$$

Algorithm 2 Pseudo-code for the computation of $\mathcal{X}_q$ on the computational domain $[N_0, N_{max}] \times [t_0, t_{max}]$, under the upstream boundary condition $\mathcal{X}^{up}$.

Input: N_0, N_{max}, t_0, t_{max}, Δt, t_q and $r_{0,q}$ {Input label domain, time domain and initial condition}

$\mathcal{X}_q \leftarrow +\infty$ {Initialization of the position function to infinity}
if $r_{0,q-1} > r_{0,q}$ **then** {Determination of the number of characteristic curves to compute}
    $n_{charac} = 2$
else
    $n_{charac} = 3$
end if
for $j = 1$ to n_{charac} **do** {Iteration on the characteristics}
    for $t = t_0$ to t_{max} **do** {Iteration on time}
        Compute $N^{(j)}(t)$ using (6.4.15) {Computation of the characteristic equation}
        Compute $\mathcal{X}_p(N^{(j)}(t), t)$ using (6.4.14) {Computation of the position along the characteristic}
    end for
end for
for $N = N_p$ to N_{max} **do** {Iteration on greater labels}
    for $t = t_N^{(1)}$ to $t_N^{(2)}$ **do** {Iteration on time}
        Compute $\mathcal{X}(N, t)$ using (6.4.20) {Computation of the position within the characteristics strip}
    end for
end for
if $n_{charac} = 3$ **then** {Case of the rarefaction fan}
    for $N = N_p$ to N_{max} **do** {Iteration on greater labels}
        for $t = t_N^{(0)}$ to $t_N^{(1)}$ **do** {Iteration on time}
            Compute $\mathcal{X}(N, t)$ using interpolation on the three closest exact values {Computation of the position within the rarefaction fan}
        end for
    end for
end if

Output: $\mathcal{X}_q(.,.)$ over $[N_0, N_{max}] \times [t_0, t_{max}]$

hence the equation yielding $r_0(t)$ (6.4.21) admits a solution only if

$$\frac{d}{dt}\xi(N(t),t) \leq \mathcal{M}(N(t),\dot{N}(t),t). \tag{6.4.22}$$

Let us describe the specific situation of $\dot{\xi}(t) = 0$ and $\dot{N}(t) \geq 0$ for any time t. This case occurs when the data originates at a fixed measurement point x_0 like a fixed detector data that is $\xi(N(t),t) = x_0$ for all time t. Then $N(t)$ represents the cumulative flow at point x_0. In this case the above compatibility condition (6.4.22) is satisfied if moreover we assume that $\dot{N} \leq \mathfrak{F}_{max}(I)$. It is quite natural to impose such a condition because $\dot{N}(t)$ is equal to the instantaneous traffic flow which is evidently bounded by $\mathfrak{F}_{max}(I)$ (see Figure 6.8). Moreover such a condition ensures that the Lagrangian stays non-negative which is coherent with its interpretation as a instantaneous speed cost.

As illustrated on Figure 6.8, there are two solutions (except in the very particular case of $\dot{N} = \mathfrak{F}_{max}$), one under-critical and the other over-critical according to classical traffic definitions. Recall that the speed-spacing fundamental diagram $\mathcal{W}$ depends on the vehicle N.

If we propagate both pairs of characteristics, then the inf-morphism property will automatically select a single solution which matches the over-critical situation (because the speed is lower than in the under-critical situation). It may happen that the congested solution is not the good one. Then to avoid any mistake, we assume that the fixed detector gives the cumulative flow and also the traffic flow speed. In this way, we can select one traffic state only.

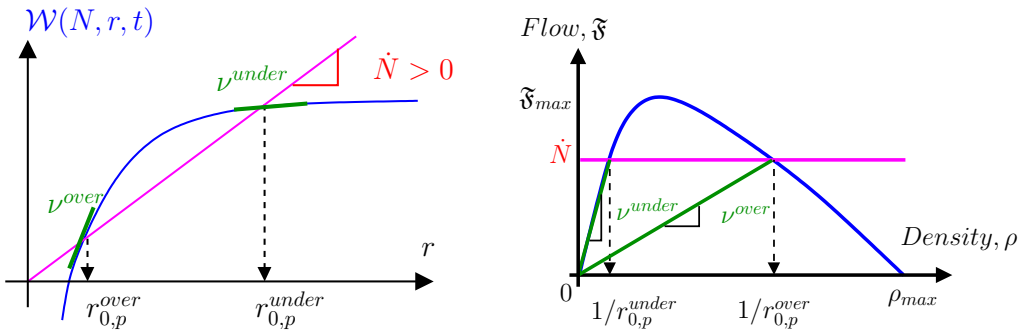

(a) Speed-spacing fundamental diagram (b) Flow-density fundamental diagram

FIGURE 6.8 – Existence of two solutions corresponding to a condition $\dot{\xi}(t) = 0$ and $\dot{N}(t) \geq 0$.

In our case, we are interested in including some Eulerian data coming from classical fixed sensors like inductive loop detectors. To achieve this aim, Eulerian data become internal boundary condition into the Lagrangian framework. We assume that a Eulerian sensor located at a fixed position x_0 gives us the incremental cumulative vehicle count which is then interpolated in a piecewise affine function $N(t)$ for $t \in [t_0, t_{max}]$. We then define by $\mathfrak{f}_{0,p}$ the value of $\dot{N}(t)$ for any $t \in [t_p, t_{p+1}]$ and we set $\hat{t}_p$ the time such that $N(\hat{t}_p) = N_p$ for any $p \in \{1, ..., P\}$.

Definition 8 (PWA internal boundary condition)**.**
Let $x_0 \geq 0$ be fixed. Then the p^{th} component of the internal boundary condition ($p = 1, ..., P$) is given by

$$\mathcal{X}^{int}(n,t) = x_0, \quad \textit{with} \quad \begin{cases} t = \mathfrak{f}_{0,p}\,(n - n_p) + \gamma_p, \\ n \in [n_p, n_{p+1}]. \end{cases}$$

Without loss of generality, we consider that $\gamma_1 = \hat{t}_1 \geq t_0$ *is given.*

To ensure continuity of the trajectory $t \mapsto n(t)$ *on which the internal boundary data* $\mathcal{X}^{int}$ *is prescribed, we require that*

$$\gamma_p = \gamma_1 + \sum_{l=1}^{p-1} \mathfrak{f}_{0,l}\ (n_{l+1} - n_l), \quad \textit{for any} \quad p = 2, ..., P.$$

We assume that N is piecewise affine on each discrete segments $[n_p, n_{p+1}]$ that is equivalent to say that $\dot{N}$ is piecewise constant (i.e. constant in each strip $[n_p, n_{p+1}] \times [t_0, t_{max}]$ for $p = 1, ..., P$). It is easy to deal with this case in the algorithm because the computational steps are similar to both previous cases for initial and upstream boundary conditions.

The only difference resides in the fact that we have a characteristic strip that matches either the under-critical or the over-critical traffic state. It is simple to verify that in the first (under-critical) case, the p^{th} component generates characteristics which are emitted with speeds $\nu^{under} > \dot{N}$ while it is the inverse in the other case (see Figure 6.9). From a traffic point of view, it is relevant with observations stating that a deceleration wave spreads over vehicles located further upstream at a slower speed than an acceleration wave.

Hence, from a computational viewpoint, if we are in the under-critical (resp. over-critical) case, then we will use the same strategy than Algorithm 1 (resp. Algorithm 2).

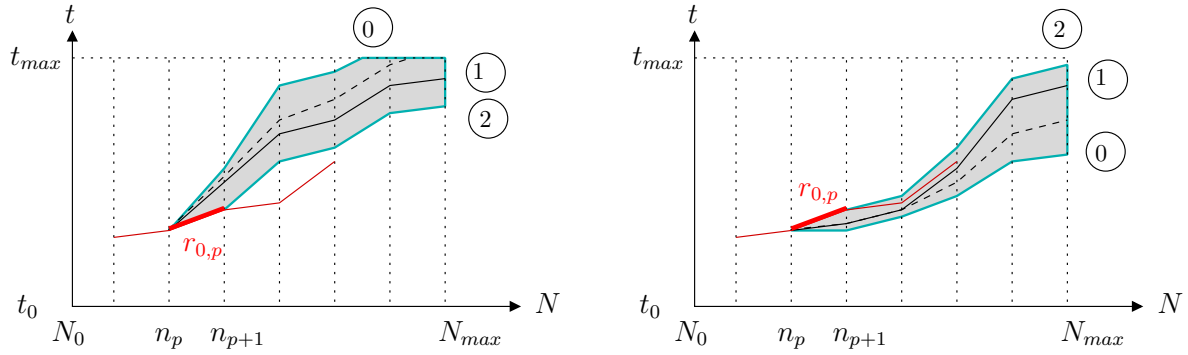

(a) Generation by the over-critical solution (b) Generation by the under-critical solution

FIGURE 6.9 – Domain of influence of an internal boundary data (in red).

4.3 Recapitulation of the overall algorithm

The different elements of the computations for piecewise affine value conditions are recapitulated in the following pseudo-code (see Algorithm 3).

Remark 4.5. *This pseudo-code underlines the property of the Lax-Hopf algorithm to treat in a parallel way the different value conditions (initial, upstream boundary and internal boundary).*

5 Numerical example

5.1 Instantiation

In order to simplify the computations and to ease the presentation of the following example, we consider that the driver attribute I is piecewise constant with respect to N

Algorithm 3 Pseudo-code implementation for the Lax-Hopf based computation of the position function $\mathcal{X}$ on the computational domain $[N_0, N_{max}] \times [t_0, t_{max}]$ prescribed by the user.

Input: N_0, N_{max}, t_0 and t_{max} {Input label domain, time domain}
$\mathcal{X} \leftarrow +\infty$ {Initialization of the position function to infinity}
for $p = 1$ to P **do** {Iteration on the initial conditions}
  for $T = t_0$ to t_{max} **do** {Iteration on time}
    for $N_T = N_p$ to N_{max} **do** {Iteration on greater labels}
      compute $\mathcal{X}_p^{ini}(N_T, T)$ using Algorithm 1 {Component induced by the initial condition $r_{0,p}$}
      if $\mathcal{X}_p^{ini}(N_T, T) < \mathcal{X}$ **then**
        $\mathcal{X} \leftarrow \mathcal{X}_p^{ini}(N_T, T)$ {Update the position function}
      end if
    end for
  end for
end for
for $q = 1$ to Q **do** {Iteration on upstream boundary conditions}
  for $T = t_q$ to t_{max} **do** {Iteration on greater times}
    for $N_T = N_0$ to N_{max} **do** {Iteration on labels}
      compute $\mathcal{X}_q^{up}(N_T, T)$ using Algorithm 2 {Component induced by the upstream boundary condition $\mathcal{X}N_0, t_q$}
      if $\mathcal{X}_q^{up}(N_T, T) < \mathcal{X}$ **then**
        $\mathcal{X} \leftarrow \mathcal{X}_q^{up}(N_T, T)$ {Update the position function}
      end if
    end for
  end for
end for
for $p = 1$ to P **do** {Iteration on internal boundary conditions}
  for $T = t_p$ to t_{max} **do** {Iteration on greater times}
    for $N_T = N_p$ to N_{max} **do** {Iteration on greater labels}
      compute $\mathcal{X}_p^{int}(N_T, T)$ {Component induced by the internal boundary condition $\mathcal{X}N_p, t_p$}
      if $\mathcal{X}_p^{int}(N_T, T) < \mathcal{X}$ **then**
        $\mathcal{X} \leftarrow \mathcal{X}_p^{int}(N_T, T)$ {Update the position function}
      end if
    end for
  end for
end for
Output: $\mathcal{X}(.,.)$ over $[N_0, N_{max}] \times [t_0, t_{max}]$

at initial time $t = t_0$. It means that there exist some platoons of vehicles which share the same driver attribute. It could be for example some vehicles of the same kind (cars and trucks), or vehicles that go to the same destination, or vehicles that have the same desired maximal speeds.

Actually, in this numerical example, we have considered a discrete step $\Delta n = 1$ for the initial condition so that the attribute I is constant for each vehicle. As $\varphi = 0$, this attribute is conserved at any time $t \geq t_0$ (see Figure 6.11 (left)).

We consider for this numerical example a Colombo 1-phase model [174] given by

$$\mathcal{W}(r, N, t) := \begin{cases} V - \dfrac{\beta}{r} & \text{if} \quad r \geq r_{crit}(I), \\ (I + q_* r)\left(1 - \dfrac{1}{rR}\right) & \text{else,} \end{cases}$$

where β, q_*, V and R are given parameters of the model. More precisely, q_* stands for the theoretical maximal flow, while V and R describe respectively the maximal speed and density. The critical spacing $r_{crit}(I)$ separating the free and congested cases is computed as the inverse of the critical density

$$\rho_{crit}(I) := \frac{1}{2\left(\beta - \dfrac{I}{R}\right)} \left[V + \frac{q_*}{R} - I - \sqrt{\left(V + \frac{q_*}{R} - I\right)^2 - 4q_*\left(\beta - \frac{I}{R}\right)} \right].$$

The numerical values considered in this example are given below

$$\begin{cases} V = 25\ m.s^{-1} \\ \hat{V} = 22\ m.s^{-1} \\ R = 1/5\ veh.m^{-1} \\ \hat{R} = 1/30\ veh.m^{-1} \end{cases} \quad \text{and} \quad \begin{cases} \beta = \dfrac{V - \hat{V}}{\hat{R}} = 90\ m^2.s^{-1} \\ q_* = 1\ veh.s^{-1} \end{cases}$$

The flow-density and speed-spacing fundamental diagrams are given on Figure 6.10. Notice that these numerical values are satisfactory for a two-lanes road section. The driver attribute I varies between 0 and $I_{max} = 5$ which is designed such that the flow-density fundamental diagram $\mathfrak{F}(\rho, I)$ stays concave with respect to ρ.

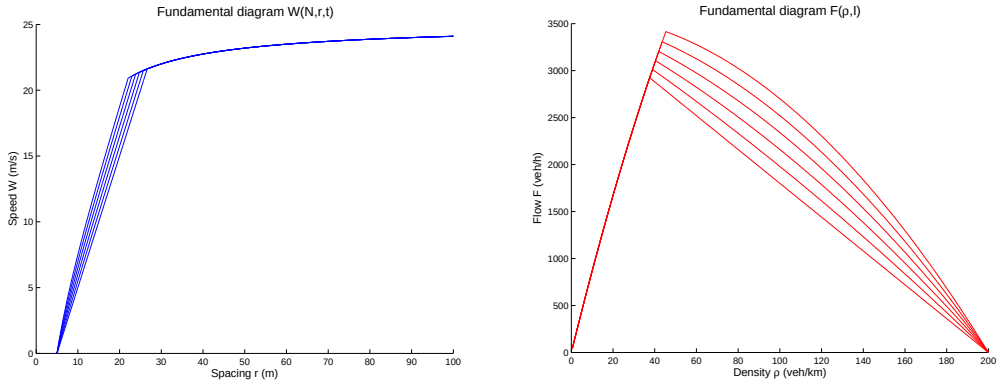

FIGURE 6.10 – Speed-spacing fundamental diagram $\mathcal{V}(r, I)$ (left) and flow-density fundamental diagram $\mathfrak{F}(\rho, I)$ (right).

The Lagrangian function $\mathcal{M}$ is given by

$$\mathcal{M}(u, I(N, t)) := \sup \left\{ \sup_{r \geq r_{crit}(I)} g_1(r, u, I), \sup_{r_{min} \leq r \leq r_{crit}(I)} g_2(r, u, I) \right\}$$

with

$$\begin{cases} g_1(r,u,I) := V - \dfrac{\beta}{r} - ru, \\ g_2(r,u,I) := (I + q^* r)\left(1 - \dfrac{1}{rR}\right) - ru. \end{cases}$$

Some simple algebra leads to

$$\sup_{r \geq r_{crit}(I)} g_1 := \begin{cases} g_1\left(r_{crit}(I)\right) & \text{if} \quad \sqrt{\dfrac{\beta}{p}} < r_{crit}(I), \\ g_1\left(\sqrt{\dfrac{\beta}{p}}\right) & \text{else} \end{cases}$$

and

$$\sup_{r_{min} \leq r \leq r_{crit}(I)} g_2 := \begin{cases} g_2\left(r_{min}\right) & \text{if} \quad q^* < p \quad \text{and} \quad \sqrt{\dfrac{I}{R(p-q^*)}} < r_{min}, \\ g_2\left(r_{crit}(I)\right) & \text{if} \quad q^* \geq p \quad \text{or if} \quad q^* < p \quad \text{and} \quad \sqrt{\dfrac{I}{R(p-q^*)}} > r_{crit}(I), \\ g_2\left(\sqrt{\dfrac{\beta}{p}}\right) & \text{if} \quad q^* < p \quad \text{and} \quad r_{min} \leq \sqrt{\dfrac{I}{R(p-q^*)}} \leq r_{crit}(I). \end{cases}$$

The Lagrangian $\mathcal{M}$ is then computed for our numerical instantiation, as illustrated on Figure 6.11 (right).

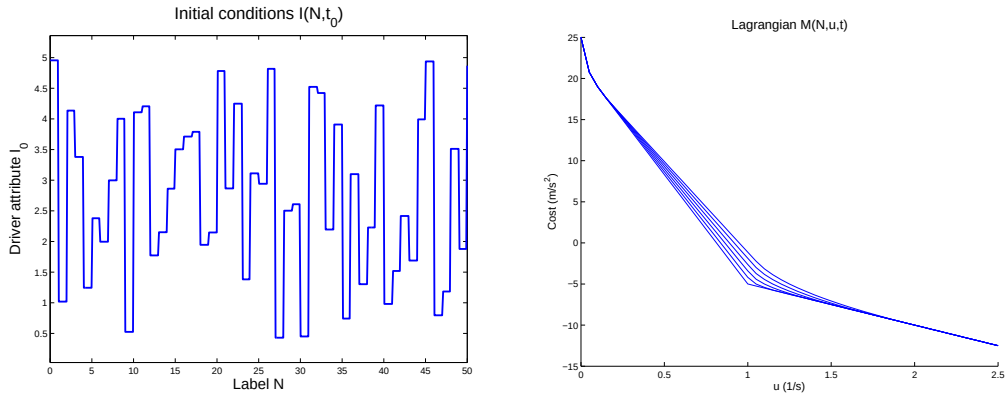

FIGURE 6.11 – Initial values of driver attribute $I(N, t_0)$ (left) and Lagrangian function $\mathcal{M}(N, u, t)$ (right).

We consider piecewise affine initial conditions that is we prescribe each vehicle position $X(t, n)$ at time $t = t_0$ for $n \in [N_0, N_{max}]$ according to a normal distribution of spacing between $r_{min} = 5$ m and a 50 m "maximal" spacing. The initial condition for this numerical test are plotted on Figure 6.12.

Moreover we prescribe piecewise affine upstream boundary condition that is the trajectory $X(t, n)$ of the first vehicle $N = N_0$ for $t \in [t_0, t_{max}]$. This upstream boundary condition is illustrated on Figure 6.13.

We also have included two (fictive) vehicle trajectories for $N = 25$ and $N = 46$ as Lagrangian internal boundary conditions. They are plotted on Figure 6.14. For these trajectories, we have considered randomly distributed speed values that are piecewise constant. Note that the speed distribution is chosen such that the mean value is equal to 18 m.s^{-1} in a first time and then to 10 m.s^{-1}. In that way, one can verify the trajectories are piecewise affine and averaging on time, vehicles are globally decelerating.

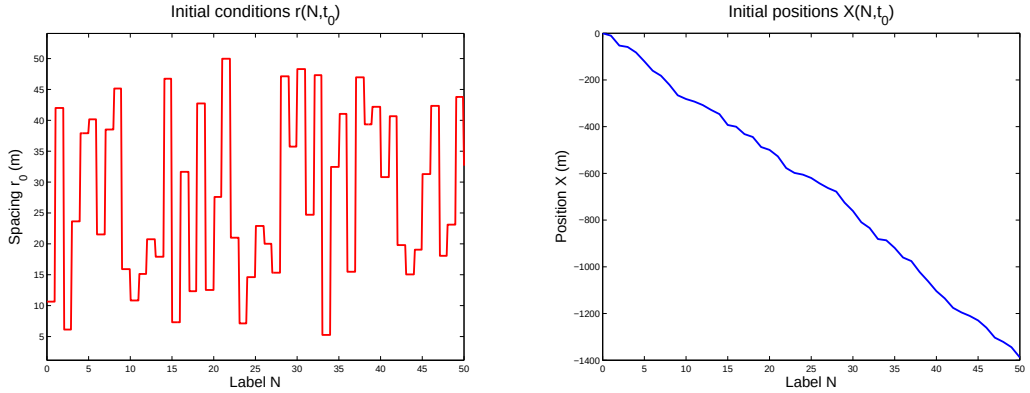

(a) Initial spacing $r(N, t_0)$ (b) Initial positions of vehicles $\mathcal{X}(N, t_0)$

FIGURE 6.12 – Initial conditions for the GSOM PDE at $t = t_0$.

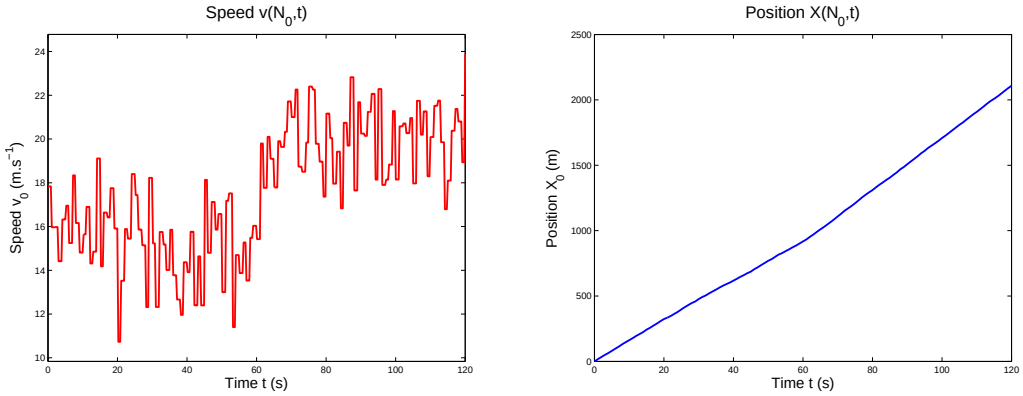

(a) Boundary speed $v(N_0, t)$ (b) First vehicle trajectory $\mathcal{X}(N_0, t)$

FIGURE 6.13 – Boundary conditions for the GSOM PDE at $N = N_0$.

Remark 5.1 (Realism of vehicle speed profiles)**.** *The profiles of speeds are voluntarily noisy and not so realistic. However, one can expect that real data coming from GPS sensors for instance, introduce such a noise.*

5.2 Numerical result and interpretation

The solution is thus given by applying the computation algorithm described in Algorithm 3. The simulations deal with 50 vehicles on a 2 minutes run. We also compare the solution with initial and upstream boundary conditions and the solution with initial, upstream and internal boundary conditions. The numerical solutions $\mathcal{X}$ are respectively plotted on Figures 6.15 (a) and (b).

In Figures 6.15 (c) and (d), we have also plotted the speeds of vehicles which are computed as the discrete gradient of the solution $\mathcal{X}(N, t)$ according to time t and for any vehicle N. One can observe the shock and rarefaction waves generated from initial and boundary conditions. Note that the internal boundary conditions are not necessarily defined for every $t \in [t_0, t_{max}]$. It is the reason why there is an area up to $N = 46$ and $t = 110$ that matches a high speed rarefaction fan since the solution is no more constrained by the internal boundary condition.

One can note that the integration of two slower vehicles ($N = 25$ and $N = 46$) in the

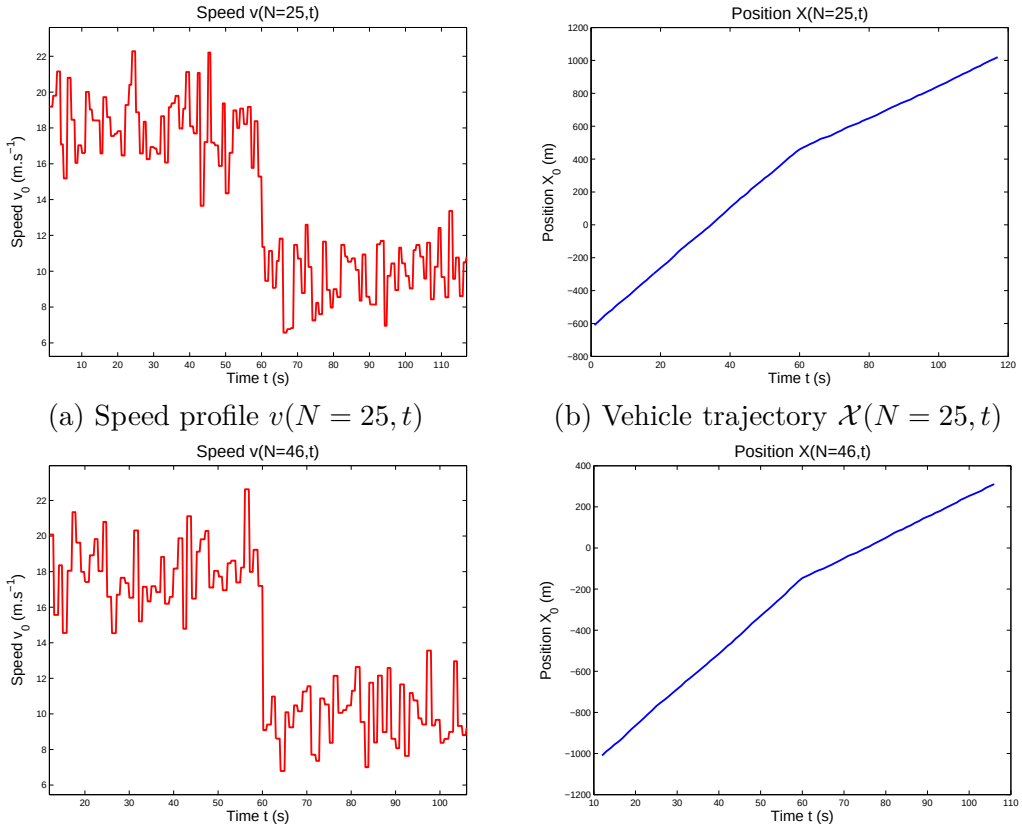

(a) Speed profile $v(N = 25, t)$ (b) Vehicle trajectory $\mathcal{X}(N = 25, t)$

(c) Speed profile $v(N = 46, t)$ (d) Vehicle trajectory $\mathcal{X}(N = 46, t)$

FIGURE 6.14 – Lagrangian internal boundary conditions for the GSOM PDE at $N = 25$ and $N = 46$.

traffic flow implies the modification of the solution. The values of $\mathcal{X}$ for $N \geq 25$ and then $N \geq 46$ are notably decreased. Indeed slower vehicles impose lower speeds to the following vehicles as it could be noticed on vehicle trajectories plotted on Figure 6.16. Thus, data assimilation allows to modify the previous over-estimation we made by considering only initial and upstream boundary conditions.

We also include a fictitious Eulerian data, i.e. Cumulative Vehicle Counts $N(t)$, coming from a fixed location $x_0 = 0$. The numerical solution is plotted on Figure 6.17 (a) and the corresponding speed locus are given on Figure 6.17 (b). One can see that according to the traffic speed, the domain of influence is either above (under-critical case) or below (over-critical case) the Eulerian curve. As it is clearly visible for the speeds (see Figure 6.17 (b)) in comparison to the "basic" case (see Figure 6.15 (d)), the propagation of under-critical values (resp. over-critical values) matches with high speeds (resp. low speeds). Vehicle trajectories are also corrected according to the position values deduced from the Eulerian data.

In the numerical example above, we do not consider real data assimilation. The next step for numerical results should be the assimilation of real data in a model of the GSOM family. As it was described in the previous section, vehicle trajectories and fixed detector measurements can be easily incorporated in the algorithm. However we need to identify a driver attribute I and to know how it evolves on the computational domain. That is the

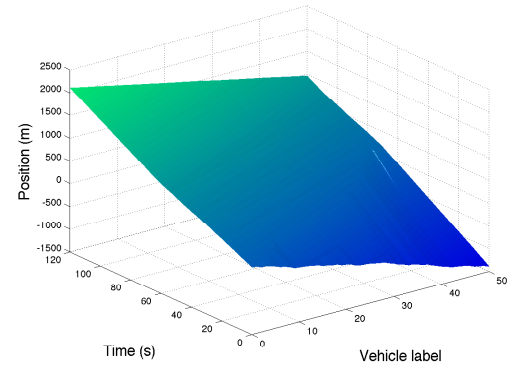

(a) Moskowitz surface $X(t,n)$

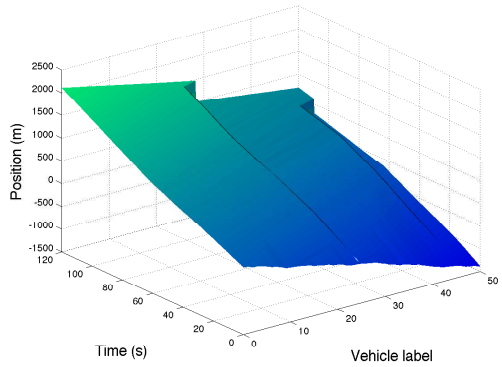

(b) Solution with Lagrangian data assimilation

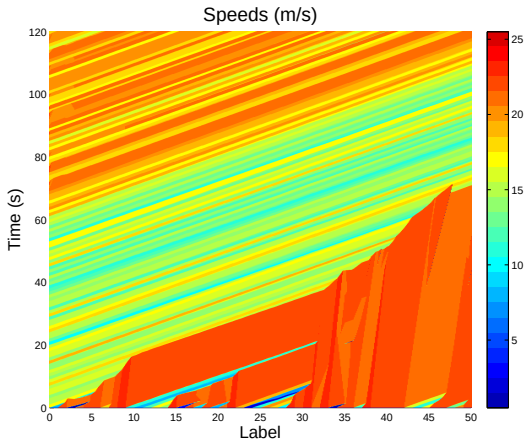

(c) Speeds

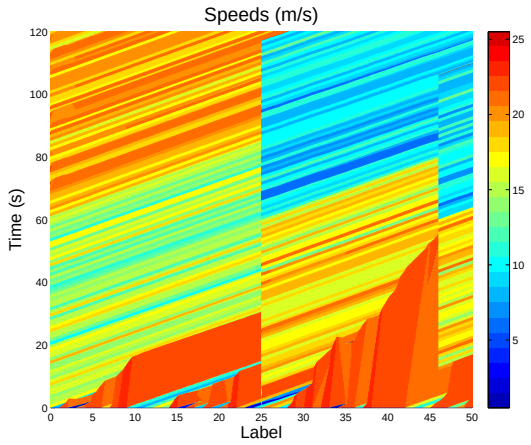

(d) Speeds with Lagrangian data assimilation

FIGURE 6.15 – Numerical solution for GSOM PDE obtained on the computation domain $[N_0, N_{max}] \times [t_0, t_{max}]$.

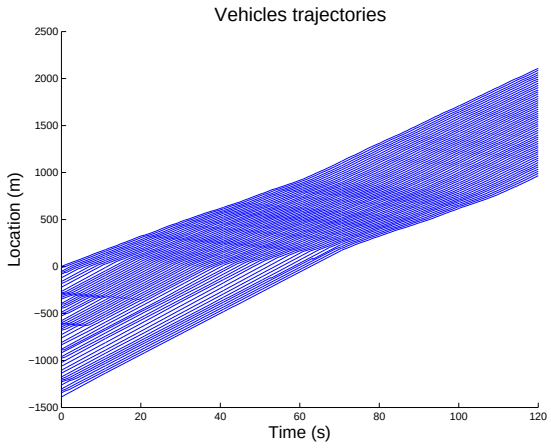

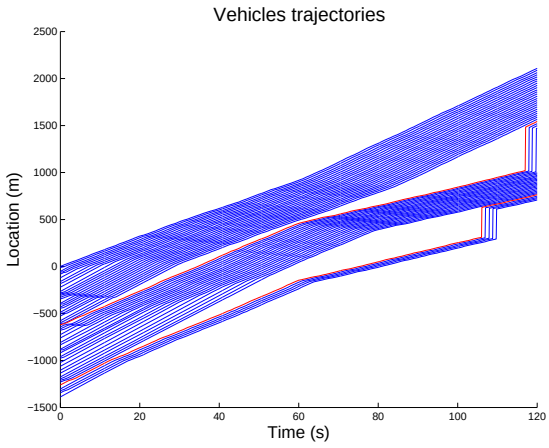

FIGURE 6.16 – Vehicle trajectories obtained for integers of the GSOM numerical solution $X(t,n)$.

tough point because it is hard to measure or to evaluate. Notice that an example of speed data assimilation with the ARZ model which is a model of the GSOM family can be found in [188].

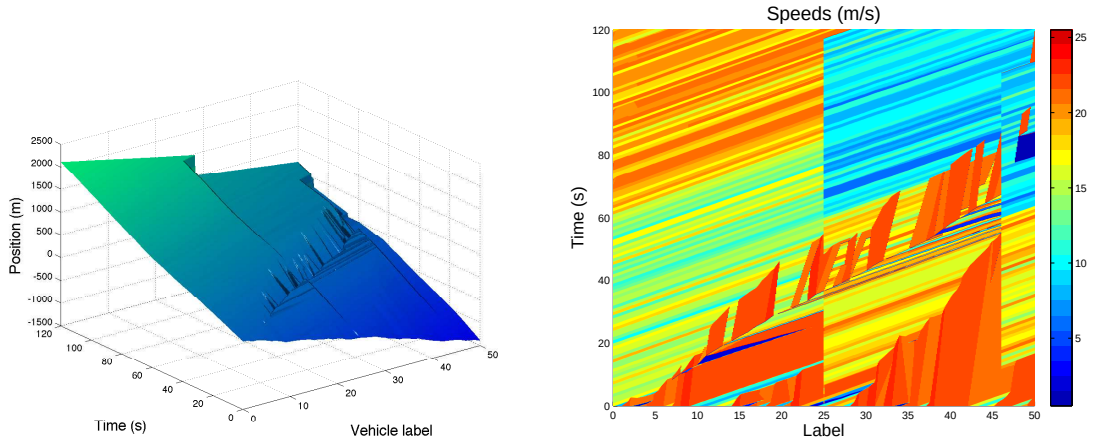

(a) Moskowitz surface $X(t, n)$ (b) Speeds

FIGURE 6.17 – Numerical solution for GSOM PDE obtained on the computation domain $[N_0, N_{max}] \times [t_0, t_{max}]$ with Lagrangian and Eulerian data assimilation.

Concerning the identification of I, a method could be deduced from [94], exploiting data-fitted fundamental diagrams. In the case of a scalar attribute I, we can use for instance speed and spacing measurements to evaluate the value of I.

6 Discussion and conclusion

In this paper, we are interested in the assimilation of different kinds of data into a generic class of macroscopic traffic flow models for improving traffic state estimation. The data come from mixed sources including Lagrangian vehicle trajectories and Eulerian cumulative vehicle counts obtained from fixed detectors. We then consider macroscopic traffic flow models of the Generic Second Order Modeling (GSOM) family in the Lagrangian system of coordinates which seems to be the most adapted framework for dealing with such data. We describe a computational method providing solutions to these models under piecewise affine initial and boundary conditions. The numerical method is based on the variational theory which has been extended to the GSOM family very recently [172]. Solution can be computed thanks to Lax-Hopf like formula and a generalization of the inf-morphism property [58]. It is possible to considerably reduce the number of integral curves by following only the characteristics which are the optimal trajectories. Another computational trick is to solve separately many partial problems (by discretizing initial and boundary conditions) instead of the general problem.

Extensions of this work could include more general assumptions on the dynamics $\varphi \neq 0$ of driver attributes, always with the assumption of piecewise affine value conditions. The computational benefits of the variational method over the finite difference method which is also presented in the paper need to be illustrated on several comparisons. We expect that the variational method has a lower computational cost (due to parallel computing e.g.) and a globally higher accuracy compared with the other method.

A still open but interesting question is the application of the algorithm to data assimilation on road networks. The challenging point is to deal with fundamental diagrams which will depend on the drivers attribute but also on the spatial position. To our best knowledge Lax-Hopf formula seems not to be so tractable in that framework because the

formula does not simplify so much for space dependent Hamiltonians. One considered possibility is to use the extended concepts of supply and demand functions to models of the GSOM family [161]. This subject is being currently investigated by the authors.

Chapitre 7

GSOM macroscopic traffic flow models on junction : Lagrangian perspective

Warning. We want to kindly warn the reader that this chapter is based on a still ongoing research. This means in particular that some of the results and the companion proofs are only proposed in a formal way. The work has greatly benefited of discussions with Asma Khelifi, University of Tunis, Tunisia, and Jean-Patrick Lebacque, Université Paris-Est, as well.

Sommaire

Abstract

In this chapter, we want to develop an intersection model which is compatible with micro and macro description, and satisfy classical constraints (the invariance principle for instance). The microscopic representation of traffic flow is particularly suited for traffic management methods involving V2X (vehicle-to-vehicle or vehicle-to-infrastructure) communication, while staying compatible with a macroscopic representation allowing global evaluation and assessment of ITS strategies.

1 Introduction

1.1 Motivation

In this chapter, we are motivated by road network modeling, thanks to macroscopic traffic flow models. First order traffic flow models have been used for quite a long time for modeling traffic flows on networks (see [106, 171] for instance). In particular, the seminal LWR model [184, 221] has been widely used. However, first order models do not allow to recapture accurately specific and meaningful traffic flow phenomena. Thus we focus on the Generic Second Order Models (GSOM) family which encompasses a large variety of higher order traffic flow models. GSOM models have been already well studied on homogeneous sections but they have attracted little attention for their implementation on junctions, as it is discussed in Section 3. However, junctions are the main source of congestion for traffic streams on a network.

In this chapter, we want to develop a junction model which is compatible with microscopic and macroscopic descriptions, and satisfies classical constraints coming from engineering, as for instance the invariance principle [67, 170, 225]. The microscopic representation of traffic flow is particularly suited for traffic management methods involving V2X (including V2V, standing for vehicle-to-vehicle and V2I, for vehicle-to-infrastructure) communications, while staying compatible with a macroscopic representation allowing global evaluation and assessment of Intelligent Transportation Systems (ITS) strategies. The key idea for conciliating both microscopic and macroscopic representations is to recast the macroscopic model under its Lagrangian coordinates. Indeed the Lagrangian framework focuses directly on the particles and incidentally it allows to keep track of individual behaviors (see for instance [177] in the case of first order LWR model).

1.2 Organization of the chapter

The article is organized as follows. In Section 2, the generic class of second order macroscopic traffic flow models called GSOM family, which is considered in this chapter, is introduced. We also give some examples of some "standard" traffic flow models which are embedded into the GSOM family. In Section 3, we review and discuss the existing approaches that were considered for solving GSOM models posed on junctions. Our aim is to show that the Lagrangian framework is well-suited for designing the solution to GSOM problems even if incorporating (moving) discontinuities. The complete numerical methodology is described in Section 4. Finally, we provide some conclusions on this work and give some insights on future research in Section 5.

2 GSOM family

2.1 Formulation of GSOM models

In [169, 174], the authors introduce a general class of macroscopic traffic flow models called the Generic Second Order Models (GSOM) family. Any model of the GSOM family can be stated in conservation form as follows

$$\begin{cases} \partial_t \rho + \partial_x(\rho v) = 0 & \text{Conservation of vehicles,} \\ \partial_t(\rho I) + \partial_x(\rho v I) = \rho\varphi(I) & \text{Dynamics of the driver attribute } I, \\ v = \mathfrak{I}(\rho, I) & \text{Fundamental diagram,} \end{cases} \tag{7.2.1}$$

where ρ stands for the density of vehicles, v for the flow speed (equal to the mean spatial velocity of vehicles), x and t for position and time. The variable I is a specific driver attribute which can represent for example the driver aggressiveness, the driver destination or the vehicle class. The flow-density fundamental diagram (FD) is defined by

$$\mathfrak{F} : (\rho, I) \mapsto \rho\mathfrak{I}(\rho, I).$$

Notice moreover that it was shown in [174] that the notions of Supply and Demand functions defined in [164] for the classical LWR model could be extended to the GSOM family. The GSOM models admit two kinds of waves :

- Kinematic waves or 1-waves as in the seminal LWR model : a wave propagates density variations at speed $\nu_1 = \partial_\rho \mathfrak{F}(\rho, I)$ while the driver attribute I is continuous across such a wave.
- Contact discontinuities or 2-waves : a wave propagates variations of driver attribute I at speed $\nu_2 = \mathfrak{I}(\rho, I)$ while the flow speed is constant across such a wave.

2.2 Examples

The GSOM family recovers a wide range of existing models :

- The LWR model [184, 221] itself is simply a GSOM model with no specific driver attribute, expressed as follows

$$\begin{cases} \partial_t \rho + \partial_x(\rho v) = 0 & \text{Conservation of vehicles,} \\ v = \mathfrak{I}(\rho, x) & \text{Fundamental diagram.} \end{cases} \tag{7.2.2}$$

  The fundamental diagram (FD) for the LWR model states that traffic flow is always at an equilibrium state. It is commonly assumed that the flow is an increasing function of density between zero (corresponding to an empty section) and a critical density and then the flow decreases until the maximal density (corresponding to a bumper-to-bumper situation). However the FD shape is always a subject of debates (see for instance [95]) and there exists a wide variety in the literature encompassing concave and triangular flow functions (see Figure 7.1 and also Chapter 3 of [106] for additional examples).

- The LWR model with bounded acceleration proposed in [165, 166, 175] is also a GSOM model in which the propagated driver attribute is simply the speed of vehicles.
- The ARZ model (standing for Aw, Rascle [11] and Zhang [241]) for which the driver attribute is taken as $I = v - V_e(\rho)$ that is $\mathfrak{I}(\rho, I) = I + V_e(\rho)$.

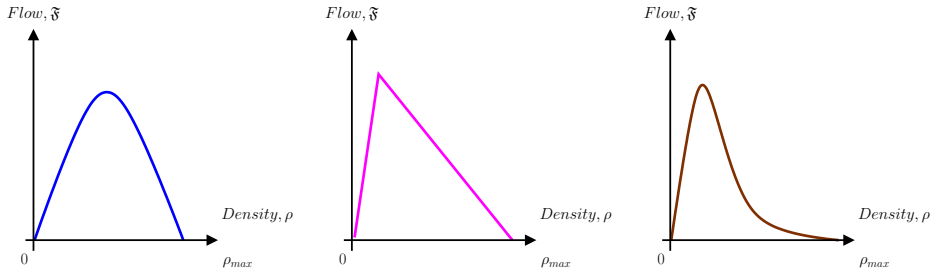

FIGURE 7.1 – Illustrations of some flow functions $\mathfrak{F}$ for the LWR model : Greenshields (left), triangular (center) and exponential (right).

- The Generalized ARZ model proposed in [94] that can be also seen as a particular case of the model described in [242]. These models introduce an interaction mechanism between two different FDs for distinguish equilibrium and non-equilibrium states.
- Multi-commodity models (multi-class, multi-lanes) of Jin and Zhang [143], Bagnerini and Rascle [12] or Herty, Kirchner, Moutari and Rascle [131]. It encompasses also the model of Klar, Greenberg and Rascle [150].
- The Colombo 1-phase model deduced in [174] from the 2-phase model of Colombo [61]. In this case, the driver attribute I is a scalar which is non-trivial in congested situation. In fluid area, the model follows the classical LWR model.
- The stochastic GSOM model of Khoshyaran and Lebacque [149]. The driver attribute I is a random variable depending on the vehicle index N and on the random event ω such that $I = I(N, t, \omega)$. The random perturbations do not affect the vehicle dynamics but affect the driver perception and its behavior.

The interested reader is referred to [172] and references therein for more details on examples.

2.3 A note on Supply-Demand functions

It is worth noticing that the notions of *supply* and *demand* functions defined in [164] for the classical LWR model and expanded to the case of the LWR model on junctions in [170], could be also extended to the GSOM family, as it was shown in [174]. These functions built on the fundamental diagram (FD) are essential to build monotone finite volume schemes for solving the hyperbolic system (7.2.1). Supply and demand functions are also particularly relevant for traffic flow modeling through junctions.

If $\mathfrak{F}$ denotes the flow-density fundamental diagram

$$\mathfrak{F}(\rho, I) := \rho \mathfrak{I}(\rho, I),$$

then equilibrium demand and supply functions are defined as follows

$$\begin{cases} \Delta(\rho, I; x) := \max\limits_{0 \le k \le \rho} \mathfrak{F}\left(k, I; x^-\right), \\ \Sigma(\rho, I; x) := \max\limits_{k \ge \rho} \mathfrak{F}\left(k, I; x^+\right). \end{cases} \tag{7.2.3}$$

In the case of GSOM models, the extension of local traffic supply and demand definitions is far from being straightforward. Indeed, it has been pointed out that downstream

supply depends on the upstream driver attribute (which has not already passed through the considered point). The upstream demand and downstream supply at a point x and time t are defined such that

$$\begin{cases} \delta(x,t) := \Delta\left(\rho(x^-,t), I(x^-,t); x\right), \\ \sigma(x,t) := \Sigma\left(\overline{\rho}(x,t), I(x^+,t); x\right), \\ \quad \text{with} \quad \overline{\rho}(x,t) := \mathfrak{I}^{-1}\left\{\mathfrak{I}\left(\rho(x^+,t), I(x^+,t); x^+\right), I(x^-,t); x^+\right\}. \end{cases} \tag{7.2.4}$$

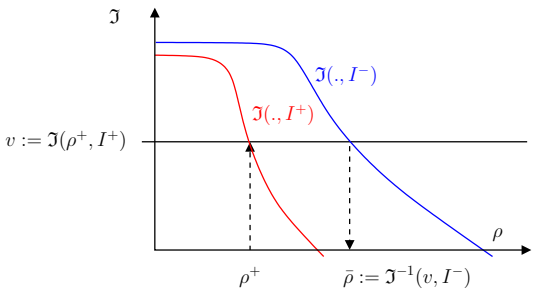

FIGURE 7.2 – The downstream supply depends on the upstream driver attribute. Here, we have defined $I^+ := I(x^+,t)$, $I^- := I(x^-,t)$ and $\rho^+ := \rho(x^+,t)$.

Let us introduce the *modified demand* for the GSOM models as follows

$$\Xi\left(\rho, I_1, I_2; x\right) := \Sigma\left(\mathfrak{I}^{-1}\left\{\mathfrak{I}\left(\rho, I_2; x^+\right), I_1; x^+\right\}, I_2; x\right), \tag{7.2.5}$$

such that the second and third formulas in (7.2.4) boils down to

$$\sigma(x,t) := \Xi\left(\rho(x,t), I(x^+,t), I(x^-,t); x^+\right).$$

It means that we need to project the observed density at x^+ on the FD depending on $I(x^-,t)$ because the immediate downstream supply depends on the perception of the available space according to the next particle that will pass at point x.

Remark 2.1 (Degenerate case due to vacuum apparition)**.** *Consider a point x separating two different traffic states $(-)$ for x^- and $(+)$ for x^+. We set $I^+ := I(x^+,t)$ and $I^- := I(x^-,t)$. It may happen that*

$$\mathfrak{I}(\rho, I^+) > \sup_{k\in\mathbb{R}} \mathfrak{I}(k, I^-) =: v^-_{max},$$

leading to an inaccuracy in (7.2.5) since $\overline{\rho} = \mathfrak{I}^{-1}\left\{\mathfrak{I}\left(\rho, I^+\right), I^-\right\}$ has no solution. In this particular case, we make the choice of $\overline{\rho} = 0$ such that $\sigma(x,t) = \sup_{k\in\mathbb{R}} \mathfrak{F}(k, I^-)$.

In Eulerian setting, it means that the group of upstream particles $(-)$ cannot accelerate enough (even increasing their speeds to v^-_{max}) to catch up with the downstream particles $(+)$. This induces the apparition of a vacuum area between both groups of particles.

The interested reader could also refer to Remark 4.4 in [68] fr more details on this case.

2.4 Lagrangian setting of the GSOM family

The common expression of GSOM models in Eulerian coordinates is given by (7.2.1). However, it is well-known that Lagrangian framework is particularly convenient for dealing

with flows of particles and it is especially true in traffic flow modeling (see [177, 232] and references therein). The Lagrangian formulation of the LWR model comes from [177] and it has been shown to be particularly convenient for numerical accuracy and state estimation.

If we set the following change of coordinates

$$\begin{cases} N(t,x) := \displaystyle\int_x^{+\infty} \rho(t,\xi)d\xi, \\ T := t \end{cases} \qquad \text{such that} \qquad \begin{cases} \partial_N = -r\partial_x, \\ \partial_T = \partial_t + v\partial_x \end{cases}$$

where v denotes the speed of particles, and if we consider the particle spacing $r := \dfrac{1}{\rho}$ and the speed-spacing fundamental diagram (see its illustration on Figure 7.3)

$$\mathcal{V}(r,I) := \mathfrak{I}\left(\frac{1}{r}, I\right) \quad \text{for any} \quad (r,I) \in (0,+\infty)\times\mathbb{R},$$

then the GSOM model (7.2.1) can be recast in Lagrangian form as follows

$$\begin{cases} \partial_T r + \partial_N \mathcal{V}(r,I) = 0 & \text{Conservation of vehicles,} \\ \partial_T I = \varphi(I) & \text{Dynamics of the driver attribute } I, \\ v = \mathcal{V}(r,I) & \text{Speed-spacing fundamental diagram.} \end{cases} \tag{7.2.6}$$

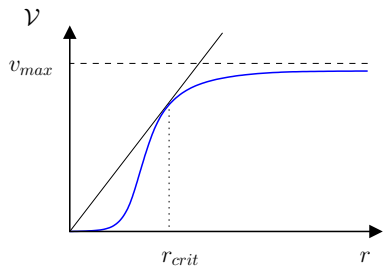

FIGURE 7.3 – The speed-spacing Fundamental Diagram.

One can notice also that we have $r = -\partial_N \mathcal{X}$ where $\mathcal{X}(N,T)$ denotes the position of particle N at time T which solves the following Hamilton-Jacobi equation

$$\begin{cases} \partial_T \mathcal{X} = \mathcal{V}\left(-\partial_N \mathcal{X}, I\right), \\ \partial_T I = \varphi(I). \end{cases} \tag{7.2.7}$$

Remark 2.2 (Supply and demand for the speed-spacing FD)**.** *Looking for supply and demand functions with respect to the speed-spacing fundamental diagram (see Figure 7.3), thanks to the monotony of function $\mathcal{V}(.,I)$, we notice that whatever the spacing, the supply is the maximal speed v_{max} while the demand is given by the speed $\mathcal{V}(r,I)$ itself. Indeed, we have*

$$\begin{cases} \Delta^{lag}(r,I) = \max\limits_{k\le r} \mathcal{V}(k,I) = \mathcal{V}(r,I), \\ \Sigma^{lag}(r,I) = \max\limits_{k\ge r} \mathcal{V}(k,I) =: v_{max}. \end{cases} \tag{7.2.8}$$

3 Critical review of the literature

At the best authors' knowledge, there is very few works on Lagrangian modeling of junctions in traffic flow modeling. One of them, namely the paper of van Wageningen-Kessels et al. [232], deals with the LWR model which is one specific model among the whole GSOM family.

3.1 Lagrangian modeling of junctions : case of the LWR model

We deal in this subsection with the paper of van Wageningen-Kessels et al. [232]. In this paper, the authors consider Eulerian discontinuities and they include them in the Lagrangian formulation of the kinematic model (say the LWR model [184,221]) for pointing out a node model. Indeed nodes are obviously Eulerian discontinuities.

The Lagrangian formulation of the LWR model comes from the work of Leclercq et al. [177] and it is particularly convenient for numerical accuracy and state estimation. As noticed by the authors, the variational approach is rather complex to apply on real network with many links and when applied to a model with for example a non-triangular fundamental diagram, it looses the advantages of higher accuracy. Thus, they use classical methods to discretize the kinematic wave model in Lagrangian formulation and extend the work to multi-class models taking into account heterogeneity of drivers and vehicles.

Recall that at a merge, flows satisfy some fixed merge ratios [15, 51] which could be time-dependent (lower in the afternoon peak than in morning peak hour for instance) but do not depend on actual flows. It is worth noticing that there are similarities in treating Eulerian discontinuities in Lagrangian formulation and treating micro-macro boundaries in hybrid approach (see for instance [33, 176, 178]).

If we consider the following change of coordinates,

$$\begin{cases} T = t, \\ N = -\displaystyle\int_x^{\infty} \rho(\xi, t) d\xi \end{cases} \qquad \text{instead of} \quad \begin{cases} t, \\ x \end{cases}$$

such that we got

$$\begin{cases} \partial_N = -r\partial_x, \\ \partial_T = \partial_t + v\partial_x, \end{cases}$$

then the LWR model $\partial_t \rho + \partial_x \left(\rho V(\rho)\right) = 0$ becomes

$$\partial_T r + \partial_N \bar{V}(r) = 0, \tag{7.3.9}$$

where r denotes the spacing (say the distance between two consecutive vehicles, front bumper to following front bumper for instance and not the net spacing). We recall that we also have $q = \rho V(\rho) = \dfrac{\bar{V}(r)}{r}$. If taking into account discontinuities in space, the model becomes

$$\partial_T r + \partial_N \bar{V}(t, x(N), r) = 0, \tag{7.3.10}$$

with a time and space dependent fundamental diagram (speed-spacing FD). From the inhomogeneous LWR model $\partial_t \rho + \partial_x \left(\rho V(\rho)\right) = f(x,t)$ (with a source-sink term), we also recover in Lagrangian formulation

$$\partial_T r + \partial_N \bar{V}(r) = -r^2 f\left(x(N), t\right).$$

The right hand side (r.h.s.) can be interpreted as the increase or decrease of platoon length per vehicle and per second (due to new platoons of vehicles entering or leaving the stream).

However, there is no description of boundary conditions in Lagrangian coordinates for the continuous model. It is only expressed as minimum between demand and supply in Eulerian formulation (classical) and for merge (Daganzo's model [77]).

Let us introduce Δt and ΔN time and particle discretization steps (see Figure 7.4).

Then the basic Lagrangian model (7.3.9) is discretized by a first order upwind method and an explicit time stepping method. Define $r_i^k = r(k\Delta t, i\Delta N)$. For a homogeneous

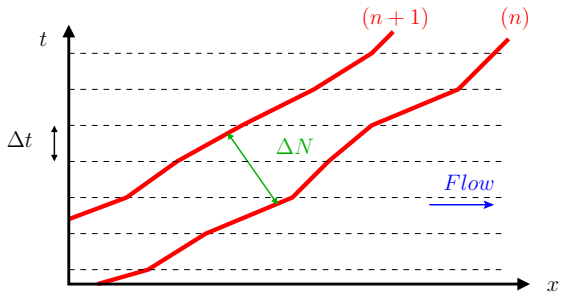

FIGURE 7.4 – Illustration of the discretization for the particle model.

section, we got

$$\begin{cases} r_i^{k+1} = r_i^k + \dfrac{\Delta t}{\Delta N}\left(v_{i-1}^k - v_i^k\right), \\ v_i^k := \bar{V}(r_i^k). \end{cases}$$

In presence of a discontinuity (and thus in case of a source/sink term in (7.3.10)), we have

$$\begin{cases} r_i^{k+1} = (1+\alpha) r_i^k + \dfrac{\Delta t}{\Delta N}\left(v_{i-1}^k - v_i^k\right), \\ v_i^k := \bar{V}(r_i^k), \\ \alpha := \Delta t r_i^k f(x(n), t) = \dfrac{\Delta N_{source}^k}{\Delta N_{initial}^k}, \end{cases} \tag{7.3.11}$$

where ΔN_{source}^k is the number of vehicles entering or leaving the node and $\Delta N_{initial}^k$ is the total number of vehicles arriving at the node at k^{th}-time step.

Remark 3.1 (Discontinuity in the Lagrangian scheme)**.** *It is worth noting that in (7.3.11) it may happen that*

(i) the speed-spacing fundamental diagram $\bar{V}$ is different before and after the discontinuity and

(ii) ΔN is different before and after the discontinuity (even if it is more tricky).

Remark 3.2 (Time discretization and passing time at the discontinuity)**.** *The time discretization introduces that group of vehicles do not arrive and exit the discontinuity at integers of the time steps. There are many strategies to solve problems caused at node that are discussed in the paper (see Figure 3 of [232]) :*

1. *Change vehicle discretization ΔN,*
2. *Adapt the time discretization step Δt,*
3. *Accept to loss accuracy by changing the trajectory only after detecting the passage to the node (for integers of time step).*

Other problems that have been taken into consideration in [232] are :

1. Change in the fundamental diagram (FD) $\bar{V}$ caused for instance by new speed limit, different number of lanes... the chosen strategy consists in waiting for the next integer time to change the FD. The change becomes effective a bit downstream of the actual change (at the discontinuity).

2. 1-2 nodes (diverge) : remove vehicles from original trajectories or bifurcations of vehicles toward other branches.

3. 2-1 nodes (merge) : add vehicles (on the considered outgoing branch)

4. Boundary conditions (inflow-outflow for a link $[0, L]$) :

   - at the inflow boundary (and not link-node interface), the number of vehicles per time unit should be prescribed as a demand-supply minimum

$$q(0,t) = \begin{cases} \min(\underbrace{\Delta(t)}_{\text{demand}}, \underbrace{C}_{\text{capacity}}), & \text{if} \quad \rho(0^+,t) \leq \rho_{crit}, \\ q(0^+,t), & \text{otherwise.} \end{cases}$$

   - At the outflow boundary, we also prescribe an external outflow restriction (the supply) as follows

$$q(0,t) = \begin{cases} \min(q(L^-,t), \underbrace{\Sigma(t)}_{\text{supply}}), & \text{if} \quad q(L^-,t) \leq \rho_{crit}, \\ min\left(C, \Sigma(t)\right), & \text{otherwise.} \end{cases}$$

   with $q(L^-,t) = q(x(0),t) = \dfrac{\bar{V}(0,t)}{r(0,t)}$ and $n = 0$ is the last group of vehicles which has left the domain.

See Figure 4 of [232] for illustrations of these considerations.

In conclusion, the authors underline that the choice of differing the change of FDs could be replaced by another one, for instance based on the minimum supply-demand scheme, which may lead to more accurate results.

3.2 Modeling of junctions with GSOM models

We refer here to the pioneer work of Khoshyaran and Lebacque [147]. They consider a GSOM model, introducing a driver specific fundamental diagram. For instance, we recall that in the ARZ model, the attribute I measures the difference between the actual speed and the equilibrium speed. Although GSOM models are macroscopic, they admit a particle (Lagrangian discretization), deduced as the Godunov scheme applied to the Lagrangian expression of the generic model. They extend this particle discretization to networks, addressing the problem of junction modeling through a supply-demand approach for link and nodes and thanks to internal state junction model.

Eulerian setting

To modelize traffic flows on network via the GSOM family, it is necessary to precise boundary conditions on branches and at the junction. In [164], link boundary conditions for the simple LWR model have been expressed under supply-demand framework, saying that a passing flow at a point is the minimum between local upstream demand and local downstream supply.

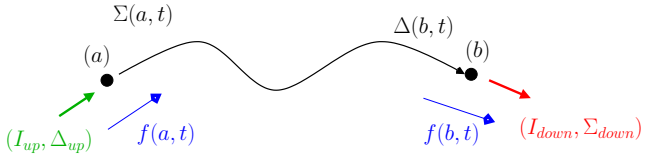

FIGURE 7.5 – Illustration of boundary conditions for a simple link.

If we consider a simple bounded link as on Figure 7.5, then boundary conditions (in Eulerian setting) are given by

$$\begin{cases} \begin{cases} \Sigma(a,t) := \Xi\left(\rho(a^+,t), I(a^+,t), I_{up}(t); a\right), \\ f(a,t) := \min\left[\Delta_{up}(t), \Sigma(a,t)\right], \end{cases} & \text{for upstream boundary,} \\ \\ \begin{cases} \Delta(b,t) := \Delta\left(\rho(b^-,t), I(b^-,t); b\right), \\ \Sigma_{down}(t) := \Xi\left(\rho(b^-,t), I_{down}(t), I(b^-,t); b\right), \\ f(b,t) := \min\left[\Delta(b,t), \Sigma_{down}(t)\right], \end{cases} & \text{for downstream boundary.} \end{cases} \tag{7.3.12}$$

For the junction model, we can consider either a point-wise model (see Figure 7.6) with an optimization of passing flows at the junction point [170],

$$\max_{Q,\ R} \sum_i \varphi_i\left(Q_i\right) + \sum_j \psi_j\left(R_j\right)$$

$$\text{s.t.} \left| \begin{array}{lll} 0 \le Q_i \le \delta_i, & \forall i, & \text{(Demand and positivity constraints)} \\ 0 \le R_j \le \sigma_j, & \forall j, & \text{(Supply and positivity constraints)} \\ R_j - \sum_i \gamma_{ij} Q_i = 0, & \forall j, & \text{(Turning fractions)} \\ R_j J_j - \sum_i \gamma_{ij} Q_i I_i = 0, & \forall j, & \text{(Traffic composition)} \end{array} \right.$$

where φ_i and ψ_j (for any i and $j \in \mathbb{N}$) are concave increasing functions,

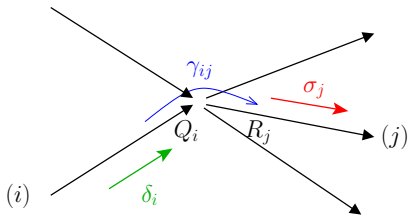

FIGURE 7.6 – Illustration of a point-wise junction model.

or we can consider an internal state model [148, 161] which assumes that the junction (noted (z)) has a physical dimension and acts like a buffer such that vehicles are stored before to exit on outgoing branches (see Figure 7.7). The internal state has some specific attributes such as

$$\begin{cases} N_z(t), & \text{total number of vehicles in the node,} \\ N_{z,j}(t), & \text{number of vehicles stored in the node and bound for link } (j), \\ I_z(t), & \text{common driver attribute of vehicles stored in the node.} \end{cases}$$

The number of vehicles stored in the node is computed thanks to a system of ordinary differential equations (ODEs) which traduces the conservation of vehicles :

$$\begin{cases} \dfrac{d}{dt}N_{z,j}(t) = -R_j + \sum_i \gamma_{ij} Q_i(t), & \forall j, \\ N_z(t) = \sum_j N_{z,j}(t), & \\ \dfrac{d}{dt}\left(N_z(t) I_z(t)\right) = \sum_i Q_i(t) I_i(z^-, t) + \sum_j R_j(t) I_z(t). & \end{cases} \tag{7.3.13}$$

Remark 3.3 (Upper bound on the capacity of the node)**.** *In my opinion, we also need to introduce an upper bound on $N_z(t)$ which correspond to the* physical *maximal number of vehicles that can be stored in the node. See also [148] for additional reference on internal state model.*

We introduce the coefficients $(\beta_i)_i$ that denote the fraction of space available for vehicles coming from (i) with respect to the total space available for all incoming branches. We then can define *partial* supply and demand functions

$$\begin{cases} \Sigma_i(t) := \beta_i \Sigma_z\left(N_z(t), I_z(t)\right), & \text{linear supply split model,} \\ \Delta_j(t); : \dfrac{N_{z,j}(t)}{N_z(t)} \Delta_z\left(N_z(t), I_z(t)\right), & \text{FIFO demand split model.} \end{cases} \tag{7.3.14}$$

The downstream supplies and upstream demands on branches are computed thanks to the *Min formula*

$$\begin{cases} Q_i(t) := \min\left[\delta_i(t), \Sigma_i(t)\right], & \text{with} \quad \delta_i(t) = \Delta_i\left(\rho_i(z^-, t), I(z^-, t)\right), \\ R_j(t) := \min\left[\Delta_j(t), \sigma_j(t)\right], & \text{with} \quad \sigma_j(t) = \Sigma_j\left(\rho_j(z^+, t), I_z(t)\right). \end{cases} \tag{7.3.15}$$

Remark 3.4 (Loss of information on driver attribute)**.** *It is worth noticing that in (7.3.15), traffic composition $I_z(t)$ at the node is assumed to be conserved on outgoing branches. One can think to a different rule since outside the junction, drivers are no longer "constrained" and they may naturally retake their initial attribute. It should be particularly true when dealing with particle (lagrangian) discretization and $\Delta N = 1$.*

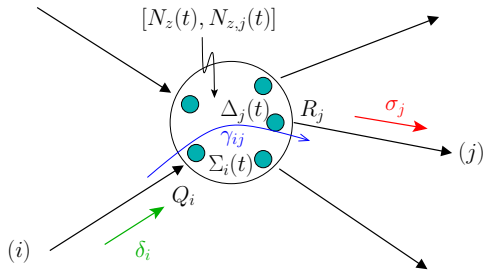

FIGURE 7.7 – Illustration of an internal state junction model.

Lagrangian setting

For deducing a particle (Lagrangian) discretization of the Eulerian model described above, it is necessary to take into consideration different elements : (i) the link model, (ii)

the internal node model and (iii) link-node and node-link interfaces (as in micro-macro or hybrid approaches [187]).

In [147], the authors make the choice to deal with densities. It imposes to work with flows, to determine at each iteration which is the traffic state (congested or fluid), and to inverse the flow function to get the corresponding density. Another solution should be to deal with spacing (or distance to the junction for incoming branches, as soon as the leader has entered the internal state).

Hereafter, we detail the Lagrangian boundary conditions for link-node and node-link interface. For node inflow on branch (i), let (a) be the closest particle to the node (z) (see Figure 7.8). We denote by $x_a(t) < 0$ its position and $I_a(t)$ its driver attribute. We can compute the local density

$$\rho_a(t) = \begin{cases} \Sigma_i^{-1}\left(Q_i(t), I_a(t)\right), & \text{if} \quad Q_i(t) = \Sigma_z(t), \quad \text{(congested)}, \\ \Delta_i^{-1}\left(Q_i(t), I_a(t)\right), & \text{if} \quad Q_i(t) = \delta_i(t), \quad \text{(fluid)}. \end{cases} \tag{7.3.16}$$

from where we can deduce the speed of particle (a). If $\Delta t v_a(t) > r_a(t)$, it means that at the next time step, particle (a) will enter the node. Thus (a) is replaced by a new particle (a) (the closest of the junction) and the number of vehicles inside the node is updated.

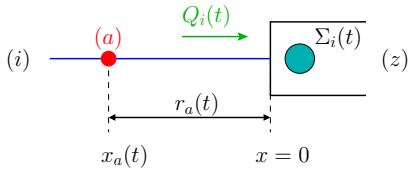

FIGURE 7.8 – Illustration of the link-node interface.

Remark 3.5 (Direct computation of the local density)**.** *To compute the local density $\rho_a(t)$ in (7.3.16), we need to know the flow $Q_i(t)$ which is assumed to be computed thanks to (7.3.15)*

$$Q_i(t) := \min\left[\delta_i(t), \Sigma_i(t)\right], \quad \textit{with} \quad \delta_i(t) = \Delta_i\left(\rho_i(z^-, t), I(z^-, t)\right).$$

However, in this formula, we need to known already $\rho_i(z^-, t)$ which seems to be strictly the same than $\rho_a(t)$ (which is by the way a macroscopic variable). It should make more sense to deal with spacing instead of density.

For the node outflow on branch (j), let (a) be the latest particle that exits the node (z) (see Figure 7.9) and $x_a(t)$ its location. We assume that there is a particle (b) stored in the node and which wants to exit it. As for inflow, we can compute the local density

$$\rho_a(t) = \begin{cases} \Sigma_i^{-1}\left(R_j(t), I_a(t)\right), & \text{if} \quad R_j(t) = \sigma_j(t), \quad \text{(congested)}, \\ \Delta_i^{-1}\left(R_j(t), I_a(t)\right), & \text{if} \quad R_j(t) = \Delta_z(t), \quad \text{(fluid)} \end{cases} \tag{7.3.17}$$

(the same remark could be done on the computation of $R_j(t)$: see Remark 3.5) from where we can deduce the local spacing $r_b(t)$ (equation (35) in [147] is not correct : it should be simply $r_b(t) := \dfrac{1}{\rho_a(t)}$) and we can deduce the position of particle (b)

$$x_b(t) = \min\left[x_a(t) - r_b(t), \frac{1}{\rho_{crit}(I_z(t))}\right]. \tag{7.3.18}$$

Remark 3.6 (Proposition of modification of (7.3.18))**.** *It would be convenient to replace previous formula (7.3.18) by*

$$x_b(t) = \min\left[\max\left\{0, x_a(t) - r_b(t)\right\}, x_a(t) - \frac{1}{\rho_{crit}(I_z(t))}\right]$$

to ensure that if the local spacing $r_b(t)$ is too high, particle (b) stays inside the node (except if one consider that negative abscissa matches with a position inside the node and not with a position on one incoming branch). Indeed it could only exit once the leader particle (a) has sufficiently advanced.

The term $\frac{1}{\rho_{crit}(I_z(t))}$ ensures that the spacing is never less than the critical spacing defined as the inverse of the critical density.

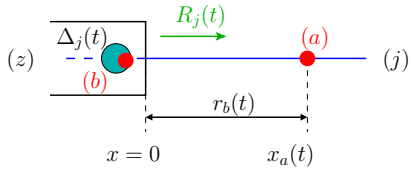

FIGURE 7.9 – Illustration of the node-link interface.

The overall algorithm is recapitulated in pseudo-code form in Algorithm 4.

Remark 3.7 (Problems to solve for a tractable algorithm)**.** *There are several problems to solve for the numerical implementation of Algorithm 4 :*

- *Vehicle labeling on branches (when $N_I > 1$ and $N_0 > 1$) : labels can be multi-defined if we give a number according to the order in which vehicles go through a pre-determined position of whatever branch. Notice that the question is also fundamental for the Hamilton-Jacobi approach and conduces to the choice of fixed coefficients to avoid these multi-definition and ensure comparison principle.*
- *Adapt the internal state model to true Lagrangian discretization (do not compute for flows for instance).*
- *Properly establish the expression of upstream and downstream boundaries (7.3.12) (and not link-node and node-link interfaces) into Lagrangian coordinates, which is not done in [147].*
- *Improve the representation of trajectories through the junction, say reduce the numerical error due to time discretization (see Figure 7.10).*

4 A new computational method for GSOM models on junctions

In this section, we describe the numerical scheme adapted for the generic Lagrangian GSOM model (7.2.6) posed on a junction. We set a *junction* as the union of N_I incoming and N_O outgoing branches that intersect at a unique point called the junction point (or the node in the traffic literature). We also highlight the specific treatment of boundary conditions. More precisely, we describe how to treat :

Algorithm 4 Pseudo-code implementation for the particle (Lagrangian) discretization of the GSOM model on a single junction, according to [147].

Input: t_0 and t_{max}, ΔN and Δt, {Input time domain, label and time steps}
$x_n(t_0)$ and $I(n, t_0)$ for all n (vehicle labels), {Input initial conditions}
L, N_I and N_0, {Input parameters of the network (length of branches, number of incoming and outgoing branches}
N_z^{max}, $N_{z,j}(t_0)$, {Input parameters of the node}
$(\gamma_{ij})_{i,j}$, {Input turning fractions}

for $t = t_0$ to t_{max} **do** {Iteration on considered time domain}
  for $i = 1$ to N_I **do** {Iteration on incoming branches}
    for all vehicles n on the branch (i) **do**
      compute $x_n(t+1)$ using (7.4.20), {Computation of the position according to Euler scheme}
      if particle (a) has no leader **then**
        compute the local density $\rho_a(t)$ using (7.3.16)
        compute the speed of particle $v_a(t) = \mathfrak{I}(\rho_a(t), I_a(t))$
        compute the position of particle (a) using (7.4.20).
        if $x_a(t+1) > 0$ **then** {The closest vehicle to the node (z) will exit the branch}
          $N_z(t+1) \leftarrow N_z(t) + 1$ {Update the number of vehicles stored in the node}
        end if
      end if
    end for
  end for
  for $j = N_I + 1$ to $N_I + N_0$ **do** {Iteration on outgoing branches}
    for all vehicles n on the branch (j) **do**
      compute $x_n(t+1)$ using (7.4.20) {Computation of the position according to Euler scheme}
      if particle (a) has no follower **then**
        compute the local flow $R_j(t)$ according to (7.3.15) and the local density following (7.3.17)
        compute the speed of following particle (b) by $v_b(t) = \mathfrak{I}(\rho_a(t), I_z(t))$
        compute the position of particle (b) using (7.4.20) knowing that $x_b(t) = 0$.
        if $x_b(t) \leq 0$ **then** {The vehicle has entered the branch (j)}
          $N_z(t+1) \leftarrow N_z(t) - 1$ {Update the number of vehicles stored in the node}
        end if
      end if
    end for
  end for
  for the node (z) **do** {Dynamics inside the node}
    compute the internal state model (7.3.13)
  end for
end for

Output: $x(.,.)$ trajectories of vehicles into the whole computational domain.

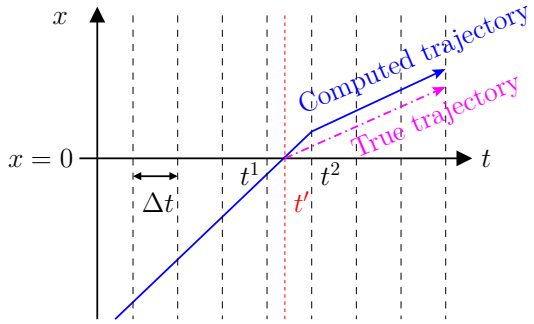

FIGURE 7.10 – Illustration of the error made due to the discrete time step when passing through the junction.

- the upstream boundary condition for any incoming branch $i \in \mathcal{I} := [\![1, N_I]\!]$,
- the downstream boundary condition for any outgoing branch $j \in \mathcal{J} := [\![N_I+1, N_I+N_O]\!]$,
- the boundaries of the junction point encompassing the link-node and node-link interfaces.

We partially follow [172] in which the authors describe boundary conditions for the Hamilton-Jacobi equation (7.2.7) associated to the Lagrangian GSOM model (7.2.6).

4.1 Lagrangian discrete model

Let us introduce time and particle discretizations. We denote by Δt and ΔN the time and particle steps respectively (see Figure 7.4). We set $I_n^t := I(t\Delta t, n\Delta N)$, for any $t \in \mathbb{N}$ and any $n \in \mathbb{Z}$.

We have the choice between two discrete models : either we deal with the discrete particle spacing defined as

$$r_n^t := r(t\Delta t, n\Delta n), \quad \text{for any} \quad (t,n) \in \mathbb{N} \times \mathbb{Z},$$

where r solves the Lagrangian GSOM model (7.2.6), or we consider the discrete particle position that reads

$$\mathcal{X}_n^t := \mathcal{X}(t\Delta t, n\Delta N), \quad \text{for any} \quad (t,n) \in \mathbb{N} \times \mathbb{Z},$$

where $(\mathcal{X}, I)$ solves the Hamilton-Jacobi problem (7.2.7) associated to (7.2.6).

Notice that the physical extension of particle $n \in \mathbb{Z}$ is $[\mathcal{X}_n^t, \mathcal{X}_{n-1}^t[$.

In the first case, we would have to solve the following numerical scheme for (7.2.6)

$$\begin{cases} r_n^{t+1} := r_n^t + \dfrac{\Delta t}{\Delta N}\left[V_{n-1}^t - V_n^t\right], \\ V_n^t := \mathcal{V}\left(r_n^t, I_n^t\right), \\ I_n^{t+1} = I_n^t + \Delta t \varphi\left(I_n^t\right) \end{cases} \tag{7.4.19}$$

while in the second case, i.e. for (7.2.7) the appropriate numerical scheme is defined as follows

$$\begin{cases} \mathcal{X}_n^{t+1} = \mathcal{X}_n^t + \Delta t V_n^t, \\ V_n^t := \mathcal{V}\left(\dfrac{\mathcal{X}_{n-1}^t - \mathcal{X}_n^t}{\Delta N}, I_n^t\right), \\ I_n^{t+1} = I_n^t + \Delta t \varphi\left(I_n^t\right) \end{cases} \tag{7.4.20}$$

Notice that both approaches are very similar and give back the same results. Indeed, one can remark that if we have

$$r_n^t := \frac{\mathcal{X}_{n-1}^t - \mathcal{X}_n^t}{\Delta N},$$

then (7.4.19) is simply deduced from (7.4.20). By the way, knowing the spacing at each numerical steps, it is easy to compute the position of all particles, thanks to a leader particle trajectory as a boundary condition.

It is worth noting that both schemes are first order schemes. The first one (7.4.19) can be interpreted as the seminal Godunov scheme [117]) applied with demand and supply defined in (7.2.8) and the second discrete model (7.4.20) is an explicit Euler scheme.

In order to the numerical scheme (7.4.20) be monotone, time and label discrete steps need to satisfy a Courant-Friedrichs-Lewy (CFL) condition given by

$$\frac{\Delta N}{\Delta t} \geq \sup_{N,r,t} \left|\partial_r \mathcal{V}(r, I(t,N))\right|. \tag{7.4.21}$$

For deducing a particle (Lagrangian) discretization of the Eulerian model described above, it is necessary to take into consideration different elements :

(i) the link model, which is given by either (7.4.20) or (7.4.19) ;

(ii) the upstream (resp. downstream) boundary conditions for an incoming (resp. outgoing) link ;

(iii) the internal junction model, say the way particles are assigned from incoming road $i \in \mathcal{I}$ to outgoing road $j \in \mathcal{J}$ and the (eventual) internal dynamics of the junction point ;

(iv) link-junction and junction-link interfaces (as in micro-macro or hybrid approaches [187]).

4.2 Downstream boundary condition

We assume that we are located at the downstream boundary of a given outgoing road $j \in \mathcal{J}$. Assume the exit point S located at x_S. The downstream boundary data at x_S is given by the downstream supply σ which is discretized as σ^t at time step t. Let n be the last particle located on the link (or at least a fraction $\eta\Delta N$ of it is still on the link, with $0 \leq \eta < 1$). See Figure 7.11.

We define the spacing associated to particle n as

$$r_n^t := \frac{x_S - \mathcal{X}_n^t}{\eta \Delta N}.$$

The fraction η is instantiated at the first time step following the exit of particle $(n-1)$, as follows

$$\eta = \frac{x_S - \mathcal{X}_n^t}{r_n^t \Delta N}.$$

Now, we have to distinguish two cases :

- either $\mathcal{V}(r_n^t, I_n^t) \leq \sigma^t r_n^t$: in this case, the downstream supply is sufficient to accommodate the demand on the link. The spacing is conserved.

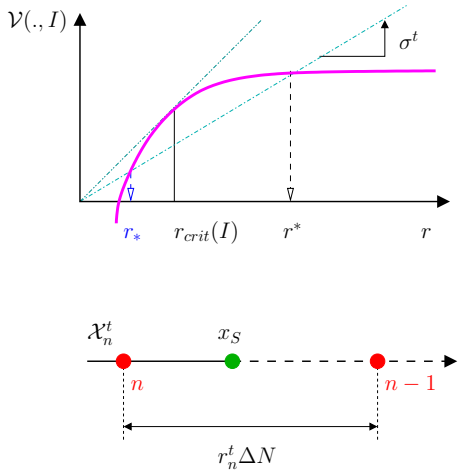

FIGURE 7.11 – Illustration of downstream boundary condition.

- or $\mathcal{V}(r_n^t, I_n^t) > \sigma^t r_n^t$: in this case, the demand on the link cannot be fully satisfied since the downstream supply limits the outflow. Then, we have to solve

$$\mathcal{V}(r_n^t, I_n^t) = \sigma^t r_n^t$$

and we choose the smallest value i.e. $r_n^t = r_*$.

Then, we still update the position of particle n as usual, using (7.4.20). We also need to update the fraction η if the particle has not totally exited the link i.e. if $\mathcal{X}_n^{t+1} < x_S$. The updated fraction is computed as follows

$$\eta \leftarrow \eta - \frac{\Delta t}{r_n^t \Delta N} \mathcal{V}\left(r_n^t, I_n^t\right).$$

Remark 4.1 (Non-satisfaction of the demand)**.** *It may seem strange to solve the equality $\mathcal{V}(r_n^t, I_n^t) = \sigma^t r_n^t$ if we are in the case of the inequality $\mathcal{V}(r_n^t, I_n^t) > \sigma^t r_n^t$. However, as the demand cannot be fully satisfied, the passing flow is actually limited to the supply. We recall that in Lagrangian, the demand and the speed $\mathcal{V}$ are the same. Thus, we have the equality.*

4.3 Upstream boundary conditions

We assume that we are located at the upstream boundary of a given incoming road $i \in \mathcal{I}$. Consider the entry point E located at position x_E. The boundary data is constituted by the upstream demand δ which is discretized as δ^t for time step t. Let n be the last particle entered in the link. The next particle $(n+1)$ is still part of the demand. See Figure 7.12. Assume that particle $(n+1)$ will enter in the link at time $(t+\varepsilon)\Delta t$. Time of entering can be computed thanks to the cumulative flow : particle $(n+1)$ can enter the link once

$$\int_0^t \dot{N}(\tau) d\tau - n = \Delta N.$$

First attempt : "pure" Lagrangian

We follow [172]. We first need to compute the spacing r_{n+1}^t associated with the particle $(n+1)$. We have that

$$\delta^t r_{n+1}^t = \mathcal{V}\left(r_{n+1}^t, I_{n+1}^t\right)$$

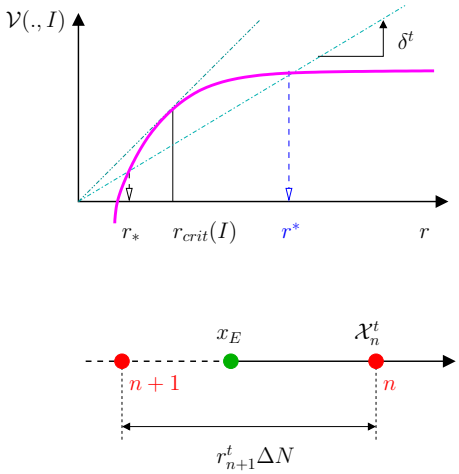

FIGURE 7.12 – Illustration of upstream boundary condition.

which leads to one ($r_{n+1}^t = r_{crit}\left(I_{n+1}^t\right)$) or two solutions. In the latter, we choose the largest value of spacing $r_{n+1}^t = r^*$.

Thus, at time $(t+1)$, we have

$$\mathcal{X}_{n+1}^{t+1} = \underbrace{\mathcal{X}_{n+1}^{t+\varepsilon}}_{=x_E} + (1-\varepsilon)\Delta t \mathcal{V}(r_{n+1}^t, I_{n+1}^t).$$

Once the particle $(n+1)$ has been created an has entered the branch, we update the algorithm for particle $(n+2)$ and so on.

If the demand is not satisfied, it means that particles have to be stored upstream the link and incoming particles are faced to the same problem throughout the time demand exceeds supply. Two solutions are possible : either we continue to consider incoming particles and we store them in a virtual buffer upstream the link with a "vertical" queue, or we can clip the unsatisfied demand and consider one single waiting particle. In our case, we make the choice of the buffer because doing that, we can reproduce the methodology to treat the node-link interface at the junction point.

Remark 4.2 (Error made by selecting the largest value of spacing)**.** *The largest value of spacing r satisfying $r\delta^t = \mathcal{V}(r, I)$ is not necessarily the physical solution. For instance, if we consider*

$$\begin{cases} \rho = \rho_0, & \text{for any} \quad x, \\ I = \begin{cases} I_l, & \text{if} \quad x < x_E, \\ I_r, & \text{if} \quad x \geq x_E. \end{cases} \end{cases}$$

with $I_l \neq I_r$, if we set

$$\rho_{eq} := \mathfrak{I}^{-1}\left\{\mathfrak{I}\left(\rho_0, I_r\right), I_l\right\},$$

then there could be a shock wave (1-wave) that propagates backward at speed

$$\frac{\mathfrak{I}(\rho_{eq}, I_l) - \mathfrak{I}(\rho_0, I_l)}{\rho_{eq} - \rho_0} < 0 \quad \textit{(Rankine-Hugoniot jump condition).}$$

Thus the corresponding density ρ_{eq} can be selected to match the reverse of the smallest *spacing r_* solution of $r\delta^t = \mathcal{V}(r, I_l)$ which is in contradiction with the systematic choice of the largest value of spacing.*

It is noteworthy that the discussion here is to estimate how important is the error made if we consider the largest value of spacing instead of the smallest one. A priori, it could be equivalent to create a particle which is further but moves quicker (say a particle with a higher spacing and a higher speed) or to create a particle nearer but moving slower (i.e. with lower spacing and speed). In this paper, we do not have completed the computations to estimate this error but this will be investigated later by the authors.

Second method : introducing passing flow

We want to adapt to the upstream boundary condition, the methodology developed for the downstream boundary condition (which is detailed in Section 4.2) by introducing a proportion η of the particle that has already entered the link. The problem we face is that, unlike for the downstream where we know exactly the position of the last particle which has exited the link, we do not know precisely the position of the next particle which will enter the link. The situation at upstream is not exactly the inverse of what happens at the downstream that is why the algorithm is not so simple. Thus, we have to position the next particle that will enter the link.

More precisely, if one consider that the last particle that has entirely entered the link at time t is labeled n, we introduce a fraction η^t of the particle $(n+1)$ which has already got into the link at time t. If we denote by q^t the effective flow at the upstream entry and at time t then the proportion η^{t+1} at time $(t+1)$ is given by

$$\eta^{t+1} = \frac{q^t(1-\varepsilon)\Delta t}{\Delta N}$$

where we assume that the particle n has entirely entered the link at time $t_n := (t+\varepsilon)\Delta t$ (see Figure 7.13).

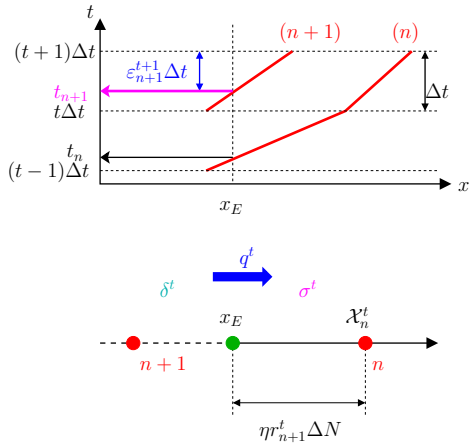

FIGURE 7.13 – Illustration of new upstream boundary condition.

Then we have to compute the flow q^t. If one consider a fictitious "junction" model just upstream the entry point, in which particles are stored before being injected into the link whenever it is possible, then we can deduce a stock model which is similar to an internal junction model : If F^t is the number of particles stored inside the fictitious junction, then the evolution of the stock is given by

$$F^{t+1} = F^t + (\delta^t - q^t)\Delta t, \tag{7.4.22}$$

where δ^t is the (cumulative) demand and q^t is the effective flow of particles which enters the link. Notice that the particle is generated at time $(t+\varepsilon)\Delta t$ if and only if

$$F^t + (\delta^t - q^t)\Delta t = \Delta N.$$

Then, with a simple test, we can distinguish two cases :

- if $F^t > 0$, then there is a (vertical) queue just upstream the entry point and we get

$$q^t = \min\left(\sigma^t, Q_{max}(I^t_{n+1}), \frac{F^t}{\Delta t} + \delta^t\right),$$

  where $Q_{max}(I^t_n)$ is the maximal flow obtained for the fundamental diagram corresponding to the attribute I^t_n.

- if $F^t = 0$, then there is no queue and the flow is simply given by the minimum between the (local) upstream demand δ^t which is given and the (local) downstream demand σ^t, say

$$q^t = \min\left(\sigma^t, \delta^t\right).$$

  We recall that the demand is defined according to (7.2.5), say

$$\sigma^t = \Xi\left(\frac{1}{r^t_n}, I^t_{n+1}, I^t_n; x_E\right) := \Sigma\left(\mathfrak{I}^{-1}\left\{\mathfrak{I}\left(\frac{1}{r^t_n}, I^t_n; x^+_E\right), I^t_{n+1}; x^+_E\right\}, I^t_n; x_E\right).$$

In summary, the algorithm is composed as follows

1. assume that we know the flow q^{t-1} passing through the entry point at time $(t-1)\Delta t$,
2. we update the fraction η^t_{n+1} of particle $(n+1)$ which has already entered the link at time t such that

$$\eta^t_{n+1} = \frac{q^{t-1}\varepsilon^t_n \Delta t}{\Delta N}$$

   where $\varepsilon^t_n \Delta t = t\Delta t - t_n$ and t_n is the exact date at which the rear of particle (n) enters the link at x_E.

3. we also compute the spacing a time t according to particle $(n+1)$

$$r^t_{n+1} = \frac{\mathcal{X}^t_n - x_E}{\eta^t_{n+1}\Delta n},$$

   and the exact position of particle $(n+1)$ and time t

$$\mathcal{X}^t_{n+1} = \mathcal{X}^t_n - r^t_{n+1}.$$

4. then we can compute the trajectory of particle $(^n{+}1)$ for following time steps as follows

$$\mathcal{X}^{t+1}_{n+1} = \mathcal{X}^t_{n+1} + \Delta t \mathcal{V}\left(r^t_{n+1}, I^t_{n+1}\right),$$

   and we distinguish two cases :

   - if $\mathcal{X}^{t+1}_{n+1} \leq x_E$, then we go back to the first step and we itemize in time.

- if $\mathcal{X}_{n+1}^{t+1} > x_E$, then (the rear of) particle $(n+1)$ has entirely entered the link and we compute the exact time of its entry t_{n+1} as follows

$$t_{n+1} = \left(t + (1 - \varepsilon_{n+1}^{t+1}\right) \Delta t, \quad \text{with} \quad \varepsilon_{n+1}^{t+1} = \frac{\mathcal{X}_{n+1}^{t+1} - x_E}{\mathcal{X}_{n+1}^{t+1} - \mathcal{X}_{n+1}^{t}}.$$

  Then we itemize by considering next particle $(n+2)$ (if it has been generated) and so on.

The algorithm in this case is a little bit longer than in the case of "pure" Lagrangian described previously but we can manage the exact arrival time of particles in the upstream buffer. Thus, the methodology can be directly applied to treat any junction-link interface as we will see in what follows.

4.4 Internal state junction model

We consider a point-wise junction model with an internal state (first introduced in [148]) that is used as a buffer between incoming and outgoing branches of the junction. We recall that this buffer has internal dynamics and we can define an internal supply which depends on the number of stored particles. In Eulerian framework, the internal state has some specific attributes such as

$$\begin{cases} N_z(t), & \text{total number of particles in the junction,} \\ N_{z,j}(t), & \text{number of particles stored in the junction and bound for outgoing link } (j), \\ I_z(t), & \text{common driver attribute of particles stored in the junction.} \end{cases}$$

Notice that the link-junction (resp. junction-link) interface is treated as a downstream (resp. upstream) boundary condition. Thus, we apply the algorithms described above, considering the local supply (resp. demand) of the buffers inside the junction point which are defined according to the number of stored particles.

There exists different strategies to deal with the assignment of particles through the junction. They are detailed here below.

- Assume that we have only the information of assignment of particles say the matrix $(\alpha_{i,j})_{i,j}$ that describe the proportion of particles coming from any road $i \in \mathcal{I}$ that want to exit the junction on road $j \in \mathcal{J}$. In that case, we consider that a particle that enters the junction from road i will exit on road j with a probability of $\alpha_{i,j}$. This probability law satisfies $\sum_j \mathbb{P}(i \to i) = \sum_j \alpha_{i,j} = 1$.

- Assume that path through the junction, say the number of the outgoing branch on which the particle $n \in \mathbb{Z}$ will exit, is directly included in the particle attribute $I(t,n)$ and that this information does not evolve in time. In that case, the choice of the outgoing branch for particle n is straightforward.

- Assume now that we consider a global network with many arcs and many junctions. We can imagine that the particle attribute $I(t,n)$ encompass the origin-destination (OD) information for particle $n \in \mathbb{Z}$. This information can depend on time, for example if the particle changes his mind about the path according to the traffic states on the network. One can assume that we can build a reactive assignment model that give us the path followed by particles. This model can be coupled with another model of command, supposed to be governed by a traffic planning agency for

instance. Let imagine that the central planners collect information on travel times on each arc of the network and that these travel times are displayed for particles that enter the network. Then any particle will select the appropriate path at each junction for going to their destination.

Moreover we can distinguish (at least) two different cases for describing the internal dynamics of the junction. Indeed, one can consider that once particles have entered the junction, whatever are their origins, they are immediately assigned to the buffer corresponding to their wished outgoing branch $j \in \mathcal{J}$. But it is also possible to consider that inside the junction point, any particle has a non-trivial travel time before to join their exit, which can be affected by the total number of particle inside the junction point or by the "physical" conflicts that can appear between the internal lanes of the junction point.

5 Discussions and future research

In this chapter, we have discussed a totally new numerical method to deal with the family of GSOM models posed on a junction. The generic GSOM model is recast in the Lagrangian framework and we have a careful look at the boundaries conditions for links and junctions. Notice that in our scheme vehicles are discretized into packets of ΔN particles. Hence, our scheme can be seen as a microscopic car-following model for the particular choice of $\Delta N = 1$.

While we do not provide numerical illustrations in our paper for lack of space, we claim that our method is very convenient for dealing with such macroscopic traffic flow models on networks. Recent models like [39] and [38] can be fully recast into the framework described in our article and solved using our algorithm. Indeed, the attribute is given by the assignment coefficients which are hopefully advected with the traffic flow (if users do not change their minds).

It has been recently proposed in [38] a methodology to solve such models incorporating an internal node (called a *buffer*). The methodology relies on a Lax-Hopf formula on branches outside the junction and it uses a simple update of queues length in the internal node. It could be convenient to compare the numerical efficiency of their numerical method and ours, knowing that Lax-Hopf formula looses part of its accuracy for non-triangular shaped fundamental diagram.

It is worth noticing also that "classical" junction models proposed in the hyperbolic literature (the interested reader could refer to [106] for instance) introduce drivers' turning preferences $(\alpha_{ij})_{i,j}$ which account for the proportion of flow coming from road i that want to exit on outgoing road j. These turning coefficients satisfy a linear transport equation. Thus, the model could be seen as a GSOM model in which the driver attribute I is defined such that $I = \alpha_{ij}$ for some (i, j) origin-destination pattern and $\varphi = 0$. Notice moreover that in this case, the FD is independant on the driver attribute.

By the way, we highlight below some interesting research directions. The discrete model (7.4.20) can be replaced by more complex time integration schemes (see for instance Runge-Kutta schemes, the trapezoidal scheme or the so-called "ballistic" scheme in [229]). Such numerical schemes can be justified mainly if we consider a source term at the r.h.s. in (7.2.6) which is not null, say $\varphi(I) \neq 0$ or depends on r, say $\varphi(I, r)$. In the particular case of $\varphi = 0$, explicit Euler scheme is very satisfying. Moreover it is also imaginable to build an implicit scheme, even if it means a higher computational cost.

Another direction of research would be to compare the numerical results obtained with our monotone scheme and those obtained from the variational approach (see [68]) adapted for junction modeling, which has not been done right now.

Conclusion et perspectives

Cette thèse a permis de mettre en avant tout l'intérêt de l'approche Hamilton-Jacobi dans la modélisation et la simulation du trafic routier sur réseau. Cette approche se veut complémentaire –et non concurrente– de la vision hyperbolique "classique" en théorie du trafic pour la modélisation macroscopique du trafic.

Il est notable que les équations d'Hamilton-Jacobi permettent de réaliser un lien rigoureux entre les échelles microscopique et macroscopique. Du point de vue des applications au trafic, il serait nécessaire de confronter les modèles et les résultats à des données réelles. Cependant, l'auteur attire l'attention du lecteur sur le fait que peu de jeux de données microscopiques sont disponibles. Cela est d'autant plus vrai pour la caractérisation fine des trajectoires des véhicules au travers d'une jonction. Une autre difficulté pour la confrontation pratique des modèles de type GSOM est l'estimation de l'attribut individuel I, qui n'est *a priori* pas mesurable par les techniques classiques. Concernant les systèmes de transports intelligents et plus particulièrement les systèmes coopératifs, ce travail pose certaines bases méthodologique pour l'étude de l'impact de ces systèmes à l'échelle macroscopique. Il ouvre également la voie à de nouveaux modèles (voir Chapitre 2) qu'il serait opportun d'étudier à la fois sur des sections homogènes mais également au travers des jonctions (voir Chapitre 7 pour cela).

Ce travail de thèse a aussi permis de dévoiler un ensemble de pistes de recherche qui sont détaillées dans ce qui suit.

Pistes de recherche

Parmi les perspectives de recherche ouvertes par ce travail, nous pouvons énoncer :

- l'homogénéisation des modèles de poursuite microscopiques avec des temps de retard non nuls $\tau \neq 0$ ainsi que l'homogénéisation stochastique de ces mêmes modèles de poursuite. Nous pouvons par exemple considérer que la loi de vitesse dépende du véhicule et donc de l'indice de celui-ci., comme ce qui suit

$$\dot{x}_i(s) = F\left(x_{i+1}(s-\tau) - x_i(s-\tau), i\right), \quad \text{pour tout} \quad i \in \mathbb{Z}, \quad s \in [0, +\infty).$$

  De façon similaire, il est possible d'introduire un aléa sur les paramètres caractéristiques de la loi de vitesse pour prendre en compte cette dépendance du comportement de conduite selon l'individu. Dans ce cas, nous nous attendons à retrouver un modèle macroscopique de second ordre de type GSOM, tenant compte de l'attribut du véhicule.

- l'homogénisation de modèles microscopiques au niveau d'une jonction, afin de pouvoir caractériser finement l'expression du limiteur du flux A et connaitre les paramètres principaux qui interviennent sur son expression. Cela peut permettre d'établir un modèle phénoménologique du limiteur de flux à la jonction au niveau macroscopique.

- pousser la théorie établie dans [140] au cas de modèles de jonction avec des coefficients $(\gamma^\alpha)_\alpha$ optimisés au cours du temps, selon les densités de véhicules en amont et en aval. Nous avons pu ébaucher quelques résultats par notre approche en simulation, au Chapitre 5. La définition de la solution de l'équation d'Hamilton-Jacobi par rapport aux densités de véhicules, fait intervenir des coefficients de partage $(\gamma^\alpha)_\alpha$ qui sont supposés fixés. Cette contrainte, nécessaire pour obtenir les bonnes propriétés mathématiques du modèle, est relativement forte car elle suppose connue *a priori* la composition du trafic entrant et sortant de la jonction. En pratique, cette composition n'est pas toujours constante dans le temps.

- utiliser la "puissance" des formules de représentation à la Lax-Hopf dans le cas de discontinuités serait également d'un intérêt majeur en théorie du trafic, pour obtenir des méthodes de calcul rapides et efficientes. Cette piste est actuellement explorée par l'auteur.

- exploiter la troisième facette du même problème évoqué en théorie de la viabilité, à savoir proposer un cadre théorique pour le contrôle individuel des mobiles sur le réseau. Ce point fait également l'objet de recherches actuelles.

Caractérisation réaliste du limiteur de flux pour le modèle d'Hamilton-Jacobi à la jonction

Afin de rendre plus réaliste pour la modélisation du trafic routier le modèle Hamilton-Jacobi à la jonction, l'auteur a suggéré à R. Monneau et C. Imbert d'inclure un flux sous-optimal à la jonction. Ils ont réussi à montrer dans [140] que le modèle était bien posé sous des hypothèses plus faibles sur l'Hamiltonien en comparaison à [141] ainsi qu'en incluant un limiteur de flux à la jonction. Cette sous-optimalité à la jonction correspond aux gênes microscopiques dus aux déplacements des véhicules à l'intérieur de la jonction, aux conflits entre mouvements tournants et aux processus d'insertion des véhicules. Notons que les conflits microscopiques sont non-négligeables à l'échelle d'une jonction en milieu urbain. Souhaitant conserver un modèle macroscopique de jonction ponctuel, cela nous amène à approximer les conflits microscopiques entre véhicules et à négliger la dimension spatiale de la zone d'entrecroisement.

Le lecteur intéressé par la littérature pourra se référer à la thèse de Ruben Corthout [64]. En particulier, le chapitre 5 de la thèse [64] est dévolu à cette question sous la forme de contraintes de demandes internes. Ces contraintes ont été également proposées dans le papier de Flötteröd et Rohde [97]. Il est intéressant de noter que ces contraintes ressemblent fortement aux notions d'offre et de demande internes définies par Khoshyaran et Lebacque dans leurs modèles à état interne (avec état dynamique ou à l'équilibre) [148]. L'idée reste similaire à la formule du minimum entre offre aval et demande amont, y compris au point de jonction.

Historiquement, le premier papier doit remonter au modèle dit SSMT (pour simulation semi-macroscopique du trafic) de Lebacque [162] en 1984. Il y a également une série de papiers orchestrés par W. Brilon et R.J. Troutbeck dans les années 2000 sur le calcul de la capacité des intersections (souvent des ronds-points) à partir de considérations microscopiques comme les temps critiques d'insertion (acceptation de créneaux). Cette question de la capacité des intersections est aussi traitée dans le Traffic Flow Theory, chapitres 8 et 9 par R.J. Troutbeck [108]. Dans les travaux de Chevallier et Leclercq [55, 56], le processus d'insertion des véhicules au niveau d'un convergent (deux voies entrantes et une voie sortante) est donné par une règle d'acceptation de créneau avec un temps inter-véhiculaire (TIV ou *headway* en anglais) critique et une distribution probabiliste des valeurs de TIV.

Ces modèles d'insertion sont agrégés au niveau macroscopique sous la forme d'un feu fictif. Les durées de temps de feu rouge et de feu vert sont déterminées selon la répartition des TIV acceptés.

Une note sur l'approche choisie

Malgré toutes les critiques que peuvent concentrer les modèles hydrodynamiques du trafic et principalement le modèle LWR, ils ont la particularité de reproduire et d'expliquer une majeure partie des phénomènes du trafic. Cependant, il est nécessaire d'aller au delà de la simple analogie entre le trafic véhiculaire sur un réseau de routes et l'écoulement d'un fluide au sein d'un réseau de tuyaux (par exemple). Là où les particules de fluide sont "inertes", les couples conducteur-véhicule sont doués de capacités supplémentaires. L'une de ces capacités est de pouvoir recevoir de l'information, la traiter et en déduire une décision amenant à une action. Cela constitue un des principaux leviers pour agir sur les problèmes de congestion en trafic. En effet, en fournissant aux véhicules les informations utiles et tout en assurant leur sécurité par des systèmes d'assistance à la conduite (voire dans un futur proche, avec des véhicules totalement autonomes), il est possible d'opérer un gain substanciel en termes de niveau de service, en "compressant" par exemple les mobiles (c'est-à-dire en réduisant les interdistances ou de manière équivalente en augmentant la densité des véhicules) tout en assurant une vitesse de circulation élevée. Cela irait donc à l'encontre de la chute du flux lorsque la densité augmente (partie décroissante du diagramme fondamental en débit-densité).

Il est vrai que cela ne constitue qu'une solution de type "technologique" à un problème de société. Cette approche n'est ni la seule possible, ni n'assure la solution optimale. C'est un parti pris assumé de la thèse. Il est également permis de réfléchir à changer en profondeur les modes de transport, tout comme il est possible de remettre en question l'organisation des villes modernes qui favorise l'étalement urbain, la polarisation de l'espace et accentue les problèmes de circulation. La réflexion dépasse le simple cadre du trafic routier, mais il semble utile de replacer ce travail de thèse dans son contexte global.

Annexe A

Etat de l'art des modèles et méthodes en trafic sur section homogène

Ce chapitre est une version longue d'un article qui a fait l'objet d'une parution dans un ouvrage collectif [66].

Sommaire

La problématique de la modélisation du trafic routier suscite un vif intérêt parmi le cercle scientifique depuis plus d'une soixantaine d'années. Il est possible de décrire le trafic routier très trivialement comme étant le processus de transport depuis une origine et vers une destination par le moyen des infrastructures routières en opposition à l'aérien, au ferroviaire, au fluvial ou au maritime. Le trafic routier résulte alors de la somme de comportements individuels des usagers cherchant à rejoindre chacun leur destination, depuis leur point d'origine sur un réseau donné. Afin de pouvoir reproduire et comprendre la réalité physique de ce phénomène réel complexe, les modèles de transports se sont développés d'une manière remarquable pendant les deux dernières décennies et désormais de nombreux acteurs proposent ou commercialisent des logiciels de simulation aux finalités très diverses. En France, plusieurs acteurs interviennent dans le domaine des transports comme les décideurs publics, les gestionnaires de réseau, les organismes de recherche et les organismes d'ingénierie ou encore les bureaux d'étude. Chacun de ces opérateurs a un rôle différent pour la modélisation et la simulation du trafic, qu'ils soient "réalisateurs" ou "consommateurs" de ces outils. Dans l'esprit de [168], ce premier chapitre se propose de peindre aussi synthétiquement que possible les évolutions récentes en termes de modélisation et de simulation dans le domaine du trafic routier. Il s'attache également à montrer les nombreuses articulations entre la modélisation ou la simulation dans ce domaine. En effet, modélisation et simulation sont deux outils toujours complémentaires et rarement concurrents.

Le chapitre est structuré de la façon suivante : la section 1 se propose de définir les principales notions usuelles dans le domaine du trafic routier. La section suivante (section 2) établit un rapide panorama historique des outils de modélisation et de simulation. Plus spécifiquement, les sections 3 et 4 présentent respectivement les différents modèles de planification et d'écoulement du trafic routier. Une présentation de certains des plus courants logiciels de simulation actuels est enfin proposée dans la section 4.4.

1 Quelques définitions

Dans l'ensemble de ce premier chapitre, nous nous intéressons au distinguo entre "modélisation" et "simulation". D'une part, la modélisation a pour but de concevoir un modèle permettant de mieux appréhender la réalité physique d'un phénomène ou d'un système déterminé, trop complexe à appréhender directement. Ainsi la modélisation exprime souvent de façon mathématique le fonctionnement d'un système de façon continue dans le temps tout en cherchant la compréhension et la simplification analytique de ce système. Un modèle a pour finalité d'être testé numériquement dans un outil de simulation.

D'autre part, la simulation va s'appuyer sur les « produits » de la modélisation afin de pouvoir étudier les effets d'une action sur ce système. La simulation cherche à décrire la dynamique de systèmes complexes et à tester différents scénarios. Ces expérimentations sont menées grâce à l'outil informatique. En somme un outil de simulation peut se réduire schématiquement à la programmation sur ordinateur d'un certain modèle. Depuis quelques années, nous avons assisté au développement des techniques informatiques et notamment la puissance et la vitesse de calcul des microprocesseurs actuels ainsi que la capacité de stockage de données des ordinateurs. Ces évolutions permettent d'envisager des applications en quasi temps réel, du moins à l'ordre de quelques secondes là où des années auparavant il aurait fallu plusieurs jours. Cette rapidité de calcul permet en outre de tester en simulation de grandes variétés de configurations. Dans le cas du trafic routier, il peut s'agir de tester plusieurs stratégies de régulation du trafic (gestion des dépassements, de la vitesse limite autorisée, gestion des carrefours à feux) mais aussi de la configuration de l'infrastructure : implantation d'un carrefour, modification du nombre de voies d'une

section, etc.

Etant une image de la réalité pour mieux comprendre un phénomène complexe, un modèle est nécessairement basé sur des hypothèses simplificatrices. A ce sujet, George E. P. Box (le désormais célèbre statisticien) déclarait que "tous les modèles sont faux mais certains sont utiles" [1]. Il est souvent nécessaire de se référer aux hypothèses initiales du modèle afin de savoir si notre cas d'utilisation correspond bien au domaine de validité du modèle. Dans le cas où le flux de véhicules est vu par le prisme de la dynamique des fluides, il est important de noter la différence entre le nombre de molécules dans une mole (donné par le nombre d'Avogadro soit $N_A = 6.2 \times 10^{23}$ éléments) et le nombre maximal de véhicules dans un kilomètre (de l'ordre de quelques centaines d'éléments). Nous voyons là un exemple d'hypothèse simplificatrice pour les modèles hydrodynamiques.

La modélisation du trafic au sens large comprend à minima deux stratégies d'approches différentes mais non indépendantes. Dans le cas qui nous intéresse, les transports se prêtent mal à la théorisation car ils sont à la fois trop complexes pour permettre une description par éléments mais ils sont aussi insuffisamment complexes pour permettre les "passages à la limite" usuels en physique. La première est reliée à l'étude du processus d'affectation des usagers sur un réseau donné. Nous définissons l'affectation comme la façon dont se répartit le volume connu d'individus (définissant une *demande*) sur un ensemble de chemins formant un réseau caractéristique d'infrastructures (formant l'*offre*). La seconde branche se propose de décrire plus finement l'écoulement des véhicules sur un chemin fixé. Elle est donc complémentaire de la première dans le sens où elle exploite les résultats de cette affectation. Il s'agit dans ce cas de comprendre les comportements des usagers en poursuite ou encore les phénomènes d'insertion et de changements de voie. L'étude de l'écoulement du trafic a aussi pour ambition de pouvoir décrire et expliquer les phénomènes de congestion.

2 La multiplicité des outils

2.1 Le constat historique

Le développement des modèles de transport trouve principalement son origine dans différents travaux des années 1950. Citons par exemple les articles de Lighthill, Whitham (1955) [184] et Richards (1956) [221] qui ont les premiers proposé un modèle hydrodynamique de trafic, mais aussi Wardrop (1952) [233] et Beckmann (1956) [25] à qui l'on doit des concepts aujourd'hui grandement utilisés pour décrire l'affectation à l'équilibre du trafic comme la différentiation entre équilibre usager et équilibre système. A compter de point de départ, le nombre de modèles et d'outils de simulation a fortement augmenté. Ainsi en 2004, dans un rapport du Department of Transportation des Etats-Unis [2], pas moins de 150 modèles/simulations de trafic véhiculaire pour la planification et la conception, la gestion et tarification ou encore le contrôle ont été recensés.

La modélisation du trafic routier permet ainsi la représentation d'un phénomène social qui est apparu avec les activités humaines et le besoin de transport (de personnes ou de marchandises) mais qui a très vite fait face aux problèmes de congestion et de sécurité. Rappelons que les véhicules automobiles se multiplient au tout début du vingtième siècle avec notamment aux Etats-Unis, le modèle de la Ford T, premier véhicule de grande série apparu en 1908. L'accès populaire à la voiture et à son utilisation entraîne une forte hausse de la demande de transport et de ce fait, l'apparition des premières congestions. Cela entraîne une augmentation des diverses pollutions (sonore, aérienne, visuelle), accentue

1. "Essentially, all models are wrong, but some are useful." Box, George EP, and Norman R. Draper. *Empirical model-building and response surfaces*. John Wiley & Sons, 1987, p. 424.
2. Accessible en ligne à http://www.ops.fhwa.dot.gov/trafficanalysistools/tat_vol2/

les risques (accidentologie, environnement, crise énergétique). Cela représente aussi une forte perte de temps pour les usagers et une diminution conséquente de la productivité tant il y a un lien fort entre système de transport et système économique. Les besoins de régulation du trafic routier en ont donc fait un sujet de recherche très important. Notons que les prérogatives changent peu au fil du temps bien qu'il y ait un intérêt accentué pour les besoins d'informations (état du système, évaluation *a posteriori*) et de gestion du système.

En règle générale, le recueil de données propres est un écueil majeur de la modélisation. Aussi les travaux de recherche sont aussi rythmés par la disponibilité ou non d'une base de données exploitable. Historiquement, les premières études afin d'appréhender empiriquement ce phénomène sont à mettre au crédit de Bruce Greenshields [120] avec en 1935 une méthode photographique de décomposition du mouvement (Figure 1). Signalons aussi les études de trafic sous le tunnel Lincoln dans les années 50 à New-York, et plus récemment le programme NGSIM à Berkeley en Californie [3] ou encore les données MoCoPo de Grenoble [4].

La modélisation et la simulation bénéficient graduellement de nouvelles ressources. Il convient de citer avant tout l'émergence des ressources informatiques avec de nouveaux matériels (ordinateurs plus puissants) et de nouveaux logiciels (langages de programmation et sorties graphiques perfectionnées). Rappelons également l'apparition de nouveaux matériels de mesure et d'acquisition de données (caméras vidéo haute définition, lecteurs de plaques minéralogiques). La modélisation profite également des avancées scientifiques d'autres disciplines en mathématique, physique ou recherche opérationnelle. La prise en compte dans les années 60 des systèmes dynamiques et de la non-linéarité c'est-à-dire de la non-proportionnalité entre les effets et les causes illustre un des apports de la mathématique à la modélisation du trafic. Autre exemple, le concept physique d'auto-organisation [27, 126, 146] prend tout son sens en trafic. L'idée est qu'un comportement d'ensemble non-trivial peut émerger des interactions entre les nombreux agents composant un système complexe. La visée applicative directive serait de conditionner le comportement individuel des agents afin d'obtenir un comportement émergent global optimal.

2.2 Modèles et simulations des transports

Dans le cadre des déplacements sur un réseau routier, il existe une grande variété d'approches en modélisation. Il est possible de les regrouper en quatre classes (à savoir les modèles d'occupation du sol, ceux de demande de déplacement, les modèles d'écoulement du trafic ou encore les modèles de gestion de réseau) qui sont regroupés ci-dessous. Nous nous intéresserons plus particulièrement aux modèles de demande ainsi qu'aux modèles d'écoulement.

3. http://ngsim-community.org/
4. http://mocopo.ifsttar.fr/

Catégorie de modèles	**But**	**Echelle temporelle**	**Echelle spatiale**
Occupation du sol	Planification, gestion	Très long terme	Global
Demande de déplacement	Planification	Long terme	Global
Ecoulement de trafic	Evaluation, planification ou gestion	Court terme	Global ou local
Gestion de réseau	Contrôle, régulation	Très court terme	Local

TABLE A.1: Classes de modèles utilisés en transport et leurs différences

D'une part, les modèles statiques sont généralement utilisés dans le cadre de la planification des transports et des réseaux. Ils permettent de disposer de prévisions de trafic pour dimensionner au mieux des infrastructures très coûteuses et construites pour le long terme. Ces modèles cherchent à connaitre ou à simuler la demande de trafic en certains points du réseau dans le but de pouvoir proposer de façon statique (d'où le terme de *planifier* dans une démarche de prévision) des méthodes de régulation soit en agissant sur la répartition de la demande, soit en modulant l'offre. Dans ce cadre-là, les modèles de trafic sont essentiellement utilisés pour estimer une affectation (statique ou dynamique) de la demande (correspondant aux véhicules) sur un réseau routier et pour pouvoir gérer cette demande de trafic selon l'offre du réseau. Aussi, en amont se trouvent des modèles de génération, de distribution (étape à laquelle est calculée la matrice origine-destination) et d'affectation. Ce modèle est classiquement appelé modèle à quatre étapes, en considérant également une étape de choix modal.

D'autre part, les modèles dynamiques permettent de décrire l'écoulement physique du trafic routier. Certains ont été bâtis sur des analogies entre l'écoulement du trafic routier et l'écoulement d'un fluide ou la cinétique des gaz. D'autres modèles considèrent le réseau comme une suite de cellules s'échangeant de l'information sous forme de véhicules. Enfin, d'autres cherchent à décrire le mouvement d'un véhicule en fonction des caractéristiques du véhicule qui le précède. Ces modèles sont notamment utilisés pour des stratégies de régulation des congestions qui se forment lorsque la demande de trafic devient supérieure à l'offre. Cela comprend des méthodes comme le délestage, la Gestion Dynamique des Voies ou la Régulation Dynamique des Vitesses. Notons aussi une autre différence entre ces deux types de modèles : tandis que les modèles de planification permettent la mise en place de méthodes sur le moyen et le long terme, les modèles dynamiques ont pour but l'utilisation de moyens de gestion sur le court terme.

3 Modèles et simulation de type planification

3.1 Affectation statique

Une étude de trafic débute lors de la commande par un opérateur qui souhaite tester une modification future soit de son réseau (ajout ou suppression de voies), soit de la demande (construction d'un centre commercial) ou encore de la stratégie de gestion de son réseau (implantation d'un feu tricolore, baisse de la vitesse maximale). Afin de pouvoir

répondre à cette commande, il est nécessaire de connaitre le réseau, la demande et la stratégie de gestion, actuels et futurs dans chacun des cas. Afin de savoir caractériser la situation existante, il faut déterminer la demande actuelle : la démarche est différente selon si l'on travaille sur un axe ou sur l'ensemble d'un réseau maillé. Dans le premier cas, la demande sera estimée en amont de la section d'étude tandis que dans le second cas, il sera nécessaire de calculer une matrice des déplacements de type origine-destination. De plus, il est important de connaitre l'offre du réseau et ses paramètres pouvant agir sur la capacité de l'infrastructure (déclivité, présence d'un convergent et/ou d'un divergent, etc.).

Concernant la description de la demande actuelle, la plupart des logiciels ne nécessite en entrée que la donnée des matrices origine-destination. Certains comme AIMSUN et SYMUVIA demandent aussi à connaitre les flux directionnels c'est-à-dire les proportions de mouvements tournants à chacun des carrefours du réseau. Notons que la matrice origine/destination fournie est déterminée de façon statique pour un instant donné. Classiquement, il s'agit de l'heure de pointe du matin ou du soir.

L'étape suivante de l'étude de trafic consiste à simuler avec un certain logiciel, la situation existante. A partir des données actuelles, le logiciel doit être en mesure de retourner des scénarios en accord avec les faits observés sur le réseau. Il est donc important de corriger les biais éventuels en agissant sur les paramètres des modèles utilisés par le logiciel. Le logiciel DYNASIM possède par exemple différents paramètres pour la loi de poursuite, pour le modèle de changement de voie ou encore pour le modèle d'insertion. Cette étape ressemble à un calage du logiciel.

La dernière étape consiste à modifier l'élément souhaité (réseau et/ou demande et/ou stratégie de gestion) et de pouvoir quantifier les impacts entraînés sur l'écoulement du trafic. Il est intéressant de noter qu'il y a pour cette étape-là du travail, une réelle dépendance des résultats fournis par le logiciel vis-à-vis du nombre de réplications effectuées.

Historiquement, le modèle statique est le modèle le plus ancien utilisé pour les études de planification. Dans les années 80 en effet, les études étaient essentiellement portées sur le domaine routier. Désormais, elles intègrent également les projets de transports en commun. Le modèle statique a pour but de déterminer une matrice des déplacements *routiers* en s'appuyant sur le principe de la modélisation à quatre étapes. Le modèle à quatre étapes comprenant génération, distribution, choix modal et affectation est un modèle éprouvé et adopté par de nombreux outils de simulation comme CUBE/TRIPS, CUBE/MINUTP, OMNITRANS, SATURN, TRANSCAD. La quatrième étape du modèle à savoir l'affectation sur les arcs du réseau, est effectuée par simulation grâce à des logiciels du type de VISUM. Il s'agit d'une affectation statique, ne permettant que le calcul des plus courts chemins, sans aucune prise en compte du phénomène de propagation du trafic. Dans VISUM, la répartition est réalisée selon le modèle LOGIT, et axé autour d'un algorithme TRIBUT, fonctionnant sur un double critère : à la fois le temps de parcours (avec une distribution de la valeur du temps) et le prix. Pour une présentation plus complète du modèle à quatre étapes, le lecteur est renvoyé à [32].

3.2 Affectation dynamique

Il est très difficile de prendre en compte la dimension temporelle des variables pour l'affectation. Il s'agit d'un domaine de recherche très actif. Les modèles actuels sont des modèles simplifiés de propagation mésoscopiques supposant que la durée de déplacement sur un tronçon est fonction du volume de véhicules. Ces modèles se rencontrent dans les logiciels CONTRAM, DYNASMART ou DYNAMIT. D'autres ont une approche macroscopique comme METACOR ou METANET.

En connaissant à la suite d'observations et/ou de simulations statiques, le volume de trafic s'écoulant par chacune des branches du réseau, il est possible d'utiliser alors des modèles dynamiques de gestion du trafic : ils s'appuient à la fois sur la gestion des carrefours (y compris des carrefours à feux), ce qui couvre la gestion des priorités ou des changements de phase de feux mais aussi la gestion de l'information routière (stationnement, état de trafic...) et de la signalisation (directionnelle et normative).

La simulation dynamique comprend non seulement l'affectation dynamique du trafic mais aussi la simulation de l'écoulement dynamique de celui-ci sur le réseau. Le principe est de pouvoir illustrer le fonctionnement du réseau mais surtout d'obtenir des données de trafic simulées, de multiples natures comme les débits, la vitesse pratiquée, le taux d'occupation et/ou la densité, etc. Un des indicateurs les plus souvent utilisés lors de la simulation dynamique est sûrement la matrice des temps de parcours sur le réseau. Cela permet de savoir quel est l'impact de la modification du réseau et/ou de la demande et/ou de la stratégie de gestion, sur les déplacements individuels des usagers. D'autres indicateurs peuvent être utilisés afin de caractériser les impacts des modifications.

La simulation dynamique s'intéresse classiquement à :

- Des points de mesure particuliers où il est possible d'avoir des données *in situ* (notamment avec la présence d'une station de comptage) ;
- Des sections du réseau pouvant engendrer de la congestion, comme les intersections, les convergents ou les divergents ;
- Des itinéraires déterminés de type Origine/Destination ;
- L'ensemble du réseau et son fonctionnement global.

Les simulations dynamiques permettent d'analyser le fonctionnement d'un aménagement à partir de plans, de matrices de déplacements Origine/Destination et de plans de feux. Elle permet également l'analyse des apports éventuels d'une régulation d'accès ou d'une gestion dynamique de trafic. Cette approche s'est par ailleurs fortement développée lors des dernières années avec la nécessité de mettre en place une gestion du trafic performante. Enfin, la simulation dynamique est utilisée pour analyser des scénarios d'événements routiers prévisibles de grande importance (accidents critiques, travaux particuliers, sous tunnel par exemple, etc.). Cela permet de mettre en place des Plans de Gestion du trafic, reprenant un catalogue de ces scénarios d'accident et la stratégie à adopter afin d'en limiter les inconvénients. Cela permet une meilleure compréhension du réseau d'infrastructures routières tout en facilitant les prises de décision et la communication avec les différents partenaires.

Les outils de simulation dynamique font bien souvent référence à la modélisation microscopique du trafic. Les véhicules sont alors pris en compte de façon individuelle. La modélisation porte sur leur cinématique propre suivant leur comportement et leur environnement proche (approche d'un point singulier comme un cédez-le-passage, manœuvre d'insertion ou de dépassement, etc.).

Les modèles implémentés dans les logiciels de simulations sont parfois de type stochastique dans la mesure où les paramètres des véhicules sont attribués de façon aléatoire, à partir de distributions statistiques. Lorsque c'est le cas, le caractère aléatoire du paramétrage impose de lancer plusieurs réplications, c'est-à-dire plusieurs simulations avec des paramètres de génération différents afin que le modèle puisse être en moyenne représentatif de l'infrastructure mais également que l'on puisse mieux appréhender les différents fonctionnements de ce réseau.

Les types de modèles qui interviennent sont les modèles de poursuite, les modèles de dépassement et d'insertion. La loi de poursuite régit la progression des véhicules qui

adoptent différentes stratégies (selon le modèle utilisé) comme maintenir une certaine distance intervéhiculaire lorsqu'ils se rapprochent de leur véhicule *leader*. Les lois de dépassement interviennent pour maintenir la vitesse désirée des véhicules, occuper les voies lorsqu'elles sont saturées ou pour se positionner sur la file adéquate lors de l'engagement d'une manœuvre de changement de direction. Pour finir, les lois d'acceptation de créneaux (traduction directe de l'anglais *gap acceptance*) permettent de prendre en compte le respect des autres véhicules en cas de situation de changement de voie, de cédez-le-passage ou de stop. Les injections de véhicules dans le réseau suivent également lois de distribution aléatoire, sous contrainte de respecter les volumes totaux de trafic entre chaque couple de la matrice origine/destination.

Liens entre les modèles d'affectation du trafic et les modèles d'écoulement sur un réseau

L'utilisation pratique de modèles en trafic vise à permettre un écoulement optimal sur un réseau, prévoir l'affectation des usagers sur un réseau selon une logique origine/destination, connaitre la charge des réseaux, prévoir la signalisation adéquate et ses caractéristiques (décomposition du cycle de feux tricolores), réduire et limiter les phénomènes de congestion, mais aussi l'ensemble des externalités du trafic.

Les modèles d'écoulement de trafic ont été développés dans le but de répondre aux besoins opérationnels en trafic, de gestion et de planification des infrastructures, de contrôle des flux et d'évaluation des niveaux de service. La plupart de ces applications nécessitent des modèles qui se doivent d'être simples et robustes, avec de modestes besoins en termes d'analyse et d'utilisation de données ainsi qu'en termes de coûts de calcul informatique. C'est ce que nous allons voir dans la partie suivante.

4 Modèles d'écoulement du trafic

Dans la grande majorité des approches de modélisation, le trafic automobile est assimilé à un fluide où les véhicules sont identifiés à des particules en interaction. Ces interactions ont été étudiées avec soin depuis le milieu du XX$^{\text{ème}}$ siècle et ont permis de dégager un grand nombre de lois de comportement. Celles-ci permettent par exemple de construire des modèles microscopiques très utiles, en particulier pour la conception et pour la simulation à petite échelle du trafic. Cependant, ces modèles microscopiques se révèlent n'être plus cohérents pour de nombreuses autres applications telles que la gestion du trafic, la planification et l'évaluation des réseaux. En effet, l'utilisation de ces modèles est parfois limitée par l'impossibilité d'avoir accès à la description détaillée des dynamiques individuelles des véhicules. Dans ces cas, l'utilisation de modèles macroscopiques s'impose.

A l'image des classifications usuelles proposées par la littérature, nous considérons les modèles de trafic selon le niveau de détail qu'ils proposent. Nous distinguerons ainsi les modèles microscopiques des modèles macroscopiques. Nous faisons volontairement l'impasse sur l'existence des modèles dits mésoscopiques qui permettent de caractériser le comportement du trafic selon des paquets de véhicules. Notons que la classification pourrait s'effectuer selon leur mise en œuvre ou encore la représentation du phénomène.

4.1 Modèles macroscopiques

Les modèles macroscopiques sont issus d'une analogie hydrodynamique de l'écoulement des véhicules. L'objet de ces modèles est de pouvoir caractériser le comportement global du trafic, à une échelle d'étude relativement importante (dizaine ou centaine de mètres

en espace et minute en temps). Ces modèles ont la particularité d'avoir une forme analytique simple et de pouvoir être discrétisés efficacement. Ils sont donc tout particulièrement utilisés dans le cadre de la modélisation des grands réseaux. Leurs applications courantes couvrent la simulation du trafic en vue de la planification et de la conception des infrastructures, mais couvrent aussi la gestion dynamique du trafic et l'évaluation de ces mesures de gestion *a posteriori*. Nous retrouvons les modèles macroscopiques discrétisés dans différents logiciels comme SSMT, NETCELL, STRADA, FREFLO, TRAF-CORFLO, METACOR ou METANET.

Dans le cas des modèles macroscopiques, nous introduisons les variables qui suivent :

- Le nombre de véhicules noté $N(x,t)$;
- Le débit noté classiquement $Q(x,t)$ correspondant au nombre de véhicules s'écoulant à un point d'abscisse x et au temps t par unité de temps :

$$Q(x,t) := \lim_{\delta t \to 0} \frac{N(x,t+\delta t) - N(x,t)}{\delta t}$$

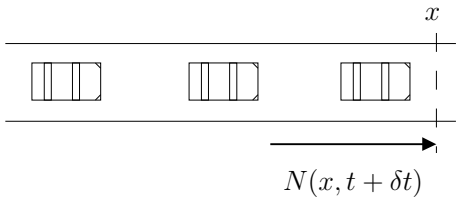

FIGURE A.1 – Illustration du *débit* en trafic

- La concentration (appelée également densité spatiale instantanée) notée $\rho(x,t)$ correspondant au nombre de véhicules par unité de longueur se trouvant sur une section voisine du point d'abscisse x, au temps t :

$$\rho(x,t) := \lim_{\delta x \to 0} \frac{N(x+\delta x,t) - N(x,t)}{\delta x}$$

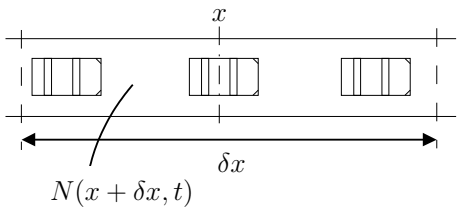

FIGURE A.2 – Illustration de la *densité* en trafic

- La vitesse de flot, notée $V(x,t)$ correspondant à la vitesse moyenne spatiale des véhicules situés dans la section $[x, x+\delta x]$ au temps t, avec $\delta t \to 0$. Cette vitesse de flot est donnée par le rapport entre le débit instantané et la concentration. En outre, il est possible de montrer que la vitesse de flot est égale à la vitesse moyenne spatiale des vitesses individuelles v_i des véhicules (i)

$$Q(x,t) = \rho(x,t)V(x,t) \quad \text{and} \quad V(x,t) = \bar{V}_s(x,t) := \frac{1}{n}\sum_{i=1}^{n} v_i(x,t).$$

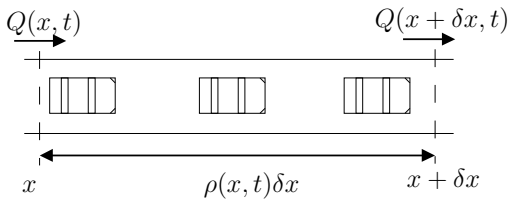

FIGURE A.3 – Illustration de la *conservation* du trafic

Modèles du premier ordre

Le modèle le plus couramment utilisé est également un des modèles pionniers en modélisation du trafic routier. Il s'agit du modèle développé simultanément par Lighthill et Whitham [184] ainsi que Richards [221], s'appuyant sur une analogie avec la dynamique des fluides. Plus communément appelé modèle LWR, ce modèle fait intervenir trois variables décrites précédemment à savoir la vitesse, le débit et la concentration. Pour que le système soit totalement déterminé, il se compose des trois équations suivantes :

- L'équation de définition de la vitesse $Q(x,t) = \rho(x,t)V(x,t)$
- L'équation de conservation, provenant de la conservation du nombre de véhicules sur une section de longueur infinitésimale et pendant un laps de temps

$$\partial_t \rho(x,t) + \partial_x Q(x,t) = 0$$

- Le diagramme fondamental $V(x,t) = V_e(\rho(x,t))$ permettant de postuler que la vitesse de flot est obtenue en permanence pour un état d'équilibre, celui-ci ne dépendant uniquement que de la concentration instantanée. Il s'agit d'une équation d'état séparant généralement une partie fluide et une partie congestionnée.

Ce système d'équations peut être condensé en une équation aux dérivées partielles, raison pour laquelle il est commun de parler de modèles de premier ordre pour cette famille de modèles. La résolution de cette équation permet de déterminer la valeur de concentration et de déduire d'après la relation d'équilibre, les valeurs de débit et de vitesse correspondantes. Il existe une grande variété de lois décrivant l'évolution du débit en fonction de la densité. Ces relations sont appelées *diagrammes fondamentaux* (DF). Dans la littérature, les DF sont généralement considérés soit linéaires par morceaux, soit quadratiques par morceaux. Les diagrammes fondamentaux doivent répondre à certaines observations expérimentales fondamentales :

- Lorsque le nombre de véhicules est suffisamment faible sur la section considérée, ces véhicules n'interagissent pas et chacun peut circuler à la vitesse désirée, appelée vitesse libre (prise généralement égale à la vitesse maximale moyenne) ;
- En augmentant le nombre de véhicules dans la section, les interactions deviennent plus importantes et les vitesses pratiquées diminuent. La vitesse de flot est donc une fonction décroissante de la concentration ;
- Dans le cas extrême où la section est saturée et donc la concentration est maximale, la vitesse et le débit sont nuls.

Les modèles type LWR sont couramment usités. Ils sont notamment appréciés pour leur robustesse, leur simplicité d'utilisation mais aussi par l'existence de solutions analytiques pour des cas simples. De plus, de nombreuses extensions en ont été déduites afin

de pouvoir permettre la prise en compte de la variabilité des usagers dans leurs comportements mais pour introduire aussi la variabilité des véhicules. Malgré tout, le modèle LWR présente certains inconvénients. Le principal est le fait qu'il considère le trafic dans un état d'équilibre à chaque instant. Les phases transitoires ne sont de ce fait pas prises en compte car le modèle considère que le trafic passe d'un état d'équilibre à un autre état d'équilibre instantanément.

Modèles du second ordre

Les modèles de second ordre permettent de prendre en compte les états de non équilibre ainsi que les situations de convergence vers un état d'équilibre. L'équation d'équilibre utilisée dans le cadre des modèles de premier ordre est ainsi remplacée par une équation dynamique exprimant l'accélération du flux. L'accélération est composée d'un terme de relaxation vers la vitesse d'équilibre $V_e(\rho)$ ainsi qu'un terme physique de comportement individuel. A l'instar de tout système dynamique, le trafic va chercher à relâcher les contraintes qui s'appliquent à lui afin de tendre vers son état d'équilibre naturel.

Les premiers travaux dans cette direction ont été proposés par Payne [214] puis Whitham [234] au début des années 1970. Ces modèles ont fait l'objet de plusieurs débats quant à leurs intérêts et leurs limites. Le renouveau des modèles de second ordre est apparu avec Aw et Rascle en 2000 [11] ainsi que Zhang en 2002 [241]. Il est possible de dégager un formalisme commun de ces modèles :

$$\begin{cases} \partial_t \rho + \partial_x \left(\rho V\right) = 0, \\ \partial_t V + V \partial_x V = \dfrac{1}{\tau}\left(V_e(\rho) - V\right) - \dfrac{1}{\rho} C^2(\rho) \partial_x \rho \end{cases}$$

Où C correspond à la célérité caractéristique du trafic et τ désigne un temps de relaxation. Le premier terme du membre de droite correspond à la relaxation qui explique la dispersion des points de mesure autour de l'équilibre. Le second terme est un terme d'anticipation. Ces modèles ont l'avantage de mieux reproduire la variabilité des comportements à l'échelle macroscopique mais ce gain par rapport au modèle LWR se fait au détriment de la simplicité de calcul.

De nombreux modèles macroscopiques de second ordre peuvent être reformulés sous le formalisme des modèles dits GSOM (Generic Second Order Modeling). Les modèles GSOM présentés pour la première fois dans Lebacque, Mammar, Haj-Salem [174] s'écrivent de la manière suivante :

$$\begin{cases} \partial_t \rho + \partial_x(\rho v) = 0, \\ \partial_t(\rho I) + \partial_x(\rho v I) = \rho \varphi(I), \\ v = \mathfrak{I}(\rho, I) \end{cases}$$

avec ρ qui définit la densité, v la vitesse, x la position et t le temps. La première équation permet de traduire la conservation des véhicules tandis que la seconde équation permet de décrire la dynamique de l'attribut comportemental I, dépendant du conducteur (cela peut être le type du véhicule, la propension à un comportement plus ou moins agressif, la destination, les flux d'informations depuis et vers le véhicule, etc.). La dernière équation reproduit la loi phénoménologique dite Diagramme Fondamental en vitesse-interdistance, qui dépend de l'attribut du conducteur. La famille GSOM englobe de nombreux modèles de la littérature comme les modèles de Aw et Rascle [11] et celui de Zhang [240, 241], les modèles multi-classes de Bagnerini et Rascle [12] ou Jin et Zhang [143], le modèle à transition de phase déduit du modèle à deux phases de Colombo [61] ou encore le modèle multivoies de Greenberg, Klar et Rascle [150].

Modèle cellulaire

Le modèle cellulaire proposé par Daganzo en 1993 [76, 77] utilise l'idée d'automates cellulaires avec une loi macroscopique de type LWR. Il s'appuie sur un diagramme fondamental linéaire par morceaux. Le réseau est divisé en cellules de longueur égale à la distance parcourue par un véhicule à la vitesse maximale. Chaque cellule (i) contient au temps t, $n_i(t)$ véhicules. Le nombre maximal de véhicules pouvant être contenus par la cellule (i) est donné par $N_i(t)$.

La loi de transmission est donnée sous la forme d'une suite récursive sur les cellules par :

$$n_i(t + \Delta t) = n_i(t) + g_i(t) - g_{i+1}(t)$$

Où $g_i(t)$ représente le flux entrant dans la cellule (i) au temps t, donné par le minimum entre l'offre de la cellule aval et la demande de la cellule amont. Ce modèle correspond au schéma numérique de Godunov [117] appliqué avec des pas d'espace et de temps unitaires. Le schéma de Godunov appliqué au trafic routier a également été utilisé par Lebacque en 1993 et 1996 [163, 164].

4.2 Modèles cinétiques

Ces modèles ont été introduits afin de prendre en compte le caractère stochastique du trafic et des flux. Ils sont basés sur une analogie avec les méthodes utilisées pour la théorie cinétique des gaz de Boltzmann. Le premier modèle de ce type a été développé par Prigogine et Herman en 1971 [218]. Il s'agit d'un modèle macroscopique qui s'appuie sur une distribution des vitesses des véhicules $f(x, v, t)$. La quantité $f(x, v, t)dxdu$ décrit alors la quantité de véhicules ayant statistiquement la vitesse v et étant contenus entre les positions x et $x + dx$ au temps t. Le modèle donne ainsi l'évolution de la densité $\rho(x, t)$ des particules comme une fonction du temps t, de la position d'une particule x et de sa vitesse v.

Ce genre de modèle plus coûteux en termes de temps de calcul par comparaison au modèle LWR, est généralement peu utilisé. De nombreuses critiques ont été formulées du fait de la difficulté de déterminer des solutions analytiques ou encore de le calibrer et de le valider. D'autres modèles cinétiques ont été développés par la suite dans le but d'améliorer le modèle de Prigogine et Herman. Il est possible de citer les travaux de Helbing [124] ou encore de Hoogendoorn et Bovy [135]. Ces travaux se sont ainsi proposés d'inclure les effets des changements de voies ou encore les hétérogénéités des véhicules.

4.3 Modèles microscopiques

Dans le cas des modèles microscopiques, les véhicules sont individualisés. Nous nous intéressons au cas des lois de poursuite entre deux véhicules consécutifs et passons sous silence les cas des conflits pour les intersections ou celui des changements de voie. Les modèles microscopiques offrent une grande richesse de détails mais nécessitent un calibrage propre du fait des nombreux paramètres individuels. Cela les rend difficiles d'utilisation pour une application temps réel. Les modèles microscopiques ont été implémentés dans de nombreux outils commerciaux comme AIMSUN, CORSIM, DRACULA, INTEGRATION, MITSIM, PARAMICS ou encore VISSIM.

Nous utiliserons les notations suivantes :

- La position du véhicule i au temps t, notée $x_i(t)$;
- La vitesse instantanée du véhicule i au temps t, notée $v_i(t) := \dot{x}_i(t)$;
- L'accélération du véhicule i au temps t, notée $a_i(t) := \ddot{x}_i(t)$;

- La longueur du véhicule i notée L_i.
- L'interdistance entre le véhicule i et son véhicule *leader* $(i-1)$ au temps t, notée $S_i(t) := x_{i-1}(t) - x_i(t)$ (pour *spacing*). On pourrait également donner l'interdistance *nette* c'est-à-dire l'interdistance mesurée etre l'arrière du véhicule leader et l'avant du véhicule suiveur $\bar{S}_i(t) := S_i(t) - L_{i-1}$;
- La vitesse relative du véhicule i par rapport à son véhicule *leader* $(i-1)$ au temps t, notée $\dot{S}_i(t) := \dot{x}_{i-1}(t) - \dot{x}_i(t)$;
- Le temps inter-véhiculaire (ou *headway* en anglais) qui est définit comme l'écart temporel entre le passage de deux véhicules successifs au droit d'une position fixée.

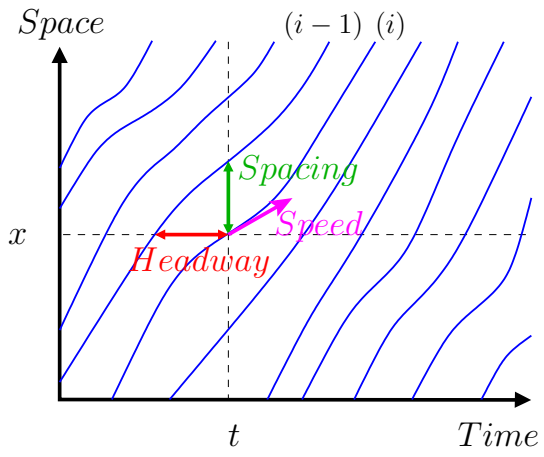

FIGURE A.4 – Notations for the microscopic car-following models

Classiquement, les modèles microscopiques ont pour principale vocation de pouvoir décrire les comportements individuels des usagers pour deux situations de conduite :

- Le comportement en poursuite, correspondant au comportement d'un conducteur en réponse aux actions du véhicule qui le précède ;
- Le comportement de changement de voie au sens large. Cela comprend les manœuvres de dépassement en section courante tout comme les manœuvres d'insertion.

Dans le cas des modèles de poursuite, il est courant de distinguer deux cas types de conduite :

- Le véhicule ne perçoit pas le véhicule qui le précède du fait d'un écart intervéhiculaire suffisamment important et dans ce cas, le conducteur circule à sa vitesse maximale désirée. Il s'agit du cas de conduite libre ;
- Le conducteur souhaite circuler à sa vitesse libre mais son véhicule *leader* ne le lui permet pas, le contraignant ainsi à adopter une vitesse inférieure à sa vitesse désirée. Il s'agit alors du cas de conduite en poursuite où le véhicule entretient de fortes interactions avec son véhicule *leader*.

Les modèles de poursuite se proposent essentiellement de reproduire le comportement de conduite d'un véhicule lorsque sa propre vitesse est contrainte par le véhicule précédent.

Modèles à distance de sécurité

Ces modèles cherchent à décrire la dynamique de poursuite sous la contrainte d'une distance minimale de sécurité. Un des premiers modèles à avoir été développé sur cette idée-là est le modèle simple de Pipes [217]. Ce modèle supposait la règle d'interdistance minimale suivante : « une bonne règle pour suivre un autre véhicule à une distance sûre est de laisser au moins l'équivalent d'une longueur de son propre véhicule tous les dix *miles* par heure [soit 16,1 km/h]». Cela nous donne la relation suivante :

$$S_i(t) = L_i \left(1 + \frac{v_i(t)}{16,1}\right). \tag{1.4.1}$$

Dans ce modèle, la distance minimale de sécurité $S_i t$ augmente linéairement avec la vitesse du véhicule v_i. D'autres auteurs ont proposé une approche relativement similaire.

Kometani et Sasaki ont proposé en 1959 [151] un modèle de prévention de collision. Ce modèle retranscrit la trajectoire d'un véhicule en fonction d'une distance de sécurité minimale permettant d'éviter toute collision. Le développement de ce type de modèle s'appuie sur une utilisation des simples équations newtoniennes du mouvement. Il s'exprime par :

$$S_i(t) = \alpha \left(v_{i-1}(t)\right)^2 + \beta \left(v_i(t-\tau)\right)^2 + \gamma v_i(t-\tau) + \delta. \tag{1.4.2}$$

Les coefficients α et β représentent l'inverse de la capacité maximale de décélération respectivement du véhicule *leader* et du véhicule suiveur. Le coefficient γ est homogène à l'inverse d'un temps et δ est homogène à une distance. Ce sont des paramètres du modèle à calibrer. Le temps τ nécessaire à la prise en compte d'une modification de vitesse du conducteur peut être interprété comme un temps de relaxation.

Les travaux de Gipps [115] ont eu pour but de compléter cette approche initiale en incorporant une vitesse maximale désirée V_i^{desir} ainsi qu'un taux de freinage maximal b_i^{max}, s'apparentant aux termes cinétiques de l'équation précédente. Ainsi, la vitesse du véhicule est définie par la valeur minimale entre la vitesse qu'il peut réellement atteindre d'un point de vue dynamique $v_i^a(t)$ et la vitesse $v_i^b(t)$ qu'il est possible d'adopter en connaissant les contraintes de sécurité liées à la présence du véhicule *leader*. Ce type de modèle semble relativement facile à calibrer. Certains auteurs ont souligné que ce modèle permettait d'obtenir des résultats bien souvent conformes aux observations. Il est par ailleurs utilisé par plusieurs logiciels de simulation du marché dont SISTIM, CARSIM mais également par AIMSUN.

L'idée que le conducteur tente de circuler à la vitesse la plus élevée possible tout en évitant la collision avec son prédécesseur a été reprise par Krauss en 1997 [152]. Ses travaux proposent un modèle discret en temps dans lequel la vitesse de sécurité est telle que le véhicule (i) n'entre pas en collision lors d'un freinage avec son véhicule *leader* $(i-1)$. Celle-ci est donnée par une relation prenant en compte des paramètres de décélération maximale, d'interdistance minimale et de vitesse désirée. De plus, le modèle prend en compte un facteur aléatoire afin de modéliser les comportements « déviants ».

Modèles de stimulus-réponse

Le principe de ces modèles peut être illustré par une relation linéaire de la forme suivante :

$$\text{réponse}(t) = \text{sensibilité} \times \text{stimulus}(t-\tau).$$

Ce type de modèles suppose l'existence d'une relation linéaire entre la vitesse ou l'accélération du véhicule à l'instant t (auquel s'ajoute parfois un temps de réaction τ non nul) et le différentiel de vitesse du véhicule et de son véhicule *leader* à l'instant t, selon un

coefficient de sensibilité. Ainsi, un véhicule réagit en réponse à un stimulus symbolisé par une modification de sa vitesse relative.

Un des modèles pionniers est le modèle linéaire de Chandler, Herman et Montroll [52] dont voici l'expression :

$$\ddot{x}_i(t) = \alpha \left(\dot{x}_{i-1}(t-\tau) - \dot{x}_i(t-\tau) \right). \tag{1.4.3}$$

Ce modèle présente l'expression de l'accélération du véhicule suiveur $(i+1)$ en fonction de la sensibilité (homogène à l'inverse d'un temps) du conducteur au différentiel de vitesse entre les deux véhicules et d'un temps de réaction. De même, les travaux entrepris considèrent un temps de relaxation $\xi := \frac{1}{\alpha}$. Ce temps de relaxation à différencier d'un temps de réaction, traduit un temps caractéristique du système nécessaire pour retourner à l'équilibre.

Le modèle de Gazis, Herman et Rothery [109], également connu sous la dénomination de modèle General Motors (GM), propose une expression généralisée pour le coefficient de sensibilité. Le modèle de poursuite ainsi proposé est non linéaire :

$$\ddot{x}_i(t) = \beta \frac{(\dot{x}_i(t))^m}{(x_{i-1}(t) - x_i(t))^l} \left(\dot{x}_{i-1}(t-\tau) - \dot{x}_i(t-\tau) \right) \tag{1.4.4}$$

Ce modèle permet de prendre en compte l'interdistance entre les deux véhicules. Les coefficients β, l et m sont des paramètres du modèle. Il est possible de retrouver le modèle linéaire de Chandler *et alii* dans le cas où $m = l = 0$. Le coefficient de sensibilité est homogène au produit d'une longueur à la puissance $(l-m)$ par un temps à la puissance $(m-1)$.

De nombreuses études ont été menées afin de déterminer la combinaison « optimale » du couple de paramètres (m, l). Ces études ont été très nombreuses durant les quinze années qui ont suivi la publication du modèle GRH ; peu de chercheurs ont persévéré ensuite dans cette voie. Le lecteur pourra se référer à [34] pour plus de détails.

Citons également l'existence du modèle linéaire d'Helly [127]. Cette approche se base sur différents indices pour l'élaboration par le conducteur de la consigne d'accélération à appliquer à son propre véhicule.

$$\begin{cases} \ddot{x}_i(t) = C_1 \left(\dot{x}_{i-1}(t-\tau) - \dot{x}_i(t-\tau) \right) + C_2 \left[(x_{i-1}(t-\tau) - x_i(t-\tau)) - S_i(t) \right], \\ S_i(t) = \alpha + \beta \dot{x}_i(t-\tau) + \gamma \ddot{x}_i(t-\tau). \end{cases} \tag{1.4.5}$$

Où S_i représente l'interdistance désirée. Egalement C_1, C_2, ainsi que α, β et δ sont des paramètres du modèle. Nous retrouvons le modèle de Chandler dans le cas où $C_2 = 0$.

Ce modèle est utilisé par les logiciels de simulation DYNASIM et également par SITRA.

Modèles à vitesse optimale

Un des premiers modèles s'appuyant sur une analyse des trajectoires des véhicules est le modèle de Newell [198]. Sa formulation est donnée par :

$$\dot{x}_i(t) = V_0 \left(x_{i-1}(t-\tau) - x_i(t-\tau) \right). \tag{1.4.6}$$

La fonction V_0 représente la vitesse optimale, correspondant à la vitesse jugée satisfaisante par le conducteur. Le temps τ ne correspond plus à un temps de réaction du conducteur mais au temps nécessaire au changement de vitesse du véhicule.

Au milieu des années 90, Bando a introduit la notion de vitesse désirée, choisie comme étant une fonction de l'interdistance [13, 14]. Cela a ouvert la voie au développement de

modèles exploitant cette idée et baptisés « *optimal velocity models* » (OVM). L'accélération du véhicule est donnée par la relation suivante :

$$\ddot{x}_i(t) = \alpha \left[V_0(x_{i-1}(t-\tau) - x_i(t-\tau) - \dot{x}_i(t-\tau) \right], \tag{1.4.7}$$

avec

$$V_0(s) = \frac{v_{max}}{2} \left[\tanh\left(s - S_c\right) + \tanh\left(S_c\right) \right].$$

La fonction V_0 est la fonction dite de vitesse optimale. Le coefficient S_c est un paramètre de la vitesse optimale à calibrer. Il correspond à une interdistance caractéristique du comportement de poursuite.

Autres modèles microscopiques

Les modèles d'automates cellulaires représentent l'écoulement du flot sous la forme d'une dynamique simple : l'évolution de cellules échangeant entre elles de l'information sous forme de véhicules. Un modèle d'automates cellulaires nécessite que les axes de l'espace et du temps soient discrétisés. Le modèle d'automate cellulaire appliqué au cas du trafic routier le plus connu est celui de Nagel et Schreckenberg [197]. Dans ce modèle, la vitesse des véhicules est considérée comme étant un nombre entier compris entre 0 et v_{max}. La voie de circulation est représentée à chaque instant par un certain nombre de sections ; une section est soit libre, soit occupée par un et un seul véhicule. L'état des cellules est actualisé chaque pas de temps, en suivant des règles faisant intervenir les caractéristiques des plus proches voisines. Une étape d'aléa est incorporée au processus. Celle-ci permet de prendre en compte les différents comportements des conducteurs et permet aussi l'apparition spontanée de la congestion, classiquement observée *in situ*.

Il existe un ensemble d'autres modèles microscopiques. Certains ouvrages comme [34], [124] ou encore [135] présentent plus précisément ces modèles originaux. Soulignons toutefois l'existence de modèles dits psychophysiques qui se basent sur les aspects psychophysiques du comportement de conduite. Les principaux modèles de ce type sont le modèle présenté par Leutzbach, [180] ainsi que le modèle de Wiedemann, [235, 236]. Ce dernier modèle représente un processus de psycho-écart entre un véhicule et son véhicule *leader*, en fonction de sa vitesse relative. Le modèle de Wiedemann est à l'origine de nombreux logiciels de simulation microscopique comme VISSIM. Il est aujourd'hui également très utilisé dans le développement de la modélisation des flux piétons.

Limites des modèles microscopiques

Classiquement, les critiques concernant les modèles de poursuite portent essentiellement sur les hypothèses simplificatrices des modèles. Ainsi il est possible de souligner que :

- La plupart des modèles microscopiques considèrent les conducteurs comme étant uniformes. Notamment, une des hypothèses simplificatrices de ces modèles est de considérer que le temps de réaction est égal entre chaque conducteur. Il n'y a donc pas de prise en compte de la variabilité des conducteurs et donc des différences de comportements entre chacun d'eux ;
- Certains des modèles supposent une optimisation continue de la vitesse. Pourtant, des éléments psychologiques tendent à prouver qu'un conducteur ne va pas forcément augmenter sa vitesse même dans le cas où son prédécesseur augmente la sienne, notamment s'il souhaite accorder moins d'attention à sa tâche de conduite ;

- A contrario, le modèle GHR suppose que pour un différentiel de vitesse nul, l'accélération sera elle-aussi nulle pour toute valeur d'interdistance ; intuitivement, si un véhicule se retrouve relativement éloigné de son véhicule *leader*, même si au temps t les deux véhicules se trouvent à la même vitesse, le véhicule suiveur peut tout à fait accélérer sa progression.
- Les modèles de poursuite semblent n'être utilisables que dans des conditions de trafic dense. En effet, si la distance intervéhiculaire est suffisamment grande, alors il n'y a plus d'interactions entre véhicules et chacun roule à sa vitesse libre.

4.4 Synthèse

Tout d'abord, rappelons que chaque modèle a ses propres limites de représentation. En effet, nous avons pu voir rapidement que chaque type de modèle a un domaine d'utilisation bien particulier et il est très difficile de pouvoir appliquer un modèle sur un domaine différent. Souvent les résultats en sont décevants car le modèle est inadapté. Pour illustrer ces propos, imaginons qu'une personne souhaite décrire finement l'écoulement du trafic en un point particulier du réseau. Son étude porte sur une section de l'ordre de quelques dizaines de mètres et dure pendant quelques minutes. Il semble tout à fait inadapté d'utiliser ici un modèle macroscopique pour plusieurs raisons : tout d'abord, il sera très difficile de pouvoir juger de la pertinence d'indicateurs macroscopiques comme la concentration (respectivement le débit) étant donné la longueur de la section concernée (respectivement la période d'agrégation). D'autre part, la variabilité des comportements individuels ne pourra pas être correctement retranscrite du fait du faible nombre de véhicules qui seront considérés. Avant de pouvoir réaliser une quelconque étude portant sur le trafic routier, il est nécessaire de préciser les échelles spatiale et temporelle de cette étude. Cela traduit en outre la volonté de l'expérimentateur d'observer plus ou moins finement le réseau. Ce choix se fait parfois en fonction des moyens (données de mesure préexistantes, moyens matériels de mesure...) dont dispose l'observateur mais principalement les échelles s'adaptent selon les objectifs qui sont poursuivis.

	General mathematical expression	**Examples of models**
(1)	$\dot{x}_i(t) = F(S_i(t))$	Pipes [217] Forbes [98]
(2)	$\dot{x}_i(t+\tau) = F(S_i(t), \dot{x}_i(t))$	Chandler [52] Gazis [109] Newell [198]
(3)	$\dot{x}_i(t+\tau) = F(S_i(t), \dot{x}_i(t), \dot{x}_{i+1}(t))$	Kometani [151] Gipps [115] Krauss [153]
(4)	$\ddot{x}_i(t+\tau) = F(S_i(t), \dot{S}_i(t), \dot{x}_i(t), \ddot{x}_i(t))$	Bando [14] Helly [127] Treiber [228]

TABLE A.2 – Car-following models classification

Nous souhaitons présenter quelques-uns des outils de simulation qui sont le plus couramment utilisés par les utilisateurs de la simulation routière en France. Nous nous préoccuperons également de relever le type de modèles utilisés afin de représenter l'écoulement dynamique du trafic. La présentation de ces outils est scindée selon si les logiciels sont purement commerciaux ou s'ils sont issus du milieu de la recherche.

microscopique	**Mésoscopique**	**macroscopique**
• AIMSUN • CORSIM • DRACULA • DYNASIM • MATSim • Quadstone PARAMICS • SimTraffic • SUMO • TransModeler • VISSIM	• Cube • DYNASMART • TRANSIMS • TransModeler	• DYNEV • Emme/2 • OmniTRANS • OREMS • TransCAD • TransModeler • VISUM

TABLE A.3: Classification de quelques exemples -sans exhaustivité- de logiciels de simulation en trafic

Pour le lecteur intéressé, le Centre d'Etudes sur les réseaux, les Transports, l'Urbanisme et les constructions publiques (CERTU) propose un site internet dédié à la simulation dynamique et qui présente une série de logiciels de simulation.

4.5 Logiciels commerciaux

Le logiciel AIMSUN a été développé peu avant le début des années 2000. Il est désormais commercialisé par la société Transport Simulation Systems (TSS), abritée par l'Université de Catalogne. Malgré cette appartenance, le produit AIMSUN ne s'inscrit pas dans un cadre académique mais bien commercial. Ce logiciel de simulation est en fait une partie de l'environnement de simulation du trafic, dénommé GETRAM (*Generic Environment for Traffic Analysis and Modeling*). GETRAM contient en plus d'AIMSUN, un éditeur de réseau, une base de données concernant le réseau d'infrastructures, un module de stockage et une interface de programmation applicative.

AIMSUN est capable de modéliser la circulation sur tout type de réseau de trafic. Il est possible de manipuler et de modifier sous AIMSUN la valeur des flux, les proportions des mouvements tournants ou encore le poids des matrices O-D. Ce sont autant de données d'entrée pour la simulation. L'utilisateur d'AIMSUN a également la possibilité d'utiliser différents modèles de choix d'itinéraire. Le logiciel permet de tester différents scénarios de trafic et il a l'avantage de prendre en compte les transports publics. De plus, les accidents et les voies réservées (par exemple les sites propres pour les transports en commun ou voie réservée pour le covoiturage) peuvent aussi être modélisés.

Le modèle de poursuite implémenté dans AIMSUN est basé sur le modèle de Gipps [115]. Plus exactement, le modèle est un développement du modèle original, classiquement fondé autour d'une composante d'accélération (modélisant la volonté d'atteindre une vitesse désirée) et une composante de décélération (traduisant la contrainte liée à la présence d'un véhicule *leader*). La spécificité du modèle implémenté dans AIMSUN est dans l'estimation de la décélération du véhicule leader.

Développé, utilisé et commercialisé par la société DYNALOGIC, le logiciel de simulation microscopique et stochastique DYNASIM a pour objectif de modéliser aussi finement que possible l'écoulement du trafic sur un réseau. Pour cela, une des idées de base du modèle est l'existence d'une zone d'influence entourant un véhicule, dans laquelle aucun

autre véhicule ne pénètre. Le modèle de poursuite sous-jacent à DYNASIM détermine l'accélération d'un véhicule selon la vitesse de ce véhicule et l'interdistance le séparant du véhicule le précédant. Le modèle utilise l'équation de l'accélération suivante :

$$\ddot{x}_i(t) = C_1\left[\dot{x}_{i-1}(t-0.25) - \dot{x}_i(t-0.25)\right] + C_2\left[(x_{i-1}(t-0.25) - x_i(t-0.25)) - \beta\dot{x}_i(t-0.25) - L\right],$$

avec L la longueur des véhicules, supposée fixe. Nous retrouvons trois paramètres C_1, C_2 et β décrivant trois types d'accélération pour le véhicule (i).

Ce modèle est issu du modèle linéaire de [127] qui pour rappel, est donné par (1.4.5) où nous prenons $\tau = 0.25$, $\alpha = L$ et $\gamma = 0$.

SITRA est un programme de simulation microscopique initialement développé à l'ONERA (Office National d'Etudes et de Recherches Aéronautiques) puis commercialisé par la société française SODIT, aujourd'hui disparue. Ce modèle était essentiellement destiné à la simulation en zone urbaine, et notamment à l'étude des intersections et des carrefours. Le modèle de poursuite utilisé par SITRA est également le modèle linéaire de Helly (1.4.5).

VISSIM est développé par la société allemande Planung Transport Verkehr (PTV). Il est le descendant des programmes réalisés dans les années 1970 à l'Université de Karlsruhe, dont par exemple [235]. VISSIM est un logiciel de simulation pour milieu urbain et interurbain. Il propose une simulation microscopique du couple véhicule-conducteur basée sur une analyse psychophysique du comportement de conduite. Ce type d'idées a été présenté brièvement avec le modèle de Wiedemann. Cette simulation est à la fois discrète et stochastique et s'effectue avec un pas de temps pris égal à 1 seconde.

VISUM est également un logiciel développé et commercialisé par la société PTV. Cependant, VISUM est un logiciel de simulation macroscopique qui se propose de déterminer les temps de parcours sur un réseau d'infrastructures. Ce calcul est réalisé de façon statique à partir des résultats d'affectation de la demande sur les branches du réseau.

PARAMICS est une série d'outils pour la simulation microscopique du trafic, dont PARAMICS Modeller constitue le noyau central. PARAMICS est susceptible de traiter des réseaux dont la taille n'est a priori pas limitée. Le logiciel PARAMICS existe conjointement sous deux versions parallèles : une version est développée par la société Quadstone tandis que la seconde est détenue par la société SIAS. Initialement développé au Centre de calcul parallèle de l'Université d'Edimbourg avant d'être repris indépendamment, et concurremment, par les sociétés SIAS (version souvent dite S-PARAMICS) et Quadstone (version quelquefois dite Q-PARAMICS). Les deux logiciels PARAMICS permettent une micro-simulation du système trafic mais sont tout aussi capables de proposer une modélisation des grands réseaux. Le modèle microscopique de poursuite de PARAMICS fait intervenir les notions d'interdistance désirée et d'interdistance cible. Afin de parvenir à atteindre ces valeurs à chaque instant, le conducteur va alors accélérer ou décélérer. Ce modèle mêle à la fois l'idée des modèles à distance de sécurité type Krauss ainsi que celle des modèles psychophysiques type Wiedemann.

Enfin, citons le cas du logiciel TRANSMODELER développé dès 2005 par la société CALIPER. Celui-ci propose des modules de simulation microscopique et macroscopique ainsi qu'une possibilité d'hybridation. Cette dernière possibilité se traduit par la capacité de simuler de larges réseaux et puis plus finement un carrefour particulier, avec un seul modèle.

4.6 Logiciels de recherche

Le logiciel SYMUVIA est développé au Laboratoire d'Ingénierie, Circulation et Transports (LICIT). SYMUVIA est basé sur un modèle macroscopique d'écoulement, utilisant un diagramme fondamental triangulaire. Deux phases sont donc mises en avant avec une

phase fluide où la position du véhicule i au temps $t+dt$ est égale à la somme de la position initiale au temps t et de la distance parcourue à la vitesse maximale (fluide) pendant dt. En phase congestionnée, la position du véhicule i est déduite de la position de véhicule *leader* $(i-1)$ à laquelle nous retranchons l'interdistance minimale, égale à l'inverse de la densité maximale de véhicules. Le pas de temps est pris de telle sorte que l'information de remontée de file d'un véhicule à l'autre, soit correctement prise en compte. Ainsi, $dt = -\frac{S_{min}}{w}$ où $-w < 0$ est la vitesse de remontée de file. Le modèle incorpore également un modèle de changements de files, des caractéristiques d'accélération bornée pour les véhicules ainsi que le comportement au niveau des convergents et des giratoires.

MITSIM est le simulateur microscopique incorporé dans le logiciel de simulation MITSIMLab, développé par le Massachussetts Institute of Technologies (MIT). MITSIMLab inclut également un simulateur de gestion de la circulation utilisé pour la simulation du contrôle du trafic et des systèmes de guidage routier. Les données d'entrée pour MITSIM sont classiquement des matrices O-D ; un modèle de choix probabiliste du trajet est ensuite utilisé pour déterminer le cheminement de chaque véhicule individuel à chaque intersection du réseau. Un modèle de choix d'itinéraire alternatif est également disponible dans lequel les véhicules sont affectés selon des chemins spécifiés dès le début de la simulation. Ces deux modèles portant sur le choix de l'itinéraire, peuvent être utilisés séparément ou simultanément lors d'une simulation. MITSIM est conçu pour être utilisé dans l'évaluation des systèmes de gestion du trafic.

Le modèle dynamique de microsimulation DRACULA (*Dynamic Route Assignment Combining User Learning and microsimulAtion*, Affectation dynamique des trajets combinant l'apprentissage des utilisateurs et la microsimulation) a été développé à l'Université de Leeds depuis 1993. C'est une nouvelle approche de modélisation de réseaux du trafic routier, dans lequel l'accent est mis sur un couplage entre un modèle d'historique de trafic et un modèle de poursuite microscopique, permettant la représentation des trajectoires individuelles des véhicules. DRACULA permet de représenter directement les choix de trajet des conducteurs à mesure que ces décisions évoluent en fonction du temps. Cette démarche prend en compte la trajectoire spatio-temporelle du véhicule *leader*, mais aussi la configuration du réseau et les règles de franchissement aux intersections. Le modèle propose donc une simulation dynamique de l'offre et de la demande.

FASTLANE est un outil logiciel développé par l'Université de Delft (Pays-Bas). Il peut être utilisé pour la prévision à court terme de l'écoulement du trafic sur les autoroutes. FASTLANE peut être utilisé par exemple par les centres de contrôle pour tester plusieurs scénarios après qu'un incident se soit produit. Les processus opérationnels dans FASTLANE peuvent être divisés en deux parties. Tout d'abord, une estimation de l'état du trafic est réalisée. Ensuite, le programme calcule et visualise le nouvel état de trafic après la mise en œuvre d'un certain scénario correspondant à l'état de trafic précédent. Dans ce logiciel, l'accent est tout particulièrement mis sur la deuxième étape du programme, à savoir la modélisation et la prédiction de l'écoulement du trafic. Le principal défi est de pouvoir mener les calculs à la fois rapidement mais tout en visant un résultat précis.

Soulignons enfin l'existence des logiciels macroscopiques METACOR (INRETS – PHOENIX ISI) et LADTA (LVMT). Issu de METANET, le programme METACOR de l'INRETS a été doté d'une interface graphique par la société Phoenix-ISI dans sa version Px-METACOR. Il s'agit d'un modèle macroscopique du second ordre destiné à l'étude de grands réseaux tels que les autoroutes ou encore les voies rapides urbaines (VRU). Notons enfin que METACOR propose une affectation dynamique.

5 Conclusion

Comme nous l'indique Joël De Rosnay [5], un modèle cherche à réunir les principaux éléments d'un système complexe pour permettre des hypothèses sur son comportement d'ensemble, tout en tenant compte de l'interdépendance des facteurs. Les modèles analogiques sont souvent utilisés en présence d'un petit nombre de variables. Pour un nombre plus important de variables (système trop complexe pour que seule la capacité de nos cerveaux puisse en appréhender tous les facteurs et toutes les coévolutions de ces facteurs dans le temps), il faut alors utiliser des moyens mécaniques ou électroniques comme les simulateurs ou les ordinateurs. Cette étape nécessite alors la construction de modèles mathématiques et la simulation. La démarche s'appuie sur trois étapes :

1. l'analyse de système à savoir définition du système par ses limites, définition des variables importantes et leurs interactions et description des variations,

2. la modélisation à partir d'un schéma des relations causales entre variables et mise en équation et sous forme de langage de programmation et

3. la simulation.

La simulation est aujourd'hui largement répandue et utilisée grâce notamment à des langages de programmation performants (plus puissants et plus simples), et grâce aux technologies de communication et informatiques (puissance de calcul permettant du calcul « temps réel », sorties graphiques...). Néanmoins il ne faut pas trop attendre de la simulation car ce n'est qu'un moyen parmi d'autres de compléter l'étude d'un système complexe. La simulation ne peut prétendre permettre de donner un optimum ou une solution exacte à un problème donné. Elle permet toutefois de donner des tendances sur les évolutions d'un système et de faire éclore de nouvelles hypothèses. La simulation reste globalement moins coûteuse que les expérimentations in situ et permet d'étudier une grande diversité de scénarios. Les résultats de simulation ne sont pas à confondre avec la réalité.

En résumé ce chapitre se proposait de mettre en avant que les modèles et simulations se distinguent par leurs champs d'application (simulations pour les tests de scénarios, modélisation pour l'analyse et l'explication) mais aussi par la multiplicité d'applications et des données disponibles. Malgré tout, ils restent complémentaires et même nécessaires l'un à l'autre. Il s'agit d'un champ en constant renouvellement, s'accommodant des nouvelles technologies à l'image des données de téléphones mobiles intelligents que l'on cherche à exploiter dorénavant. Historiquement, modélisation et simulation ont conjointement permis l'éclosion de concepts théoriques comme l'équilibre entre offre et demande des systèmes, l'affectation statique, les lois de poursuite, les lois d'offre et demande locales de trafic ou encore la notion d'utilité de l'usager.

Notons toutefois quelques limites à la parfaite harmonie entre modélisation et simulation. Premier élément, la plupart des logiciels commerciaux fonctionnent sur le principe de « boîtes noires ». L'utilisateur n'a pas la possibilité d'intervenir sur le cœur du logiciel et de savoir exactement comment les paramètres qu'il manipule ont été calibrés et validés. Cela rend difficile l'utilisation critique de l'outil puisque nous ne savons pas si les hypothèses simplificatrices du ou des modèles sous-jacents sont respectées. Egalement, il subsiste certains doutes concernant la capacité du logiciel à représenter les stratégies de gestion dynamiques, notamment du fait de l'incertitude sur la prise en compte des changements de voie. En effet, il est très difficile de calculer une longueur de voie d'insertion par exemple de par les lois d'insertion et les lois de changements de voie qui sont utilisées.

5. Joël, De Rosnay. "Le macroscope, vers une vision globale." Paris, Seuil (1975) : 137 pages.

Le pas de temps choisi a également une grande influence sur le nombre de changements de voies effectués. Un petit pas de temps provoquera une augmentation de la possibilité de changements de voies tandis qu'un pas de temps important limitera ce nombre de possibilités.

Soulignons enfin une perspective de recherche. Une étude de trafic doit nécessairement débuter par un choix d'échelle. En effet, la précision choisie pour l'étude conditionne la finesse des données à obtenir, les temps de calculs nécessaires mais aussi la précision finale des résultats. Devant la multiplicité des modèles, l'utilisateur doit réaliser un choix en connaissant les spécificités de chacun de ses modèles, leurs domaines de validité et les cas précis d'application. Le problème de l'échelle est une difficulté récurrente dans le domaine des transports. Il apparait que lors des études de trafic, les échelles microscopiques et macroscopiques sont clairement dissociées. Cela est principalement dû au fait que les modèles spatio-temporels utilisés aux niveaux microscopique et macroscopique sont distincts les uns des autres et *a priori*, indépendants entre eux. Or, l'enjeu serait de pouvoir justifier la cohérence de chaque outil de simulation voire de regrouper sous le même outil, simulations microscopique et macroscopique.

Bibliographie

[1] Y. Achdou, F. Camilli, A. Cutrì, and N. Tchou, *Hamilton–Jacobi equations on networks*, (2010).

[2] ———, *Hamilton–Jacobi equations constrained on networks*, Nonlinear Differential Equations and Applications NoDEA, 20 (2013), pp. 413–445.

[3] Y. Achdou, S. Oudet, and N. Tchou, *Hamilton–Jacobi equations for optimal control on junctions and networks*, (2013).

[4] B. Andreianov, K. H. Karlsen, and N. H. Risebro, *A theory of L1–dissipative solvers for scalar conservation laws with discontinuous flux*, Archive for rational mechanics and analysis, 201 (2011), pp. 27–86.

[5] D. Aregba-Driollet and R. Natalini, *Discrete kinetic schemes for multidimensional systems of conservation laws*, SIAM Journal on Numerical Analysis, 37 (2000), pp. 1973–2004.

[6] V. I. Arnol'd, *Mathematical methods of classical mechanics*, vol. 60, Springer, 1989.

[7] V. Astarita, *Node and link models for network traffic flow simulation*, Mathematical and Computer Modelling, 35 (2002), pp. 643–656.

[8] J.-P. Aubin, A. M. Bayen, and P. Saint-Pierre, *Dirichlet problems for some Hamilton–Jacobi equations with inequality constraints*, SIAM Journal on Control and Optimization, 47 (2008), pp. 2348–2380.

[9] ———, *Viability theory : new directions*, Springer, 2011.

[10] A. Aw, A. Klar, M. Rascle, and T. Materne, *Derivation of continuum traffic flow models from microscopic follow-the-leader models*, SIAM Journal on Applied Mathematics, 63 (2002), pp. 259–278.

[11] A. Aw and M. Rascle, *Resurrection of "second order" models of traffic flow*, SIAM journal on applied mathematics, 60 (2000), pp. 916–938.

[12] P. Bagnerini and M. Rascle, *A multiclass homogenized hyperbolic model of traffic flow*, SIAM journal on mathematical analysis, 35 (2003), pp. 949–973.

[13] M. Bando, K. Hasebe, K. Nakanishi, A. Nakayama, A. Shibata, and Y. Sugiyama, *Phenomenological study of dynamical model of traffic flow*, Journal de Physique I, 5 (1995), pp. 1389–1399.

[14] M. Bando, K. Hasebe, A. Nakayama, A. Shibata, and Y. Sugiyama, *Dynamical model of traffic congestion and numerical simulation*, Physical Review E, 51 (1995), pp. 1035–1042.

[15] H. Bar-Gera and S. Ahn, *Empirical macroscopic evaluation of freeway merge-ratios*, Transportation Research Part C : Emerging Technologies, 18 (2010), pp. 457–470.

[16] M. Bardi and I. Capuzzo-Dolcetta, *Optimal control and viscosity solutions of Hamilton–Jacobi–Bellman equations*, Springer, 2008.

[17] M. Bardi and L. Evans, *On Hopf's formulas for solutions of Hamilton–Jacobi equations*, Nonlinear Analysis : Theory, Methods & Applications, 8 (1984), pp. 1373–1381.

[18] C. Bardos, A. Y. Leroux, and J.-C. Nédélec, *First order quasilinear equations with boundary conditions*, Communications in partial differential equations, 4 (1979), pp. 1017–1034.

[19] G. Barles, *Solutions de viscosité des équations de Hamilton-Jacobi*, Springer Verlag, 1994.

[20] G. Barles, A. Briani, and E. Chasseigne, *A Bellman approach for regional optimal control problems in* $\mathbb{R}^N$, SIAM Journal on Control and Optimization, 52 (2014), pp. 1712–1744.

[21] G. Barles and E. R. Jakobsen, *On the convergence rate of approximation schemes for Hamilton–Jacobi–Bellman equations*, ESAIM : Mathematical Modelling and Numerical Analysis, 36 (2002), pp. 33–54.

[22] G. Barles and E. R. Jakobsen, *Error bounds for monotone approximation schemes for Hamilton–Jacobi–Bellman equations*, SIAM journal on numerical analysis, 43 (2005), pp. 540–558.

[23] G. Barles and P. E. Souganidis, *Convergence of approximation schemes for fully nonlinear second order equations*, Asymptotic analysis, 4 (1991), pp. 271–283.

[24] E. Barron and R. Jensen, *Semicontinuous viscosity solutions for Hamilton–Jacobi equations with convex Hamiltonians*, Communications in Partial Differential Equations, 15 (1990), pp. 293–309.

[25] M. Beckmann, C. McGuire, and C. B. Winsten, *Studies in the economics of transportation*, tech. rep., 1956.

[26] S. Bexelius, *An extended model for car-following*, Transportation Research, 2 (1968), pp. 13–21.

[27] O. Biham, A. A. Middleton, and D. Levine, *Self organization and a dynamical transition in traffic flow models*, arXiv preprint cond-mat/9206001, (1992).

[28] R. Billot, C. Chalons, F. De Vuyst, N.-E. El Faouzi, and J. Sau, *A conditionally linearly stable second–order traffic model derived from a Vlasov kinetic description*, Comptes Rendus Mécaniques, 338 (2010), pp. 529–537.

[29] S. Blandin, J. Argote, A. M. Bayen, and D. B. Work, *Phase transition model of non-stationary traffic flow : Definition, properties and solution method*, Transportation Research Part B : Methodological, 52 (2013), pp. 31–55.

[30] O. Bokanowski, Y. Cheng, and C.-W. Shu, *A discontinuous Galerkin solver for front propagation*, SIAM Journal on Scientific Computing, 33 (2011), pp. 923–938.

[31] O. Bokanowski and H. Zidani, *Anti–dissipative schemes for advection and application to Hamilton–Jacobi–Bellman equations*, Journal of Scientific Computing, 30 (2007), pp. 1–33.

[32] P. Bonnel, *Prévoir la demande de transport*, Presses de l'Ecole Nationale des Ponts et Chaussées, 2004.

[33] E. Bourrel, *Modélisation dynamique de l'écoulement du trafic routier : du macroscopique au microscopique*, PhD thesis, INSA de Lyon, 2003.

[34] M. Brackstone and M. McDonald, *Car-following : a historical review*, Transportation Research Part F : Traffic Psychology and Behaviour, 2 (1999), pp. 181–196.

[35] Y. Brenier, *Un algorithme rapide pour le calcul de transformées de Legendre-Fenchel discrètes*, Comptes rendus de l'Académie des Sciences. Série 1, Mathématique, 308 (1989), pp. 587–589.

[36] A. Bressan, *Hyperbolic systems of conservation laws : the one-dimensional Cauchy problem*, vol. 20, Oxford University Press, 2000.

[37] A. Bressan, S. Canic, M. Garavello, M. Herty, and B. Piccoli, *Flows on networks : recent results and perspectives*, EMS Surveys in Mathematical Sciences, (2014).

[38] A. Bressan and K. Nguyen, *Conservation law models for traffic flow on a network of roads*, to appear, (2014).

[39] A. Bressan and F. Yu, *Continuous riemann solvers for traffic flow at a junction*, Discr. Cont. Dyn. Syst., submitted, (2014).

[40] G. Bretti, R. Natalini, and B. Piccoli, *Fast algorithms for the approximation of a traffic flow model on networks*, Discrete and Continuous Dynamical Systems-Series B, 6 (2006).

[41] ———, *Numerical approximations of a traffic flow model on networks*, Networks and Heterogeneous Media, 1 (2006), pp. 57–84.

[42] ———, *A fluid-dynamic traffic model on road networks*, Archives of Computational Methods in Engineering, 14 (2007), pp. 139–172.

[43] ———, *Numerical algorithms for simulations of a traffic model on road networks*, Journal of Computational and Applied Mathematics, 210 (2007), pp. 71–77.

[44] C. Buisson and C. Ladier, *Exploring the impact of homogeneity of traffic measurements on the existence of macroscopic fundamental diagrams*, Transportation Research Record : Journal of the Transportation Research Board, 2124 (2009), pp. 127–136.

[45] C. Buisson and J.-P. Lebacque, *Le modèle de trafic STRADA*, Actes INRETS, (1997), pp. 69–90.

[46] C. Buisson, J.-P. Lebacque, and J.-B. Lesort, *STRADA, a discretized macroscopic model of vehicular traffic flow in complex networks based on the Godunov scheme*, in CESA'96 IMACS Multiconference : computational engineering in systems applications, 1996, pp. 976–981.

[47] C. Buisson, J.-B. Lesort, and J.-P. Lebacque, *Macroscopic modelling of traffic flow and assignment in mixed networks*, in Computing in Civil and Building Engineering. Proceedings of the Sixth International Conference on Computing in Civil and Building Engineering, Berlin, Germany 12-15 July 1995. Volume 2, 1995.

[48] F. Camilli, A. Festa, and D. Schieborn, *An approximation scheme for a Hamilton–Jacobi equation defined on a network*, Applied Numerical Mathematics, 73 (2013), pp. 33–47.

[49] F. Camilli and C. Marchi, *A comparison among various notions of viscosity solution for hamilton–jacobi equations on networks*, Journal of Mathematical Analysis and applications, 407 (2013), pp. 112–118.

[50] F. Camilli, C. Marchi, and D. Schieborn, *The vanishing viscosity limit for Hamilton–Jacobi equations on networks*, Journal of Differential Equations, 254 (2013), pp. 4122–4143.

[51] M. J. Cassidy and S. Ahn, *Driver turn-taking behavior in congested freeway merges*, Transportation Research Record : Journal of the Transportation Research Board, 1934 (2005), pp. 140–147.

[52] R. E. Chandler, R. Herman, and E. W. Montroll, *Traffic dynamics : studies in car following*, Operations research, 6 (1958), pp. 165–184.

[53] Y. Cheng and C.-W. Shu, *A discontinuous Galerkin finite element method for directly solving the Hamilton–Jacobi equations*, Journal of Computational Physics, 223 (2007), pp. 398–415.

[54] ———, *Superconvergence of discontinuous Galerkin and local discontinuous Galerkin schemes for linear hyperbolic and convection–diffusion equations in one space dimension*, SIAM Journal on Numerical Analysis, 47 (2010), pp. 4044–4072.

[55] E. Chevallier and L. Leclercq, *A macroscopic theory for unsignalized intersections*, Transportation Research Part B : Methodological, 41 (2007), pp. 1139–1150.

[56] ———, *A macroscopic single-lane roundabout model to account for insertion delays and O–D patterns*, Computer-Aided Civil and Infrastructure Engineering, 23 (2008), pp. 104–115.

[57] C. G. Claudel, *Convex formulations of inverse modeling problems on systems modeled by Hamilton–Jacobi equations. Applications to traffic flow engineering*, PhD thesis, University of California, 2010.

[58] C. G. Claudel and A. M. Bayen, *Lax–Hopf based incorporation of internal boundary conditions into Hamilton–Jacobi equation. Part i : Theory*, Automatic Control, IEEE Transactions on, 55 (2010), pp. 1142–1157.

[59] ———, *Lax–Hopf based incorporation of internal boundary conditions into Hamilton–Jacobi equation. Part ii : Computational methods*, Automatic Control, IEEE Transactions on, 55 (2010), pp. 1158–1174.

[60] G. M. Coclite, M. Garavello, and B. Piccoli, *Traffic flow on a road network*, SIAM journal on mathematical analysis, 36 (2005), pp. 1862–1886.

[61] R. M. Colombo, *A 2×2 hyperbolic traffic flow model*, Mathematical and computer modelling, 35 (2002), pp. 683–688.

[62] R. M. Colombo and E. Rossi, *On the micro–macro limit in traffic flow*, Rend. Sem. Mat. Univ. Padova, 131 (2014), pp. 217–235.

[63] L. Corrias, *Fast Legendre–Fenchel transform and applications to Hamilton–Jacobi equations and conservation laws*, SIAM journal on numerical analysis, 33 (1996), pp. 1534–1558.

[64] R. Corthout, *Intersection Modelling and Marginal Simulation in Macroscopic Dynamic Network Loading*, PhD thesis, KU Leuven, 2012.

[65] R. Corthout, G. Flötteröd, F. Viti, and C. M. Tampère, *Non-unique flows in macroscopic first-order intersection models*, Transportation Research Part B : Methodological, 46 (2012), pp. 343–359.

[66] G. Costeseque, *Modélisation et simulation dans le contexte du trafic routier*, Modéliser et simuler. Epistémologies et pratiques de la modélisation et de la simulation, (2013).

[67] G. Costeseque and J.-P. Lebacque, *Discussion about traffic junction modelling : conservation laws vs Hamilton–Jacobi equations*, Discrete Cont. Dyn. Syst. S, 7 (2014), pp. 411–433.

[68] ———, *A variational formulation for higher order macroscopic traffic flow models : numerical investigation*, Transp. Res. Part B : Methodological, (2014).

[69] G. Costeseque, J.-P. Lebacque, and R. Monneau, *A convergent scheme for Hamilton–Jacobi equations on a junction : application to traffic*, Num. Math., (2014).

[70] R. Courant, K. Friedrichs, and H. Lewy, *On the partial difference equations of mathematical physics*, IBM journal of Research and Development, 11 (1967), pp. 215–234.

[71] M. G. Crandall, L. C. Evans, and P.-L. Lions, *Some properties of viscosity solutions of Hamilton–Jacobi equations*, Transactions of the American Mathematical Society, 282 (1984), pp. 487–502.

[72] M. G. Crandall, H. Ishii, and P.-L. Lions, *User's guide to viscosity solutions of second order partial differential equations*, Bulletin of the American Mathematical Society, 27 (1992), pp. 1–67.

[73] M. G. Crandall and P.-L. Lions, *Viscosity solutions of Hamilton–Jacobi equations*, Transactions of the American Mathematical Society, 277 (1983), pp. 1–42.

[74] M. G. Crandall and P.-L. Lions, *Two approximations of solutions of Hamilton–Jacobi equations*, Mathematics of Computation, 43 (1984), pp. 1–19.

[75] C. M. Dafermos, *Hyperbolic conservation laws in continuum physics*, vol. 325 of Grundlehren der Mathematischen Wissenschaften [Fundamental Principles of Mathematical Sciences], Springer-Verlag, Berlin„ 2005.

[76] C. F. Daganzo, *The cell transmission model : A dynamic representation of highway traffic consistent with the hydrodynamic theory*, Transportation Research Part B : Methodological, 28 (1994), pp. 269–287.

[77] ———, *The cell transmission model, part ii : network traffic*, Transportation Research Part B : Methodological, 29 (1995), pp. 79–93.

[78] ———, *A variational formulation of kinematic waves : basic theory and complex boundary conditions*, Transportation Research Part B : Methodological, 39 (2005), pp. 187–196.

[79] ———, *A variational formulation of kinematic waves : Solution methods*, Transportation Research Part B : Methodological, 39 (2005), pp. 934–950.

[80] ———, *On the variational theory of traffic flow : well-posedness, duality and applications*, (2006).

[81] C. F. Daganzo and N. Geroliminis, *An analytical approximation for the macroscopic fundamental diagram of urban traffic*, Transportation Research Part B : Methodological, 42 (2008), pp. 771–781.

[82] I. C. Dolcetta, *On a discrete approximation of the Hamilton–Jacobi equation of dynamic programming*, Applied Mathematics and Optimization, 10 (1983), pp. 367–377.

[83] I. C. Dolcetta and H. Ishii, *Approximate solutions of the Bellman equation of deterministic control theory*, Applied Mathematics and Optimization, 11 (1984), pp. 161–181.

[84] J. S. Drake, J. L. Schofer, and A. May, *A statistical analysis of speed-density hypotheses in vehicular traffic science*, in proceedings of the Third International Symposium on the Theory of Traffic Flow, 1967.

[85] D. R. Drew, *Deterministic aspects of freeway operations and control*, Texas Transportation Institute College Station, TX, 1965.

[86] F. Dubois and P. Le Floch, *Boundary conditions for nonlinear hyperbolic systems of conservation laws*, Journal of Differential Equations, 71 (1988), pp. 93–122.

[87] A. Duret, J. Bouffier, and C. Buisson, *Onset of congestion from low-speed merging maneuvers within free-flow traffic stream*, Transportation Research Record : Journal of the Transportation Research Board, 2188 (2010), pp. 96–107.

[88] L. C. Edie, *Car-following and steady-state theory for noncongested traffic*, Operations Research, 9 (1961), pp. 66–76.

[89] L. C. Evans, *Partial differential equations (graduate studies in mathematics, vol. 19)*, American Mathematics Society, 2009.

[90] M. Falcone, *A numerical approach to the infinite horizon problem of deterministic control theory*, Applied Mathematics and Optimization, 15 (1987), pp. 1–13.

[91] M. Falcone and R. Ferretti, *Discrete time high-order schemes for viscosity solutions of Hamilton–Jacobi–Bellman equations*, Numerische Mathematik, 67 (1994), pp. 315–344.

[92] M. Falcone and R. Ferretti, *Semi-lagrangian schemes for Hamilton–Jacobi equations, discrete representation formulae and godunov methods*, Journal of computational physics, 175 (2002), pp. 559–575.

[93] ———, *Semi-Lagrangian approximation schemes for linear and Hamilton–Jacobi equations*, SIAM, 2013.

[94] S. Fan, M. Herty, and B. Seibold, *Comparative model accuracy of a data-fitted generalized Aw-Rascle-Zhang model*, arXiv preprint arXiv :1310.8219, (2013).

[95] S. Fan and B. Seibold, *A comparison of data-fitted first order traffic models and their second order generalizations via trajectory and sensor data*, arXiv preprint arXiv :1208.0382, (2012).

[96] N. Farhi, H. Haj-Salem, and J.-P. Lebacque, *Multianticipative piecewise-linear car-following model*, Transportation Research Record : Journal of the Transportation Research Board, 2315 (2012), pp. 100–109.

[97] G. Flötteröd and J. Rohde, *Operational macroscopic modeling of complex urban road intersections*, Transportation Research Part B : Methodological, 45 (2011), pp. 903–922.

[98] T. Forbes, H. Zagorski, E. Holshouser, and W. Deterline, *Measurement of driver reactions to tunnel conditions*, in Highway Research Board Proceedings, vol. 37, 1958.

[99] N. Forcadel, C. Imbert, and R. Monneau, *Homogenization of fully overdamped frenkel–kontorova models*, Journal of Differential Equations, 246 (2009), pp. 1057–1097.

[100] ———, *Homogenization of accelerated Frenkel-Kontorova models with n types of particles*, Transactions of the American Mathematical Society, 364 (2012), pp. 6187–6227.

[101] N. Forcadel and W. Salazar, *Homogenization of second order discrete model and application to traffic flow*, preprint, (2014).

[102] H. Frankowska, *Lower semicontinuous solutions of Hamilton–Jacobi–Bellman equations*, SIAM Journal on Control and Optimization, 31 (1993), pp. 257–272.

[103] G. Galise, C. Imbert, and R. Monneau, *A junction condition by precised homogenization*, (2014).

[104] M. Garavello, P. Goatin, et al., *The cauchy problem at a node with buffer*, Discrete Contin. Dyn. Syst. Ser. A, (2012).

[105] M. Garavello, R. Natalini, B. Piccoli, and A. Terracina, *Conservation laws with discontinuous flux*, Networks and Heterogeneous Media, 2 (2007), pp. 159–179.

[106] M. Garavello and B. Piccoli, *Traffic flow on networks*, American institute of mathematical sciences Springfield, MO, USA, 2006.

[107] ———, *Conservation laws on complex networks*, Annales de l'Institut Henri Poincaré (C) Non Linear Analysis, 26 (2009), pp. 1925–1951.

[108] N. H. Gartner, C. J. Messer, and A. K. Rathi, *Traffic flow theory : A state-of-the-art report*, Committe on Traffic Flow Theory and Characteristics (AHB45), 2001.

[109] D. C. Gazis, R. Herman, and R. W. Rothery, *Nonlinear follow-the-leader models of traffic flow*, Operations Research, 9 (1961), pp. 545–567.

[110] N. Geroliminis and C. F. Daganzo, *Existence of urban-scale macroscopic fundamental diagrams : Some experimental findings*, Transportation Research Part B : Methodological, 42 (2008), pp. 759–770.

[111] N. Geroliminis and J. Sun, *Properties of a well-defined macroscopic fundamental diagram for urban traffic*, Transportation Research Part B : Methodological, 45 (2011), pp. 605–617.

[112] A. Ghorbel and R. Monneau, *Existence and non-existence of semi-discrete shocks for a car-following model in traffic flow*, (2012).

[113] J. Gibb, *Model of traffic flow capacity constraint through nodes for dynamic network loading with queue spillback*, Transportation Research Record : Journal of the Transportation Research Board, 2263 (2011), pp. 113–122.

[114] Y. Giga and N. Hamamuki, *Hamilton–Jacobi equations with discontinuous source terms*, Communications in Partial Differential Equations, 38 (2012), pp. 199–243.

[115] P. G. Gipps, *A behavioural car-following model for computer simulation*, Transportation Research Part B : Methodological, 15 (1981), pp. 105–111.

[116] E. Godlewski and P.-A. Raviart, *Hyperbolic systems of conservation laws*, Ellipses, 1991.

[117] S. K. Godunov, *A difference method for numerical calculation of discontinuous solutions of the equations of hydrodynamics*, Matematicheskii Sbornik, 89 (1959), pp. 271–306.

[118] S. Göttlich, U. Ziegler, and M. Herty, *Numerical discretization of Hamilton-Jacobi equations on networks*, Networks & Heterogeneous Media, 8 (2013).

[119] H. Greenberg, *An analysis of traffic flow*, Operations research, 7 (1959), pp. 79–85.

[120] B. D. Greenshields, J. Bibbins, W. Channing, and H. Miller, *A study of traffic capacity*, in Highway research board proceedings, vol. 14, 1935.

[121] K. Han, *An Analytical Approach to Sustainable Transportation Network Design*, PhD thesis, The Pennsylvania State University, 2013.

[122] K. Han, B. Piccoli, T. L. Friesz, and T. Yao, *A continuous-time link-based kinematic wave model for dynamic traffic networks*, arXiv preprint arXiv :1208.5141, (2012).

[123] K. Han, T. Yao, and T. L. Friesz, *Lagrangian-based hydrodynamic model : Freeway traffic estimation*, arXiv preprint arXiv :1211.4619, (2012).

[124] D. Helbing, *Traffic and related self-driven many-particle systems*, Reviews of modern physics, 73 (2001), p. 1067.

[125] ———, *Derivation of a fundamental diagram for urban traffic flow*, The European Physical Journal B, 70 (2009), pp. 229–241.

[126] D. Helbing, S. Lämmer, and J.-P. Lebacque, *Self-organized control of irregular or perturbed network traffic*, in Optimal control and dynamic games, Springer, 2005, pp. 239–274.

[127] W. Helly, *Simulation of bottlenecks in single-lane traffic flow*, in (Herman R.C. Ed.), Proc. Symp. Theory of Traffic Flow, Elsevier, Amsterdam, 1961, pp. 207–238.

[128] V. Henn, *A wave-based resolution scheme for the hydrodynamic LWR traffic flow model*, in Traffic and Granular Flow'03, Springer, 2005, pp. 105–124.

[129] J. C. Herrera and A. M. Bayen, *Incorporation of lagrangian measurements in freeway traffic state estimation*, Transportation Research Part B : Methodological, 44 (2010), pp. 460–481.

[130] J. C. Herrera, D. B. Work, R. Herring, X. J. Ban, Q. Jacobson, and A. M. Bayen, *Evaluation of traffic data obtained via GPS-enabled mobile phones : The* Mobile Century *field experiment*, Transportation Research Part C : Emerging Technologies, 18 (2010), pp. 568–583.

[131] M. Herty, C. Kirchner, S. Moutari, and M. Rascle, *Multicommodity flows on road networks*, Communications in Mathematical Sciences, 6 (2008), pp. 171–187.

[132] M. Herty and A. Klar, *Modeling, simulation, and optimization of traffic flow networks*, SIAM Journal on Scientific Computing, 25 (2003), pp. 1066–1087.

[133] H. Holden and N. H. Risebro, *A mathematical model of traffic flow on a network of unidirectional roads*, SIAM Journal on Mathematical Analysis, 26 (1995), pp. 999–1017.

[134] ———, *Front tracking for hyperbolic conservation laws*, vol. 152, Springer, 2011.

[135] S. P. Hoogendoorn and P. H. Bovy, *State-of-the-art of vehicular traffic flow modelling*, Proceedings of the Institution of Mechanical Engineers, Part I : Journal of Systems and Control Engineering, 215 (2001), pp. 283–303.

[136] S. P. Hoogendoorn, S. Ossen, and M. Schreuder, *Properties of a microscopic heterogeneous multi-anticipative traffic flow model*, in Transportation and Traffic Theory 2007. Papers Selected for Presentation at ISTTT17, 2007.

[137] E. Hopf, *Generalized solutions of non-linear equations of first order*, Journal of Mathematics and Mechanics, 14 (1965), pp. 951–973.

[138] C. Hu and C.-W. Shu, *A discontinuous galerkin finite element method for Hamilton–Jacobi equations*, SIAM Journal on Scientific computing, 21 (1999), pp. 666–690.

[139] C. Imbert and R. Monneau, *Flux-limited solutions for quasi-convex Hamilton–Jacobi equations on networks*, (2014).

[140] ———, *Level-set convex Hamilton–Jacobi equations on networks*, (2014).

[141] C. Imbert, R. Monneau, and H. Zidani, *A Hamilton–Jacobi approach to junction problems and application to traffic flows*, ESAIM : Control, Optimisation and Calculus of Variations, 19 (2013), pp. 129–166.

[142] H. Ishii, *Perron's method for Hamilton-Jacobi equations*, Duke Mathematical Journal, 55 (1987), pp. 369–384.

[143] W. Jin and H. M. Zhang, *Multicommodity kinematic wave simulation model for network traffic flow*, Transportation Research Record : Journal of the Transportation Research Board, 1883 (2004), pp. 59–67.

[144] W.-L. Jin and W. W. Recker, *Instantaneous information propagation in a traffic stream through inter-vehicle communication*, Transportation Research Part B : Methodological, 40 (2006), pp. 230–250.

[145] W.-L. Jin and Y. Yu, *Asymptotic solution and effective hamiltonian of a Hamilton–Jacobi equation in the modeling of traffic flow on a homogeneous signalized road*. 2014.

[146] B. S. Kerner, *Experimental features of self–organization in traffic flow*, Physical Review Letters, 81 (1998), pp. 3797–3800.

[147] M. M. Khoshyaran and J.-P. Lebacque, *Lagrangian modelling of intersections for the GSOM generic macroscopic traffic flow model*, in Proceedings of the 10th International Conference on Application of Advanced Technologies in Transportation (AATT2008), Athens, Greece, 2008.

[148] ———, *Internal state models for intersections in macroscopic traffic flow models*, in conference of Traffic and Granular Flow, Shanghai, 2009.

[149] ———, *A stochastic macroscopic traffic model devoid of diffusion*, in Traffic and Granular Flow'07, Springer, 2009, pp. 139–150.

[150] A. Klar, J. Greenberg, and M. Rascle, *Congestion on multilane highways*, SIAM Journal on Applied Mathematics, 63 (2003), pp. 818–833.

[151] E. Kometani and T. Sasaki, *A safety index for traffic with linear spacing*, Operations Research, 7 (1959), pp. 704–720.

[152] S. Krauss, *Microscopic modeling of traffic flow : Investigation of collision free vehicle dynamics*, PhD thesis, Universitat zu Koln., 1998.

[153] S. Krauss, P. Wagner, and C. Gawron, *Metastable states in a microscopic model of traffic flow*, Physical Review E, 55 (1997), p. 5597.

[154] N. Krylov, *On the rate of convergence of finite-difference approximations for Bellman equations with variable coefficients*, Probability Theory and Related Fields, 117 (2000), pp. 1–16.

[155] N. V. Krylov, *The rate of convergence of finite-difference approximations for Bellman equations with Lipschitz coefficients*, Applied Mathematics & Optimization, 52 (2005), pp. 365–399.

[156] H. J. Kushner and P. Dupuis, *Numerical methods for stochastic control problems in continuous time*, vol. 24, Springer, 2001.

[157] C. Lattanzio and P. Marcati, *The zero relaxation limit for the hydrodynamic whitham traffic flow model*, Journal of differential equations, 141 (1997), pp. 150–178.

[158] J. A. Laval and L. Leclercq, *The Hamilton–Jacobi partial differential equation and the three representations of traffic flow*, Transportation Research Part B : Methodological, 52 (2013), pp. 17–30.

[159] P. D. Lax, *Hyperbolic systems of conservation laws II*, Communications on Pure and Applied Mathematics, 10 (1957), pp. 537–566.

[160] ———, *Hyperbolic systems of conservation laws and the mathematical theory of shock waves*, vol. 11, SIAM, 1973.

[161] J. Lebacque, S. Mammar, and H. Haj-Salem, *An intersection model based on the GSOM model*, in Proceedings of the 17th World Congress, The International Federation of Automatic Control, Seoul, Korea, 2008, pp. 7148–7153.

[162] J.-P. Lebacque, *Semimacroscopic simulation of urban traffic*, in Proc. of the Int. 84 Minneapolis Summer Conference. AMSE, vol. 4, 1984, pp. 273–291.

[163] ———, *Les modèles macroscopiques de trafic*, in Annales des Ponts et chaussées, no. 67, Elsevier, 1993, pp. 24–45.

[164] ———, *The Godunov scheme and what it means for first order traffic flow models*, in Internaional symposium on transportation and traffic theory, 1996, pp. 647–677.

[165] ———, *A two phase extension of the LWR model based on the boundedness of traffic acceleration*, in Transportation and Traffic Theory in the 21st Century. Proceedings of the 15th International Symposium on Transportation and Traffic Theory, 2002.

[166] ———, *Two-phase bounded-acceleration traffic flow model : analytical solutions and applications*, Transportation Research Record : Journal of the Transportation Research Board, 1852 (2003), pp. 220–230.

[167] ———, *Intersection modeling, application to macroscopic network traffic flow models and traffic management*, in Traffic and Granular Flow'03, Springer, 2005, pp. 261–278.

[168] ———, *Modélisation et simulation des transports : un panorama*, Génie logiciel, (2005), pp. 43–54.

[169] J.-P. Lebacque, H. Haj-Salem, and S. Mammar, *Second order traffic flow modeling : supply-demand analysis of the inhomogeneous Riemann problem and of boundary conditions*, Proceedings of the 10th Euro Working Group on Transportation (EWGT), 3 (2005).

[170] J.-P. Lebacque and M. M. Khoshyaran, *First order macroscopic traffic flow models for networks in the context of dynamic assignment*, in Transportation Planning, Springer, 2002, pp. 119–140.

[171] ———, *First-order macroscopic traffic flow models : Intersection modeling, network modeling*, in Transportation and Traffic Theory. Flow, Dynamics and Human Interaction. 16th International Symposium on Transportation and Traffic Theory, 2005.

[172] ———, *A variational formulation for higher order macroscopic traffic flow models of the GSOM family*, Procedia-Social and Behavioral Sciences, 80 (2013), pp. 370–394.

[173] J.-P. Lebacque, X. Louis, S. Mammar, B. Schnetzler, and H. Haj-Salem, *Modélisation du trafic autoroutier au second ordre*, Comptes Rendus Mathematique, 346 (2008), pp. 1203–1206.

[174] J.-P. Lebacque, S. Mammar, and H. H. Salem, *Generic second order traffic flow modelling*, in Transportation and Traffic Theory 2007. Papers Selected for Presentation at ISTTT17, 2007.

[175] L. Leclercq, *Bounded acceleration close to fixed and moving bottlenecks*, Transportation Research Part B : Methodological, 41 (2007), pp. 309–319.

[176] ———, *Hybrid approaches to the solutions of the "Lighthill–Whitham–Richards" model*, Transportation Research Part B : Methodological, 41 (2007), pp. 701–709.

[177] L. Leclercq, J. A. Laval, and E. Chevallier, *The lagrangian coordinates and what it means for first order traffic flow models*, in Transportation and Traffic Theory 2007. Papers Selected for Presentation at ISTTT17, 2007.

[178] L. Leclercq and S. Moutari, *Hybridization of a class of "second order" models of traffic flow*, Simulation modelling practice and theory, 15 (2007), pp. 918–934.

[179] H. Lenz, C. Wagner, and R. Sollacher, *Multi-anticipative car-following model*, The European Physical Journal B-Condensed Matter and Complex Systems, 7 (1999), pp. 331–335.

[180] W. Leutzbach and R. Wiedemann, *Development and applications of traffic simulation models at the Karlsruhe Institut für Verkehrswesen*, Traffic engineering & control, 27 (1986), pp. 270–278.

[181] R. J. LeVeque, *Finite volume methods for hyperbolic problems*, vol. 31, Cambridge university press, 2002.

[182] J. Li and H. Zhang, *Modeling space–time inhomogeneities with the kinematic wave theory*, Transportation Research Part B : Methodological, 54 (2013), pp. 113–125.

[183] ———, *The variational formulation of a non-equilibrium traffic flow model : Theory and implications*, Procedia-Social and Behavioral Sciences, 80 (2013), pp. 327–340.

[184] M. J. Lighthill and G. B. Whitham, *On kinematic waves II. A theory of traffic flow on long crowded roads*, Proceedings of the Royal Society of London. Series A. Mathematical and Physical Sciences, 229 (1955), pp. 317–345.

[185] Y. Lucet, *Faster than the fast Legendre transform, the linear-time Legendre transform*, Numerical Algorithms, 16 (1997), pp. 171–185.

[186] Y. Makigami, G. Newell, and R. Rothery, *Three-dimensional representation of traffic flow*, Transportation Science, 5 (1971), pp. 302–313.

[187] S. Mammar, J.-P. Lebacque, and H. H. Salem, *Intersection modeling based on the second order traffic flow model ARZ*, in Proceedings of the 11th EWGT Meeting, 2006, pp. 435–440.

[188] ———, *Riemann problem resolution and Godunov scheme for the Aw-Rascle-Zhang model*, Transportation science, 43 (2009), pp. 531–545.

[189] A. May Jr and H. Keller, *Non–integer car–following models*, Highway Research Record, 199 (1967), pp. 19–32.

[190] P.-E. Mazaré, A. H. Dehwah, C. G. Claudel, and A. M. Bayen, *Analytical and grid-free solutions to the Lighthill–Whitham–Richards traffic flow model*, Transportation Research Part B : Methodological, 45 (2011), pp. 1727–1748.

[191] T. Monamy, *Private discussions*.

[192] R. Monneau, *Homogenization of some traffic vehicular models*. private lectures, 2011.

[193] R. Monneau, M. Roussignol, and A. Tordeux, *Invariance and homogenization of an adaptive time gap car-following model*, Nonlinear Differential Equations and Applications NoDEA, (2012), pp. 1–27.

[194] J. Monteil, *Investigating the effects of cooperative vehicles on highway traffic flow homogenization : analytical and simulation studies*, PhD thesis, INSA Lyon, Villeurbanne, 2014.

[195] J. Monteil, R. Billot, and N. E. EL FAOUZI, *Véhicules coopératifs pour une gestion dynamique du trafic : approche théorique et simulation.*, Recherche Transports Sécurité, (2013).

[196] K. Moskowitz and L. Newan, *Notes on freeway capacity*, Highway Research Record, (1963).

[197] K. Nagel and M. Schreckenberg, *A cellular automaton model for traffic flow*, J. Physique I, 2 (1992), p. 102.

[198] G. F. Newell, *Nonlinear effects in the dynamics of car following*, Operations Research, 9 (1961), pp. 209–229.

[199] G. F. Newell, *A simplified theory of kinematic waves in highway traffic, part i : general theory*, Transportation Research Part B : Methodological, 27 (1993), pp. 281–287.

[200] ———, *A simplified theory of kinematic waves in highway traffic, part ii : Queueing at freeway bottlenecks*, Transportation Research Part B : Methodological, 27 (1993), pp. 289–303.

[201] ———, *A simplified theory of kinematic waves in highway traffic, part iii : Multi-destination flows*, Transportation Research Part B : Methodological, 27 (1993), pp. 305–313.

[202] D. Ngoduy, *Application of gas-kinetic theory to modelling mixed traffic of manual and ACC vehicles*, Transportmetrica, 8 (2012), pp. 43–60.

[203] ———, *Instability of cooperative adaptive cruise control traffic flow : A macroscopic approach*, Communications in Nonlinear Science and Numerical Simulation, 18 (2013), pp. 2838–2851.

[204] D. Ngoduy, S. Hoogendoorn, and R. Liu, *Continuum modeling of cooperative traffic flow dynamics*, Physica A : Statistical Mechanics and its Applications, 388 (2009), pp. 2705–2716.

[205] D. Ngoduy and C. Tampère, *Macroscopic effects of reaction time on traffic flow characteristics*, Physica Scripta, 80 (2009), p. 025802.

[206] D. Ngoduy and R. Wilson, *Multianticipative nonlocal macroscopic traffic model*, Computer-Aided Civil and Infrastructure Engineering, (2013).

[207] O. Oleinik, *Construction of a generalized solution of the cauchy problem for a quasi-linear equation of first order by the introduction of vanishing viscosity*, Amer. Math. Soc. Transl. Ser, 2 (1963), pp. 277–283.

[208] G. Orosz, B. Krauskopf, and R. E. Wilson, *Bifurcations and multiple traffic jams in a car-following model with reaction-time delay*, Physica D : Nonlinear Phenomena, 211 (2005), pp. 277–293.

[209] G. Orosz and G. Stépán, *Subcritical Hopf bifurcations in a car-following model with reaction-time delay*, Proceedings of the Royal Society A : Mathematical, Physical and Engineering Science, 462 (2006), pp. 2643–2670.

[210] G. Orosz, R. E. Wilson, and B. Krauskopf, *Global bifurcation investigation of an optimal velocity traffic model with driver reaction time*, Physical Review-Series E-, 70 (2004), pp. 026207–026207.

[211] S. Osher and J. A. Sethian, *Fronts propagating with curvature-dependent speed : algorithms based on Hamilton–Jacobi formulations*, Journal of computational physics, 79 (1988), pp. 12–49.

[212] S. Osher and C.-W. Shu, *High-order essentially nonoscillatory schemes for Hamilton–Jacobi equations*, SIAM Journal on Numerical Analysis, 28 (1991), pp. 907–922.

[213] S. Ossen and S. P. Hoogendoorn, *Multi-anticipation and heterogeneity in car-following empirics and a first exploration of their implications*, in Intelligent Transportation Systems Conference, 2006. ITSC'06. IEEE, IEEE, 2006, pp. 1615–1620.

[214] H. J. Payne, *Models of freeway traffic and control.*, Mathematical models of public systems, (1971).

[215] B. Perthame, *Kinetic formulation of conservation laws*, vol. 21, Oxford University Press, 2002.

[216] B. Piccoli, K. Han, T. L. Friesz, and T. Yao, *Second order models and traffic data from mobile sensors*, arXiv preprint arXiv :1211.0319, (2012).

[217] L. A. Pipes, *An operational analysis of traffic dynamics*, Journal of applied physics, 24 (1953), pp. 274–281.

[218] I. Prigogine and R. Herman, *Kinetic theory of vehicular traffic*, tech. rep., 1971.

[219] R. Prud'homme, *La congestion et ses coûts*, Annales des Ponts et Chaussées, 94 (2000), pp. 13–19.

[220] S. Qiu, M. Abdelaziz, F. Abdellatif, and C. G. Claudel, *Exact and grid-free solutions to the Lighthill–Whitham–Richards traffic flow model with bounded acceleration for a class of fundamental diagrams*, Transportation Research Part B : Methodological, 55 (2013), pp. 282–306.

[221] P. I. Richards, *Shock waves on the highway*, Operations research, 4 (1956), pp. 42–51.

[222] D. Serre, *Systemes de lois de conservation*, Diderot Paris, 1996.

[223] J. A. Sethian, *Level set methods and fast marching methods : evolving interfaces in computational geometry, fluid mechanics, computer vision, and materials science*, vol. 3, Cambridge university press, 1999.

[224] C. M. Tampère, *Human-kinetic multiclass traffic flow theory and modelling*, Civil Engineering and Geosciences, Department Transport & Planning, (2004), p. 309.

[225] C. M. Tampère, R. Corthout, D. Cattrysse, and L. H. Immers, *A generic class of first order node models for dynamic macroscopic simulation of traffic flows*, Transportation Research Part B : Methodological, 45 (2011), pp. 289–309.

[226] C. M. Tampère, S. P. Hoogendoorn, and B. Van Arem, *Continuous traffic flow modeling of driver support systems in multiclass traffic with intervehicle communication and drivers in the loop*, Intelligent Transportation Systems, IEEE Transactions on, 10 (2009), pp. 649–657.

[227] A. Tordeux, *Étude de processus en temps continu modélisant l'écoulement de flux de trafic routier*, PhD thesis, Université Paris-Est, 2010.

[228] M. Treiber, A. Hennecke, and D. Helbing, *Congested traffic states in empirical observations and microscopic simulations*, Physical Review E, 62 (2000), p. 1805.

[229] M. Treiber and V. Kanagaraj, *Comparing numerical integration schemes for time-continuous car-following models*, arXiv preprint arXiv :1403.4881, (2014).

[230] M. Treiber, A. Kesting, and D. Helbing, *Delays, inaccuracies and anticipation in microscopic traffic models*, Physica A : Statistical Mechanics and its Applications, 360 (2006), pp. 71–88.

[231] J. N. Tsitsiklis, *Efficient algorithms for globally optimal trajectories*, Automatic Control, IEEE Transactions on, 40 (1995), pp. 1528–1538.

[232] F. van Wageningen-Kessels, Y. Yuan, S. P. Hoogendoorn, H. Van Lint, and K. Vuik, *Discontinuities in the lagrangian formulation of the kinematic wave model*, Transportation Research Part C : Emerging Technologies, 34 (2013), pp. 148–161.

[233] J. G. Wardrop, *Some theorical aspects of road traffic research*, Proceedings of the Institute of Civil Engineers, Part II, Vol.1 (1952), pp. 325–378.

[234] G. B. Whitham, *Linear and nonlinear waves*, vol. 42, John Wiley & Sons, 1974.

[235] R. Wiedemann, *Simulation des verkehrsflusses schriftenreihe des instituts für verkehrswesen*, Universität Karlsruhe, (1974).

[236] R. Wiedemann and U. Reiter, *Microscopic traffic simulation : the simulation system mission, background and actual state*, Project ICARUS (V1052) Final Report. Brussels, CEC, 2 (1992).

[237] D. B. Work, O.-P. Tossavainen, Q. Jacobson, and A. M. Bayen, *Lagrangian sensing : traffic estimation with mobile devices*, in American Control Conference, 2009. ACC'09., IEEE, 2009, pp. 1536–1543.

[238] Z. Xu, C.-W. Shu, et al., *Anti-diffusive high order WENO schemes for Hamilton–Jacobi equations*, Methods and Applications of Analysis, 12 (2005), pp. 169–190.

[239] I. Yperman, *The link transmission model for dynamic network loading*, PhD thesis, KU Leuven, 2007.

[240] H. M. Zhang, *A theory of nonequilibrium traffic flow*, Transportation Research Part B : Methodological, 32 (1998), pp. 485–498.

[241] ———, *A non-equilibrium traffic model devoid of gas-like behavior*, Transportation Research Part B : Methodological, 36 (2002), pp. 275–290.

[242] P. Zhang, S. Wong, and S. Dai, *A conserved higher-order anisotropic traffic flow model : description of equilibrium and non-equilibrium flows*, Transportation Research Part B : Methodological, 43 (2009), pp. 562–574.

[243] Y.-T. Zhang and C.-W. Shu, *High-order WENO schemes for Hamilton–Jacobi equations on triangular meshes*, SIAM Journal on Scientific Computing, 24 (2003), pp. 1005–1030.

Table des figures

Liste des tableaux

Liste des algorithmes

Index

Titre

Contribution à l'étude du trafic routier sur réseaux à l'aide des équations d'Hamilton-Jacobi

Résumé

Ce travail porte sur la modélisation et la simulation du trafic routier sur un réseau. Modéliser le trafic sur une section homogène (c'est-à-dire sans entrée, ni sortie) trouve ses racines au milieu du XX$^{\text{ème}}$ siècle et a généré une importante littérature depuis. Cependant, la prise en compte des discontinuités des réseaux comme les jonctions, n'a attiré l'attention du cercle scientifique que bien plus récemment. Pourtant, ces discontinuités sont les sources majeures des congestions, récurrentes ou non, qui dégradent la qualité de service des infrastructures. Ce travail se propose donc d'apporter un éclairage particulier sur cette question, tout en s'intéressant aux problèmes d'échelle et plus particulièrement au passage microscopique-macroscopique dans les modèles existants.

La première partie de cette thèse est consacrée au lien existant entre les modèles de poursuite microscopiques et les modèles d'écoulement macroscopiques. Le passage asymptotique est assuré par une technique d'homogénéisation pour les équations d'Hamilton-Jacobi. Dans une deuxième partie, nous nous intéressons à la modélisation et à la simulation des flux de véhicules au travers d'une jonction. Le modèle macroscopique considéré est bâti autour des équations d'Hamilton-Jacobi. La troisième partie enfin, se concentre sur la recherche de solutions analytiques ou semi-analytiques, grâce à l'utilisation de formules de représentation permettant de résoudre les équations d'Hamilton-Jacobi sous de bonnes hypothèses. Nous nous intéressons également dans cette thèse, à l'application des techniques Hamilton-Jacobi à la classe générique des modèles macroscopiques de trafic de second ordre, dits *modèles GSOM*.

Mots-clés

Trafic routier, micro, macro, réseau, jonction, Hamilton-Jacobi, schéma numérique, Lax-Hopf

Title

Contribution to road traffic flow modeling on networks using Hamilton-Jacobi equations

Abstract

This work focuses on modeling and simulation of traffic flows on a network. Modeling road traffic on a homogeneous section takes its roots in the middle of XX$^{\text{th}}$ century and it has generated a substantial literature since then. However, taking into account discontinuities of the network such as junctions, has attracted the attention of the scientific circle more recently. However, these discontinuities are the major sources of traffic congestion, recurring or not, that basically degrades the level of service of road infrastructure. This work therefore aims to provide a unique perspective on this issue, while focusing on scale problems and more precisely on microscopic-macroscopic passage in existing models.

The first part of this thesis is devoted to the relationship between microscopic car-following models and macroscopic continuous flow models. The asymptotic passage is based on a homogenization technique for Hamilton-Jacobi equations. In a second part, we focus on the modeling and simulation of vehicular traffic flow through a junction. The considered macroscopic model is built on Hamilton-Jacobi equations as well. Finally, the third part focuses on finding analytical or semi-analytical solutions, through representation formulas aiming to solve Hamilton-Jacobi equations under adequate assumptions. In this thesis, we are also interested in the application of Hamilton-Jacobi technique to a generic class of second order macroscopic traffic flow models, the so-called *GSOM models*.

Keywords

Traffic flow, micro, macro, network, junction, Hamilton-Jacobi, numerical scheme, Lax-Hopf